

**MODELING SPACE-TIME RAINFALL AT THE MESOSCALE  
USING RANDOM CASCADES**

by

**Thomas Mark Over**

S.B. Civil Engineering, Massachusetts Institute of Technology, 1983

M.S. Water Resources Engineering, Stanford University, 1984

A thesis submitted to the  
Faculty of the Graduate School of the  
University of Colorado in partial fulfillment  
of the requirements for the degree of  
Doctor of Philosophy  
Program in Geophysics

1995

This thesis for the Doctor of Philosophy degree by

Thomas Mark Over

has been approved for the

Program in Geophysics

by

---

Vijay K. Gupta (thesis advisor)

---

Thomas J. Warner

Date \_\_\_\_\_

Over, Thomas Mark (Ph.D., Geophysics)

Modeling Space-Time Rainfall at the Mesoscale Using Random Cascades

Thesis directed by Professor Vijay K. Gupta

Contemporary problems in hydrology require a simple, testable and accurate theory for mesoscale rainfall fields in space and time. The author's thesis is that evolving multiplicative random cascades provide such a theory. This theory requires only a few parameters to model the observed intermittency and hierarchy of scales in space-time rainfall. Random cascades are first tested as a spatial theory on radar snapshots of mesoscale rainfall fields. In this application, three tasks are accomplished: (1) a class of approximate cascade *generators* is developed; (2) an existing estimation theorem is generalized to include the new class of generators; and (3) the statistical fluctuations associated with the estimation procedure are characterized. The third task is accomplished using comparisons with a new method of simulating "off-grid" cascades.

For a large set of tropical oceanic radar data, it is seen that first-order parameter of the theory, which governs the structure of rainy versus dry regions, varies smoothly as a one-to-one function with the large-scale spatial average rain rate. However, the second-order parameter, which governs the fluctuations within the rainy region, is invariant. These results have important implication physical and theoretical implications.

The spatial cascade theory is extended to space-time by developing a new theory of "evolving" cascades, which results from generalizing the iid cascade generators to iid stochastic processes indexed by time. These stochastic processes may be quite general; the only necessary conditions are that they marginally satisfy the conditions for cascade generators and that they *causal*. To accomodate forcing by the large-scale conditions, the generator processes are non-stationary.

The space-time theory is tested by considering the evolution of a “tracked” rainfall field. A space-time extension of the spatial estimation theorem is used to test the theory and estimate the temporal parameters. Additional tests of the space-time theory are provided by the Lagrangian and Eulerian covariance. The latter, under stationary conditions, is used to determine the conditions under which the theory satisfies Taylor’s hypothesis.

## **Acknowledgements**

This research was supported by grants from NASA and NSF, and by a student position with the USGS, Water Resources Division. Data for the study was kindly provided by Dave Short and Tom Bell of NASA, Rick Lawford of the Atmospheric Environment Service (Canada), and Isztar Zawadzki of McGill University.

I would like to thank my advisor, Vijay Gupta, first for taking a risk on an engineer whose main qualification was probably an eagerness to learn, and, subsequently for years of guidance through the process of becoming a “theoretical hydrologist”. I hope you are not disappointed!

Second, I would like to thank Ed Waymire, Brent Troutman, and Skip Vecchia for patiently answering my seemingly endless questions about stochastic processes.

Third, thanks to my officemates and other co-workers over the years who helped make my life as a graduate student a human rather than just intellectual affair.

Fourth, thanks to my thesis committee for your time and patience.

Last but by no means least, many thanks to family and friends who encouraged, listened, suffered, and prayed with me through this thesis. It would never have gotten finished without you!

## CONTENTS

### Chapter 1:

Introduction.....	1
-------------------	---

### Chapter 2:

Background.....	9
2.1 The Observed Space-Time Structure of Rainfall Fields.....	9
2.1.1 Extratropical Cyclones.....	10
2.1.2 Midlatitude Convective Systems.....	12
2.1.3 Tropical Cloud Systems.....	15
2.2 Previous Approaches to Modeling Space-Time Rainfall.....	16
2.2.1 Point Process Models.....	16
2.2.2 Gaussian Random Field Models.....	21
2.2.3 Notions of Scaling Invariance in Rainfall and their Testing.....	22
2.2.4 Additive, Simple-Scaling Models.....	27
2.2.5 Multiplicative, Multi-Scaling Models.....	28

### Chapter 3:

The Theory of Random Cascades with Applications to Spatial Rainfall.....	31
3.1 Motivation.....	31
3.2 An Introduction to the Theory of Discrete IID Random Cascades.....	36
3.3 Estimation and the Moments of Discrete IID Random Cascades.....	49
3.3.1 Marginal Moments.....	49
3.3.2 Derivatives of the Marginal Moments.....	55
3.3.3 Cross Moments.....	56
3.4 Some Modeling Considerations.....	59
3.4.1 Difficulties Arising from Discreteness.....	59

3.4.1.1	Nonhomogeneity and Anisotropy .....	59
3.4.1.2	“On-grid” versus “Off-grid” Cascades .....	62
3.4.1.3	The Role of the Branching Number.....	63
3.4.2	Some Relevant Examples of Generators .....	67
3.4.2.1	General Results for Generators with Atoms at Zero.....	67
3.4.2.2	The Beta-Model .....	69
3.4.2.3	The Log-Poisson Model.....	71
3.4.2.4	The Log-Normal Model.....	74
3.4.3	A Notion of a $k$ th-order Approximation to an MKP function .....	78
3.4.4	A Notion of $k$ th-order Generator Homogeneity.....	82

#### **Chapter 4:**

Applications of the Theory of Random Cascades to Spatial Rainfall .....		84
4.1	Introduction.....	84
4.2	Description of Data.....	84
4.3	A Method for Constructing Homogeneous and Isotropic Cascades.....	86
4.4	Tests of the Random Cascade Theory.....	95
4.4.1	Tests of the Theory Using the Scaling of Marginal Moments .....	95
4.4.2	Tests of the Theory Using Cross Moments.....	109
4.5	Parameter Estimation .....	124
4.6	Dependence of Cascade Parameters on Large-Scale Average Rain Rate	136
4.6.1	Results.....	136
4.6.2	Interpretation.....	143

#### **Chapter 5:**

A Theory of Space-Time Rainfall Using Random Cascades.....		150
5.1	Introduction.....	150
5.2	A General Theory of Space-Time Cascades .....	151
5.2.1	The Construction.....	152

5.2.2	Scaling of the Moments: Testing and Parameter Estimation .....	154
5.3	Implications for Lagrangian and Eulerian Correlations .....	167
5.3.1	Lagrangian Correlation .....	167
5.3.2	Eulerian Correlation and Taylor's Hypothesis.....	171
5.4	A Specific Example of a Space-Time Construction .....	179
5.4.1	The Second-Order Process.....	180
5.4.2	The First-Order Process .....	183
5.4.3	Parameter Estimation .....	189
<b>Chapter 6:</b>		
	Conclusions.....	192
	<b>References.....</b>	<b>196</b>
APPENDIX A:		
	<b>A Few Concepts from Measure Theory .....</b>	<b>206</b>
APPENDIX B:		
	<b>Hausdorff Measure and Dimension .....</b>	<b>208</b>
APPENDIX C:		
	<b>Calculation of the Moments of the Cascade Limit Mass.....</b>	<b>211</b>
APPENDIX D:		
	<b>The Ensemble Average Cross Moments for a One-Dimensional Cascade .....</b>	<b>215</b>
APPENDIX E:		
	<b>Proof of Convergence of the Spatial Average Temporal Cross Moments.....</b>	<b>220</b>
APPENDIX F:		
	<b>Finite-State Non-Homogeneous Birth-Death Processes .....</b>	<b>225</b>
APPENDIX G:		
	<b>Cross Moments of the Stationary Log-Normal Diffusion .....</b>	<b>233</b>

**LIST OF TABLES**

Table 2.1	The scaling hierarchy of structures in extratropical cyclones.....	11
Table 2.2	The scaling hierarchy of dynamics in a decaying typhoon.....	12
Table F.1	Properties of a Birth-Death Process: Example 1 .....	231
Table F.2	Properties of a Birth-Death Process: Example 2 .....	231
Table F.3	Properties of a Birth-Death Process: Example 3 .....	232

## LIST OF FIGURES

Figure 3.1	Scaling analysis of a spatial rainfall scene.....	32
Figure 3.2	Construction of a cascade model of a spatial rainfall scene .....	34
Figure 3.3	Binary tree induced by the subdivision of the unit interval .....	39
Figure 3.4	Cascade construction sequences .....	42
Figure 3.5	Three classes of MKP functions .....	46
Figure 3.6	Cascade grid for $b=9$ and $n=2$ .....	61
Figure 4.1	Schematic of “on-grid” versus “off-grid” cascades .....	88
Figure 4.2	The Voronoi polygon of a point .....	91
Figure 4.3	The sub-tessellation of a Voronoi polygon into sub-polygons.....	94
Figure 4.4	Standard error of scaling of moments of spatial rainfall, $q=0$ .....	98
Figure 4.5	Standard error of scaling of moments of spatial rainfall, $q=2$ .....	99
Figure 4.6	Logarithm of moments of limit mass for the beta model, $b=4$ .....	100
Figure 4.7	Intercepts of moments of spatial rainfall, $q=0$ .....	103
Figure 4.8	Intercepts of moments of spatial rainfall, $q=2$ .....	104
Figure 4.9	Typical scaling of moments .....	105
Figure 4.10	E-W cross moment exponent vs. $t(q)$ cross moment exponent.....	113
Figure 4.11	E-W cross moment exponent vs. $t(q)$ cross moment exponent.....	114
Figure 4.12	E-W cross moment exponent vs. $t(q)$ cross moment exponent.....	115
Figure 4.13	N-S cross moment exponent vs. $t(q)$ cross moment exponent.....	116
Figure 4.14	N-S cross moment exponent vs. $t(q)$ cross moment exponent.....	117
Figure 4.15	N-S cross moment exponent vs. $t(q)$ cross moment exponent.....	118
Figure 4.16	E-W cross moment, $p=q=0$ .....	119
Figure 4.17	E-W cross moment, $p=q=1$ .....	120
Figure 4.18	N-S cross moment, $p=q=0$ .....	121

Figure 4.19	N-S cross moment, $p=q=1$ .....	122
Figure 4.20	Estimate of $t(0)$ from $t^{(1)}(0)$ vs. estimate from scaling of moments ..	127
Figure 4.21	$\tau^{(2)}(0.5)$ vs. beta .....	130
Figure 4.22	$\tau^{(2)}(1)$ vs. beta .....	131
Figure 4.23	$\tau^{(2)}(1.5)$ vs. beta .....	132
Figure 4.24	$\tau^{(2)}(2)$ vs. beta .....	133
Figure 4.25	First and second-order MKP functions with equal slopes at $q=1$ .....	137
Figure 4.26	Beta estimated from $\tau(0)$ vs. average rain rate .....	140
Figure 4.27	Beta estimated from $\tau^{(1)}(1)$ vs. average rain rate.....	141
Figure 4.28	Beta estimated from $\tau^{(1)}(0.5)$ vs. average rain rate.....	142
Figure 5.1	Time-evolving cascade construction with $d=1, b=2$ .....	153
Figure 5.2	Estimated spatial $\tau(q)$ vs. time .....	161
Figure 5.3	Scaling of temporal cross moments, $t_1 = 17:00$ .....	162
Figure 5.4	Space-time MKP functions estimated from Figure 5.3. ....	163
Figure 5.5	Decay of space-time MKP function with time .....	164
Figure 5.6	Decay of curvature of space-time MKP function with time .....	166
Figure 5.7	Behavior of the Lagrangian cross moments .....	172
Figure 5.8	Space-time MKP function from Lagrangian cross moments.....	173
Figure 5.9	Estimator of first-order fluctuation rate .....	191

# Chapter 1

## Introduction

The spatial or space-time variability of rainfall is central to a number of important problems in surface hydrology. This means specifically that the average rain rate over some region is not sufficient to determine its hydrologic behavior to a first-order approximation. The sensitivity of hydrologic behavior to the variability of the rainfall field is usually the result of a non-linear interaction between the rainfall and some other component of the system. For example, the generation of runoff, depending as it does on partitioning of rainfall into interception, infiltration, and runoff is non-linear in the rain rate because interception and infiltration involve thresholds. Hence the same amount of rain applied uniformly will lead to a smaller amount of runoff than if it is applied in a highly non-uniform manner. This has been most clearly recognized in the development of parameterizations of the land surface in atmospheric models (Johnson et al. 1993; Pitman et al. 1993); for a clear demonstration of this effect in distributed hydrologic modeling, see Ogden and Julien (1994). Another example of sensitivity to rainfall variability arising from non-linearity is the problem of rainfall measurement using both radar and passive microwave sensors. For both types of sensors, the strength of the signal received by the sensor depends non-linearly on the rain rate. Hence when the rain rate is variable within the field-of-view, the variability must be known in order to convert the signal into an average rain rate applicable to the whole field-of-view (Chiu et al. 1990; Ha and North 1995; Zawadzki 1982; Lovejoy and Schertzer 1990). A third example is the problem of the prediction of floods. In this case, not only is the variability of the rainfall critical to the system's behavior, but also

the spatial structure of this variability, because it is the interaction of the rainfall structure with river basin structure that determines the size and timing of the peak flow. These effects are seen indirectly in the “multiscaling” of floods (Gupta and Dawdy 1995); for a direct demonstration, see Gupta et al. (1995).

The chief feature of space-time rainfall at the mesoscale that must be captured by any model or theory is its scaling hierarchy of structures in space and time. It is generally observed in mesoscale rainfall events that instead of a homogeneous rainfall field extending over a large region in space and time, there is a hierarchy of structures, each with its associated space and time scales and intensity, with a number of the smaller structures comprising the larger. As might be expected, the temporal scale (typical lifetime) of a given structure grows with spatial scale, while the average rainfall intensity over it decreases. For example, as found by Austin and Houze (1970, 1972) in extratropical cyclones, the highest intensity element of a rainfall field is a convective cell, which lies at the small-scale end of the mesoscale range and has a spatial scale of about  $2\text{ km}$ , a lifetime of 30 minutes to an hour, and a rainfall intensity typically on the order of  $100\text{ mm/hr}$ . At the large-scale limit of the mesoscale is the cyclone itself, which typically has a spatial scale of about  $1000\text{ km}$ , a lifetime of several days, and a typical average rainfall intensity on the order of  $1\text{ mm/hr}$ . Empirical evidence for the space-time structure of rainfall fields will be reviewed in greater detail in Chapter 2.

The first stochastic theory to model this scaling hierarchy of space-time structures was that of LeCam (1961), who used the theory of clustered point processes to construct a general approach to the problem. The basic idea of clustered point process theories of spatial rainfall is to identify the convective cells as randomly-located points in space-time, associating with them some spatial extent, lifetime and intensity. The larger-scale structures are modeled through the clustering of the points. Clustered point process models are attractive because they use the well-developed mathematical theo-

ry of point processes and random fields to directly model the hierarchy of scales observed in space-time rainfall. However, this also leads to their main disadvantage. Because the structure at each scale is modeled separately, it has its own set of parameters, a minimum of three. Thus a complete model with three scales would include nine parameters. Parameter sets of this size require sophisticated estimation techniques, especially if the parameters are possibly varying in space and time.

An attractive means of reducing the number of parameters required in a stochastic rainfall theory is to assume some kind of *scale invariance*, which might hold over the whole mesoscale range and thus require only a few parameters to model the whole observed hierarchy of structures. This approach assumes that the distinct scales associated with the hierarchy structures in rainfall systems are an artifact of the observation process.

New ideas lead to new ways of looking at data and thence to new results, and scaling invariance was no exception. Lovejoy (1981, 1982) found fractal characteristics in the spatial structure of rain and cloud fields and extreme (hyperbolic) variability in the rain rate fluctuations in space and time. On the basis of these results, Lovejoy and Mandelbrot (1985) constructed an additive, simple-scaling space-time rainfall model on the basis of these results, the so-called fractal sum of pulses (FSP) model. Lovejoy and Schertzer (1985) generalized this to a multiscaling form, but retained the additivity.

The work of Waymire (1985) provides a conceptual bridge between the point process theories that preceded it and the scale-invariant theories that followed. He showed how a large class of processes, including many that have been proposed as models of rainfall, have “scaling limits”. This means that under properly normalized averaging over successively larger domains in space or time, they converge to self-similar or simple-scaling processes. This provides theoretical justification for developing models

that are self-similar in the first place, such as the FSP.

Lovejoy and Schertzer (1985) also pointed out the applicability of theory of multiplicative random cascades (Mandelbrot 1974) to the modeling of rainfall fields, and subsequently developed this approach extensively; see the review by Tessier et al. (1993) and the discussion in Chapter 2. As multiplicative random cascades form the heart of the theory presented and tested here, their construction and properties of multiplicative random cascades are described in detail in Chapter 3. They have a number of advantages over additive scale-invariant theories in modelling rain, as will be described in Chapter 2.

From the present point of view, the theory Lovejoy and Schertzer developed is lacking in two respects. First, it is oriented almost entirely toward the ensemble properties of geophysical fields and their estimation. This approach assumes the stationarity of the processes being modelled. However, it is to be expected that the structure of such fields vary in space and time according to the variation of their physical environment. In the rainfall context one might ask for example whether it is reasonable to suppose that a model of spatial rainfall should have the same parameters regardless of whether it is tropical convection or an extratropical cyclone. Thus the development of a “path-wise” theory that allows estimation of parameters from a single realization of a random cascade field is crucial. Second, since they had in view general applications to geophysical fields, a number of basic issues necessary to constructing a theory of space-time rainfall in particular remained unexplored, including: How well and over what range of scales and for what types of rainfall does the theory explain data? What types of generators are most appropriate? Are the parameters of the generators homogeneous in space and time or do they vary as a function of the meteorological conditions? What effect does the “off-grid” nature of data have on the estimation problem? In view of the observed anisotropy of space and time dimensions, how can this theory

be extended into the time domain to make it into a space-time theory?

A fundamental step in the development of a path-wise random cascade theory was taken by Holley and Waymire (1992), who give conditions on the generator  $W$  of the cascade under which the small-scale limit of the scaling of the spatial moments of a random cascade measure converge almost surely to its characteristic function, the so-called MKP function. These conditions are however rather restrictive and exclude generators that one would want to use in modeling rainfall, including those that have an “atom” at the value zero with positive probability, which is necessary in order to have regions without rain. Their result is also asymptotic, i.e., the theorem applies in the small-scale, high-resolution limit, and does not address the statistical issues involved in estimation from finite resolution data. A more subtle issue is that the result applies strictly only to the process of averaging up over the same subdivision of the domain of the cascade measure that was used in its construction. Since the method of subdivision is typically a grid, if the grid’s location, orientation, or existence is in doubt, we have what will be called here an “off-grid” cascade. Clearly data must be thought of an off-grid cascade; the effect of this on the estimation problem is unknown.

In order to begin to answer these questions, the research described here was undertaken. It is divided into three parts. Chapter 3 presents a review of the theory of random cascades with some extensions for the purpose of modeling spatial rainfall. Chapter 4 gives results of the application of the theory presented in Chapter 3 to a large set of radar-derived rainfall scenes, and Chapter 5 presents an extension of the theory to space-time.

Following the review of the theory of random cascades given in Section 3.2, developments in the spatial theory of rainfall using random cascades begin with extensions to the theory of Holley and Waymire (1992). It was found that one of the conditions stated in the theorem is not used in its proof. Relaxing the condition made it

possible to show that the asymptotic convergence of the scaling of the moments holds for a range of non-negative moment orders for a more general class of generators, including those with an atom at zero. This is described in Section 3.3. Second, a class of generators appropriate for modeling spatial rainfall was developed. The approach taken was to investigate the notion of approximate generators. First and second-order approximate generators were defined, requiring one parameter for the first-order approximation and an additional parameter for the second. This study of appropriate cascade generators also led to clarification of the role of the branching number of the cascade and its relation to the log-infinite divisibility of the generator. These results are given in Section 3.4. In order to provide a consistency check on the results obtained using the scaling of the moments, the prediction of the theory regarding two-point spatial cross moments is also given in Section 3.3.

The statistical issues were explored primarily through simulations. This is due not only to the inherent difficulty of the theoretical issues involved even in the ideal “on-grid” case, but also because as described above, data is inherently “off-grid”. Thus a means of simulating off-grid cascades was developed and simulations of the same resolution as the data were made. Then the same estimation techniques were applied to both. This procedure made it possible to explore questions of goodness-of-fit, bias and variance in estimation by comparison of results from data with those from simulations. The simulation of off-grid cascades is described in Section 4.3.

The theoretical ideas were tested on a database of radar-derived spatial rainfall consisting of more than 3200 scans obtained nominally every fifteen minutes over a fixed location in the tropical Atlantic in the summer of 1974. The predictions of the theory and parameter estimation techniques were applied to these scans, one at a time. The results of this analysis were compared to the results of applying the same analysis to simulated off-grid cascade fields of the same resolution, so that the effects of resolu-

tion and the off-grid nature of the data could be taken into account. This analysis had two goals: (a) to provide a test of the hypothesis of scaling invariance which lies at the heart of the theory, and (b) assuming that scale invariance was found to hold, to estimate the parameters of the theory and to investigate their dependence on the large-scale meteorological conditions. It was found that the hypothesis of scaling of the spatial moments was reasonably well-satisfied. This is described in Section 4.4.

We proceeded then to estimate the parameters and compare them to the large-scale meteorological conditions. Direct measures of the large-scale meteorological conditions would only have been available from a re-analysis of the raw data of the experiment, which was beyond the scope of the thesis and the expertise of the researcher to undertake. Instead the large-scale average rain rate, which is available from the radar simply by averaging, was employed as a measure of the large-scale meteorological conditions. Review of the theoretical as well as empirical literature regarding the generation of rainfall in general and in GATE in particular reveals that this is a useful measure in any case. It was found that the parameter of the first-order approximate cascade depends strongly and according to a simple one-to-one function of the large-scale average rain rate (Over and Gupta 1994), while the “second-order” parameter is largely independent of the large-scale average rain rate. This result is described in Section 4.5. It is interpreted in Section 4.6 to suggest that there is a small scale at which the probability distribution of rainfall, conditioned on positive rain, is independent of the large-scale average rain rate. This interpretation is also compared with the conclusions of other empirical and theoretical studies.

The second main part of the thesis involves the development and testing of a theory of space-time rainfall, and is given in Chapter 5. This theory is based on the notion that the spatial rainfall field *evolves* in time, a fact which underlies the observed anisotropy of space and time noted above. First, this means that the future can depend

only on the past. Second, the field at time  $t + \tau$  will look quite similar to the field at time  $t$ , for a small lag  $\tau$ . Third, since, as was observed in the analysis of the spatial data, the cascade parameters of the spatial rainfall field depend on the large-scale meteorological conditions in which it is embedded, the theory must allow for evolution according to a non-stationary forcing. One basic implication of these requirements is that the space-time theory will naturally lie in the Lagrangian reference frame (that is, following the flow). This is because a Lagrangian description separates the variation occurring due to temporal evolution from that due to advection of the field. The basic notion that is used to develop a space-time theory here is to construct cascades of iid stochastic processes  $W_t$  indexed by time in place of the generators of the spatial cascades which are iid random variables (Over and Gupta 1995). Such cascades are easily shown to satisfy the requirements just described, and in addition lead to a number of other interesting and important testable predictions, including those regarding the breakdown of Taylor's hypothesis (Zawadzki 1973; Crane 1990). Space-time versions of the first and second-order spatial models described above are also developed. Due to the requirement of tracking rainfall fields in order to test a Lagrangian space-time theory, it is tested on a different set of data than is the spatial theory.

## **Chapter 2**

### **Background**

As stated in the introduction, the chief feature of spatial and space-time rainfall at the mesoscale that models have attempted to capture is what we have called a “scaling hierarchy” of structures. The goal of the first section of this chapter is to present the evidence for this notion. It first arose in essentially qualitative studies of the rainfall fields associated with extratropical cyclones, but it is also observed in most varieties of convective rainfall, both tropical and subtropical. Following this discussion of rainfall observations, the second section reviews developments in theories space-time rainfall. It is organized essentially in chronological order, and intends to show how theories were proposed, tested and improved upon from one generation to the next.

#### **2.1 The Observed Space-Time Structure of Rainfall Fields**

In the general reviews of the structure of precipitation systems of Houze (1981) and Houze and Hobbs (1982), precipitating weather systems are divided into three main types: extratropical cyclones, midlatitude convective systems (including thunderstorms), and tropical cloud systems (including hurricanes). Since our concern is with the space-time structure of rainfall fields, essentially, their space-time geometry, we will not discuss their dynamics to much depth. As described in the introduction, and to be amplified below, the notion of a scaling hierarchy of embedded structures forms the basis for most stochastic theories of space-time rainfall. Thus this review will focus on whether such a hierarchy is observed, and where it is observed, what are the geometry and space and time scales of its elements.

### 2.1.1 Extratropical Cyclones

The traditional approach to stochastic space-time rainfall modeling, the clustered point process approach, which will be described in detail below, had its origins in the structures observed in the precipitation fields associated with extratropical cyclones by weather radars, which were increasingly employed in research and operational contexts following the discovery of their usefulness for meteorological purposes late in World War II. The general picture that emerged from these studies is, as we have said, a “scaling hierarchy” of structures, in which structures are embedded within successively larger structures, leading to a regular variation as a function of scale of the basic properties (rainfall intensity, duration, etc.) of these structures. One of the earliest such studies was that of Austin (1960), who identified the four-level hierarchy that provided the basic form of the studies that followed:

- (a) a synoptic scale low pressure center with associated warm and cold fronts;
- (b) banded mesoscale areas of precipitation (“rainbands”);
- (c) areas of heavy rain within the mesoscale bands with scales of 30-50 miles and durations of a few hours; and
- (d) individual convective showers with scales of 2-5 miles and durations typically less than an hour.

Perhaps the classic papers in this area are those of Austin and Houze (1970) and Austin and Houze (1972). Analysis of additional cases of cyclones over New England led them to maintain the same four-level hierarchy but added some additional detail. Table 2.1 was extracted from these papers. This table shows the decrease in intensity and increase in duration that is observed to accompany an increase in spatial scale in rainfall coming from extratropical cyclones. In fact, if the intensity and duration are plotted against scale on a log-log plot, both are approximately power laws.

**Table 2.1 The scaling hierarchy of structures in extratropical cyclones**

	Synoptic Systems	Large Mesoscale Areas	Small Mesoscale Areas	Cells
Scale <i>km<sup>2</sup></i>	> 10, 000	1300-2600	250-400	5-10
Intensity <i>mm/hr</i>	1	2	5	10-50
Duration <i>hours</i>	24-72	2-5	1	0.1-0.5
Occurrence		several per synoptic system	3-6 within LMSA	1-7 within SMSA
Motion		same as associated SMSA	same as associated cells	with wind at mid-cell height

While it is not from an extratropical cyclone, it is worthwhile considering for purposes of comparison the three-level hierarchy that was presented in the study of a decaying typhoon over Japan by Matsumoto (1968). The hierarchy consists of synoptic, meso- and convective scales, with which were associated typical vertical velocities and divergences, as shown in Table 2.2. One interesting aspect of this study is that it consists of scaling of the dynamical properties of the precipitation areas. Matsumoto notes that the rainfall amount that would be predicted from the synoptic-scale moisture convergence is only one-third of what was observed. This provides an additional example of how variability can be a first-order effect in non-linear systems, as discussed in the introduction.

Further research revealed the same basic structures as in the research of Austin

**Table 2.2 The scaling hierarchy of dynamics in a decaying typhoon**

	Synoptic	Mesoscale	Convective
Scale <i>km</i>	1000	100	10
Vertical Velocity <i>ms<sup>-1</sup></i>	0.01	0.1	1.0
Divergence <i>s<sup>-1</sup></i>	$10^{-5}$	$10^{-4}$	$10^{-3}$

and Houze in extratropical cyclones over the United Kingdom (Harrold 1973; Browning 1974; Harrold and Austin 1974) and the Pacific Northwest (Houze et al. 1976; Hobbs and Locatelli 1978; Hobbs 1978), and in subtropical cyclones near Japan (Nozumi and Arakawa 1968). The research in the Pacific Northwest led to the classification of the rainbands into six types, depending on their location with respect to the warm and cold fronts associated with the cyclone. In terms of rain intensity and geometry, the various types of rainbands do not differ greatly, except for the “narrow cold-frontal” rainband, which is narrower (5 *km* as opposed to 50 *km*) and has deeper, more intense convection. These researchers also tended to classify the structures into three scales (synoptic, large mesoscale (rainband), and small mesoscale precipitation cores), with the cores having a length scale on the order of five *km*.

### 2.1.2 Midlatitude Convective Systems

Working from the smallest to the largest, midlatitude convective systems consist of single, supercell, and multicell thunderstorms, which are meso- $\gamma$  (2-20 *km*) and meso- $\beta$  (20-200 *km*) scale phenomena, and mesoscale convective complexes and squall lines, which are meso- $\alpha$  (200-2000 *km*) scale phenomena. All these phenomena include the thunderstorm cell as a basic element, either alone or grouped together in

some way, usually then including a cirrus anvil with stratiform precipitation.

The classic research on the structure of single and multicell thunderstorms was the Thunderstorm Project (Byers and Braham 1949). This research concerned summer “air-mass” thunderstorms, which occur in large masses of convectively unstable air with little vertical wind shear. It showed that each thunderstorm cell follows a certain life cycle. In the developing stage, a single strong updraft characterizes the cell. Precipitation is forming, but its fall is inhibited by the updraft. Eventually, however, the weight of the precipitation overcomes the strength of the updraft and a downdraft associated with rain forms. This is the mature stage. At the dissipating stage, the updraft has died and the downdraft continues until the precipitation has rained out. The whole cycle takes about an hour.

It is commonly observed that a group of such cells appears together, often in different stages of their life cycles, and the whole group is usually defined as single thunderstorm. Such a multicell cell storm will typically have a life time of several hours. It is thought that the downdrafts created by the falling precipitation are responsible for the clustering of thunderstorm cells because they induce updrafts nearby, though the cause of the clustering of thunderstorms is not completely understood. Indeed there are physical reasons (the convective stabilization of the environment of the cloud) and observations to support the notion that cumulus clouds are regularly-distributed rather than clustered (Ramirez and Bras 1990; Ramirez et al. 1990; see also Weger et al. 1993 and references therein). However, it seems clear empirically that storms of hydrologic importance are indeed clustered, since it is only isolated air-mass thunderstorms that are observed apart from clusters, and these generally produce only minor amounts of precipitation.

In weak ambient vertical wind shear a multicell storm will tend to consist of a disorganized clumping of cells, while in somewhat stronger wind shear, it will tend to be-

come organized, with new cells forming on the leading edge of the storm and dissipating on the trailing edge. In this case there is possibly a storm-wide air inflow-outflow pattern, though this may possibly just be the aggregate effect of the individual cells.

In strong vertical wind shear and strong instability, a supercell storm sometimes forms. These are of the scale of a multicell storm, but consist of a single large cell with a strong updraft and downdraft pair. The strong wind shear allows the storm to tilt over such that the downdraft associated with the precipitation on the leading side does not kill the updraft in the rear that supply the moisture. The tilting due to the shear also enhances the size of the anvil cloud and leads to a gradation of precipitation intensities from the leading edge where there is light rain back to the storm center, where there is strong hail and possibly a tornado. Since these storms are associated with severe weather such as tornados and large hail, they have been studied extensively observationally as well as by modeling and many typical features have been isolated. However, for our present purposes it is sufficient merely to note that there are conditions under which the scale of the convective cell is considerably larger than under other conditions.

When several thunderstorms are grouped together, we have added the third scale to the sequence *cell, storm, mesoscale convective complex (MCC)*. As noted above, they are meso- $\alpha$  scale phenomena, including meso- $\alpha$  scale airflow and cloud shield. The cloud shield is a source of stratiform precipitation. The mesoscale airflow appears to be initiated by the aggregate effect of the thunderstorms, but as the system matures, mesoscale phenomena, such as the stratiform precipitation and radiative transfer associated with the cloud shield, become increasingly important. Thus in the mature stage of an MCC, the thunderstorms may have died out. It has been estimated that MCCs are responsible for 50-60% of the summertime precipitation over the Great Plains of the

US (Fritsch et al. 1981), so clearly they are a hydrologically important phenomenon in that region. Again the focus here is not so much on the dynamics of MCCs as on the elements of their structure that are relevant to stochastic modeling.

While MCCs are round or oval, sometimes groups of thunderstorms develop along a line, which is then called a squall line. These develop under a variety of conditions, may occur in groups, and usually include a trailing stratiform region of precipitation. Their linear or curvilinear form, like that of rainbands associated with extratropical cyclones, has important implications for the geometric modeling being discussed here. In particular, at the scale of the squall line, the model would have to be spatially anisotropic. Because of this, general theories of space-time rainfall have not usually taken them directly into account.

### **2.1.3 Tropical Cloud Systems**

The structure of tropical precipitation, apparently since it is also of convective origin, is similar to that of midlatitude convective systems. We refer the reader again to Houze and Hobbs (1982) for a more in-depth review. As in the midlatitudes, tropical rainfall is sometimes due to isolated cumulonimbus. Tropical cumulonimbus (isolated or not) are generally not as violent as severe midlatitude thunderstorms, as measured for example by updraft velocities; see Jorgensen and LeMone (1989) and references therein. However, the bulk of precipitation in the tropics, as in midlatitude convective systems, comes from larger-scale systems with a hierarchical structure. These occur in two basic forms. One is disorganized clumps of convective clouds with a large cirrus shield like an MCC; they are called simply tropical cloud clusters. The other is the tropical squall line, again with a form similar to its midlatitude cousin.

Organization of tropical convection on the synoptic and yet larger scales is also observed. In the GARP Atlantic Tropical Experiment (GATE), whose data we use to test our theory in Chapter 4, it was observed that easterly waves with a time interval of

three to four days organized the convection on the synoptic scale (Reed et al. 1977; Thompson et al. 1979). An overview of the precipitation systems observed in GATE is given in Houze and Betts (1981). In the Pacific, synoptic and larger scale organization takes the form of so-called tropical super cloud clusters (SCCs). These have spatial scales of 2000-4000 *km* and lifetimes of 10-15 days, and propagate eastward, while the cloud clusters of which they consist propagate westward (Nakazawa 1988; Lau et al 1991; Sui and Lau 1992; Mapes and Houze 1993).

## **2.2 Previous Approaches to Modeling Space-Time Rainfall**

The development of stochastic theories or models of rainfall in space and time has been approached from many points of view. A common difficulty has been to make the model or theory simple enough to realize two goals: testing the model structure and estimating the model parameters. We will review previously developed models on the basis of these criteria below. A model is testable if predictions can be made based on its assumptions that can be tested against data. The testability of a model is usually in inverse proportion to the number of free parameters it contains, although model structure is also important. It will be seen in particular that the scaling hierarchy of structures observed in most hydrologically significant precipitation systems reviewed above can be modeled with particular parsimony of parameters by the use of scaling invariant theories. Because our review is concerned with the development of the theory of space-time rainfall, models that operate in a purely simulation mode with essentially no testability will not be considered.

### **2.2.1 Point Process Models**

The work of LeCam (1961) underlies a large class of stochastic space-time rainfall models, those which are constructed from spatial point processes. Informally, a point process is a random means of distributing points in some space. These points be-

come the basic building block of the stochastic model. Most such models consider the points to be convective storm cells, which are assigned intensity, shape, velocity, and temporal behavior. Their occurrence is also usually clustered in space and time.

In particular, LeCam proposed the following elements for his model. He pictured the points of a point process being used to represent convective cells with random diameter and intensity, possibly with variable intensity structure interior to the cell diameter, that moved with random velocity. These cells in turn occur randomly in clusters, which possibly may be shaped like fronts. The clusters themselves will have some random motion and dissipation behavior. And at a third level, the clusters occur in clusters, which constitute a storm.

So LeCam's basic construction is quite general. There are a number of unspecified functions that could possibly include stochastic dependence and nonhomogeneities. His basic assumption is that within a storm, the fronts are placed independently of one another, and within a front, the cells are placed independently of one another, which makes the process a two-stage Neyman-Scott clustering process and permits computation of the Laplace transform of the rainfall process in terms of the unspecified functions.

The first work to develop LeCam's basic structure into a fully specified stochastic space-time model was that of Waymire et al. (1984), which presents what is commonly called the WGR model. The WGR model adopts the two-stage clustering of convective cells of LeCam and makes simple (and homogeneous) assumptions on the size, shape, intensity, and space-time occurrence of the elements of the cells and their clusters, such that the first-order (mean) and second-order (space-time covariance) behavior of the model could be computed. In its most basic form, it has nine parameters, which the authors specified using typical values obtained from the extratropical cyclone literature described above.

The main purpose of the development of the WGR model was to create an example of a model or theory which obeyed Taylor's hypothesis of fluid turbulence up to a short time, as had been shown to hold in rainfall by Zawadzki (1973). For a definition of this hypothesis and further discussion, see Chapter 5.3.2. This purpose was indeed accomplished, and later Gupta and Waymire (1987) showed that a whole class of point process-type models would obey Taylor's hypothesis up to the characteristic time of dissipation of their rainfall cells.

Despite the fact that the goal of the development of the WGR model was to explore Taylor's hypothesis and its breakdown in space-time rainfall, it has been subsequently used simply as a stochastic model, i.e., to generate sequences of rainfall fields used for other purposes. One of the basic issues involved in such use is parameter estimation. Its nine parameters makes this a somewhat difficult task, and, as discussed above, has a negative impact on its testability. Since the second-order moment properties of the theory were known, Valdes et al. (1985) used the method of moments to estimate parameters. Since rain gauges record rainfall aggregated over time intervals, a basic advance in parameter estimation was to compute the time-integrated first and second-order behavior of the WGR model, which was accomplished and applied to a small basin with a dense network of gauges by Islam et al. (1988). They also tested the sensitivity of the model to variation in the parameters and the consistency of parameter estimation over a range of time scales. Valdes et al. (1990) wanted to estimate parameters for the WGR model from radar data, so they performed the analogous integration in space and likewise tested the consistency of parameter estimation over a range of spatial scales.

The fact that it was possible to compute the second-order moment properties of the WGR model and its spatially and temporally integrated forms, so that the parameters of the model could be estimated from data and the breakdown of Taylor's hypoth-

esis could be predicted shows that the WGR model is a relatively simple construct. However, as described, the information derived obtained from these calculations was mostly used in parameter estimation, so that testable predictions were not emphasized. However, see Valdes et al. (1994) for a test of the WGR model vis-a-vis some Gaussian random field models using their spectra compared to the spectra of the GATE rainfall data. Note also that the parameter estimation requirements make testing for non-stationarity or non-homogeneity in the data virtually impossible.

An extension of the WGR model by Phelan and Goodall (1990) addresses some of concerns; see also Goodall and Phelan (1991). They allow each cell its own constant but random water content, intensification rate, aging rate, velocity and spatial extent. They develop an estimation procedure that involves tracking individual cells in the sample rainfall intensity process, which is a radical departure from the fitting of second-order moments that was used previously. After fitting the model, the residuals showed a lot of spatial structure in the dissipative stage of the rainfall field, so Phelan (1991, 1992) considered estimating a non-parametric aging function as an alternative to the previously assumed exponential. The intensive tracking procedure used to estimate parameters for these models clearly yields a lot of information; however, it comes at the price of a much more complicated theory. It seems unlikely that it will be possible to fully specify in a meaningful way a model of such complexity.

To avoid the parameter estimation difficulties of the more realistic models, some very simple point process models have also been developed, often with more analytical than modeling goals. For example, Smith and Karr (1985) studied maximum likelihood and method moments parameter estimation techniques for a five-parameter model of daily totals of space-time rainfall. They found that the method moments approach is analytically simpler and note that the cell radius parameter is difficult if not impossible to estimate from rain gauge data. Cox and Isham (1988) study space-time

extensions of the temporal models of Rodriguez-Iturbe et al. (1987). In these models, storms consisting of single disks with random radii, velocities, lifetimes, and rain rates arrive according to Poissonian and clustered point processes in time. It was found, as might be expected, that the second-order properties, including conditions of validity of Taylor's hypothesis, and other quantities of interest such as the distribution of storm duration at a point can be computed for the Poissonian case, while these computations are quite difficult for the clustered case. In the Poissonian case, Taylor's hypothesis is satisfied for times short relative to the mean lifetime of a cell when the velocity of cells does not vary much from one to another.

Point process models that are simple because they involve little or no clustering seem applicable to air-mass thunderstorms. Using assumptions applicable to this case, Rodriguez-Iturbe et al. (1986), in an extension of the work of Eagleson (1984), computed the second-order and fractional wetting properties of a spatial model of total storm depth in which the cells are either located independently using a Poisson process or by a two-level Neyman-Scott clustering process. The other parameters of the model are the distribution of rainfall depths and the cell spread function. Eagleson et al. (1987) applied the model in its Poissonian form against data from Walnut Gulch experimental watershed in Arizona to determine which of the three spread functions studied was most appropriate. A single-event (non-stationary) space-time extension of the model of Rodriguez-Iturbe et al. (1986) was studied by Rodriguez-Iturbe and Eagleson (1987). They computed the second-order properties of the rainfall intensity and cumulative rainfall depth fields.

An interesting extension of these ideas is the model of Cowpertwait (1995). In this model, storms are again modeled as disks with random radius, lifetime and intensity, but now the storms are randomly selected from a finite number of types, each with its own set of distributions of cell properties. Thus the properties of an arbitrary

cell are correlated. The cell arrivals are according to a generalization of the Neyman-Scott clustering process. The spatial distribution of the cells is Poissonian. Second-order properties of the model are calculated in order to allow fitting of the model from multi-site temporal data.

### **2.2.2 Gaussian Random Field Models**

A second class of models that has been developed and used extensively are those based on Gaussian random fields or functions thereof. The model of Bras and Rodriguez-Iturbe (1976) models storm “exteriors” essentially according to a point process, parameterized by the time between events, storm duration, total depth and storm velocity for various types of events, but the “interior” follows a non-stationary hyetograph with a superimposed space-time correlated Gaussian random field, for which Taylor’s hypothesis is assumed valid for all times. The resulting field is rather smooth compared to instantaneous rainfall fields obtained from radar. This model has been used in a number of simulation studies, including that of Wilson et al. (1979).

One particular weakness of the model of Bras and Rodriguez-Iturbe is its Gaussian distribution of rainfall residuals, whereas rain rates conditioned on rain are usually found to be closer to lognormally distributed. Using this idea, Bell (1987) produced a model in which he transformed a Gaussian random field into a field with a mixed lognormal distribution, including an atom at zero. The model requires the prescription of the marginal distribution of rain rates and the spatial and temporal correlation structure of the original Gaussian random field, which reproduces the realistic feature that the temporal correlations at larger scales are longer than those at smaller scales. The model may include motion by advection. The model was fitted to the observations of GATE in order to study the accuracy of satellite measurements of GATE-like rain (Bell et al. 1990).

Gaussian random field models, without transformation into a mixed lognormal

form and only a single time and length scale, i.e., Gaussian noise-forced diffusive models, have also been extensively used to study satellite estimation problems. Models of this type without (North and Nakamoto 1989) and with advection (Nakamoto et al. 1990) have been used. The temporal and spatial spectra of these models as well as the WGR model are compared with the GATE data in Valdes et al. (1994), and it is found that the Gaussian random field models fit the spectra of data much better. They have also been applied to rainfall over land (Polyak et al. 1994).

### 2.2.3 Notions of Scaling Invariance in Rainfall and their Testing

Before proceeding to the discussion of full-fledged models of spatial and space-time rainfall that utilize scaling invariance ideas, it is worthwhile presenting these ideas so that some basic ideas are clear. The basic notions underlying theoretical approaches to scale-invariant descriptions of rainfall fields are the properties of random fields called “simple scaling” and its generalization “multiscaling”. The notion of simple scaling has its origin in the characterization of the “stable distributions”, and was generalized to its present form by Lamperti (1962). We will generally follow the exposition of Gupta and Waymire (1990).

Consider an arbitrary random field  $\{Y(\hat{x})\}$  indexed by  $\hat{x} \in D \subseteq \mathfrak{R}^d$ . It is said to be “simple scaling” if for each  $\lambda$  there exists a positive function  $C_\lambda$  such that for any arbitrary set of points  $\hat{x}_1, \hat{x}_2, \dots, \hat{x}_n$ , the following equality of joint distributions holds:

$$\begin{aligned} &P[C_\lambda^{-1} Y_\lambda(\hat{x}_1) < y_1, C_\lambda^{-1} Y_\lambda(\hat{x}_2) < y_2, \dots, C_\lambda^{-1} Y_\lambda(\hat{x}_n) < y_n] \\ &= P[Y_\lambda(\hat{x}_1) < y_1, Y_\lambda(\hat{x}_2) < y_2, \dots, Y_\lambda(\hat{x}_n) < y_n], \end{aligned} \quad (2.1)$$

where  $Y_\lambda(\hat{x}) = Y(\lambda\hat{x})$ . If we consider equality in distribution, and (2.1) can be written simply

$$\{C_\lambda^{-1}Y_\lambda(\hat{x})\} = \{Y(\hat{x})\}. \quad (2.2)$$

While this may seem quite abstract, a significant consequence is that if the scaling function  $C_\lambda$  exists and is continuous, it must have the form

$$C_\lambda = \lambda^\theta, \quad (2.3)$$

i.e., a power law in  $\lambda$ . Then equation (2.2) becomes

$$\lambda^{-\theta}\{Y_\lambda(\hat{x})\} = \{Y(\hat{x})\}, \quad (2.4)$$

where again we have equality in distribution. So a multiplication by  $\lambda^{-\theta}$  converts the joint distribution of the field under rescaling of its index back to that of the field with the original index. This suggests why simple scaling is also called “self-similar”.

This becomes applicable to spatial rainfall by considering the  $\lambda$ -scale averages of the simple scaling field  $\{Y(\hat{x})\}$ , i.e.,

$$Y_\lambda = \lambda^{-2} \int_{D_\lambda} Y(\hat{x}) d\hat{x}, \quad (2.5)$$

where  $D_\lambda$  is a subset of  $\mathfrak{R}^2$  of area  $\lambda^2$ . As shown by Gupta and Waymire (1991),  $Y_\lambda$  is also simple scaling with the same exponent  $\theta$  as  $\{Y(\hat{x})\}$ , i.e.,

$$\lambda^{-\theta}Y_\lambda = Y_1, \quad (2.6)$$

where again we have equality in distribution.

Using these representations, Kedem and Chiu (1987) showed that empirically reasonable rain rate processes in space and time cannot be simple scaling. In space, they observed that the probability of positive rain increases with scale, whereas self-similarity requires that it be constant. In time, they assumed that the process had stationary

increments. Then self-similarity requires that if it ever stops raining, it can never start again, which is clearly unphysical. Thus if we define intermittency to mean the presence of zeroes in the rainfall field, simple scaling founders on intermittency both in space and in time (assuming stationary increments).

Gupta and Waymire (1991) investigated theoretical issues involving random fields with homogeneous simple-scaling fluctuations, with an eye toward application to rainfall. Their results are generally negative. First they note the result of Dobrushin (1980), which is that if an ordinary random field (that is, a random function where point values  $y = f(\hat{x})$  are defined) is homogeneous, simple-scaling, and continuous in probability, then it is with probability one a random constant. They also showed, following the Mandelbrot (1972, 1974) that a random field that is lognormal at all scales of resolution cannot have simple-scaling fluctuations.

Some simple considerations regarding moments suggest the proper direction for generalization of the notion of simple scaling to something that is useful in the rainfall context. It follows from equation (2.6) that

$$EY_\lambda^h = \lambda^{h\theta} EY_1^h, \quad (2.7)$$

or,

$$\log EY_\lambda^h = h\theta \log \lambda + \log EY_1^h \quad (2.8)$$

(Gupta and Waymire 1990). If  $Y_\lambda$  is as in equation (2.6) an average rain rate at resolution  $\lambda$ , then it is non-negative. In order to avoid dividing by zero, we restrict the moment order to  $h \geq 0$ . Equation (2.8) shows an easily tested implication of simple scaling: the moments are log-log linear versus scale of resolution  $\lambda$  with slope function

$$s(h) = h\theta. \quad (2.9)$$

Since  $EY^0 = P(Y > 0)$  for a non-negative random variable  $Y$ , taking  $h = 0$  in equation (2.9) demonstrates the result of Kedem and Chiu noted above regarding the incompatibility of simple scaling for spatial rainfall with the observation that the probability of positive rain depends on resolution.

What is commonly observed instead of equation (2.9) is the following:

$$\log EY_\lambda^h = s(h)\theta \log \lambda + \log EY_1^h \quad (2.10)$$

for some non-linear function  $s(h)$ . In this case, the moments are still log-log linear with scale, but the slope of the moments versus scale is no longer linear. It is shown by Gupta and Waymire (1990) that this behavior is implied by a scale invariance property quite similar in form to the simple scaling relation equation (2.2):

$$\{C_\lambda^{-1} Y_\lambda(\hat{x})\} \equiv \{Y(\hat{x})\}. \quad (2.11)$$

Now, however, the scale function  $C_\lambda > 0$  is *random* and the scale change can only go in one direction. Gupta and Waymire show that  $s(h)$  concave, as is observed in data, the scale change is limited to magnification, so we take  $\lambda \leq 1$ . The general solution of the scale function is no longer  $C_\lambda = \lambda^\theta$  but

$$C_\lambda = \lambda^\mu \exp(Z_{-\log \lambda}), \quad \lambda \leq 1, \quad (2.12)$$

where  $\mu$  is an arbitrary real number and  $Z_a$  is a process with stationary increments.

Since processes with stationary increments have natural representations as sums of identically distributed (id) random variables,  $C_\lambda$  is essentially a product of id random variables. If  $C_\lambda$  is limited to the subclass where  $Z_a$  is a process with independent and stationary increments, then  $C_\lambda$  has the representation as a product of independent and identically distributed (iid) random variables. If we call these iid random variables  $W$  then from equation (2.11) we have

$$Y_\lambda \equiv Y_1 \prod_i W_i. \quad (2.13)$$

To see that this essentially gives the marginal representation of a random cascade, compare equation (3.20) in Section 3.2. This connection is explained more thoroughly in Gupta and Waymire (1993).

While these theoretical investigations point to the necessity of generalizing the notion of scaling invariance beyond simple scaling, some recent research involving wavelet transforms has attempted to resurrect simple scaling in rainfall. This line of research was introduced by Kumar and Foufoula-Georgiou (1993a, b). They used Haar wavelets to decompose rainfall fields into a sequence of average and fluctuation fields at each scale, and then studied the distributions of the fluctuations as a function of scale, by fitting them to the symmetric subclass of Levy-stable laws. The range of spatial resolutions where the scale parameter of the symmetric stable law varied log-log linearly with spatial resolution, which is the test of simple scaling of the wavelet fluctuations in this framework, was usually found from 2 km up to 25-30 km. However, this result must be considered somewhat tentatively, as the fits to the stable laws were not generally very good and the fluctuations were seen to depend strongly on their associated local averages. This latter point is important because it means that the fluctuations at a given scale are not homogeneous, i.e., they do not come from a common distribution. Thus it is not clear what can be learned fitting a single distribution to them.

This latter difficulty can be remedied at least to a large degree by “standardizing” the fluctuations, i.e., dividing them by their local averages. Then, as shown by Perica and Foufoula-Georgiou (1995a), the fluctuations are well-fitted by Gaussian distributions, and the scale parameters suggested self-similarity over a similar range of scales as for the non-standardized fluctuations. Though the same authors have proposed a

procedure for disaggregating rainfall fields from coarser to finer resolution based on their results (Perica and Foufoula-Georgiou 1995b), it nevertheless remains true that wavelet transforms are fundamentally a data analysis framework, not a modeling framework or theory. Additionally, while we have not in this review precisely defined wavelet fluctuations, they are essentially just the difference between the local rain rate at one resolution and the local average rain rate at the next coarser resolution. Thus a wavelet analysis is an additive decomposition. As such, they do not yield information regarding the non-rainy regions of the field. The homogenization of the fluctuations that resulted from division by the local averages suggests what was concluded previously by Lovejoy and Schertzer (1985) and Gupta and Waymire (1990): rainfall fields are fundamentally multiplicative, not additive. Thus a connection between the standardized fluctuations of a Haar wavelet decomposition and the multipliers of a random cascade seems a possibility; however, an attempt to establish one by Over and Gupta (1993) was largely unsuccessful. This is an important question that ought to be pursued further.

#### **2.2.4 Additive, Simple-Scaling Models**

As described in the introduction, empirical evidence for scale invariance in rainfall fields apparently began with Lovejoy (1981, 1982), who showed that the perimeter-area relation of rain and cloud fields over a wide range of scales suggests fractal characteristics and provided evidence that distributions of fluctuations of rainfall rates in space and time have hyperbolic (power-law) tails, which is an indication of the presence of extreme variability in rain rates. Lovejoy and Mandelbrot (1985) constructed a space-time rainfall model on the basis of these results, the so-called fractal sum of pulses (FSP) model. As the name implies, one generic feature of this model is that it is an additive model, consisting of the sum of basic random elements (“pulses”) whose size and intensity distributions are chosen to match the spatial and intensity properties

observed by Lovejoy (1981, 1982). In particular, in two dimensions, these pulses are cylindrical with random base areas with the distribution  $P(A > a) = a^{-1}$  for  $a > 1$  and height (rain rate) fluctuations with the distribution  $\Delta R \equiv \pm A^{1/\alpha}$  (i.e., a fluctuation is equally likely to be positive or negative). This construction gives a spatial scaling exponent of  $H = 1/\alpha$ , so that like any simple scaling theory, the process is governed by a single exponent.

They observed however in radar data that  $H \cong 0.5 \neq 1/\alpha \cong 0.6$  (Lovejoy and Schertzer 1985). They solved this problem by locating the pulses only on a fractal subset of the two-dimensional space, giving what they called the “scaling cluster of pulses” (SCP) model. Since this model involves two independent exponents, it cannot be simple-scaling. But it is still an additive model and it shares with the FSP model and indeed any additive random model a common difficulty: negative values always have some probability of occurrence. Thus they discovered what is described above, that generalization to more than one scaling exponent is more naturally accomplished in a multiplicative framework.

An important development of Lovejoy and Schertzer (1985) that applies to both additive and multiplicative models is the notion of generalized scale invariance. This allows general forms of anisotropy applicable to the vertical stratification, differential rotation, or space-time anisotropy to be modeled in a scale-invariant framework. They carried these ideas over into the multiplicative framework (Lovejoy and Schertzer 1987), but their utility has been limited by the difficulty of deriving simple testable predictions from theories involving such anisotropies.

### **2.2.5 Multiplicative, Multi-Scaling Models**

As just noted, Lovejoy and co-workers introduced some interesting additive models, but their major contribution was to apply and develop the theory of multiplicative random cascades for applications to atmospheric phenomena, including rainfall fields.

This theory has its conceptual roots in the statistical theory of turbulence (Kolmogorov 1941), but was introduced in its basic mathematical form by Mandelbrot (1974). Multiplicative random cascades, like the FSP process, are constructed using a basic random element, but a product of them arranged according to a hierarchical structure called a cascade. The basic random element is a random variable with non-negative support denoted by  $W$  and called the *generator* of the cascade. The construction and properties of multiplicative random cascades will be described in detail in Chapter 3. Multiplicative random cascades have a number of advantages over additive theories such as the FSP model. We note three. First, the fractal spatial properties and extreme variability observed in data arise naturally from the construction. Second, the FSP process and additive models in general have difficulty modeling regions of zero rain rate, whereas zeroes may be obtained from multiplicative models simply by multiplying by zero. Third, under suitable conditions on  $W$ , there is a one-to-one correspondence between quantities that are simple to compute from data and the parameters of the model. Thus such models, as scale invariant constructions, not only have few parameters, but in addition, these parameters are relatively straightforward to estimate.

Schertzer and Lovejoy added a number of enhancements to the basic theory proposed by Mandelbrot. In addition to the notion of generalized scale invariance described above, they proposed an important class of generators (the “universal” (extremal) log-Levy generators, (Schertzer and Lovejoy 1987), developed data analysis and parameter estimation techniques (“functional box counting” and “elliptical dimensional sampling” (Lovejoy et al. 1987), “double trace moments” (Lavalley et al. 1992), and “probability distribution multiple scaling” (Lavalley et al. 1991)), and recognized the inherent limitations of parameter estimation techniques (the notion of the “sampling dimension” (Lavalley et al. 1991)). As described in the introduction, despite their general importance, these developments do not address a number of the basic

questions required for theories of space-time rainfall and left open the need for the research described here.

It should also be noted that, as conceived by Lovejoy and coworkers (see, e.g., the review by Tessier et al. (1993)), rain rates are not to be directly modeled by multiplicative random cascades. Instead, using a parameter derived from the Fourier spectrum of the rainfield, the multiplicative cascade is power-law filtered (i.e., smoothed). The idea behind this point of view seems to be an analogy with the statistical theory (Kolmogorov 1941), in which the conserved quantity (energy) is modeled purely multiplicatively as a *measure* (Mandelbrot 1974), but an associated fluctuation field (the velocities) is essentially additive. Lovejoy and co-workers take it that the rainfall field is in analogy with the velocity field in turbulence, while the conserved quantity is some unknown potential. While it is agreed that it is not exactly clear how this analogy should extend in the case of rainfall, the non-negativity and conservation properties of rainfall rate suggests that instead that as a working hypothesis, rainfall rate should be taken in analogy with energy rather than velocity. The relatively good fit of random cascades directly to rainfall fields shown in this thesis serves to confirm this hypothesis.

## Chapter 3

# The Theory of Random Cascades with Applications to Spatial Rainfall

### 3.1 Motivation

The random cascade construction can be developed from an analysis of the following situation. Consider an instantaneous snapshot of rain rates over some region, for example, a single scan of weather radar data. Assume that the data has been binned into  $2^{2n}$  square boxes with side length  $l_{min}$ , and associate with each box the spatial average rain rate over the box, denoting this by  $R_i(l_{min})$ ,  $i = 1, 2, \dots, 2^{2n}$ . This is illustrated for  $n = 3$  in Figure 3.1(a). In the GATE data that will be used extensively here,  $l_{min} = 4$  km and  $n = 6$ , so the whole snapshot is 64 by 64 boxes, or 256 by 256 km. Now consider the boxes constructed by taking contiguous groups of boxes of side length  $l_{min}$ . There are  $2^{n-1}$  boxes of side length  $2l_{min}$  (Figure 3.1(b)),  $2^{n-2}$  boxes of side length  $4l_{min}$ , and so on up to a single box of side length  $l_{max} = 2^n l_{min}$  (Figure 3.1(c)). It will be convenient to use a normalized side length parameter  $\lambda = l/l_{max}$ , which will be called the “scale”. Associated with each box at each scale is the rain rate averaged over the region enclosed by the boxes, denoted  $R_i(\lambda)$ ,  $i = 1, 2, \dots, N(\lambda)$ , where  $N(\lambda) = \lambda^{-2}$  denotes the number of boxes at scale  $\lambda$ . A “scaling” analysis of this snapshot of data is performed by considering the statistical properties of the rain rates  $R_i(\lambda)$  as a function of scale  $\lambda$ .

Now, for real (convective) rain, typically a significant number of the  $R_i(\lambda)$  at all but the largest scale will have a value of zero, i.e., it will not be raining anywhere in

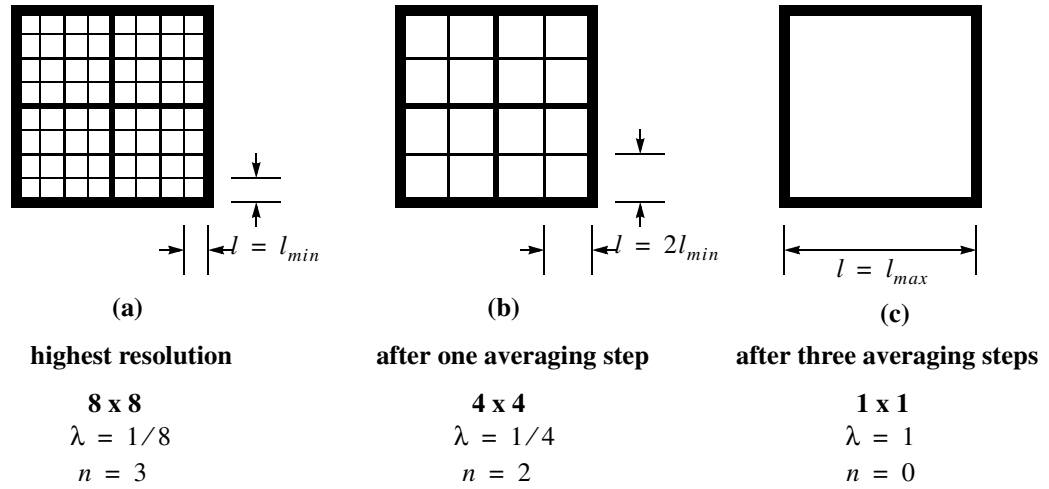


**Figure 3.1** Scaling analysis of a spatial rainfall scene

them. The first “scaling” question one might ask then is how the fraction  $f(\lambda)$  of boxes with rain rate greater than zero changes as a function of scale. Performing this computation on the empirical data we will examine below yields the following:

$$f(\lambda) \approx c\lambda^k \quad (3.1)$$

To analyze this result briefly, consider first the largest scale ( $\lambda = 1$ ). Then  $f(\lambda) = c$ , but since there is only one box at that scale, if there is any rain we have  $c = 1$ . Next consider minimum and maximum values of  $k$ . If  $k = 0$ , then  $f(\lambda) = 1$  at all scales, so  $k = 0$  corresponds to rain everywhere. If  $k = 2$ , first notice by definition that

$$f(\lambda) = \frac{N^+(\lambda)}{N(\lambda)}, \quad (3.2)$$

where  $N^+(\lambda)$  is the number of boxes with rain at scale  $\lambda$ . Since by assumption  $f(\lambda) \sim \lambda^2 = (N(\lambda))^{-1}$ , we have  $N^+(\lambda) \sim \lambda^0$ , so there is a single box with rain at each

scale. So it appears that  $k$  has the range  $0 \leq k \leq 2$ , with increasing  $k$  indicating increasing sparsity of the set where there is rain. Since the dimension of a point is zero and the dimension of a planar region is two, it appears that  $2 - k$  indicates the dimension of the set that has rain. Those familiar with fractals will know that we have been performing a dimension estimate by so-called box-counting on this set.

As a point of comparison, consider the result of such a scaling analysis when the boxes are assigned to be rainy or dry independently, as was done by Gupta and Waymire (1993). In this case, the fraction of boxes with rain is only power law with scale in the limit as  $\lambda \rightarrow 0$ , and always has an exponent of  $k = 2$ .

Of course we are interested in more than just the region where there is rain. We are also interested in how much rain is falling in the boxes that have rain, and, in the present context, how that rain rate changes as a function of scale. Let's ask a specific question: how does the average rain rate in the boxes where there is rain vary as a function of scale? Let's denote the rain rates in boxes at scale  $\lambda$  that have non-zero rain rates as  $R_i^+(\lambda)$ ,  $i = 1, 2, \dots, N^+(\lambda)$  and the average of these by  $\overline{R^+(\lambda)}$ . This could also be computed empirically, but you would find that

$$\overline{R^+(\lambda)} = \frac{\bar{R}}{f(\lambda)} \approx \bar{R}\lambda^{-k}, \quad (3.3)$$

where  $\bar{R} = N(\lambda)^{-1} \sum_i R_i(\lambda)$  is the spatial average rain rate. The result may be computed as follows. Notice that  $\bar{R}$  can be written in terms of  $\overline{R^+(\lambda)}$  as follows:

$$\bar{R} = \frac{N^+(\lambda)}{N(\lambda)} \frac{1}{N^+(\lambda)} \sum_i R_i^+(\lambda) = f(\lambda) \overline{R^+(\lambda)}. \quad (3.4)$$

Solving for  $\overline{R^+(\lambda)}$  gives equation (3.3).

From this simple analysis a stochastic model can be constructed that has the properties of the data. Consider the same  $l_{max}$  by  $l_{max}$  region (Figure 3.2(a)). Assign the

uniform rain rate  $R_0$  to the whole region as an initial condition. Divide the region into four  $l_{max}/2$  by  $l_{max}/2$  boxes (Figure 3.2(b)). Assume the rain rate in the  $i$ th box can be written as the product  $R_0 W_i(1)$ , where the  $W_i(\lambda)$  are random variables. As the simplest possibility, assume additionally that the  $W_i(\lambda)$  are independent and identically distributed (iid) for all  $\lambda$  and all  $i$ , i.e., independent of each other and scale and space. The distribution of the  $W_i(\lambda)$  will be derived from the results of our analysis above. Assume  $P(R_i(\lambda) > 0) = f(\lambda) = \lambda^k$ , which implies at  $\lambda = 1/2$  that

$$P(R_0 W_i > 0) = P(W_i > 0) = (1/2)^k. \quad (3.5)$$

Similarly, following equation (3.3), assume  $E[R_i^+(\lambda)] = R_0 \lambda^{-k}$ , which implies at  $\lambda = 1/2$  that

$$E[R_0 W_i^+] = R_0 E[W_i^+] = R_0 (1/2)^{-k} \quad (3.6)$$

where  $W_i^+ = W_i \parallel W_i > 0$ , hence  $E[W_i^+] = (1/2)^{-k}$ .

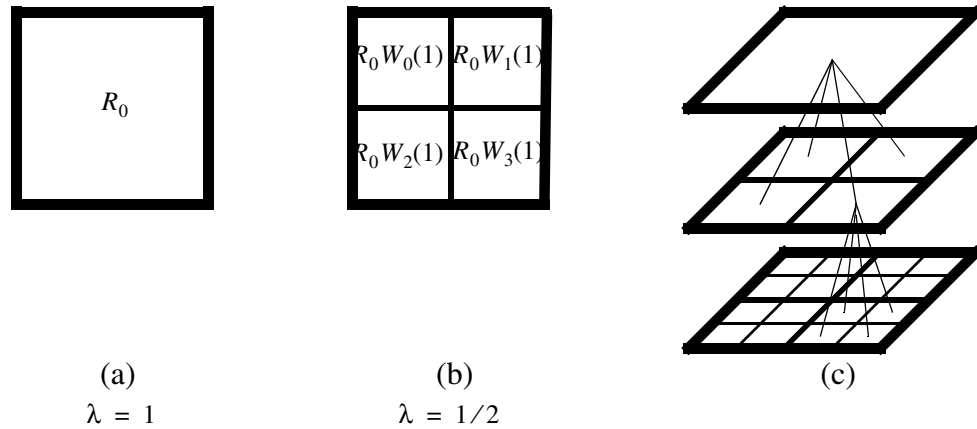


**Figure 3.2 Construction of a cascade model of a spatial rainfall scene**

Now consider further subdivision of the region into boxes of size  $l_{max}/4$ ,  $l_{max}/8$ , and so on with additional multiplications by iid random variables  $W$  (Figure

3.2(c)). After  $n$  subdivisions and multiplications, we have

$$R_i(\lambda_n) = R_0 \prod_{j=1}^n W_i(j), \quad i = 1, \dots, 2^{2n}, \quad (3.7)$$

where  $\lambda = 2^{-n}$ , for which

$$P(R_i(\lambda_n) > 0) = P\left(\prod_{j=1}^n W_i(j) > 0\right) = (1/2)^{nk} = (\lambda_n)^k \quad (3.8)$$

since the  $W_i(j)$  are iid. Similarly,

$$E[R_i^+(\lambda_n)] = R_0 E\left[\prod_{j=1}^n W_i^+(j)\right] = R_0 (1/2)^{-nk} = R_0 (\lambda_n)^{-k}, \quad (3.9)$$

so it can be seen that this choice of multiplicative structure and distribution for the  $W$  reproduces the empirical scaling properties of the data.

Let's examine the distribution of  $W$  further, as far as we have determined it. We have

$$P(W > 0) = (1/2)^k, \quad (3.10)$$

which implies

$$P(W = 0) = 1 - (1/2)^k \quad (3.11)$$

and

$$E[W^+] = (1/2)^{-k}. \quad (3.12)$$

We have not determined anything about the distribution of  $W^+$ , the positive part of  $W$ , beyond its expectation. So the distribution of  $W^+$  is arbitrary insofar as matching the empirical results noted thus far, apart from being positive and having the appropriate expectation. As we will see below, simply taking  $W^+$  to be an atom at its expected value, i.e.,  $P(W = E[W^+]) = (1/2)^{-k} = (1/2)^k$ , gives a first-order model of spatial rain

rates for convective rain.

Notice that  $E[W] = 1$  implies a condition of conservation of rain rate on average as the model proceeds from scale to scale. To see this, consider that the expected value of the average rain rate is given by

$$E\left[\frac{1}{N(\lambda_n)} \sum_{i=1}^{N(\lambda_n)} R_i(\lambda_n)\right] = E[R_i(\lambda_n)] = R_0(E[W])^n = R_0, \quad (3.13)$$

and thus is independent of scale. This does not mean that the average rain rate will be exactly  $R_0$  at every scale; it is easy to see for example that there is some probability that with the choice of the random variable  $W$  that we have made here that the rain rate will become zero everywhere. Exact (pathwise) conservation was assumed in the data analysis. The conservation condition will turn out to be an important condition for theorems describing the result of letting this process continue to the limit of small scales.

In the limit of small scales (i.e.,  $\lambda \rightarrow 0$  and  $n \rightarrow \infty$ ), the process we have constructed from our data analysis is an iid discrete random cascade with generator  $W$ . A more rigorous treatment of the construction and behavior of iid discrete random cascades is the subject of the remaining sections of this chapter. Some notation is developed and the basic theory is described in the next section. The scaling properties of the moments of random cascade measures and their relation to testing the theory and estimating its parameters are presented in Section 3.3. In the final section, issues relating to the use of this theory for rainfall modeling and a few examples of cascades relevant to modeling spatial rainfall are examined.

### 3.2 An Introduction to the Theory of Discrete IID Random Cascades

Discrete random cascades with iid generators as they are presented here were introduced by Mandelbrot (1974) as a contribution to the statistical theory of fluid turbu-

lence. The phenomenology of a self-similar cascade of turbulent eddies has underlain turbulence theories at least since the time of Richardson's famous ditty: "big whirls have little whirls that feed on their velocity, and little whirls have lesser whirls and so on to viscosity - in the molecular sense" (Richardson 1965; first published in 1922). Mandelbrot's motivation in particular was to test the hypothesis of marginal lognormality of the energy dissipation rate, which had been proposed by Kolmogorov (1962) and Oboukhov (1962) and apparently proven for a cascade-like construction by Yaglom (1966). Mandelbrot showed, however, that the mathematics of random cascades are rather subtle, and that in fact a variety of marginal distributions may be obtained, from those that are nearly lognormal to others that are vastly different from lognormal.

The basic theory is developed in Mandelbrot (1974), Kahane (1974), and Peyriere (1974). Kahane and Peyriere (1976) summarized the results to that point. They obtained a number of important results regarding the limit of the process as  $\lambda \rightarrow 0$ . Before giving their results, we must develop a some more notation.

The motivation given in Section 3.1 above used rain rates averaged over a box at scale  $\lambda$  (denoted  $R_i(\lambda)$ ) to describe the cascade because this quantity arises in the data that we are considering. However, to describe the mathematical results related to random cascades, it is necessary to use the concepts of measure theory, which we briefly introduce in Appendix A. Because a measure is a distribution of "mass" or "stuff", rain rate at some scale  $\lambda$  cannot be a measure. Intuitively, this is because a rain rate is not an amount of "stuff", and mathematically, because it fails the additivity criterion given by equation (A.1). However, the rain rate is closely related to two physical quantities that are an amount of stuff and thus can be modeled as a measure, which are, first, the amount rain falling in some time on some region, or, second, the amount of rain falling in some time on some region divided by the elapsed time. Thus the measure with which we will be concerned is the function that maps (Borel) subsets of the

earth's surface to a non-negative real number which denotes the amount of rain falling on it in a short time. What we call the rain rate then is simply this measure divided by the area (Lebesgue measure) of the corresponding subset. Of course, since the data we will be examining is obtained from weather radars, the data actually corresponds to a somewhat different measure, namely, the scatter caused by the hydrometeors intersected by the radar beam as it rotates through its scanning pattern, from which the amount of rain falling can be estimated. Either measure obviously has a temporal as well as a spatial component, but at first we will suppress the temporal aspect and consider only the spatial properties of the measure for a sequence of short time intervals. The properties of the temporal evolution of the measure will be considered in Chapter 5.

An unambiguous presentation of the construction and theory of random cascades unfortunately requires some rather cumbersome notation. Things become cumbersome because we would like to keep track of the sub-square at all the previous levels that leads to a particular sub-square at the level of interest. The presentation here will closely follow that of Gupta and Waymire (1995). The case of interest is as in Section 3.1 a square region of side length  $l_{max}$ , which may be now precisely defined as  $J = [0, l_{max}]^2 \subset \mathfrak{R}^2$ . However, for sake of simplicity of presentation, consider first the one-dimensional unit domain  $J = [0, 1] \subset \mathfrak{R}$ . Extension to general  $l_{max}$  and two-dimensional domains will be fairly straightforward.

To begin, fix a *branching number*  $b \geq 2$ , an integer. Consider the  $b$ -ary expansion of the real numbers in the unit interval. This can be written as the sequence  $t = (t_1, t_2, \dots, t_n, \dots)$  where  $t_i \in \{0, 1, \dots, b-1\}$ . When the sequence is truncated at some level  $n$  we will write  $\hat{t}_n = (t_1, t_2, \dots, t_n)$ . Notice this expansion induces an  $b$ -ary tree, which is sketched in Figure 3.3 for  $b = 2$  and  $n = 3$ . Each unique (infinite) sequence  $t$  designates a different path through this tree, of which there are uncountably

many, since there are uncountably many real numbers in any interval. For finite  $n$ , there are  $b^n$  truncated paths  $\tilde{t}_n$ , denoted  $\tilde{t}_n^i$ ,  $i = 1, 2, \dots, b^n$ .

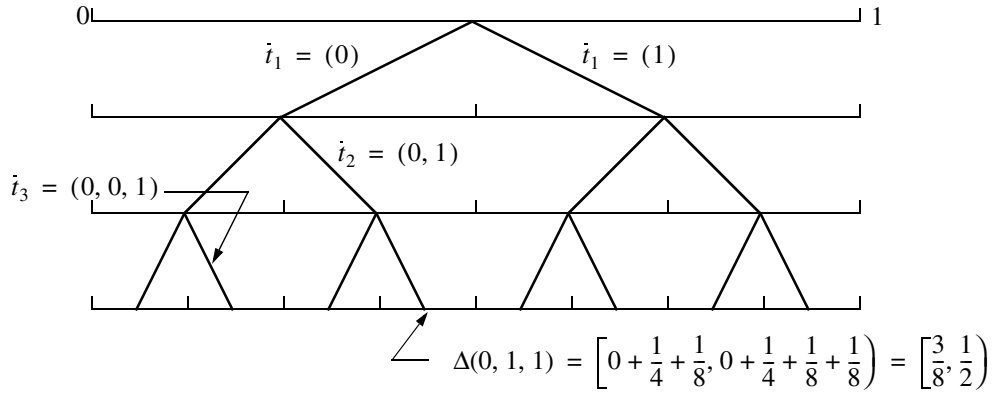


**Figure 3.3** Binary tree induced by the subdivision of the unit interval

Next associate with each finite path  $\tilde{t}_n$  the sub-interval

$$\Delta(\tilde{t}_n^i) = \Delta(t_1^i, \dots, t_n^i) = \left[ \sum_{j=1}^n t_j^i b^{-j}, \sum_{j=1}^n t_j^i b^{-j} + b^{-n} \right) \quad (3.14)$$

(again see Figure 3.3). Notice the  $\Delta(\tilde{t}_n^i)$ ,  $i = 1, \dots, b^n$ , are disjoint sets which generate a partition of the unit interval with resolution  $b^{-n}$ , i.e.,  $\lambda = \|\Delta(\tilde{t}_n^i)\| = b^{-n}$  and  $[0, 1) = \bigcup_{i=1}^{b^n} \Delta(\tilde{t}_n^i)$ . When the path to a sub-square at level  $n$  is not of concern, we simply denote the  $i$ th such sub-square by  $\Delta_n^i$ ,  $i = 1, 2, \dots, b^n$ .

Finally associate with each finite path independent and identically distributed non-negative mean one random weights denoted  $W_{\tilde{t}_n^i} = W_{t_1^i t_2^i \dots t_n^i}$ . A generic random variable with the common distribution of the  $W_{\tilde{t}_n^i}$  will be denoted simply as  $W$  and will be called the *generator* of the random cascade. The weights  $W_{\tilde{t}_n^i}$  are used to multiplicatively generate a measure on  $J$  as shown in Figure 3.4.

In order to explain Figure 3.4, we must first backtrack and consider a generalization of the discrete iid random cascade construction, called a *positive martingale*, which is constructed as follows. First, assign an arbitrary (finite) initial mass distribu-

tion (measure)  $\mu_0$  to  $J$ . Next define  $\mu_n$ , the mass distribution at level  $n$ , by the integral

$$\mu_n(A) = \int_A Q_n(x) \mu_0(dx), \quad (3.15)$$

where  $A$  is a (Borel) subset of  $J$  and  $Q_n(x)$  is a *martingale sequence* in  $n$  for all  $x$  with

$$\int_J E[Q_n(x)] \mu_0(dx) < \infty. \quad (3.16)$$

A martingale sequence (or simply *martingale*) is a sequence of random variables,  $X_1, X_2, \dots$ , with an associated sequence of events  $F_1, F_2, \dots$  in the probability space on which the random variables are defined, such that the following conditions hold:

- (a)  $F_n \subset F_{n+1}$ ;
- (b) the set of events  $F_n$  determines the value of  $X_n$ ;
- (c)  $E[|X_n|] < \infty$ ; and
- (d)  $E[X_{n+1} \mid F_n] = X_n$  with probability one.

Martingales sequences have convergence properties that make possible the final step in the construction, which is to take the limit  $n \rightarrow \infty$ , i.e., consider the measure

$$\mu_\infty(A) = \lim_{n \rightarrow \infty} \mu_n(A). \quad (3.17)$$

For the existence of the limit measure defined by equation (3.17) see, for example, Kahane (1989) or Waymire and Williams (1995) and references therein.

The positive martingale construction may be reduced to a random cascade as follows. First, take the initial mass distribution  $\mu_0$  to have a uniform density  $R_0$ . Second, specify the martingale sequence  $Q_n(x)$  to be

$$Q_n(x) = \prod_{j=1}^n P_j(x), \quad (3.18)$$

where  $P_n(x)$  are iid with  $EP_n(x) = 1$ . Notice that this way of specifying  $Q_n(x)$  makes two important assumptions: first, independence of  $P_n(x)$  from level to level, and second, a conservation condition induced by  $EP_n(x) = 1$ , which in turn implies that  $EQ_n(x) = 1$  and that  $E\mu_n(A) = \int \mu_0(dx)$ .

Finally  $P_n(x)$  may be defined<sup>A</sup> in terms of the iid weights  $W_{t_n^i}$  assigned to the recursive subdivision of the domain  $J$  defined by the sub-intervals  $\Delta(t_n^i)$  as follows:

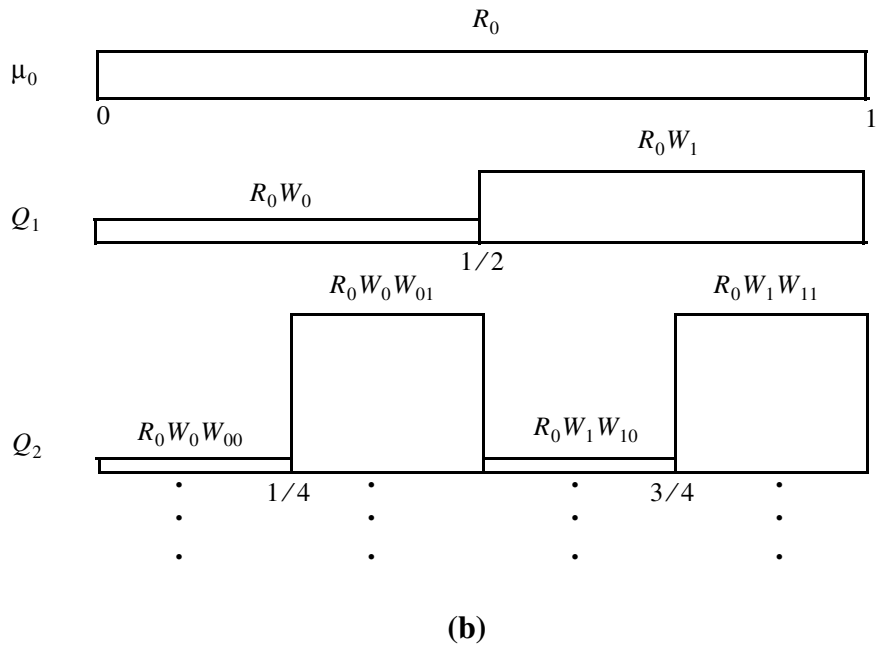
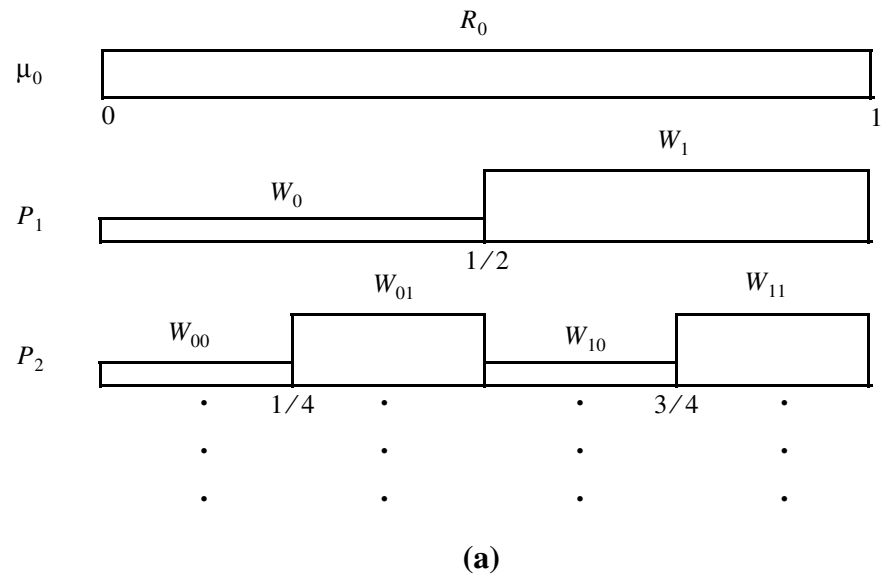
$$P_n(x) = \begin{cases} W(t_n^1) & \text{on } x \in \Delta(t_n^1) \\ \dots & \\ W(t_n^{b^n}) & \text{on } x \in \Delta(t_n^{b^n}) \end{cases} \quad (3.19)$$

Figure 3.4 is a schematic of this construction. Figure 3.4(a) shows the construction of the  $P_n(x)$  from the weights  $W_{t_n^i}$  for  $n = 2$  while Figure 3.4(b) shows the  $Q_n(x)$  that result from application of equation (3.18) to the  $P_n(x)$  shown in Figure 3.4(a). Notice that in specifying  $P_n(x)$  in this way, we are making many assumptions. In general,  $P_n(x)$  could be an arbitrary non-negative stochastic process as long as the condition  $EP_n(x) = 1$  and independence from level to level are preserved. Thus for the discrete iid random cascade construction, the  $Q_n(x)$  are piecewise constant over the sub-intervals  $\Delta(t_n^i)$  so that

$$\mu_n(\Delta(t_n^i)) = \int_{\Delta(t_n^i)} \mu_n(dx) = R_0 b^{-n} W_{t_1^i} W_{t_2^i} \dots W_{t_n^i}. \quad (3.20)$$

Before giving further specific results regarding discrete iid random cascades, consider the generalization of this construction to the two-dimensional domain

$J = [0, l_{max}]^2$ . In general, the branching number is the ordered pair  $(b^{(x)}, b^{(y)})$ ,



**Figure 3.4** Cascade construction sequences  
 (a)  $P_n$ , (b)  $Q_n$

where  $b^{(x)}$  and  $b^{(y)}$  are integers greater than or equal to two, but we will only consider the case where  $b^{(x)} = b^{(y)} = \sqrt{b}$  for some integer and perfect square  $b$ , with  $b \geq 4$ .

The infinite paths

$$t^i = (t^{x,i}, t^{y,i}), \quad (3.21)$$

where

$$t^{x,i} = (t_1^{x,i}, t_2^{x,i}, \dots, t_n^{x,i}, \dots), t_n^{x,i} \in \{0, \dots, \sqrt{b} - 1\}, \quad (3.22)$$

and likewise for  $t^{y,i}$ , now give a  $\sqrt{b}$ -ary expansion of a real number in the square  $J = [0, l_{max}]^2$ . A finite path  $t_n^i$  is now simply  $(t_n^{x,i}, t_n^{y,i})$ , where

$$\tilde{t}^{x,i} = (t_1^{x,i}, t_2^{x,i}, \dots, t_n^{x,i}), \quad (3.23)$$

and likewise for  $\tilde{t}^{y,i}$ .

The sub-square of  $J$  associated with a finite path  $t_n^i$  is given by the Cartesian product

$$\Delta(t_n^i) = \Delta(\tilde{t}_n^{x,i}) \times \Delta(\tilde{t}_n^{y,i}), \quad (3.24)$$

where

$$\Delta(\tilde{t}_n^{x,i}) = \Delta(t_1^{x,i}, \dots, t_n^{x,i}) = \left[ \sum_{j=1}^n t_j^{x,i} \sqrt{b}^{-j}, \sum_{j=1}^n t_j^{x,i} b^{-j} + \sqrt{b}^{-n} \right). \quad (3.25)$$

A sub-square at level  $n$  has a side length of  $l_n = l_{max} b^{-n/2}$ , or a normalized side length of  $\lambda_n = l_n / l_{max} = b^{-n/2}$ .

We can now proceed to give specific results concerning a discrete iid random cascade on the domain  $J = [0, l_{max}]^2$  with an initial mass distribution having a constant density  $R_0$ , which is our primary case of interest. Then  $\mu_0(J) = R_0 l_{max}^2$ . From equa-

tion (3.20), the mass in the box  $\Delta(\tilde{t}_n^i)$  is given by

$$\mu_n(\Delta(\tilde{t}_n^i)) = R_0 l_{max}^2 b^{-n} \prod_{j=1}^n W(\tilde{t}_j^i). \quad (3.26)$$

Notice in equation (3.26) the presence of the normalizing factor  $b^{-n}$ , which corrects the mass for the decreasing size of the box as  $n$  increases, whereas such a correction would not be necessary for the sequence of rain rates. Recall that the  $W(\tilde{t}_j^i)$  are iid non-negative mean one random variables. Because the  $W(\tilde{t}_j^i)$  are identically distributed, the masses  $\mu_n(\Delta(\tilde{t}_n^i))$  for all sub-squares  $\Delta(\tilde{t}_n^i)$  are identically distributed. As such, the particular sub-square is not important for present purposes so we write  $\Delta_n^i$  for the  $i$ th box at level  $n$  and  $\mu_n(\Delta_n^i)$  for the mass in it. This mass is distributed as

$$\mu_n(\Delta_n^i) = R_0 l_{max}^2 b^{-n} \prod_{j=1}^n W_j. \quad (3.27)$$

We use the notation  $W$  to refer a generic random variable with the distribution of the  $W_j(\Delta_n^i)$ , the generator of the random cascade.

Taking the limit  $n \rightarrow \infty$  yields the limit measure  $\mu_\infty$ . Choose a sub-square at level  $n$  with mass  $\mu_n(\Delta_n^i)$ . The cascade below this sub-square is just an independent cascade with the same generator and initial mass  $\mu_n(\Delta_n^i)$ . Thus there is a very recursive character to a random cascade. This results in the following recursion relation (Holley and Waymire 1992)

$$\mu_\infty(\Delta_n^i) = \mu_n(\Delta_n^i) Z_\infty(\Delta_n^i), \quad i = 1, 2, \dots, b^{-n} \quad (3.28)$$

where the random variables  $Z_\infty(\Delta_n^i)$  are mutually independent, identically distributed as  $\mu_\infty(J)/\mu_0(J)$  for all  $i$  and all  $n$ , and are independent of the  $\mu_n(\Delta_n^i)$ . Like the  $W_j(\Delta_n^i)$ , the  $Z_\infty(\Delta_n^i)$  are identically distributed, so we will denote by  $Z_\infty$  a generic random variable with the distribution of the  $Z_\infty(\Delta_n^i)$ . Equation (3.28) indicates that in the limit, the

mass in a sub-square is given by the product of a large-scale component  $\mu_n(\Delta_n^i)$  and a small-scale component  $Z_\infty(\Delta_n^i)$ . Thus it gives an explicit representation of the effect of “subgrid-scale variability” that is so sought after in turbulence theory and environmental modeling.

If we set  $n = 1$  in equation (3.28), sum over all  $i$ , and note that  $\mu_1 = \mu_0(J)b^{-1}W$  and  $\sum_i \mu_\infty(\Delta_1^i) = Z_\infty$  in distribution, we obtain a means of obtaining (in principle, at least) the distribution of  $Z_\infty$  from the distribution of  $W$  (Holley and Waymire 1992):

$$Z_\infty = b^{-1} \sum_{i=1}^b W(i)Z_\infty(i). \quad (3.29)$$

To my knowledge, the distribution of  $Z_\infty$  has been obtained explicitly for only one class of cascades, but equation (3.29) can also be used to find the integer moments of  $Z_\infty$  in general. This calculation is given in Appendix C, as it is rather long, but we will use the result below.

The above notation and a few results provides the necessary background for the basic results of Kahane and Peyriere (1976) regarding the limit measure. First, we must define the so-called MKP (Mandelbrot-Kahane-Peyriere) function:

$$\chi_b(q) = \log_b E W^q - (q - 1). \quad (3.30)$$

As we shall see, the MKP function contains a great deal of information about the random cascade generated by  $W$ . Two basic facts about MKP functions are that they are convex and  $\chi_b(1) = 0$ . As defined by Mandelbrot (1974), there are three basic classes of MKP functions, depending on the existence of the moments of  $Z_\infty$ , and designated as *regular*, *irregular*, and *degenerate*. Schematic MKP function for each of these three types are shown in Figure 3.5.

Now we are truly ready to give the results of Kahane and Peyriere (1976) regarding the limit measure of a random cascade. Their results concern three properties of

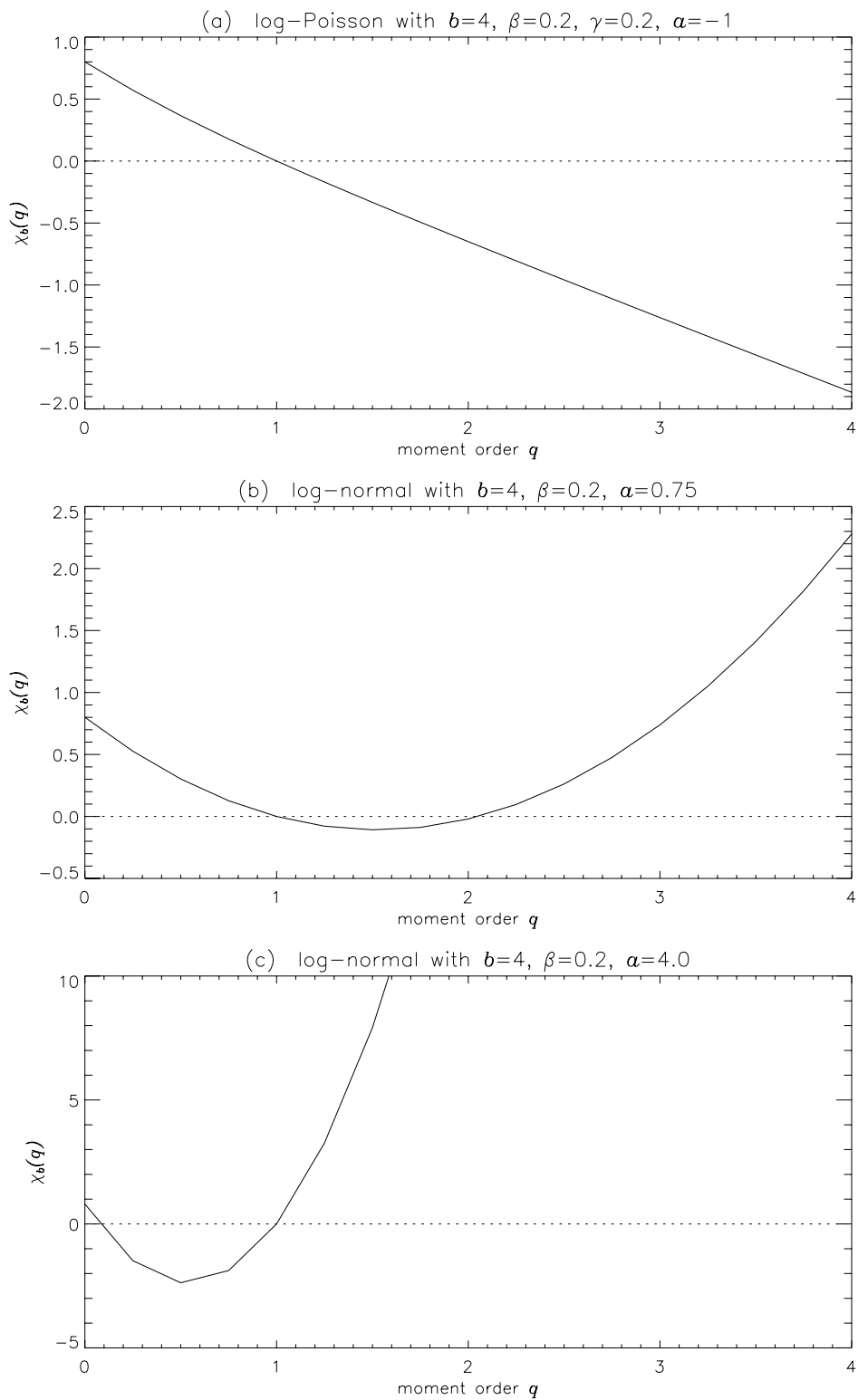


**Figure 3.5 Three classes of MKP functions**  
**(a) regular, (b) irregular, (c) degenerate (after Mandelbrot (1974))**

the limit measure: (a) the non-degeneracy of the limit mass  $\mu_\infty(J)$  - under what conditions is it possible that the limit mass is greater than zero; (b) the divergence of statistical moments of the limit mass; and (c) the dimension of support of the limit measure.

Theorem 3.1 (Kahane and Peyriere 1976). Let  $W$  be the generator of a discrete iid random cascade with MKP function  $\chi_b(q)$  and branching number  $b$ , then

(a) If  $\chi_b^{(1)}(1) < 0$ , then  $EZ_\infty > 0$  and  $EZ_\infty = 1$ .

(b) For  $q > 1$ ,  $\mu_\infty(J)$  has a finite moment of order  $q$  if and only if  $q < q_c$ , where  $q_c = \inf\{q \geq 1; \chi_b(q) \geq 0\}$ . Moreover,  $EZ_\infty^q$  exists for all  $q > 0$  if and only if  $W$  is essentially bounded by  $b$  and  $P(W = b) < 1/b$ .

(c) If  $E[Z_\infty \log Z_\infty] < \infty$ , then the limit measure  $\mu_\infty$  is almost surely supported by a Borel subset of  $J$  of Hausdorff dimension  $D = -d\chi_b^{(1)}(1)$ .

Definitions of a few terms in this theorem are probably in order before proceeding to any discussion. In part (b), “essentially bounded by  $b$ ” means that the probability that  $W$  exceeds  $b$  is zero and  $\inf\{A\}$  denotes the “infimum” of the set  $A$ , which is a generalization of the notion of a minimum and is defined in Appendix B. In part (c), note that Borel subsets are defined in the introduction to measure theory in Appendix A. Hausdorff dimension is a generalization of the notion of Euclidean dimension and is also defined in Appendix B. The “support” of a measure is formally the smallest closed set  $A$  such that  $\mu_\infty(A^c) = 0$ , where  $A^c$  denotes the complement of the set  $A$  with respect to the space  $J$  (i.e.,  $J - A$ ), so the support is the closure of the subset of  $J$  where the measure “lives”.

Now for some discussion. Part (a) indicates that if the slope of the MKP function at  $q = 1$  is negative, then the expected value of the limit mass is positive, and in particular one. The MKP function in Figure 3.5c fails this criterion and thus indicates a degenerate cascade, while those in Figure 3.5a and Figure 3.5b fulfill it. In non-degenerate cascades whose generators include an “atom” at zero, as we shall see, the limit

mass may still be zero with positive probability, but it would be degenerate if it were zero with probability one. Part (b) gives necessary and sufficient conditions on the existence of the moments of the limit mass, one for moments in the range  $1 < q < q_c$ , and the other for all moments  $q > 0$ . As shown in Figure 3.5, the critical moment  $q_c$  is infinite (all positive moments exist) for the regular class, while for the irregular class  $q_c$  is finite, and it is undefined for the degenerate class. Part (c) gives the Hausdorff dimension of the support of the limit measure. The condition  $E[Z_\infty \log Z_\infty] < \infty$  cannot be checked directly from the MKP function like the other conditions in this theorem, because as we noted, while the distribution of  $Z_\infty$  is given in principle by the solution of equation (3.29), it has been solved only in a certain special cases. However, Waymire and Williams (1995) note that Kahane (1989) found a way to remove this condition. So we will not concern ourselves with it.

The Hausdorff dimension of the support of the limit measure may be used to prove the *singularity* of the limit measure with respect to Lebesgue measure. A measure  $\mu$  is singular with respect to another measure  $\nu$  if there exist sets  $S_\mu$  and  $S_\nu$  such that  $\mu(S_\mu^c) = 0$ ,  $\nu(S_\nu^c) = 0$ , and  $S_\mu \cap S_\nu = \emptyset$ , where  $S^c$  denotes the complement of  $S$  (Billingsley 1986, p. 442). The singularity of the cascade limit measure follows from the fact that any subset of Hausdorff dimension  $D < d$  has  $d$ -dimensional Lebesgue measure zero. This is because Hausdorff measure, properly normalized, is identical to Lebesgue measure (see Appendix B), and the Hausdorff dimension of a set in  $\mathfrak{R}^d$  is given by the exponent  $D$  such that  $0 \leq D \leq d$  where the Hausdorff measure jumps from infinity to zero. Thus when  $D < d$ , the  $d$ -dimensional Hausdorff measure is zero, implying that  $d$ -dimensional Lebesgue measure is also zero. Thus the support of any iid discrete random cascade has Lebesgue measure zero unless the MKP function has slope  $\chi_b^{(1)}(1) = -1$ , which only occurs in the trivial case where  $W = 1$  with probability one. Hence consider the two measures  $\mu_\infty$ , the cascade limit measure, and  $\Lambda$ ,  $d$ -

dimensional Lebesgue measure. Denoting the support of the random cascade limit measure by  $S_{\mu_\infty}$ , then  $\mu_\infty(S_{\mu_\infty}^c) = 0$  by the definition of the support of a measure, and  $\Lambda(S_{\mu_\infty}) = 0$  when  $D < d$ , and by definition  $S_{\mu_\infty} \cap S_{\mu_\infty}^c = \emptyset$ , thus satisfying the definition of mutually singular measures.

Perhaps it seems strange to suggest that it rains only in a region of zero area. Two complementary responses can be made. First, one should not expect to directly observe it to be so, since all observation involves averaging over some region. Second, apart from observation, the physical implications of this kind of result are usually avoided by recognizing that there is a minimum scale below which the cascade structure no longer holds. In the study of fluid turbulence, the minimum scale is fairly well understood as the scale where dissipation due to viscosity overcomes and smooths out the cascade of turbulent eddies. In convective rainfall, one might expect that the size of a convective cell (on the order of  $2 \text{ km}$  in diameter) would constitute a minimum scale. Unfortunately, this scale is approximately the same as the reliable resolution of a weather radar, so it is difficult to empirically test this hypothesis. We discuss in Chapter 4 evidence for a break in scaling at about  $2 \text{ km}$  that is suggested by the present analysis.

### 3.3 Estimation and the Moments of Discrete IID Random Cascades

#### 3.3.1 Marginal Moments

The centrality of the MKP function  $\chi_b(q)$  to the study of random cascades is derived not only from the convenience of the statement of results regarding the moments of the limit mass  $Z_\infty$  as in Theorem 3.1, but in applications even more so from the fact that it describes the scaling of the ensemble moments of the cascade measure. To show this, we first define the scaling of the ensemble moments as

$$\lim_{\lambda \rightarrow 0} \frac{\log EM_n(q)}{-\log \lambda} = \lim_{n \rightarrow \infty} \frac{\log_b EM_n(q)}{n/d}, \quad (3.31)$$

where

$$M_n(q) = \sum_{i=1}^{b^n} \mu_\infty^q(\Delta_n^i). \quad (3.32)$$

By equation (3.27)

$$EM_n(q) = b^n E[\mu_\infty^q(\Delta_n^i)] = \mu_0^q(J) b^n b^{-nq} (EW^q)^n EZ_\infty^q, \quad (3.33)$$

so

$$\lim_{n \rightarrow \infty} \frac{\log_b EM_n(q)}{n/d} = \lim_{n \rightarrow \infty} \frac{\log_b \left\{ (b^{1-q} EW^q)^n EZ_\infty^q \mu_0^q(J) \right\}}{n/d} \quad (3.34)$$

$$= \lim_{n \rightarrow \infty} \frac{n[(1-q) + \log_b EW^q] + \log_b(EZ_\infty^q) + q \log_b \mu_0(J)}{n/d} \quad (3.35)$$

$$= d(1-q + \log_b EW^q) = d\chi_b(q). \quad (3.36)$$

This result is significant because it provides a way of estimating the generator  $W$  in physical situations where a large number of presumably iid realizations of random fields are available (e.g., fully developed turbulence). In this case, the ensemble average moments can be estimated and their scaling computed to give an estimate of the MKP function.

The situation in rainfall is somewhat different. It is difficult to justify *a priori* the assumption that a sequence of instantaneous rainfall fields is homogeneous. Instead, one would like to estimate the MKP function from the scaling of the moments for each field in the sequence to construct a sequence of estimated MKP functions. This re-

quires a somewhat different theory. We denote what we will call the scaling of the *spatial* average moments, that is, the scaling of the moments from a single spatial field, by the function  $\tau(q)$  and define it as

$$\tau(q) = \lim_{n \rightarrow \infty} \frac{\log_b M_n(q)}{n/d}. \quad (3.37)$$

Conditions under which it has been shown that this limit exists and equals the scaling of the *ensemble* average moments are given by the following theorem.

Theorem 3.2 (adapted from Holley and Waymire 1992). Consider a discrete iid random cascade with generator  $W$  and branching number  $b$ . For moments  $q$  where

$$EW^{2q}/E^2W^q < b \quad (3.38)$$

and

$$EZ_\infty^{2q} < \infty, \quad (3.39)$$

then

$$\tau(q) = \lim_{n \rightarrow \infty} \frac{\log_b M_n(q)}{n} = d\chi_b(q), \quad (3.40)$$

where  $d$  is the dimension of the domain  $J$  of the cascade.

Furthermore,

$$\lim_{n \rightarrow \infty} \frac{M_n(q)}{EM_n(q)} = \lim_{n \rightarrow \infty} \frac{M_n(q)}{\mu_0^q(J)b^{n\chi_b(q)}EZ_\infty^q} = Y(q), \quad (3.41)$$

where  $Y(q)$  is a random variable for each  $q$ .

So, according to theorem, while the moments of a single realization of a cascade measure do not converge to their expected values, the scaling of the moments do (un-

der certain conditions), and thus the generator can be estimated from a single realization. The moments (normalized by their expected values) do converge, but not to a constant, rather to a random variable denoted here by  $Y(q)$ . This fact demonstrates the *non-ergodicity* of the cascade limit measure.

A few comments regarding this theorem are in order. First, the theorem stated in Holley and Waymire (1992) from which this theorem is adapted (Theorem 2.7, p. 830) includes a rather restrictive condition called *strong boundedness*, which, among other things, excludes generators with atoms at zero (that is,  $P(W=0) > 0$ ). However, the proof in Holley and Waymire (1992) does not require this condition, so the less restrictive condition (3.39) is substituted.

Second, let us consider the range of  $q$  for which the conditions of the theorem are satisfied. Let us restrict ourselves to non-degenerate cascades (i.e.,  $q_c > 1$ ) and  $q \geq 0$ . We make the latter restriction because negative moments are unusable in analyzing data, since they only serve to amplify the noise that is invariably present. We first note that from the definition of the MKP function that the moment ratio condition is equivalent to the condition

$$2\chi_b(q) > \chi_b(2q). \quad (3.42)$$

Since we have assumed a non-degenerate cascade ( $q_c > 1$ ), consider first the condition  $1 < q_c < 2$ . Then  $EZ_\infty^{2q} < \infty$  if and only if  $q < q_c/2 < 1$ . However,

$$2\chi_b(q_c/2) > 0 > \chi_b(q_c) = 0, \quad (3.43)$$

so the moment ratio condition is satisfied for  $q \leq q_c/2$ . Thus for  $1 < q_c < 2$ , the  $EZ_\infty^{2q} < \infty$  condition is the more restrictive condition. Thus when we consider the applicability of Theorem 3.2 for specific models and we have  $1 < q_c < 2$ , we need consider only the condition  $EZ_\infty^{2q} < \infty$ . In particular, the conditions of Theorem 3.2 will be

satisfied for  $q < q_c/2$ .

For  $q_c = 2$ , it is easy to verify that both conditions hold only for  $q < 1$ . Thus this case can be combined with the previous case, yielding the result that the conditions of Theorem 3.2 will be satisfied for  $q < q_c/2$  when  $1 < q_c \leq 2$ .

When  $q_c > 2$ ,  $EZ_\infty^{2q} < \infty$  still holds if and only if  $q < q_c/2$ . However, at  $q = q_c/2$ , the moment ratio condition fails, since

$$\chi_b(q) < 0 < 2\chi_b(2q) = 0. \quad (3.44)$$

Thus when  $q_c > 2$ , the moment ratio condition determines the applicability of Theorem 3.2. Since this condition depends on the form of the MKP function, the complete range of  $q$  where the conditions of Theorem 3.2 are satisfied cannot be determined in a model-independent way as was possible for  $1 < q_c \leq 2$ , and thus we will investigate this on a case-by-case basis when  $q_c > 2$ . At a minimum, we can show in general that the conditions of Theorem 3.2 are satisfied for  $q \leq 1$ , since then the moment ratio condition is satisfied since  $\chi_b(q) \geq 0$  and  $\chi_b(2q) < 0$ .

To summarize, for non-degenerate cascades, the conditions of Theorem 3.2 are satisfied if and only if  $q$  is in the half-open interval  $[0, q_c/2)$  when  $q_c \leq 2$ , and for  $q$  in at least the closed interval  $[0, 1]$  when  $q_c > 2$ .

Third, the theorem gives convergence in the limit  $n \rightarrow \infty$  (i.e.,  $\lambda \rightarrow 0$ ). Infinite resolution data is obviously unavailable. An approximate theory based on the infinite resolution result is required for data analysis. Taking logs of both sides we rewrite equation (3.41) for large but finite  $n$  as

$$\log M_n(q) \cong \log Y(q) + q \log \mu_0(J) + \log EZ_\infty^q + n \log b \chi_b(q). \quad (3.45)$$

Now, since  $\lambda_n = b^{-n/d}$  and  $\tau(q) = d\chi_b(q)$  using Theorem 3.2, we can rewrite equation (3.45) as

$$\log M_n(q) \cong \log Y(q) + q \log \mu_0(J) + \log EZ_\infty^q - \tau(q) \log \lambda_n. \quad (3.46)$$

This is the fundamental data analysis relation. Using it, we expect that if our data came from a random cascade satisfying the conditions of Theorem 3.2 that plots of  $\log M_n(q)$  versus  $-\log \lambda_n$  will be linear with slopes giving an estimate of  $\tau(q)$  and intercepts estimating the sum of the remaining terms in equation (3.45). Thus the linearity of such plots provides a test of applicability of any random cascade to the data, while the slopes give an estimate of the function  $\tau(q)$ , and thereby, in principle, an estimate of the generator  $W$  because of equation (3.40). The significance of deviations from linearity are difficult to evaluate quantitatively, since the necessary theory has not been developed. In Chapter 4 we apply this test by computing a measure of the goodness of the log-log linear fit for the data and compare it to the same measure computed from simulated cascades.

The intercepts provide a further test, though also not without difficulties. From equation (3.45), the intercept which we denote by  $I(q)$  gives an estimate of

$$I(q) \approx \log Y(q) + q \log \mu_0(J) + \log EZ_\infty^q. \quad (3.47)$$

The difficulties arise for the following reasons. First, we do not know the distribution of  $Y(q)$ , let alone  $\log Y(q)$ , though since  $EY_n(q) = E[M_n(q)/EM_n(q)] = 1$ , we might expect a central tendency of  $\log Y(q)$  near 0. This expectation is borne out in simulations, as we shall see in Chapter 4. Second, we must estimate the  $q \log \mu_0(J)$  term, because the cascade conserves mass only on the average. Since

$$E[\mu_\infty([0, l_{max}]^2)] = E[\bar{R}l_{max}^2] = R_0 l_{max}^2 = \mu_0(J), \quad (3.48)$$

we estimate  $\mu_0(J)$  by  $\bar{R}l_{max}^2$ . Finally, the  $\log EZ_\infty^q$  term is difficult to estimate. Its value (see Appendix C) depends not only on the moments of the generator, for which

$\tau(q)$  provides an estimate, but also on the value of the branching number  $b$ , which is in principle non-estimable. However,  $\log EZ_\infty^q$  can often be argued (see Figure 4.6) to be small relative to the other terms in equation (3.47). Because of these difficulties, as well as additional ones introduced by the “off-grid” nature of the data described below, we will use simulations to generate a set of intercepts to which those from data can be compared.

Simulations are also required to apply this theory to data for a more fundamental reason which can be described as follows. Notice that the scaling of moments function  $\tau(q)$  is computed by integrating over the same boxes  $\{\Delta_n^i\}$  that were used to generate the cascade. Thus Theorem 3.2 depends on this fact, and it is unclear whether the theorem will hold if the location of the boundaries of the boxes that generated the cascade are unknown, or if they do not exist at all, as one might suppose would be true of data. While perhaps analytical approaches to this problem can be worked out (as indeed has been done to a degree in the case of Kahane’s (1985) analysis of Mandelbrot’s (1972; 1983, pp. 379-380) “continuous” lognormal cascades, though they do not give a spatial moment result like Theorem 3.2), the sensitivity of the results to various spatial subdivision methods can be easily explored using simulated cascades. Simulation methods and results will be given preceding the data analysis in Chapter 4.

### 3.3.2 Derivatives of the Marginal Moments

The first and second derivatives of the MKP function will be used below for the purposes of estimating its parameters and testing its linearity. In addition, while we will not use the “multifractal spectrum  $f(\alpha)$ ” of the general theory of multifractals here, it is the Legendre transform of  $\tau(q)$  (Falconer 1990, ch. 17), hence when  $\tau(q)$  is differentiable,  $\alpha(q)$  is given by  $-\tau^{(1)}(q)$ . In fact, because of this, the estimation method we will give for the derivatives of  $\tau(q)$  was originally developed as part of a means of estimating  $f(q)$  and  $\alpha(q)$ , since direct methods are subject to the need for logarith-

mic corrections and other difficulties (Chhabra and Jensen 1989).

The method is obtained from the definition of  $\tau(q)$  (equation (3.40)) by differentiating, i.e.,

$$\tau^{(1)}(q) = \frac{d}{dq} \lim_{n \rightarrow \infty} \frac{\log \sum_{i=1}^{b^n} \mu_{\infty}^q(\Delta_n^i)}{n \log b} = \lim_{n \rightarrow \infty} \frac{\frac{d}{dq} \log \sum_{i=1}^{b^n} \mu_{\infty}^q(\Delta_n^i)}{n \log b} \quad (3.49)$$

$$= \lim_{n \rightarrow \infty} \frac{\sum_{i=1}^{b^n} \mu_{\infty}^q(\Delta_n^i) \log \mu_{\infty}(\Delta_n^i)}{n \log b \sum_{i=1}^{b^n} \mu_{\infty}^q(\Delta_n^i)}. \quad (3.50)$$

Similarly, the second derivative of  $\tau(q)$  is estimated as

$$\tau^{(2)}(q) = \frac{d}{dq} \lim_{n \rightarrow \infty} \frac{\sum_{i=1}^{b^n} \mu_{\infty}^q(\Delta_n^i) \log \mu_{\infty}(\Delta_n^i)}{n \log b \sum_{i=1}^{b^n} \mu_{\infty}^q(\Delta_n^i)} \quad (3.51)$$

$$= \lim_{n \rightarrow \infty} \frac{\left[ \sum_{i=1}^{b^n} \mu_{\infty}^q(\Delta_n^i) (\log \mu_{\infty}(\Delta_n^i))^2 \right] \left[ \sum_{i=1}^{b^n} \mu_{\infty}^q(\Delta_n^i) \right] - \left[ \sum_{i=1}^{b^n} \mu_{\infty}^q(\Delta_n^i) \log \mu_{\infty}(\Delta_n^i) \right]^2}{n \log b \left[ \sum_{i=1}^{b^n} \mu_{\infty}^q(\Delta_n^i) \right]^2}. \quad (3.52)$$

In actual practice, of course, the small-scale limit is not attainable, and a straight-line fit of the sums versus  $n \log b$  is used to estimate the derivatives of  $\tau(q)$ , in the same way as with the estimate of  $\tau(q)$  itself. A proof that the derivative and limit can be exchanged as was done in going from equation (3.49) to equation (3.50) and from equation (3.51) to equation (3.52) has not been worked out, but the results obtained by this method and those from numerical differentiation of the estimated  $\tau(q)$  curve were compared and were found to be quite similar.

### 3.3.3 Cross Moments

In many applications of random measures (e.g., the statistical theory of turbulence), the spatial correlation or cross moment properties are very important. In turbulence theory, two-point cross moment properties have been computed by a number of authors for multifractal or cascade-like constructions via heuristic arguments (Yaglom 1966; Cates and Deutsch 1987; Siebesma and Pietronero 1988; Lee and Halsey 1990; Meneveau and Chhabra 1990). To our knowledge, a rigorous calculation has not been previously performed. We will present results only for the simplest case, two masses at the same level of a  $d$ -dimensional random cascade with a separation vector  $\hat{r} = (r, 0, \dots, 0)$ , i.e., the separation distance is zero in all but one of the  $d$  dimensions. Solution of this simple case will be enough to make an important consistency check on the rainfall data. More general calculations involving more than two masses, more than one level, and separation vectors involving more than one non-zero element have been carried out but are not yet published (B. M. Troutman, personal communication).

As in the case of the marginal moments, we will first compute the ensemble average or expectation of the cross moments. Following that, the question of whether the sample cross moments can be shown to converge in any sense to the ensemble average cross moments will be examined. As we will suggest but not prove rigorously, the cross moments mimic the marginal moments with regard to this question: the *scaling* of the sample cross moments does converge to the *scaling* of the ensemble average cross moments.

The (normalized) ensemble average cross moments are as follows. The calculation is presented in Appendix D, as it is rather lengthy.

$$\frac{E[\mu_\infty^p(\Delta_n^i)\mu_\infty^q(\Delta_n^{i+b^{m/2}})]}{E[\mu_\infty^{p+q}(\Delta_n^i)]} = C_n(p, q) \frac{1 - \left(\frac{r_n}{l_{max}}\right)^{1 + \log_{\sqrt{b}} R(p, q)}}{1 - r_n/l_{max}} \left(\frac{r_n}{l_{max}}\right)^{-\log_{\sqrt{b}} R(p, q)}, \quad (3.53)$$

where

$$C_n(p, q) = \frac{EZ_\infty^p EZ_\infty^q}{EZ_\infty^{p+q}} R(p, q)^{-n} \frac{\sqrt{b} - 1}{\sqrt{b} R(p, q) - 1}, \quad (3.54)$$

$$R(p, q) = \frac{EW^{p+q}}{EW^p EW^q}, \quad (3.55)$$

and  $\mu_\infty(\Delta_n^i)$  denotes the limit measure in a box at level  $n$  chosen randomly from among the boxes where  $1 \leq i + b^{m/2} \leq b^{n/2}$ . Then  $\mu_\infty(\Delta_n^{i+b^{m/2}})$  is the limit measure in a box a distance  $r_n = l_{max} b^{(m-n)/2}$  away. Note that in using  $\sqrt{b}$  we are assuming  $d = 2$ ; in general we would have  $b^{1/d}$  for a  $d$ -dimensional cascade where  $b^{1/d}$  branchings occur at each level in each dimension.

The interesting part of the behavior of the cross moment is its  $r_n$ -dependence, which is evidently approximately power law with exponent

$$\kappa_{\sqrt{b}}(p, q) = -\log_{\sqrt{b}} R(p, q). \quad (3.56)$$

Approximate power law dependence on  $r_n$  depends on the fact that for  $n$  large,  $r_n/l_{max} \ll 1$ , and in for many generators of interest  $0 \leq \log_b R(p, q) \leq 1$  (see Appendix D for discussion), so

$$\frac{1 - (r_n/l_{max})^{1 + \log_{\sqrt{b}} R(p, q)}}{1 - r_n/l_{max}} \approx 1. \quad (3.57)$$

The cross-moment exponent  $\kappa_{\sqrt{b}}(p, q)$  can also be written in terms of the MKP function  $\chi_b(q) = \log_b E(W^q) - (q - 1)$  as

$$\kappa_{\sqrt{b}}(p, q) = 2(\chi_b(p+q) - \chi_b(p) - \chi_b(q) + 1). \quad (3.58)$$

If Theorem 3.2 holds, we have for  $d = 2$  that  $\tau(q) = 2\chi_b(q)$ , so equation (3.58) can be re-written as

$$\kappa_{\sqrt{b}}(p, q) = \tau(p+q) - \tau(p) - \tau(q) + 1. \quad (3.59)$$

This relation provides a consistency check between the marginal and cross moments of empirical data.

Equation (3.59) is also suggestive that the exponents  $\kappa_{\sqrt{b}}(p, q)$  of the spatial cross moments (i.e., those from a single realization) might converge under certain conditions to their ensemble average values, which is our next subject.

The following hypothesis is due to B. M. Troutman and A. V. Vecchia (personal communication). It has not been proven but it can be tested for large but finite  $n$  using simulated cascades.

Hypothesis: Under certain conditions on the generator  $W$ ,

$$\lim_{n \rightarrow \infty} \left( \log \frac{\left( \frac{1}{b^n - b^m} \right) \sum_{i=1}^{b^n - b^m} \mu_{\infty}^p(\Delta_n^i) \mu_{\infty}^q(\Delta_n^{i+b^m})}{b^{-n} \sum_{i=1}^{b^n} \mu_{\infty}^{p+q}(\Delta_n^i)} \right) / (-\log r_n) = -\log_b R(p, q). \quad (3.60)$$

This hypothesis is suggested by equation (3.53) by replacing the ensemble averages on the left-hand side with spatial averages. As usual, in finite resolution data or simulations, a relation such as equation (3.60) is tested by assuming that the ratio on the left-hand side is sufficiently close to convergence that log-log linearity will hold in plots of the numerator versus the denominator, whose slope then gives an estimate of the exponent on the right-hand side. This procedure was used on simulated cascade realizations to test the hypothesis and is used to explore the cross moment behavior of rainfall data in Chapter 4.

### 3.4 Some Modeling Considerations

In this section we consider some issues in the application of discrete random cascades as defined and described above to modeling spatial measures. In the first subsection a few facts about the spatial structure of discrete random cascades arising from their discreteness (in space and scale) that make their literal application to spatial modeling problematic are examined and solutions are proposed. In the second subsection, the features of generators appropriate to modeling spatial rainfall are examined in general and through a few specific examples.

#### 3.4.1 Difficulties Arising from Discreteness

##### 3.4.1.1 Nonhomogeneity and Anisotropy

As noted above, the limit measure of a cascade is singular and hence does not qualify as a (random) function. However, if the cascade measure is integrated over its boxes

$$\{\Delta_n^i\}, i = 1, 2, \dots, b^n \quad (3.61)$$

at a finite resolution, it can be treated as random function or stochastic process on a finite lattice, where a point in the lattice is associated with the center of each box. Consider the properties of the resulting process

$$\{\mu_\infty(\Delta_n^i)\}, i = 1, 2, \dots, b^n. \quad (3.62)$$

Recall that a stochastic process is *homogeneous* if the joint distributions of the random variables making up the process are invariant under translation and it is *isotropic* if the joint distributions are invariant under rotation. The joint distributions of the masses are composed of the marginal distributions of the masses, which in this case are identical, and the dependency between them. The dependency of two masses in the

process given by (3.62) is determined by the number of common multipliers. To see this, consider two masses  $\mu_\infty(\Delta_n^i)$  and  $\mu_\infty(\Delta_n^j)$ , with  $i \neq j$ . Recall that these are given by

$$\mu_\infty(\Delta_n^i) = \mu_0(J)b^{-n} \left( \prod_{k=1}^n W_k^i \right) Z_\infty(\Delta_n^i), \quad (3.63)$$

and likewise for  $\mu_\infty(\Delta_n^j)$ . For each mass, the multipliers  $W_k$  are independent, but up to  $n - 1$  of them may be common between the two masses (the multiplier  $W_n$  cannot be in common, and the high frequency factors are likewise always independent). How the number of common multipliers is distributed in space determines the homogeneity and isotropy properties. In Appendix D this fact is used to compute the two-point spatial cross moments  $E[\mu_\infty^p(\Delta_n^i)\mu_\infty^q(\Delta_n^j)]$  of the process (3.62).

As an example, consider the boxes from a cascade with  $\sqrt{b} = 3$  integrated up to  $n = 2$  as shown in Figure 3.6. It should be clear that the masses in each first-level box (demarcated by heavy lines) have one common multiplier, while those from different first-level boxes have no common multipliers. Thus the joint distributions of masses within one of the first-level boxes are of one type (dependent), while those that involve masses from more than one first-level box are of another type (independent). The homogeneity and isotropy properties of the integrated cascade follow from this.

Taking homogeneity first, consider two of the two-point joint distributions of the masses in the boxes labeled in Figure 3.6, mass  $i$  with mass  $j$  ( $F_{i,j}$ ) and mass  $j$  with mass  $k$  ( $F_{j,k}$ ). First notice that the lattice itself limits separation and translation distances to integer multiples of the lattice spacing, and limits the direction of separation and translation to the axes of the lattice. But even under these conditions, the process fails to be homogeneous, because  $F_{i,j}$  involves masses from different first-level boxes while  $F_{j,k}$  does not. Hence the integrated cascade fails to be invariant under transla-

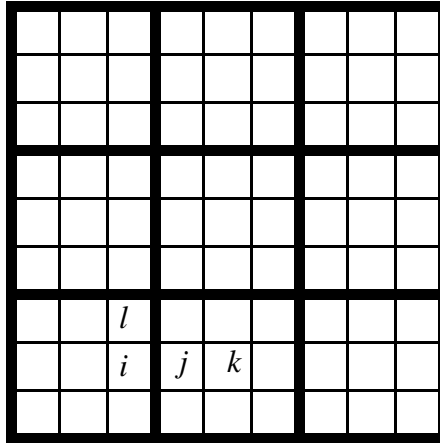


**Figure 3.6** Cascade grid for  $b=9$  and  $n=2$

tion and is thus a nonhomogeneous stochastic process. Because the individual masses are identically distributed, however, we might say the process is “marginally” homogeneous.

As regards isotropy, consider the joint distributions of mass  $i$  with mass  $j$  ( $F_{i,j}$ ) and mass  $i$  with mass  $l$  ( $F_{i,l}$ ) in Figure 3.6. Notice again here the constraints of the lattice in which we can only consider directions along one of the axes. Again even under these constraints the process is anisotropic because  $F_{i,j}$  involves masses from different first-level boxes and  $F_{i,l}$  does not.

In applications, we may find that we want a random field model that is anisotropic and nonhomogeneous, but in a way that is controllable using model parameters, not simply inherent to the model, and we would most likely want to use a homogeneous and isotropic model as a null hypothesis unless physical considerations determined otherwise. So the failure of discrete random cascades to be homogeneous or isotropic is a serious concern, but it is not too serious because homogeneous and isotropic cas-

acades can be constructed by making the method of spatial subdivision at each scale homogeneous and isotropic. We will describe a method of doing this in the following chapter. The difficulty with this method is that analytical calculations have not been carried out. Thus our approach will be to use the method to simulate homogeneous and isotropic cascades and then use the simulations to determine if the analytical results that have been obtained for discrete cascades on a square lattice still hold.

### 3.4.1.2 “On-grid” versus “Off-grid” Cascades

Even if one expected his data to arise exactly as a discrete random cascade with a particular branching number in square boxes on a regular lattice, it would be impossible to directly employ the regular lattice theory because one would not know the location or orientation of the lattice in the data. And it would be necessary to know this, since the theory described above, most importantly Theorem 3.2 that allows estimation of the MKP function of the generator of a cascade from the scaling of the moments of the cascade limit measure, applies strictly only to the cascade limit measure integrated over the exact boxes  $\Delta_n^i$ ,  $i = 1, \dots, b^n$  that subdivide the cascade domain  $J$  at each level  $n$ . In other words, in the basic representation of the integrated limit mass,

$$\mu_\infty(\Delta_n^i) = \mu_n(\Delta_n^i)Z_\infty(\Delta_n^i), \quad (3.64)$$

the boxes  $\Delta_n^i$ ,  $i = 1, \dots, b^n$  over which the limit measure is integrated must be the boxes used to subdivide the domain at level  $n$ . They cannot be any collection of square sets of side length  $l_{max}b^{-n/d}$  that covers the domain, let alone non-square sets.

When a cascade limit measure is sampled by integrating over the boxes used to generate it, we will say this is an “on-grid” cascade, while if it is sampled otherwise, we will call it an “off-grid cascade”. Obviously any sampling of real data is an off-grid cascade if it is a cascade at all; on-grid cascades can only be obtained by simulation.

In addition, it is by no means clear that such a lattice of boxes ever did exist in the

generation of any real-world data set. The spatial structure used to generate a cascade is merely a phenomenology suggested by a mathematical construct that leads to spatial mass distributions that have certain properties in common with the data, of which the square gridding is not one. In the rainfall context, the binning of the radar data constitutes the imposition of a square grid of essentially random orientation and location onto a field which, as noted above, we would like to assume as an initial hypothesis to be homogeneous and isotropic. This difficulty can also be overcome by the use of simulations of the type discussed above.

### 3.4.1.3 The Role of the Branching Number

The two difficulties discussed above arise from the most-likely unphysical spatial subdivision method used to generate regular lattice discrete random cascades. A difficulty also arises from the choice of a branching number (which amounts to discreteness in scale), which is, that we have presented no means of estimating it. To see this, notice that a value for  $b$  must be assumed in order to compute  $\tau(q)$ , which gives by Theorem 3.2 the MKP function as a function of this assumed  $b$ . If it were true that the distribution of any random variable  $W$  satisfying the requirements of a cascade generator could be made a function of  $b$  for any  $b > 1$  in such a way that the cascade limit measure did not vary with  $b$ , then the value of  $b$  would be truly arbitrary and ignorance of it would be of no concern. However, we will show next that (1) the limit measure depends on the value of  $b$  directly, not only through the MKP function; and (2) if we limit the arbitrariness of  $b$  to invariance of the MKP function rather than the limit measure itself, then only a certain class of generators are allowable, which are said to be *log-infinitely divisible*.

To show that the limit measure depends on the value of  $b$  directly as well as the MKP function, consider the moments of the limit mass  $Z_\infty$  as computed in Appendix C. In particular, consider the second moment

$$EZ_\infty^2 = \frac{b-1}{b-EW^2}. \quad (3.65)$$

Since  $\chi_b(2) = \log_b EW^2 - 1$  then  $EW^2 = b^{\chi_b(2)+1}$  and

$$EZ_\infty^2 = \frac{b-1}{b-b^{\chi_b(2)+1}} = \frac{1-b^{-1}}{1-b^{\chi_b(2)}}. \quad (3.66)$$

Since  $\chi_b(2) = -1$  if and only if  $P(W=1) = 1$ , thus even if  $W$  and  $b$  are adjusted together so that the MKP function is invariant, the distribution of the limit mass and hence the limit measure depends on  $b$  directly for any non-trivial cascade. This fact would actually provide a means of estimating  $b$  from the distribution of  $Z_\infty$  obtained from an ‘‘on-grid’’ cascade, but, as argued above, we will not find on-grid cascades in real data nor do we expect it to have some fixed  $b$ .

If we do not worry about all the properties of the limit mass, but just ask that  $W$  is such that the scaling properties of the limit measure as captured by the MKP function can be made invariant under changes in  $b$ , it turns out that this is equivalent to requiring that  $W$  be of the form

$$W = e^X, \quad (3.67)$$

where  $X$  has an infinitely divisible distribution. Following Waymire and Williams (1993), we say in this case that the distribution of  $W$  is *log-infinitely divisible*.

A probability distribution  $Q$  is said to be infinitely divisible if for all  $n \geq 1$ , it can be factored as an  $n$ -fold convolution of a probability distribution  $Q_n$ . It follows from this definition that the characteristic function

$$\varphi(\xi) = \int e^{i\xi x} Q(dx) \quad (3.68)$$

of an infinitely divisible distribution has the property that  $(\varphi(\xi))^t$  is also the character-

istic of an infinitely divisible distribution for any real, positive  $t$  (Lukacs 1970, p. 111). Using this result, it follows that given an infinitely divisible distribution  $Q$ , there is a family of (infinitely divisible) probability distributions  $Q_t$ ,  $t \geq 0$ , such that  $Q_1 = Q$  and  $Q_t * Q_s = Q_{t+s}$ . For  $t \neq 1$ ,  $Q_t$  can be obtained from the characteristic function

$$\varphi_t(\xi) = \int e^{i\xi x} Q_t(dx) = E[e^{i\xi X_t}] = (\varphi_1(\xi))^t \quad (3.69)$$

where  $X_t$  is a random variable with distribution  $Q_t$  (Bhattacharya and Waymire 1990, p. 349).

Now consider the family of distributions of the random variables  $W_b = e^{X_t}$  where  $\log b = t$  (then  $t \geq 0$  requires  $b \geq 1$ ) and  $X_t$  has a distribution that is a member of an infinitely divisible family as described above. When the expectations exist, the representation (3.69) can be written as

$$E[e^{qX_t}] = (E[e^{qX_1}])^t, \quad (3.70)$$

or, in terms of  $W_b$ ,

$$EW_b^q = (EW_e^q)^{\log b}. \quad (3.71)$$

With a little algebra, equation (3.71) can be re-written as

$$\log_b EW_b^q = \log_e EW_e^q, \quad (3.72)$$

which shows that the MKP function of  $W_b$  with branching number  $b$  is the same as that of  $W_e$  with branching number  $e$ . Notice taking  $q = 1$  in equation (3.71) shows that the mean one condition on cascade generators is preserved by this transformation.

The above argument shows that the log-infinite divisibility of the distribution of  $W_e$  induces a family of probability distributions of random variables  $W_b$ ,  $b \geq 1$ , with

invariant MKP functions. Reversing the steps of the argument shows that the assumption of invariant MKP functions implies the log-infinite divisibility of the distribution of  $W_b$ .

The upshot of this is that only if  $W$  is taken to have a log-infinitely divisible distribution can it be transformed as a function of  $b$  such that the MKP function does not change. Since  $b$  is in fact unknowable in applications, this is a crucial property for cascade generators used in spatial modeling to have. In light of this, we will consider in what follows only cascade generators with log-infinitely divisible distributions. We will examine below in detail three log-infinitely divisible generators. In order to analyze these, we need two more facts about infinite divisibility:

(a) If a random variable  $X$  has an infinitely divisible distribution, then  $X' = aX$  also has an infinitely divisible distribution, for any real number  $a$ .

(b) If two independent random variables  $X$  and  $Y$  have infinitely divisible distributions, then the sum  $X + Y$  has an infinitely divisible distribution, i.e., the class of infinitely divisible distributions is closed under finite convolutions (Lukacs 1970, p. 109). This implies that for two independent random variables  $e^X$  and  $e^Y$  with log-infinitely divisible distributions, the product  $e^X e^Y = e^{X+Y}$  has a log-infinitely divisible distribution.

### 3.4.2 Some Relevant Examples of Generators

#### 3.4.2.1 General Results for Generators with Atoms at Zero

A very important feature of the cascade theory for applications to spatial rainfall is that it can model regions of zero rain rate. This is accomplished by allowing the generator  $W$  to have a so-called *atom* at zero, i.e.,

$$P(W = 0) = 1 - b^{-\beta} \text{ and } P(W = W^+) = b^{-\beta}, \quad (3.73)$$

where  $W^+$  is the positive part of  $W$  (i.e.,  $P(W^+ > 0) = 1$ ). The parameter  $\beta$  will be restricted to be non-negative because we need  $P(W = W^+) \leq 1$ .

The following very simple observation will be central to all that follows. A generator  $W$  with an atom at zero can thus be written as the *composition*  $W = BY$  where

- (a)  $B$  and  $Y$  are independent cascade generators;
- (b)  $B$  has the distribution  $P(B = 0) = 1 - b^{-\beta}$  and  $P(B = b^\beta) = b^{-\beta}$ ; and
- (c)  $Y = b^{-\beta}W^+$  (in particular,  $P(Y > 0) = 1$ ).

Using the composition theorem of Waymire and Williams (1995), a *composition* of cascades may be defined equivalently as the cascade that results from using a generator that is the product of two independent cascade generators, as  $W = BY$  here, or, the cascade that results from using the limit measure of one cascade as the initial measure for the second, independent, cascade.

Since  $B$  has a log-infinitely divisible distribution (Waymire and Williams 1993), if  $Y$  has a log-infinitely divisible distribution, then so does  $W$  because the class of infinitely divisible distributions is closed under convolution. Several choices for the distribution of  $Y$  will be considered below.

The MKP function for a generator whose distribution is given by (3.73) is

$$\chi_b(q) = \log_b(b^{-\beta}E[(W^+)^q]) - (q - 1) \quad (3.74)$$

$$= -\beta + \log_b E[(W^+)^q] - (q - 1). \quad (3.75)$$

In terms of  $Y$  this is

$$\chi_b(q) = \log_b(b^{-\beta}E[(b^\beta Y)^q]) - (q - 1) \quad (3.76)$$

$$= \beta(q - 1) + \log_b EY^q - (q - 1) \quad (3.77)$$

$$= (\beta - 1)(q - 1) + \log_b EY^q. \quad (3.78)$$

The values of the MKP function at  $q = 0$  and  $q = 1$  are particularly useful. We have

$$\chi_b(0) = -\beta + 1 \quad (3.79)$$

and

$$\chi_b(1) = -\beta + \log_b EW^+ = \log_b EY. \quad (3.80)$$

The MKP function at  $q = 1$  implies

$$EW^+ = b^\beta \text{ and } EY = 1. \quad (3.81)$$

In view of equation (3.40), equation (3.79) provides a means of estimating the parameter  $\beta$ :

$$\hat{\beta} = 1 - \tau(0)/d. \quad (3.82)$$

Additional ways of estimating  $\beta$  will be considered below.

Because the generator  $W$  in this case can take on the value zero, the limit mass can be zero without the cascade being degenerate (see Theorem 3.1a for the definition and a criterion for degeneracy). The probability that  $Z_\infty = 0$  is computed by Holley and Waymire (1992) and is given by the smallest positive solution to

$$\gamma = (1 - b^{-\beta} + b^{-\beta}\gamma)^b, \quad (3.83)$$

where  $\gamma = P(Z_\infty = 0)$ .

Several specific choices for the distribution of  $Y$  are considered next.

### 3.4.2.2 The Beta-Model

If  $P(Y = 1) = 1$  (or, equivalently,  $W^+$  is specified by an atom at its expected val-

ue  $b^\beta$ ), then the representation given by (3.73) can be further simplified, yielding

$$P(W = b^\beta) = b^{-\beta} \text{ and } P(W = 0) = 1 - b^{-\beta}, \quad (3.84)$$

with an MKP function given by

$$\chi_b(q) = (q - 1)(\beta - 1). \quad (3.85)$$

Notice that in this case the generator  $W$  is completely parameterized by  $\beta$ . A deterministic cascade with this generator was first proposed as a model for the spatial structure of energy dissipation in fluid turbulence by Novikov and Stewart (1964). Because it has a single parameter that has been traditionally denoted by  $\beta$ , this model is often called the  $\beta$ -model, a usage that is adopted here.

It is easy to see from equation (3.85) that the slope of the MKP function in the case of the  $\beta$ -model is constant and is given by

$$\chi_b^{(1)}(q) = \beta - 1, \quad (3.86)$$

which shows, using Theorem 3.1a, that we must have  $\beta < 1$  to obtain a non-degenerate cascade. As shown in Over and Gupta (1994), the MKP function of an iid random cascade has a constant slope if and only if it has a  $\beta$ -model generator. Equation (3.86) suggests another estimate  $\tilde{\beta}$  for  $\beta$  in the case of a  $\beta$ -model generator, derived from the slope of the  $\tau(q)$  curve at  $q$ :

$$\tilde{\beta} = 1 + \tau^{(1)}(q)/d. \quad (3.87)$$

It can also be shown from the MKP function of the  $\beta$ -model (equation (3.85)) that it satisfies the conditions of Theorem 3.2 for all  $q \geq 0$ . To do so, first notice that this model satisfies the condition for the existence of  $EZ_\infty^q$  for all  $q > 0$  from Theorem 3.1b for any  $\beta < 1$ . Next recall that the moment ratio condition in terms of the MKP

function is

$$2\chi_b(q) > \chi_b(2q). \quad (3.88)$$

In terms of the  $\beta$ -model MKP function, this is

$$2(\beta - 1)(q - 1) > (\beta - 1)(2q - 1), \quad (3.89)$$

which implies

$$2(\beta - 1)q + 2(1 - \beta) > 2(\beta - 1)q + 1 - \beta, \quad (3.90)$$

or

$$2(1 - \beta) > 1 - \beta, \quad (3.91)$$

which is satisfied for any  $\beta < 1$ . Thus in principle Theorem 3.2 may be used to estimate the MKP function for a  $\beta$ -model for any  $q$ .

We shall see in Chapter 4 that this very simple model gives a good approximation to the spatial structure of convective rain rates. However, this simple assumption does not hold in exactly and in general  $Y$  must have some variance. So we give next two examples of  $Y$  with log-infinitely divisible distributions that have non-zero variance.

### 3.4.2.3 The Log-Poisson Model

The first example is the following log-Poisson form patterned after the generator introduced into the theory of turbulence by Dubrulle (1994) and She and Waymire (1995):

$$Y = b^{\gamma + aX_\lambda}, \quad (3.92)$$

where  $a$  and  $\gamma$  are free parameters and  $X_\lambda$  is a Poisson random variable with parameter  $\lambda$ , whose value, as we shall see, is determined by the other parameters. Since  $X_\lambda$  is

Poisson, this generator takes on a countably infinite number of discrete values and its distribution is log-infinitely divisible. The parameters  $a$  and  $\gamma$  under various conditions can take on positive or negative values, but they have certain inter-relationships that should be noted. When  $a = 0$ ,  $Y$  reduces to an atom at  $b^\gamma$ , so we must have  $\gamma = 0$  in order preserve  $EY = 1$ , giving again the  $\beta$ -model. When  $a > 0$ ,  $Y$  has the minimum value  $b^\gamma$ , hence we must have  $\gamma < 0$  in order to have  $EY = 1$ . And when  $a < 0$ ,  $Y$  has the maximum value  $b^\gamma$ , so  $\gamma > 0$  is required for  $EY = 1$ .

The MKP function for this model may be computed as follows. Referring to the general representation for generators with an atom at zero (equation (3.78)), we see that the value of  $EY^q$  is needed. To compute this, notice

$$EY^q = E[b^{q\gamma + qaX_\lambda}] = b^{\gamma q} E[b^{qaX_\lambda}]. \quad (3.93)$$

Since by assumption  $X_\lambda$  is Poisson with parameter  $\lambda$ , we have

$$P(X_\lambda = m) = e^{-\lambda} \frac{\lambda^m}{m!}, \quad (3.94)$$

so

$$E[b^{qaX_\lambda}] = \sum_{m=0}^{\infty} e^{-\lambda} b^{qam} \frac{\lambda^m}{m!} = e^{-\lambda} \sum_{m=0}^{\infty} \frac{(\lambda b^{aq})^m}{m!} = e^{-\lambda} e^{\lambda b^{aq}} = e^{\lambda(b^{aq} - 1)}, \quad (3.95)$$

so we have

$$EY^q = b^{\gamma q + \frac{\lambda(b^{aq} - 1)}{\log b}}, \quad (3.96)$$

and the MKP function is given by

$$\chi_b(q) = (\beta - 1)(q - 1) + \gamma q + \frac{\lambda(b^{aq} - 1)}{\log b}. \quad (3.97)$$

The parameter  $\lambda$  is determined by the condition  $EY = 1$ ,

$$EY = 1 = b^{\gamma + \frac{\lambda(b^a - 1)}{\log b}}, \quad (3.98)$$

which implies

$$\lambda = \frac{-\gamma \log b}{b^a - 1}, \quad (3.99)$$

so the MKP function can be written

$$\chi_b(q) = (\beta - 1)(q - 1) + \gamma \left( q - \frac{b^{aq} - 1}{b^a - 1} \right). \quad (3.100)$$

We will use the first two derivatives of the MKP functions in several ways below, so we compute them now:

$$\chi_b^{(1)}(q) = \beta - 1 + \gamma \left( 1 - \frac{b^{aq} a \log b}{b^a - 1} \right) \quad (3.101)$$

and

$$\chi_b^{(2)}(q) = \frac{-\gamma b^{aq} (a \log b)^2}{b^a - 1}. \quad (3.102)$$

Cascades with log-Poisson generators can exhibit a large range of properties, and now that we have computed the MKP function and two derivatives, some discussion of these properties for various values of the parameters is in order. Consider first the case  $a < 0$ . As noted above, in this case, the maximum value of  $Y$  is  $b^\gamma$  (hence the

maximum of  $W$  is  $b^{\gamma+\beta}$ ), and as  $X$  gets large,  $Y$  approaches zero. Hence according to equation Theorem 3.1b, for  $a < 0$ , the cascade limit mass  $Z_\infty$  will have moments of all orders if  $\gamma + \beta < 1$ , and will not if  $\gamma + \beta > 1$ .

Now consider the case  $a > 0$ . Then the minimum value of  $Y$  is given by  $b^\gamma$  (hence the minimum of  $W^+$  is  $b^{\gamma+\beta}$ ) and the maximum value diverges to infinity. Thus such cascades cannot satisfy the conditions on the existence of all moments of the limit mass. These cascades can also fail the non-degeneracy condition. The non-degeneracy condition (see Theorem 3.1a) is

$$\chi_b^{(1)}(1) = \beta - 1 + \gamma \left( 1 - \frac{b^a a \log b}{b^a - 1} \right) < 0. \quad (3.103)$$

This shows that for given  $\gamma$ ,  $a$  and  $b$ , a critical  $\beta_c$  can be defined where for  $\beta \geq \beta_c$ , the non-degeneracy condition will fail, i.e.,

$$\beta_c = 1 - \gamma \left( 1 - \frac{b^a a \log b}{b^a - 1} \right). \quad (3.104)$$

For example, take  $\gamma = -1$ ,  $a = 1$  and  $b = 4$ , then the cascade limit measure is degenerate for

$$\beta \geq \beta_c = 2 - \frac{4 \log 4}{3} = 0.1516\dots \quad (3.105)$$

With regard to applications, as we shall see in Chapter 4, this is a fairly small value of  $\beta$ , so it will pay to be careful of degeneracy when using the log-Poisson model with  $a > 0$ .

The properties of the log-Poisson model may be summarized as follows:

- (a) for  $a \neq 0$ , its positive part  $W^+ = b^\beta Y = b^{\beta + \gamma + aX_\lambda}$  is discrete with an infinite

number of atoms on a finite (if  $a < 0$ ) or infinite (if  $a > 0$ ) support;

(b) if  $a = 0$ , it reduces to the  $\beta$ -model;

(c) for  $a < 0$ , the distribution of the limit mass may or may not have moments of all positive orders (see Theorem 3.1b);

(d) for  $a > 0$ , the distribution of the limit mass fails to have moments of all positive orders;

(e) for  $a > 0$ , the generator may fail the non-degeneracy criterion (Theorem 3.1a);

(f) because  $X$  is Poisson, the distribution of the generator is log-infinitely divisible.

#### 3.4.2.4 The Log-Normal Model

The second example is constructed by again taking

$$Y = b^{\gamma + \sigma X} \quad (3.106)$$

as in equation (3.92), but now  $X$  is a standard Gaussian random variable, i.e., it is Gaussian with zero mean and unit variance, so  $Y$  is lognormal. This model can be thought as having been implicit in the lognormal hypothesis of turbulent energy dissipation of Kolmogorov (1962) and Obhukov (1962). They did not, however, propose their hypothesis within a random cascade framework. Mandelbrot (1972) was the first to use a lognormal random cascade generator, also as a turbulence model, and as a log-Levy generator, it lies in the class of “universal” cascade generators of D. Schertzer and S. Lovejoy (see, for example, Lovejoy and Schertzer (1987)). In none of these previous uses did it include an atom at zero.

The MKP function can be computed as follows. First we compute

$$EY^q = b^{\gamma q} E[b^{q\sigma X}]. \quad (3.107)$$

Now

$$E[b^{q\sigma X}] = E[e^{q\sigma X \log b}] = E[e^{qX'}], \quad (3.108)$$

where  $X'$  is Gaussian with zero mean and variance  $(\sigma \log b)^2$ . Thus  $e^{X'}$  is lognormal and has moments

$$E[e^{qX'}] = e^{(\sigma \log b)^2 q^2 / 2}. \quad (3.109)$$

So we have

$$EY^q = b^{\gamma q + \sigma^2 \log b q^2 / 2}. \quad (3.110)$$

Since  $EW = 1$  implies  $EY = 1$ , we have

$$1 = b^{\gamma + \sigma^2 \log b / 2}, \quad (3.111)$$

so  $\gamma$  can be written in terms of  $\sigma$  and  $b$  as

$$\gamma = -\sigma^2 \log b / 2, \quad (3.112)$$

so

$$EY^q = b^{\frac{\sigma^2 \log b}{2}(q^2 - q)}. \quad (3.113)$$

Thus the distribution of the generator  $W$  is

$$P(W = 0) = 1 - b^{-\beta} \text{ and } P(W = b^\beta Y) = b^{\beta - \sigma^2 \log b / 2 + \sigma X'} = b^{-\beta}, \quad (3.114)$$

with

$$EW^q = b^{-\beta} E[(b^\beta Y)^q] = b^{-\beta + \beta q + \frac{\sigma^2 \log b}{2}(q^2 - q)} \quad (3.115)$$

and MKP function

$$\begin{aligned}
\chi_b(q) &= \log_b EW^q - (q-1) \\
&= (\beta-1)(q-1) + \frac{\sigma^2 \log b}{2}(q^2 - q).
\end{aligned} \tag{3.116}$$

The first two derivatives of the MKP function are given by

$$\chi_b^{(1)}(q) = \beta - 1 + \left( \frac{\sigma^2 (\log b)}{2} \right) (2q - 1) \tag{3.117}$$

and

$$\chi_b^{(2)}(q) = \sigma^2 \log b. \tag{3.118}$$

To determine parameter values under which the conditions of Theorem 3.2 are satisfied, we first need to determine the critical value of moment order  $q_c$  (see Theorem 3.1b). Since  $\chi_b(q)$  is quadratic, it is easy to solve for its zeroes, one of which occurs at  $q = 1$  and the other at

$$q_c = \frac{2(1-\beta)}{\sigma^2 \log b}. \tag{3.119}$$

As would be expected,  $q_c$  increases as  $\beta$  and  $\sigma$  decrease. As noted in the discussion following Theorem 3.2, assuming the cascade is non-degenerate, when  $q_c \leq 2$ , the condition  $EZ_\infty^{2q} < \infty$  governs the satisfaction of the conditions of the theorem. From equation (3.119),  $EZ_\infty^{2q} < \infty$  for

$$q < \frac{q_c}{2} = \frac{1-\beta}{\sigma^2 \log b}. \tag{3.120}$$

When  $q_c > 2$ , on the other hand, the moment ratio condition is the governing condition instead. For the lognormal model, the moment ratio condition (equation (3.42))

reduces to

$$1 - \beta > \sigma^2 (\log b) q^2, \quad (3.121)$$

which shows that it will be satisfied for

$$q < \sqrt{\frac{1 - \beta}{\sigma^2 \log b}}. \quad (3.122)$$

We summarize the properties of the lognormal model as follows:

(a) its positive part  $W^+ = b^\beta Y$  has a continuous density with unbounded positive support;

(b) because of the unbounded positive support of  $W^+$ , the distribution of its limit mass  $Z_\infty$  fails to have moments of all positive orders (see Theorem 3.1b); in fact,  $EZ_\infty^q$  exists only for

$$q < q_c = \frac{2(1 - \beta)}{\sigma^2 \log b}; \quad (3.123)$$

(c) because  $\chi_b^{(1)}(1) = \beta - 1 + \sigma^2 \log b / 2$ , for large enough  $\sigma$ ,  $Z_\infty$  fails the degeneracy criterion  $\chi_b^{(1)}(1) < 0$  (see Theorem 3.1a);

(d) when  $q_c \leq 2$  and the cascade is non-degenerate, the range of non-negative  $q$  in which the scaling of the moments estimates the MKP function by Theorem 3.2 is

$$0 \leq q < \frac{q_c}{2} = \frac{1 - \beta}{\sigma^2 \log b}; \quad (3.124)$$

(e) when  $q_c > 2$ , the range of non-negative  $q$  in which the scaling of the moments estimates the MKP function by Theorem 3.2 is  $0 \leq q < \sqrt{\frac{1 - \beta}{\sigma^2 \log b}}$ ;

(f) because  $X$  is Gaussian, the distribution of the generator is log-infinitely divisible;

- (g) its MKP function has a constant second derivative; and
- (h) it has only one parameter  $\sigma$  in addition to  $\beta$ .

As we will see in the two remaining subsections, writing generators with atoms at zero as the composition of independent generators  $W = BY$ , where  $B$  is a  $\beta$ -model generator and  $Y$  is a positive generator, as we have been doing, also suggests simple ways of defining notions of approximations and homogeneity for sequences of data.

### 3.4.3 A Notion of a $k$ th-order Approximation to an MKP function

As we saw in Section 3.3, the exact MKP function cannot be obtained from finite resolution data even when Theorem 3.2 is applicable. Because of this, we define here a notion of a  $k$ th-order approximation to the actual MKP function, which will be used extensively in the data analysis that follows in Chapter 4.

The basic idea behind the approximation scheme to follow is to construct successively higher order approximations  $\chi_{b,(1)}(q)$ ,  $\chi_{b,(2)}(q)$ ,  $\dots$ , where each  $\chi_{b,(i)}$  is an MKP function, to the true MKP function  $\chi_b(q)$ . We will also make use of two auxiliary ideas. First, because of its connections to the idea of a composition of cascades introduced above, it is convenient to write the  $k$ th-order approximation  $W_{(k)}$  to the true generator  $W$  as the product of  $k$  independent component generators, i.e.,

$$W_{(k)} = \prod_{i=1}^k W_i. \quad (3.125)$$

Notice that  $W_{(1)} = W_1$ . Equation (3.125) also implies, using the definition of an MKP function, that

$$\chi_{b,(k)}(q) = \sum_{i=1}^k \chi_{b,i}(q) + (k-1)(q-1). \quad (3.126)$$

Second, we will characterize the behavior of the true MKP function by its derivatives  $\chi_b^{(j)}(q)$  evaluated at  $q = 1$  because this corresponds to the behavior of its mean.

Because of the constraints on a valid MKP function,  $\chi_b(1) = 0$ ,  $0 < \chi_b(0) \leq 1$ , and  $\chi_b^{(2)}(q) \geq 0$ , general approximation schemes such Taylor series expansion of  $\chi_b(q)$  cannot generally be applied. However, a Taylor series expansion of  $\chi_b(q)$  about  $q = 1$  truncated to first order works quite well for the first-order model,  $\chi_{b,1}(q)$ . Using this idea, we have

$$\chi_{b,1}(q) = \chi_b^{(1)}(1)(q - 1). \quad (3.127)$$

Thus the first-order MKP function is a straight line with slope  $\chi_b^{(1)}(1)$ . Thus the  $\beta$ -model with varying slopes dependent on the value of  $\chi_b^{(1)}(1)$  is the unique choice of a first-order model according to the present definition since, as we have seen, the  $\beta$ -model is the unique random cascade model with straight-line MKP functions. Notice that a first-order approximation, as we have defined it, would map data without zeroes to a  $\beta$ -model cascade and would thus introduce zeroes into the approximate form. Recalling that the dimension of the support of the random cascade measure is given by  $-\chi_b^{(1)}(1)$ , one sees that essentially the first-order approximation is the simplest cascade that preserves the support of the measure.

Consider now a second-order approximation. Using again the idea of extrapolating the behavior near  $q = 1$ , let us assume that  $\chi_{b,(2)}^{(2)}(q)$  is a constant given by  $\chi_b^{(2)}(1)$ . This implies that  $\chi_{b,(2)}(q)$  is quadratic. Assume further that

$$\chi_{b,(2)}(0) = \chi_{b,1}(0) = 1 - \beta, \quad (3.128)$$

so that the second-order component  $W_2$  is a positive random variable and the partitioning between rainy and non-rainy regions continues to be governed by the first-order component  $W_1$ . Then using the general constraint  $\chi_b(1) = 0$  and equation (3.126) gives the MKP function of  $W_2$  as

$$\chi_{b,2}(q) = \chi_b^{(2)}(1)(q^2 - q) - (q - 1), \quad (3.129)$$

which implies from the definition of an MKP function that

$$EW_2^q = b^{\chi_b^{(2)}(1)(q^2 - q)}. \quad (3.130)$$

It is easy to check that this relation is satisfied by taking  $W_2$  to be lognormal, i.e.,  $W_2 = b^{\gamma + \sigma X}$ , where  $X$  is a unit Gaussian random variable. The condition  $EW_2 = 1$  implies that  $\gamma = -\sigma^2 \log b / 2$ , so the second-order component has the distribution

$$W_2 = b^{(-\sigma^2 \log b / 2) + \sigma X}, \quad (3.131)$$

and corresponding MKP function

$$\chi_{b,2}(q) = \frac{\sigma^2 \log b}{2}(q^2 - q) - (q - 1). \quad (3.132)$$

Thus the second-order approximation  $W_{(2)} \equiv W_1 W_2$  of the generator has the distribution

$$P(W_{(2)} = 0) = 1 - b^{-\beta} \text{ and } P(W_{(2)} = b^\beta W_2 = b^{\beta - \sigma^2 \log b / 2 + \sigma X}) = b^{-\beta}, \quad (3.133)$$

and the MKP function

$$\chi_{b,(2)}(q) = (\beta - 1)(q - 1) + \frac{\sigma^2 \log b}{2}(q^2 - q). \quad (3.134)$$

Thus the second-order approximation is just the lognormal model discussed above.

Following the philosophy of looking at the behavior near  $q = 1$ , the parameters of the models can be estimated from the derivatives at  $q = 1$ . For the first-order model we set

$$\chi_{b,1}^{(1)}(q) = \hat{\tau}^{(1)}(1)/d, \quad (3.135)$$

and for the second-order model

$$\chi_{b,(2)}^{(2)}(q) = \chi_{b,2}^{(2)}(q) = \sigma^2 \log b = \hat{\tau}^{(2)}(1)/d \quad (3.136)$$

and

$$\chi_{b,(2)}^{(1)}(q) = \beta - 1 + \frac{\sigma^2 \log b}{2}(2q - 1) = \hat{\tau}^{(1)}(1)/d. \quad (3.137)$$

Notice that  $\beta$  estimated for a second-order approximation using equation (3.137) would differ from that estimated by equation (3.135) for a first-order approximation for the same value of  $\hat{\tau}^{(1)}(1)/d$ .

To extend this notion of approximation beyond the second order presents difficulties. For example, for the third order, one expects a third-order polynomial MKP function. However, MKP functions must be convex for all  $q$ , which third-order polynomials generally are not. Perhaps the proper direction for generalization is to keep the number of parameters at two, but to vary the exponent of the term which is here quadratic. This would lead to a class of generators similar to those used by S. Lovejoy, D. Schertzer and coworkers, so-called “universal cascades” (see, e.g., Tessier et al. 1993). This class includes the lognormal model (without zeroes) as the member with a quadratic MKP function and the  $\beta$ -model. The difference is that “universal cascades” do not in general have atoms at zero (in fact, only the  $\beta$ -model does). Their view is that regions of zero rain rate that are observed in data may be thought of in their modeling framework as regions where the rain rate is simply extremely small (Y. Tessier, personal communication). I believe that this view is incorrect on the grounds that such regions are not anything like the regions of zero rain rate actually observed in

data. In data, the regions of zero rain rate are finite-sized; in the “universal” model, regions of “very small rain rate” are fractal sets, i.e., they have zero area.

### 3.4.4 A Notion of $k$ th-order Generator Homogeneity

In view of the data we are about to analyze, it is useful to propose a notion of  $k$ th-order generator homogeneity, which is closely related to the notion of  $k$ th-order approximation which was just defined. Consider the following situation. Given a data set, i.e., a sequence of instantaneous spatial measures taken at times  $t_i$ ,  $i = 1, 2, \dots, n$ . We just showed that by examining the derivatives of the  $\tau(q)$  function evaluated at  $q = 1$  we could obtain a series of approximations to the true MKP function of the generators  $W^i$  of the spatial measures in the sequence of data. Writing  $W^i$  in the form (3.125), the results would be particularly simple and useful if there was an order of approximation  $k^*$  beyond which (i.e., for  $k \geq k^*$ ) the estimated generators  $W_k^i$  did not depend on  $i$ ; i.e., the  $k$  and higher order generators were constant. We will call this property of a sequence of spatial measures  *$k$ th-order generator homogeneity*, and will say that any sequence having it is  *$k$ th-order generator homogeneous*.

We will see that second-order generator homogeneity holds in the data rather well. Hence we will write the sequence of generators for the data set as

$$W^i = B^i Y, \quad (3.138)$$

which shows that all the variation in the generators  $W^i$  arises from variation in the  $\beta$ -model generator  $B^i$ ; the positive generator  $Y$  is invariant.

Notice that  $k$ th-order generator homogeneity does not in general require  $k$ th-order approximate generators  $W_{(k)}^i = \prod_{j=1}^k W_j^i$ , it merely requires that the  $k$ th and higher order generators are invariant. Because of this, it does not require any specific form for the generators  $W_j^i, j \geq k^*$ . For example, consider  $W^i = B^i Y^i$ , where the  $Y^i$  are log-Poisson. Now since in this case  $\chi_{b,Y}^{(2)}(q)$  varies with  $q$ ,  $W^i$  is not in this case second-or-

der, i.e., it is not fit perfectly by a second-order approximation  $W^i = B^i Y^i$  where  $Y^i$  is lognormal, but it could still be second-order generator homogeneous, as long as the  $Y^i$  do not vary with  $i$ .

## **Chapter 4**

# **Applications of the Theory of Random Cascades to Spatial Rainfall**

### **4.1 Introduction**

The purpose of this chapter is to apply the theory of random cascades developed in Chapter 3 to sequences of spatial rainfall to test the applicability of the random cascade theory to spatial rainfall. First, in Section 4.2, the rainfall data to be used in testing the theory is described. Then in Section 4.3, a method used to simulate “off-grid” cascades used for comparison with data is discussed. In Section 4.4 the random cascade theory is tested against the data, using the theory developed in Chapter 3 and the aforementioned simulations. Given that the theory is found to be applicable, we will estimate parameters and test the notion of second-order generator homogeneity in Section 4.5. This sequence of parameter estimates then forms the database from which to study the dependence of the spatial pattern, captured in the parameter estimate sequence, against a measure of large-scale forcing of the rainfall, the large-scale average rain rate. This study is carried out and interpreted in Section 4.6.

### **4.2 Description of Data**

The primary data set used to test the spatial cascade theory here is radar rain rate data from the Global Atmospheric Research Program Atlantic Tropical Experiment (GATE), phases I and II. The GATE radar data was obtained from by ships stationed in the tropical Atlantic off west Africa (centered at  $8^{\circ}30'$  N. latitude and  $23^{\circ}30'$  W.

longitude) in the summer of 1974, and is nominally available every fifteen minutes, although there are brief gaps in the record. Phase I lasted from June 28 to July 16 and the radar data consists of 1713 scans; phase II lasted from July 28 to August 15 and has 1512 scans of radar data. Such a sheer quantity of processed radar rainfall data is seldom available. For these phases of the experiment, the radar data was primarily obtained from one C-band (approximately 10 *cm* wavelength) radar stationed at the center of the experimental region, with another C-band radar used to fill in regions where the primary radar had an obstructed view.

The processing of the GATE radar data is described in detail in Patterson et al. (1979). A general introductory guide to radar rainfall data is given by Collier (1989). As with any such data set, two primary transformations are required, one to convert the radar returned signal (reflectivity) into rainfall rates, and the other to convert from the original spherical coordinates of the radar into a Cartesian coordinate system that is amenable to analyses such as are performed here. The reflectivity-rain rate conversion is performed using a “*Z-R* relationship”, in this case,

$$R = 0.013Z_e^{0.8}, \quad (4.1)$$

where  $R$  is rainfall rate in  $mm/hr$  and  $Z_e$  is the “equivalent reflectivity factor” in units of  $mm^6 m^{-3}$ . The equivalent reflectivity factor is defined as “the summation per unit volume of the sixth power of the diameter of spherical water drops in the Rayleigh scattering region which would back scatter the same power as the measured reflectivity” (Collier 1989, p. 25), which explains the units as diameter in  $mm$  to the sixth power divided by volume in  $m^3$ . The Rayleigh scattering region obtains when the radar wavelength is much larger than the rain drop diameter, e.g., for diameters smaller than 3.2  $mm$  for C-band radars (Collier 1989, p. 25). The conversion to Cartesian coordinates is performed using the interpolation scheme described in Patterson et al. (1979)

and results in a circular array of square pixels with a side length of 4 *km*. The diameter of the circular array is 100 pixels. Beyond the two primary transformations, corrections for a variety of sources of attenuation were performed.

In order to provide some preliminary sense of the applicability of the results obtained by testing the cascade theory on the GATE radar data to continental convective rainfall, we also make use of some radar data from a C-band radar located at Elbow, Saskatchewan, between Saskatoon and Regina. This radar is operated by the Atmospheric Environment Service (AES) of Canada and the data was kindly provided by R. L. Lawford of the AES. This data was converted by the AES into a square array 120 pixels on a side, each pixel being square with a side length of 2 *km*. The *Z-R* relationship used for this data was

$$Z_e = 200R^{1.6}, \quad (4.2)$$

which corresponds to

$$R = 0.005Z_e^{0.625}, \quad (4.3)$$

in the same units as equation (4.1) above.

### 4.3 A Method for Constructing Homogeneous and Isotropic Cascades

Three kinds of difficulties are discussed in Section 3.4 that arise from the discreteness in space and scale of the method of constructing the random cascades for which the theory is presented in Chapter 3. One of them, the arbitrariness of the branching number, can be overcome by the use of log-infinitely divisible generators. The effects of having “off-grid” data to compare to an “on-grid” theory can be partially accounted for by the use of simulations of discrete random cascades, as will be discussed below. However, as will also be noted, this method is not completely satisfactory and such

cascades remain nonhomogeneous and anisotropic. To remove these properties, cascades must be constructed using a homogeneous and isotropic method of spatial subdivision. The main purpose of this section is to present such a method and discuss the simulation of cascades via the method. Cascades simulated by this method will often constitute “the theory” in the subsequent sections in which the random cascade theory is compared with spatial rainfall data.

The essence of “off-grid” data, even if it came from a standard discrete cascade, is that the sampling method included no knowledge of the location and orientation of the boxes used to subdivide space when constructing the cascade. The effect of lack of knowledge of the location of the boxes is easy to test using computer simulations as follows.

(a) Simulate a standard discrete random cascade down to a relatively high resolution using some branching number  $b_d$  (the subscript  $d$  signifies “down”.) For example, take  $b_d = 4$  in two dimensions and simulate down to  $n_d = 10$  levels, giving a cascade of  $\sqrt{b_d^n} = 1024$  pixels on a side.

(b) Select randomly a square subset of the cascade of size  $\sqrt{b_d^{n-1}}$ . Thus for the example above, one would randomly locate a square subset 512 pixels on a side.

(c) Select an “on-grid” square subset also of size  $\sqrt{b_d^{n-1}}$ . For  $b_d = 4$ , this would mean choosing one of the four quadrants of the cascade at level  $n_d$ .

(d) Compare the  $\tau(q)$  function (or any other quantity of interest) obtained from the subset selected in step (b) with that obtained from the subset selected in step (c).

A selection of the “on-grid” and “off-grid” subsets is illustrated for  $b_d = 4$  and  $n_d = 3$  in Figure 4.1.

A variant of this approach uses a randomly located square subset of a size corresponding to an integer multiple of a different branching number  $b_u$  (the subscript  $u$

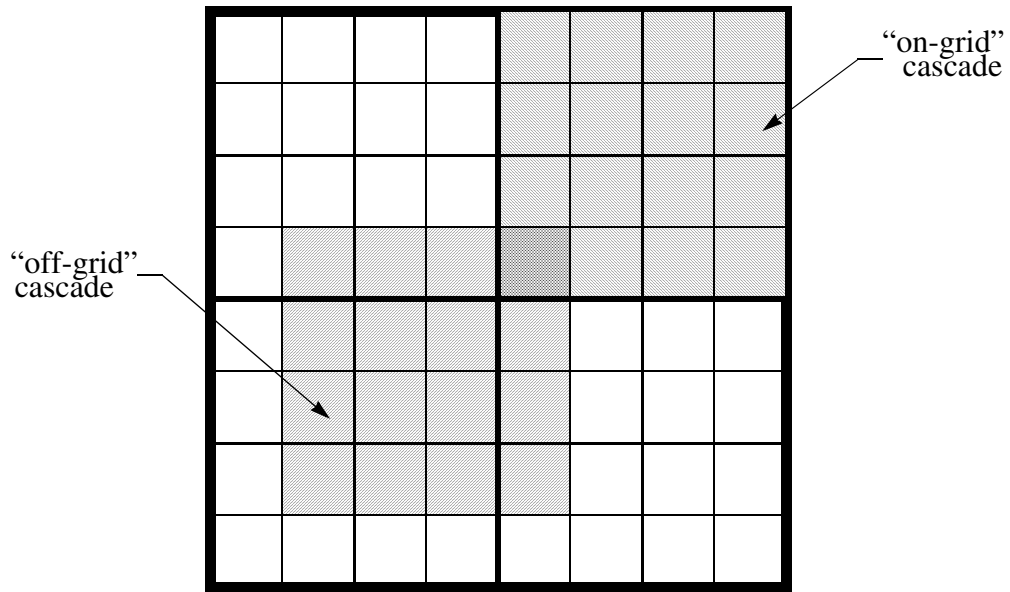


**Figure 4.1** Schematic of “on-grid” versus “off-grid” cascades

signifies “up”). For the example in step (a) above, one could take  $b_u = 9$  and select a random subset 729 pixels on a side, and average over the boxes six times, since  $\sqrt{b_u^6} = 729$ . Then comparison of the scaling properties requires an adjustment for the effect of changing the branching number, which presumes the use of a log-infinitely divisible generator.

The effect of random orientation of boxes obviously cannot be simulated by such a method. However, this is not a great concern because next we present a method of simulating homogeneous and isotropic cascades, which by definition lack preferred locations or orientations.

The homogeneous and isotropic cascade simulation method we present may be thought of as a discrete form of the lognormal cascade simulation method used by Mandelbrot (1972), which is presented more clearly in Mandelbrot (1983, pp. 379-380). In this method, one generates a cascade by multiplication of lognormal random fields, i.e., the martingale sequence  $Q_n(x)$  (see equation (3.15)) is composed of the

product of random factors  $P_1(x), \dots, P_n(x)$ , where  $P_i(x) = e^{X_i(x)}$ ,  $i = 1, \dots, n$ , and  $X_i(x)$  is a homogeneous Gaussian random field, with mean one and some variance  $\sigma^2$ . To completely specify the random field requires additionally the spatial structure of the variance. This can be specified by assuming isotropy and a correlation length. It is the correlation length alone that varies with scale, as can be seen to be appropriate by considering the random field  $P_n(x)$  that one obtains from a discrete random cascade at level  $n$ . In this case, the value of the random field is different in every box, so it has a correlation length on the order of the box size,  $b^{-n/2}$  in two dimensions. So Mandelbrot assigns an exponential decay of correlation with characteristic length  $b^{-n/2}$ , i.e., the covariance is taken to be  $\sigma^2 e^{-|\tau|/b^{-n/2}}$ . It should be noted that Kahane (1985) has analyzed this construction and verified that certain results conjectured by Mandelbrot (such as the Hausdorff dimension of support of the measure and the degeneracy criterion) carry over from the discrete case to this one, showing that certain basic aspects of the theory of such cascades are the same as that of discrete cascades.

One could imagine generalizations of this method by taking  $X_i(x)$  to be other kinds of finite variance random fields, such marginally gamma-distributed, or infinite variance fields. As noted in Chapter 3, the “universal generators” employed by D. Schertzer and S. Lovejoy employ a whole family of such random fields, which are constructed from (extremal) log-Levy stable distributions, of which the Gaussian distribution is the only finite variance case.

Here we generalize Mandelbrot’s construction in a direction which is determined by the properties of rainfall fields. In Chapter 3, the zeroes of rainfall fields are incorporated into discrete random cascades by allowing the generators to have an atom at zero. To incorporate this effect into the present context where we are specifying the whole field  $P_n(x)$  at once, we assume that the marginal distribution of  $P_n(x)$  also has an atom at zero that results from regions that are zero, and that the marginal distribu-

tion need not be supported on a connected set (take, for example, the marginal distribution of  $P_n(x)$  to be the  $\beta$ -model). The latter fact precludes  $P_n(x)$  being a continuous function, and the existence of regions that are zero suggests that the appropriate way to construct  $P_n(x)$  is to perform a discrete but nevertheless homogeneous and isotropic subdivision of space and assign iid realizations of a random cascade generator to each subdivision. In order to maintain the increasing variability of  $P_n(x)$  as  $n$  increases, the spatial subdivision must have a decreasing characteristic length  $\lambda = b^{-n/2}$  (in two dimensions).

A classic way of subdividing the plane homogeneously and isotropically into discrete regions of some characteristic size is through the use of Voronoi tessellations “generated” by a homogeneous and isotropic point process. If we designate the set of points in some bounded region  $J$  of the plane arising from such a point process by

$$P = \{p_1, p_2, \dots, p_n\}, \quad (4.4)$$

where the locations of the points,  $x_i$ ,  $i \in I_n = \{1, \dots, n\}$  are distinct and  $2 \leq n \leq \infty$ , then the Voronoi tessellation induced by  $P$  is the set of polygons

$$V = \{V(p_1), V(p_2), \dots, V(p_n)\} \quad (4.5)$$

where

$$V(p_i) = \{x \mid \|x - x_i\| \leq \|x - x_j\| \text{ for } i \neq j, i \in I_n\} \quad (4.6)$$

(Okabe et al. 1992, p. 67). In other words, the polygons  $V(p_i)$  consist of the points in the plane that are closest to  $p_i$ . An example is shown in Figure 4.2. Notice that there are points in the plane that are equidistant from two or more generator points in  $P$ . These constitute the boundaries or edges of the polygons and are included in two or more polygons. Also notice that some of the polygons will have infinite area, since we

are subdividing the whole plane, and that the polygons are convex sets.

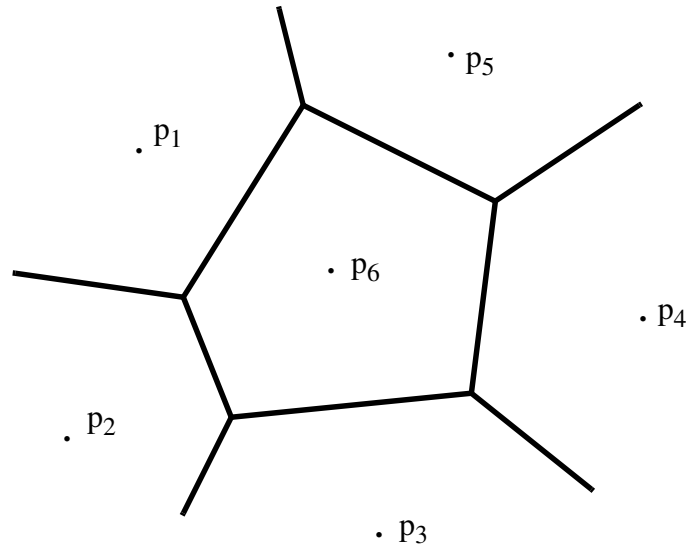


Figure 4.2 The Voronoi polygon of a point

The point process from which the points  $P$  that generate the polygons are obtained must be homogeneous and isotropic so that the tessellation it generates and the random fields  $P_n(t)$  are also homogeneous and isotropic. We will consider two examples with these properties, the binomial point process and the Poisson point process.

The binomial point process can be thought of as the process by which a fixed number, say  $m$ , of points are located independently with the uniform distribution over some bounded subset  $J$  of the plane (Okabe et al. 1992, pp. 56-57). Just as on some interval  $[a, b]$  the density of the uniform distribution is given by

$$f(x) = \frac{1}{b-a}, \quad (4.7)$$

the uniform distribution on  $J$  has the density

$$f(x) = \frac{1}{\|J\|}, \quad (4.8)$$

where  $\|J\|$  denotes the area of the set  $J$ . The binomial point process is so-called because it has the property that the number of points in a subset  $S$  of  $J$ , denoted  $N(S)$ , has the binomial distribution with  $m$  trials and success rate  $\theta = \|S\|/\|J\|$ . The *intensity* of a point process, which we designate by  $\nu$ , is defined as the expected number of points per unit area, so over some  $S \subseteq J$  we have  $\nu = m\theta/\|J\|$ . The problem with the binomial point process is that it does not extend homogeneously to regions outside  $J$ . Consider a region  $T$  disjoint from  $J$  such that  $\|T\| \neq \|J\|$ . In order to have a homogeneous process, the intensities  $\nu_T$  in  $T$  and  $\nu_J$  in  $J$  must be equal. But since  $\nu_T = m_T/\|T\|$  and  $\nu_J = m_J/\|J\|$ , where  $m_T$  and  $m_J$  are positive integers,  $\nu_T = \nu_J$  requires

$$\frac{m_T}{m_J} = \frac{\|T\|}{\|J\|}. \quad (4.9)$$

But since  $\|T\|$  and  $\|J\|$  are not necessarily integers, it is not in general possible to satisfy equation (4.9) nor  $\nu_T = \nu_J$ .

The Poisson point process resolves the above difficulty by making the number of points in  $J$  no longer fixed at  $m$  but random, with a Poisson distribution with parameter  $m$ . Then the intensity  $\nu$  is given by  $m/\|J\|$ , and in any subset  $S$  of  $J$  the number of points  $N(S)$  has a Poisson distribution with parameter  $m\|S\|/\|J\|$ . Notice that unlike in the binomial point process, in an arbitrary region  $T$  disjoint from  $J$  we can have the same intensity, by taking the number of points to be selected from the Poisson distribution with parameter

$$\nu\|T\| = m\|T\|/\|J\|. \quad (4.10)$$

Because of this property, we will use the Poisson point process to generate Voronoi tessellations of the portions of the plane on which the homogeneous and isotropic cascades are simulated. Notice we can define the characteristic length of the polygons generated by a point process of intensity  $\nu$  as  $\lambda = \nu^{-1/2}$ , since  $\nu^{-1}$  is the expected

area of each polygon.

Thus the basic construction of homogeneous and isotropic random cascades to be employed here is as follows:

(a) Define a region  $J$  of the plane on which to construct the cascade; we will usually use a square region of side length  $l_{max}$ , say,  $J = [0, l_{max}]^2$ .

(b) Choose some branching number  $b > 1$  (not necessarily an integer).

(c) At each level  $n$ , simulate points from a Poisson point process with intensity  $\nu = b^n$  such that the characteristic size of the polygons generated by the points will be  $\lambda = b^{-n/2}$ . Do this sufficiently far beyond the boundary of  $J$  (say, a few characteristic lengths) such that edge effects (e.g., the infinite polygons in Figure 4.2) do not affect the region inside  $J$ .

(d) Construct the Voronoi polygons associated with the points of the Poisson point process.

(e) Construct the random field  $P_n(x)$  on  $J$  by assigning an iid realization of a cascade generator  $W$  (with a log-infinitely divisible generator) to each polygon.

(f) Construct the martingale sequence  $Q_n(x) = \prod_{i=1}^n P_i(x)$ .

The construction outlined above satisfies the requirements we have stated, but the discreteness of the random fields  $P_n(x)$  introduces an unforeseen difficulty. Because the subdivision of space at each level is independent of that at the other levels, the product of the  $P_n(x)$ ,  $Q_n(x)$ , has a very fragmented set where  $Q_n(x) = 0$ . The problem with the set where  $Q_n(x) = 0$  is that the overlap of independent polygons from different scales leads to lots of regions where  $Q_n(x) = 0$  that have length scales much smaller than  $\lambda = b^{-n/2}$ .

In view of this, the construction outlined above was modified to prevent this problem by tessellating the plane in the standard manner at the first level only, followed by

“sub-tessellations” at subsequent levels. A sub-tessellation takes each polygon in a tessellation, simulates a (modified) Poisson point process over it, and subdivides the polygon into “sub-polygons” essentially by a Voronoi tessellation of the region inside the polygon. An example of the sub-tessellation of a polygon is shown in Figure 4.3. The sub-tessellation is generated by a modified Poisson point process because the number of points inside the polygon tells how many sub-polygons into which to divide it. Thus one point means no subdivision and zero points has no meaning. Thus the number of points must come from a distribution that excludes zero. This is accomplished by taking the number of points to be  $1 + M$ , where  $M$  is a Poisson random variable with parameter

$$m = \nu \|S\| - 1 = b^n \|S\| - 1, \quad (4.11)$$

where  $\|S\|$  is the area of the polygon  $S$ . Notice that to sub-tessellate the original square  $J = [0, l_{max}]^2$  would destroy the isotropy of the cascade, since the boundaries of  $J$  have fixed orientations.

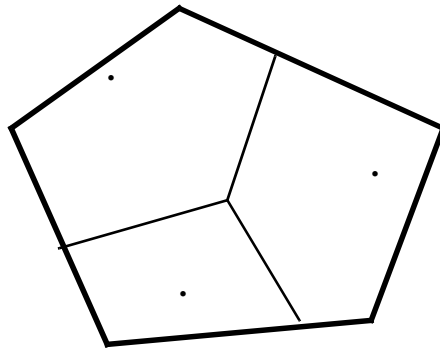


**Figure 4.3** The sub-tessellation of a Voronoi polygon into sub-polygons

## 4.4 Tests of the Random Cascade Theory

### 4.4.1 Tests of the Theory Using the Scaling of Marginal Moments

We first test the scaling of the marginal moments of the spatial rainfall field. As described in Section 3.3 (see equation (3.46)), the random cascade theory predicts that the moments of the field versus the length scale of the boxes over which it is integrated will be log-log linear. In order to provide a quantitative measure of the “goodness” of the log-log linear fit, a measure of the error of the weighted linear regression fit is computed and compared to the same quantity computed from off-grid simulations. A more informative test is provided by comparing the intercepts of the log-moment versus log-scale relationship obtained from data versus those obtained from simulations. This test is more informative than the linearity test because the direction of the deviation from the theoretical result gives information about the scaling of the data.

Because our primary data set is that from the GATE experiment, for which the largest  $2^n$  by  $2^n$  set of pixels is 64 by 64, we use 64 by 64-pixel (actually, a 64 by 64-pixel grid laid over a homogeneous and isotropic cascade simulated by the means described in the previous section)  $\beta$ -model simulations for comparison purposes, of which 400 were simulated with  $\beta$  values,

$$\beta_i = 0.0025i + 0.00125, \quad i = 0, \dots, 399, \quad (4.12)$$

so the  $\beta$  values are evenly spaced between 0.00125 and 0.99875. A  $\beta$ -model generator was used in order to avoid questions of generator type and parameter values. In any case, the quantities used in this section that were obtained from simulations were found to be relatively insensitive to the distribution of the positive part of the generator.

The linear regression of the log of the moments versus the log of the scale is performed by the method of least squares. A weight function

$$w_n = b^n \quad (4.13)$$

was applied in order to cause the small-scale values to determine the line. It is given this form because the number of boxes grows in that way. The optimal method for determining the weight function is not available because the variance of the slope of the regression as a function of the weighting scheme is not known.

The first test we apply concerns the “goodness” of the fit of the linear regression to the data. This is measured by a quantity we will call the “standard error”  $S(q)$ . It is a function of the moment order  $q$ , and is defined as follows:

$$S(q) = \sqrt{n_{max}^{-1} \sum_{n=0}^{n_{max}} (\hat{y}_n(q) - \log M_n(q))^2 w_n}, \quad (4.14)$$

where  $n$  is the cascade level,  $\hat{y}_n(q)$  is the weighted least squares fit to  $\log M_n(q)$ ,  $M_n(q)$  is the  $q$ th moment of the rainfall data at level  $n$ ,  $w_n$  is the weighting function defined above, and  $n_{max}$  is the maximum level in the data (here  $n_{max} = \log_2 64 = 6$ ).

In Figures 4.4 and 4.5 the standard error  $S(q)$  for  $q = 0$  and  $q = 2$ , respectively, are plotted against the estimate of  $\tau(q)$  (the regression slope) for the  $\beta$ -model simulations and the data from GATE phases I and II. The simulations and GATE data show similar behavior for  $q = 0$ ; for  $1 < \tau < 2$ , the standard error is small (on the order of one or smaller), while for  $0 < \tau < 1$ , much larger values are sometimes (often in the case of the simulations) obtained. This trend in error as a function of  $\tau(0)$  is to be expected, since  $\tau(0) = 2$  corresponds to a scene completely full of rain, while  $\tau(0) = 0$  indicates only a single pixel with rain at each scale. It is curious however that the simulations tend to have larger standard errors in the small  $\tau$  range. Note that  $q = 0$  treats each box with mass the same, effectively giving them all unit mass, so the  $q = 0$  analysis is an analysis of the rainy versus non-rainy area. Because of this, one issue

that will need to be kept in mind when  $q = 0$  is the effect of data processing on the rainfall field, because of the classic difficulty of distinguishing small rain rates from zero. We will spend considerable time in this chapter with further analyses of the  $q = 0$  scaling. So for now, as a preliminary conclusion, we may evidently take it that the standard error analysis for  $q = 0$  provides no strong evidence that the hypothesis that the rainfall field is a random cascade needs to be rejected.

When  $q = 2$ , the GATE rainfall fields tend to have somewhat larger standard errors than the simulations, especially in the region around  $\tau(2) = -1.5$  where most of the GATE rainfall scans cluster, though not by a large amount. Since taking  $q = 2$  emphasizes the larger values of the measure, it might be thought that the choice of the positive part of the cascade generator might affect the standard error for  $q = 2$ , but examination of standard errors from other simulations indicates that the differences are very slight.

The second test concerns the intercepts of the log-log linear fits. As shown in Section 3.3 (equation (3.47)), the intercepts  $I(q)$  are given by

$$I(q) \approx \log Y(q) + q \log \mu_0(J) + \log EZ_\infty^q. \quad (4.15)$$

It is useful to think of the intercepts as providing a realization of  $\log Y(q)$ , but since  $\log EZ_\infty^q$  depends on  $b$  and hence can't really be estimated, we keep  $\log Y(q)$  and  $\log EZ_\infty^q$  together and re-write equation (4.15) as

$$\log Y(q) + \log EZ_\infty^q \approx I(q) - q \log \mu_0(J), \quad (4.16)$$

where the initial mass term  $q \log \mu_0(J)$  is estimated by

$$q \log \mu_0(J) = q \log (R_0 l_{max}^2) \approx q \log (\bar{R} l_{max}^2) \quad (4.17)$$

(from equation (3.48)).

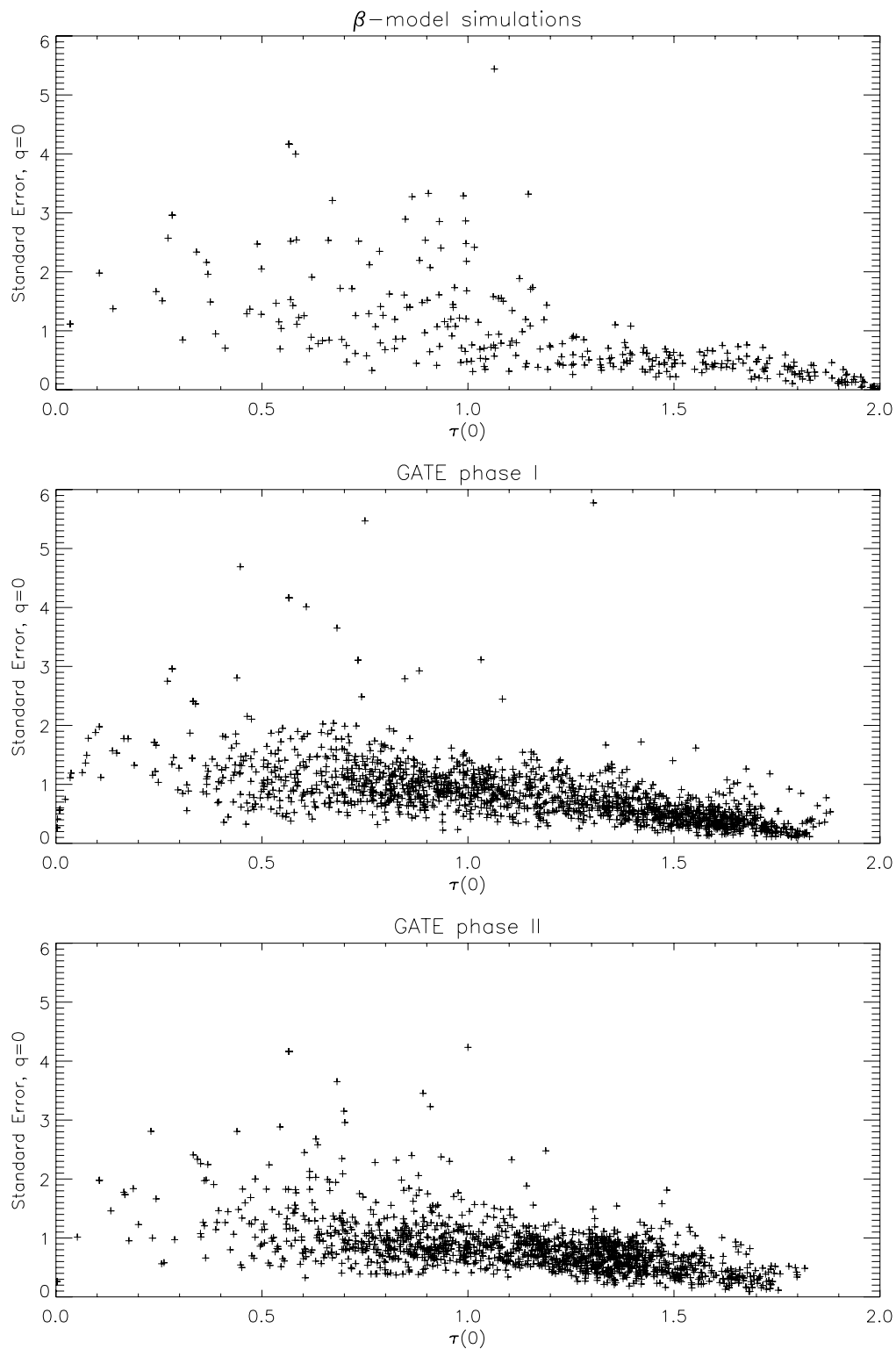


**Figure 4.4** Standard error of scaling of moments of spatial rainfall,  $q=0$

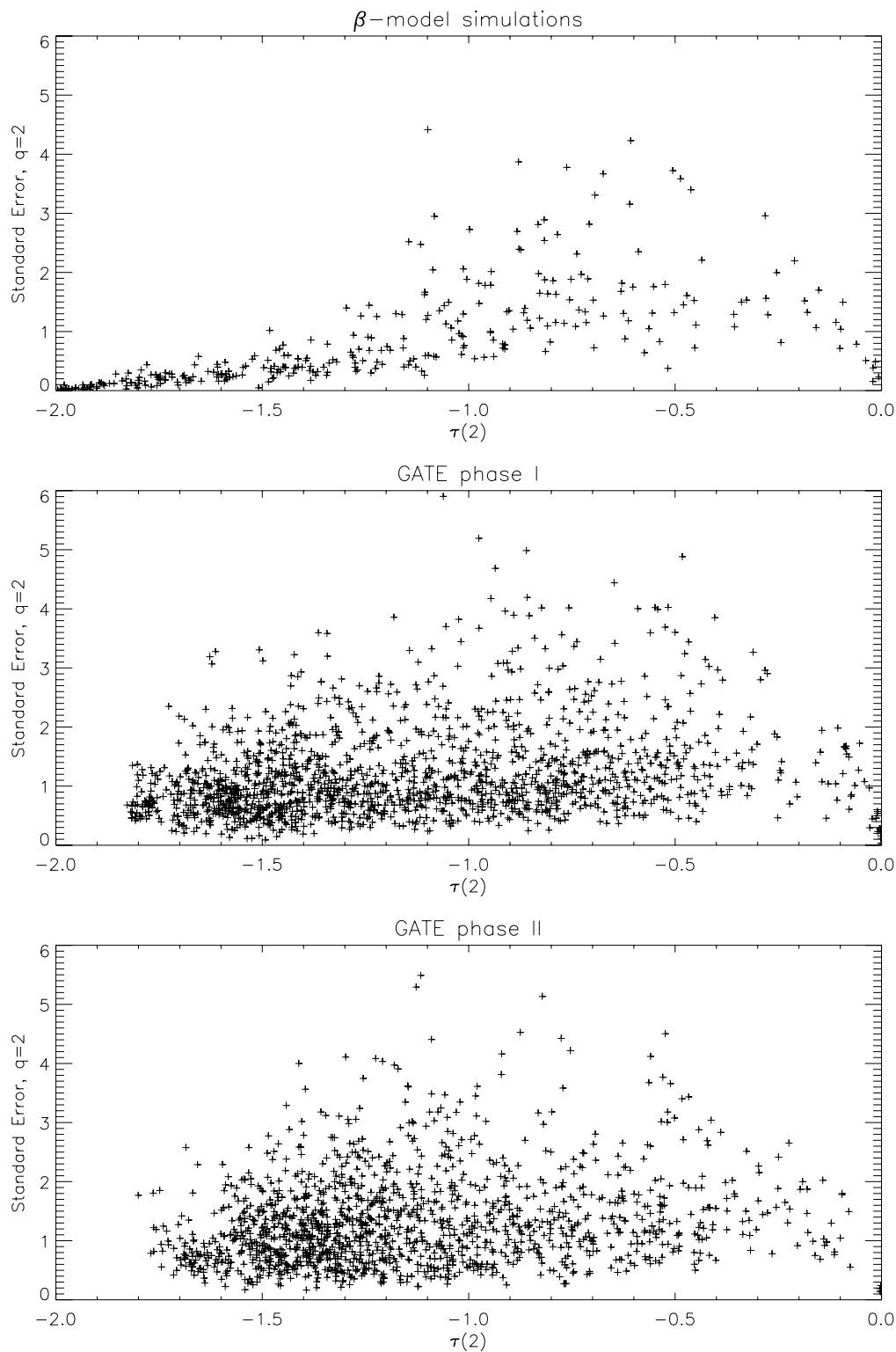


**Figure 4.5** Standard error of scaling of moments of spatial rainfall,  $q=2$

To provide some idea of what is going on with the  $\log EZ_\infty^q$  term, one can assume a value of  $b$  and a generator and compute the quantity  $\log EZ_\infty^q$ . For  $q = 0$ ,  $EZ_\infty^q = P(Z_\infty > 0)$ , for which a formula is given in Chapter 3 (equation (3.83)). From Appendix C,  $EZ_\infty^2 = (b - 1)/(b - EW^2)$ . Since  $b = 4$  is used in the data analysis and the simulations are for the  $\beta$ -model, we made those assumptions on branching number and generator and produced Figure 4.6. We will comment on the results given in Figure 4.6 as the need arises.

Before proceeding to the data analysis, we make one more adjustment to equation (4.16). The data we use is actually rain rates averaged over boxes of size  $l_{min}^2$ , i.e., we have  $l_{min}^2 R_\infty(\Delta_{n_{max}}^i) = \mu_\infty(\Delta_{n_{max}}^i)$ . So if the sum  $M_n(q)$  is written in terms of rain rates, we obtain

$$M_n(q) = \sum_{i=1}^{b^n} \mu_\infty^q(\Delta_n^i) = l_{min}^{2q} \sum_{i=1}^{b^n} R_\infty^q(\Delta_n^i), \quad (4.18)$$

which introduces an additional term  $q \log l_{min}^2$  into the intercept of log-log plots, in which case equation (4.16) becomes

$$\begin{aligned} \log Y(q) + \log EZ_\infty^q &\approx I_R(q) - q \log(\bar{R} l_{max}^2) + q \log l_{min}^2, \\ &\approx I_R(q) - q \log(\bar{R} b^{n_{max}}) = I_N(q), \end{aligned} \quad (4.19)$$

since  $l_{min}^2/l_{max}^2 = b^{-n_{max}}$ . The notation  $I_R(q)$  is introduced to denote intercepts obtained when using rain rates as the data. The quantity  $I_R(q) - q \log(\bar{R} b^{n_{max}})$  is given the shorthand  $I_N(q)$  because these can be thought of as ‘‘normalized’’ intercepts. Notice that when the data is rain rates, we have

$$\frac{M_0(q)}{(\bar{R} b^{n_{max}})^q} = \frac{(\sum_i R_i)^q}{(b^{-n_{max}} (\sum_i R_i) b^{n_{max}})^q} = 1. \quad (4.20)$$

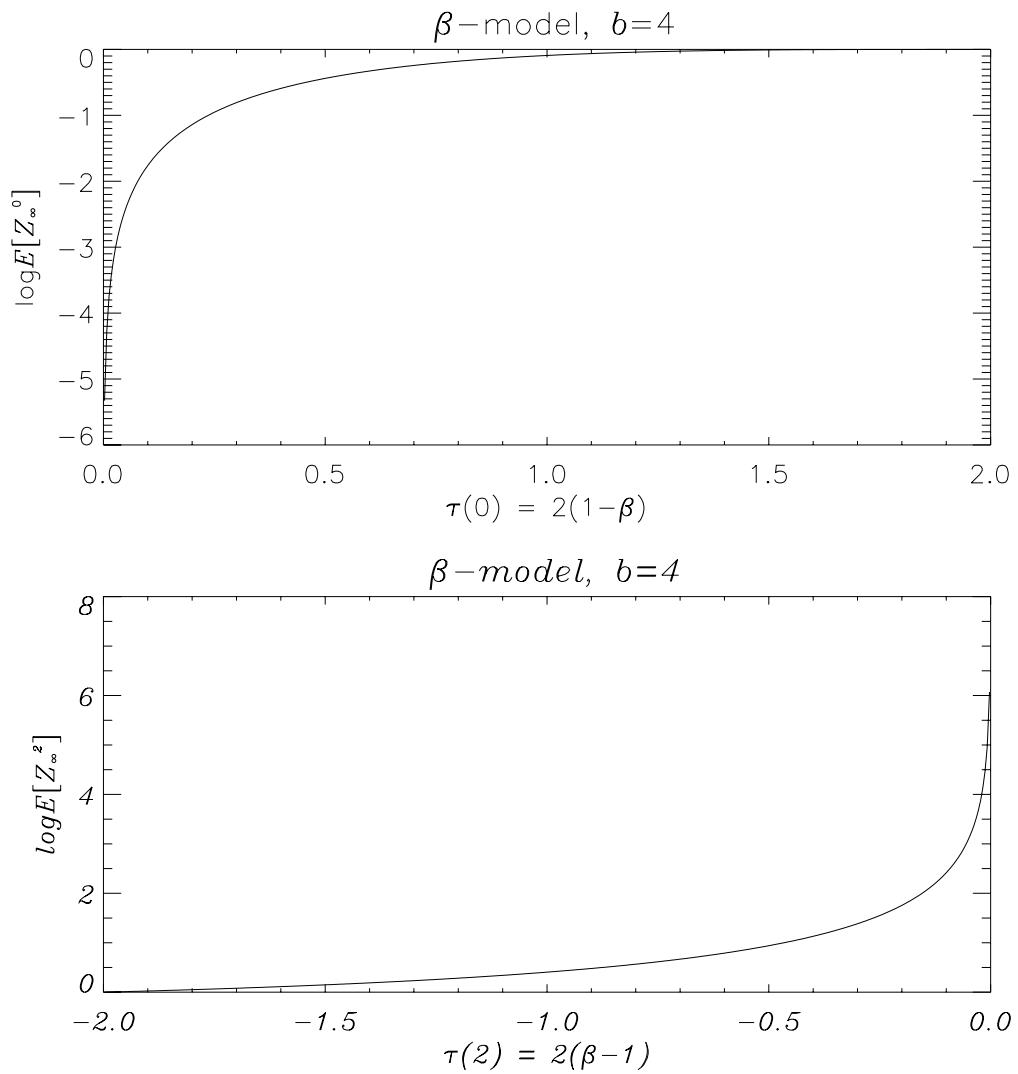


**Figure 4.6** Logarithm of moments of limit mass for the beta model,  $b=4$

This fact will be useful in interpreting the results.

Figures 4.7 and 4.8 contain the same set of plots as Figures 4.4 and 4.5, but for the normalized intercepts  $I_N(q)$  instead of slopes. Consider the simulation results first.

These confirm the conjecture made in Section 3.3 that  $\log Y(q)$  would be centered around zero. This is seen most clearly near the values for the rain-filled scene,

$\tau(0) = 2$  and  $\tau(2) = -2$ . Notice from Figure 4.6 that  $\log EZ_\infty^q$  is likely quite small in

this region. For  $q = 0$ , moving away from  $\tau(0) = 2$ , there appears to be a weak upward trend as a function of  $\tau$ . The plots from the data have similar but stronger trends, and do not appear to have  $\log Y(q) = 0$  for the rain-filled scenes as the simulations do. In fact, for  $q = 0$ , the  $\tau(0) = 2$  asymptote appears to be negative, and the intercepts grow as  $\tau$  decreases, passing through zero in the neighborhood of  $\tau(0) = 1.7$ . On the other hand, for  $q = 2$ , the  $\tau(2) = -2$  asymptote is positive for the data, and the  $\log Y(q)$  estimate decreases as  $\tau$  increases, passing through zero in the neighborhood of  $\tau(2) = -1$ .

We will use the schematics in Figure 4.9 to help interpret these results. As can be seen there, failure for the fitted log-log linear curves to pass through or near the point  $M_0(q)/(Rb^{n_{max}})^q = 1$  signals imperfect scaling of the moments. Because of the weighting of the regression, the standard error is quite sensitive to the scaling of the moments at smaller scales, but not at the larger scales. Thus the intercepts are important in measuring whether the scaling that is obtained at the smaller scales holds through to the larger scales. This sort of information is very important, because if random cascades or some other scale-invariant theory is to apply to rainfall in any meaningful or useful sense, it needs to apply over a range of scales. The most reasonable default hypothesis is that a significantly non-zero intercept indicates a failure of scaling, unless another explanation can be found.

But the deviations of the simulations from perfect scaling, defined by the zero normalized intercept criterion, while not as great as those in the data, suggest that there are indeed other at least partial explanations of this behavior. First, as already described, the theory actually indicates that the intercepts will on average deviate from zero by the amount of the  $\log EZ_\infty^q$  term, which we have neglected. Figure 4.6 provides an estimate of the size of this term. In the case of  $q = 0$ , this term is negative but small for all but the smallest values of  $\tau$ . The trend in the intercepts of the data is

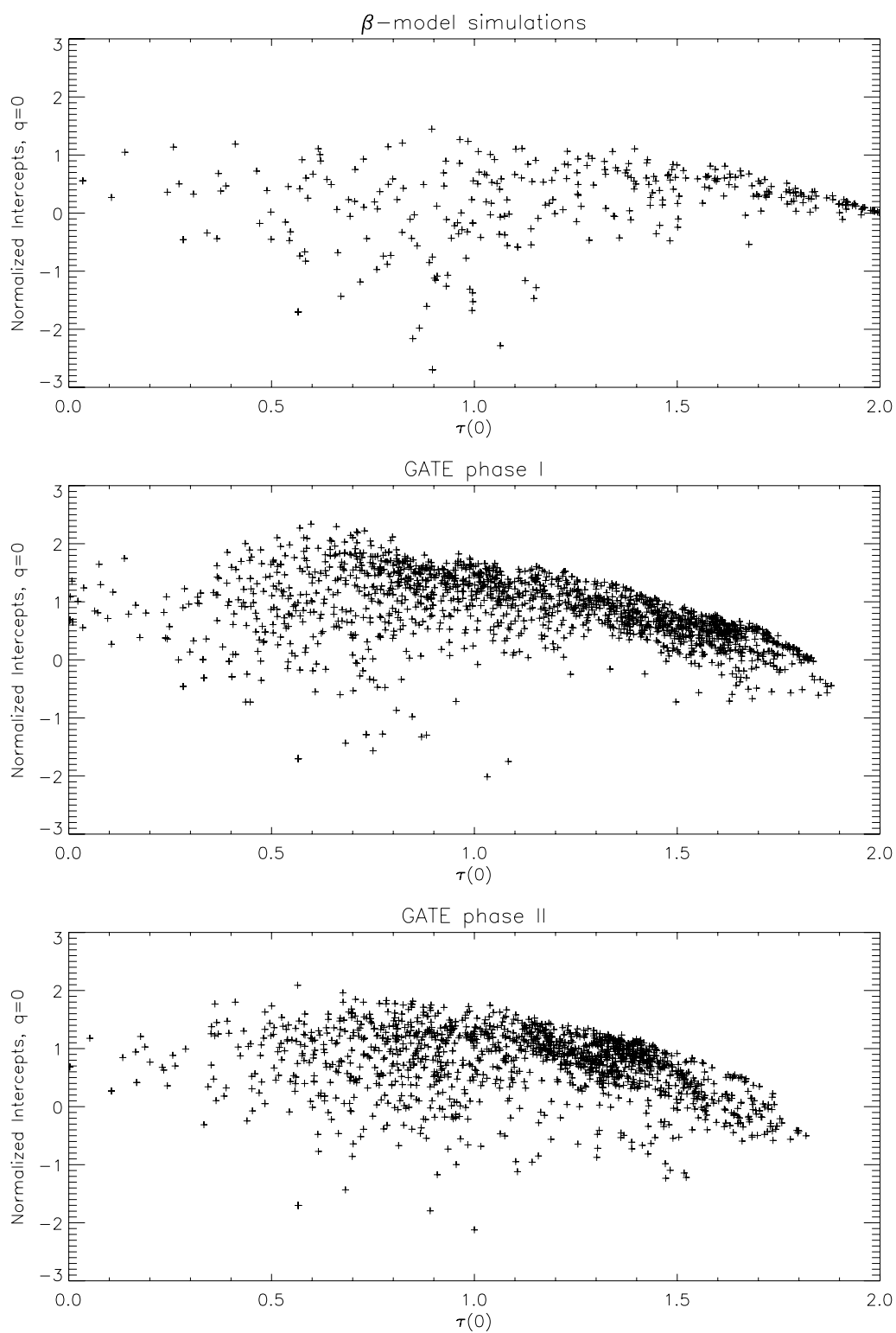


**Figure 4.7** Intercepts of moments of spatial rainfall,  $q=0$

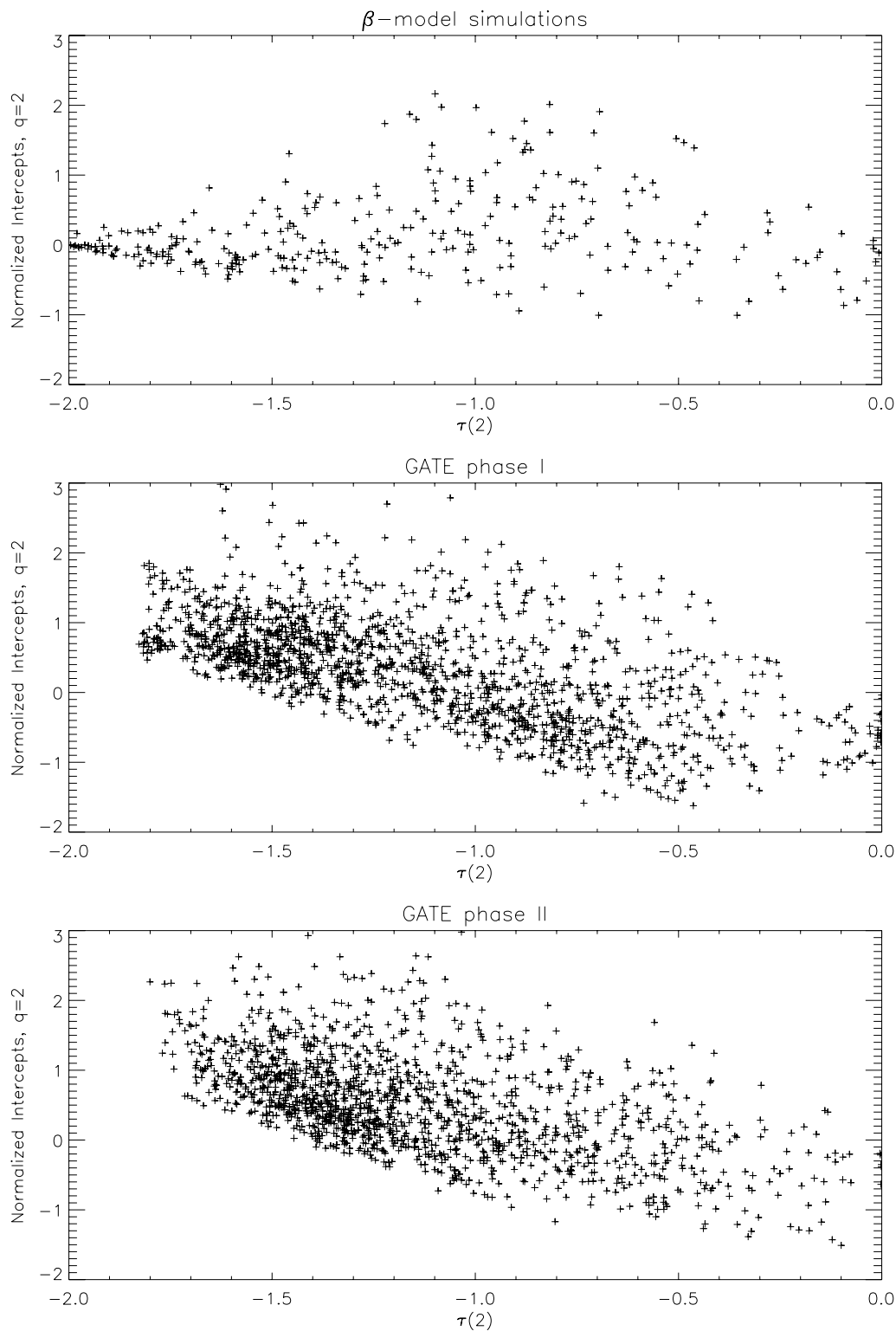


**Figure 4.8** Intercepts of moments of spatial rainfall,  $q=2$

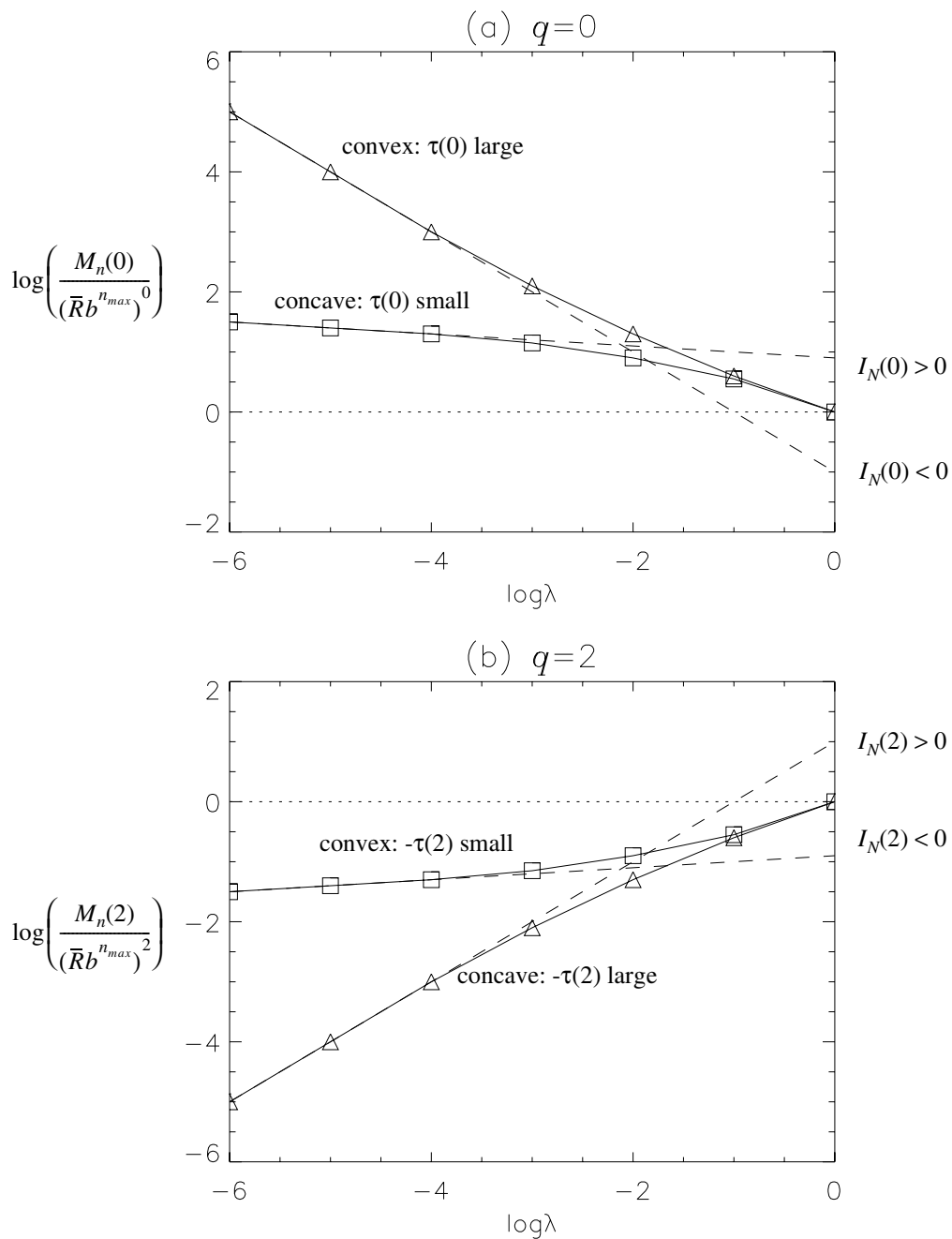


**Figure 4.9** Typical scaling of moments

positive to the left, so the direction of the theoretical effect is opposite to that observed in the data. The  $q = 2$  case is similar: while here the  $\log EZ_\infty^q$  term is somewhat larger, the direction of its effect is again wrong.

The other way in which we expect the data to be different from the theory, even if it had come from a scale-invariant random cascade, is that the data is, as discussed in Section 4.3, “off-grid” (as are the simulations), while the theory is “on-grid”. Let us see if we can develop some intuition regarding the effect of this difference. When  $q = 0$ , throwing down a data analysis grid randomly on a random cascade measure with zeroes in it will cause a lot of the non-zero regions to straddle boxes in the data analysis grid, with the effect that the number of boxes with mass at each scale will be anomalously large. This will have the effect of shifting each data point up. However, at the larger scales, the number of boxes is small and there is only so much room to shift upward. Thus it is reasonable to expect concavity to arise in the scaling of the moments from this source. This situation of course obtains for the simulations as well as the data and probably explains the increase in  $I_N(0)$  observed in Figure 4.7a as you move away from  $\tau = 2$ .

The  $q = 2$  case is basically opposite. Taking  $q > 1$  emphasizes the larger values of the mass; these occur when some box at some scale in the generation process receives an unusually large value of the multiplier, but such a box will be split up and spread across two or more adjacent boxes when a random grid is applied. This will result in shifting the moments down from their theoretical “on-grid” locations. Again at the larger scales, the shifting is less likely to occur, in this case, because the large boxes are less likely to cross the large values of the mass, and again the moment of the mass in the largest box is independent of the gridding. Thus we expect convexity in the scaling of the moments, as perhaps occurs weakly for the simulations in Figure 4.8a.

The effect in the  $q > 1$  case is generally weaker than in the  $q = 0$  case, because in the  $q = 0$  case, *any* amount of mass that appears in a box has the same effect as a lot of mass. The  $q > 1$  case would be more strongly affected by the gridding in the case of a very large  $q$ .

So we have examined two sources of deviations from perfect scaling of the moments that would appear in realizations of a random cascade, and found that while one of them seems to appear in the simulations, and by extension in the data, the deviations in the data are much larger than those in the simulations, and hence require some additional explanation. At this point, it seems unlikely that there is any explanation other than nonhomogeneity of scaling. Let's observe what the results are saying about the nature of this nonhomogeneity by comparing the results in Figures 4.7 and 4.8 with the schematics in Figure 4.9.

For  $q = 0$ , the intercepts in the data are positive for the moderate to small values of  $\tau$ . This indicates the concave curve in Figure 4.9a. In addition to the effect of gridding discussed above, there appears then to be a tendency for the rainfall pattern to deviate from what would be observed in a random cascade in the sense that relative to what occurs at smaller scales, too many boxes at larger scales have mass. This means that the regions with mass are too uniformly distributed in space, or, equivalently, there are not enough holes at larger scales.

For the values of  $\tau$  at which most of the GATE scans cluster, the deviations from the behavior of the simulations are fairly minor, a helpful fact for modeling GATE-like rain with random cascades. But as mentioned before, for the largest values of  $\tau$ , the intercepts become negative, which indicates the convex curve in Figure 4.9a. This means that there are too many large regions *without* mass at the larger scales; the large value of  $\tau$  indicates that at smaller scales there are few regions without mass - the rainy regions are almost without holes.

For  $q = 2$ , these same scans of rainfall have the smallest (most negative) values of  $\tau$  and positive intercepts, indicating they have scaling curves like the concave one in Figure 4.9b. This behavior is consistent with that observed in these scans for  $q = 0$ , as may be seen by considering the change in moment as scale is decreased. It decreases

es more slowly at large scales than at small, which means that at large scales all the intense rainfall tends to be concentrated in a few regions, while at smaller scales, it is more uniformly distributed. This picture is thus consistent with that at the  $q = 0$  where, for these scans, we saw that the large scale had a lot of empty regions relative to an iid random cascade, while the small scale did not. Hence at the large scales, the rainy area is relatively small, but where it is rainy, the rain rate is large. At small scales, the situation is reversed - the rainy area is relatively large and the rain rate is relatively small. Of course, “relative” here means in relation to what would be obtained from a scale-homogeneous multiplicative cascade with the same values of  $\tau$ .

Again, as in the  $q = 0$  case, as the value of  $\tau$  moves away from its maximum magnitude, the data intercepts pass through a region where they are not so anomalous, near where most of the GATE scans are clustered. At smaller magnitudes of  $\tau$ , the intercepts are negative, which indicates the convex scaling curve in Figure 4.9b. This means the rainfall is more uniformly distributed at larger scales than it is at smaller scales, relative to a cascade. Again this is consistent with what was found for  $q = 0$ .

So a consistent picture emerges from this analysis of the intercepts and their implications for the scaling of the moments. Relative to what would be observed from a random cascade, GATE scenes with a lot of rain are over-clustered (too non-uniform) at large scales and under-clustered (too uniform) at small scales, while scenes with little rain are too uniform at large scales and too non-uniform at small scales. This is not to say that the homogeneous scaling assumption is not a useful one in characterizing these scenes - as noted above, the deviations where the majority of the scenes are clustered are not large - but anything the data analysis can tell us about the extent and nature of the deviations of data from a theory is that much more information available for an improved or new theory.

Before examining other tests of the data, let us use Figure 4.9 to briefly describe

what implications a failure in scaling would have for modeling using random cascades. Consider the concave curve through the data in Figure 4.9a. As noted, this is the typical situation for data for  $q = 0$  for all but the largest values of  $\tau(0)$ . For  $q = 0$ , the moments simply count the number of pixels at each scale that contain rainfall. The slope of the line between the data points at each scale indicates the rate at which this number decreases as scale increases. If this “rate” - quantitatively, the ratio between the number at each scale - is constant, perfect scaling is obtained. If it has a trend - for example, the concave curve indicates a decreasing rate - the scaling is nonhomogeneous. That is, it appears that the process moves from scale to scale differently at different scales. We will not prove this assertion, but it should be reasonably clear intuitively that such a situation could be modeled as a random cascade with generators whose distributions depend on scale. In the case of the concave curve in Figure 4.9a, these generators would have a variance that increases as scale decreases. We will not discuss such nonhomogeneous cascades further; our present purpose is to further explore the applicability of homogeneous cascade theory to rainfall.

#### 4.4.2 Tests of the Theory Using Cross Moments

The second set of tests is developed from the scaling of the spatial average cross moments, that is, the dependence of quantities of the form

$$M_n(p, q; r) = \frac{\left(\frac{1}{b^n - b^m}\right) \sum_{i=1}^{b^n - b^m} \mu_\infty^p(\Delta_n^i) \mu_\infty^q(\Delta_n^{i+b^m})}{b^{-n} \sum_{i=1}^{b^n} \mu_\infty^{p+q}(\Delta_n^i)}, \quad (4.21)$$

on  $r_n/l_{max} = b^{(m-n)/2}$ ,  $0 \leq m < n$ , where  $r_n$  is a distance along on axis of a two-dimensional cascade. As shown in Section 3.3, the corresponding ensemble average quantity has the scaling

$$\frac{E[\mu_\infty^p(\Delta_n^i)\mu_\infty^q(\Delta_n^{i+b^m})]}{E[\mu_\infty^{p+q}(\Delta_n^i)]} \sim \left(\frac{r_n}{l_{max}}\right)^{-\log_{\sqrt{b}}R(p,q)}, \quad (4.22)$$

where the scaling exponent is

$$\kappa_{\sqrt{b}}(p,q) = -\log_{\sqrt{b}}R(p,q) = -\log_{\sqrt{b}}\frac{EW^{p+q}}{EW^p EW^q}. \quad (4.23)$$

The conjecture is made in Section 3.3 that the spatial average cross moment has the same scaling as the ensemble average cross moment, i.e.,

$$M_n(p,q;r) \sim \left(\frac{r_n}{l_{max}}\right)^{-\log_{\sqrt{b}}R(p,q)}. \quad (4.24)$$

A side effect of the present discussion will be testing this conjecture using simulated cascades.

The cross moment scaling can be used to make a consistency check because the exponent  $\kappa_{\sqrt{b}}(p,q)$  can be written in terms of the MKP function or the  $\tau(q)$  function of the generator as follows:

$$\kappa_{\sqrt{b}}(p,q) = 2(\chi_b(p+q) - \chi_b(p) - \chi_b(q) + 1) \quad (4.25)$$

$$= \tau(p+q) - \tau(p) - \tau(q) + 1 \quad (4.26)$$

(see Section 3.3). To perform the test,  $\kappa_{\sqrt{b}}(p,q)$  is estimated from the scaling of the spatial average cross moments (equation (4.24)) and  $\tau(q)$  from the scaling of spatial average marginal moments (equation (3.45)); then the equality (4.26) can be tested.

Tests of equation (4.26) for three choices of moment order for the  $\beta$ -model simulations and GATE phases I and II are given in Figures 4.10 through 4.15. The first set of three figures contains the scaling exponents of the cross moments in the East-West direction for the GATE data, and the second set of three contains the scaling exponents

in the North-South direction. Consider first the case where  $p = q = 0$  (Figures 4.10 and 4.13). In this case, the cross moment exponents from simulations and data in both directions lie above the value computed from the scaling of the marginal moments according to equation (4.26), but the East-West direction is higher. Since for other moment orders, the cross moment exponents from simulations lie fairly well centered on the value predicted by equation (4.26), it is reasonable to assume that this is not evidence of the failure of the conjecture that equation (4.26) holds, but instead an effect of the off-grid nature of the simulations. Apparently the effect of the failure to match the generation and analysis grids has somewhat different effects for the marginal and cross moments for  $p = q = 0$ , making the cross moment exponents smaller in magnitude (hence indicating larger correlation) than what would be expected from the scaling of the marginal moments.

However, the cross moment exponents computed from the data have generally larger deviations from the predicted value than do the simulations, hence giving further evidence of disagreement with the random cascade theory. The size and sign of this deviation as a function of the moment order and direction of the cross moment exponent is quite interesting. For  $p = q = 0$  (Figures 4.10 and 4.13), the cross moment exponents for both directions lie generally above the predicted value, but the East-West cross moment exponent is clearly higher. This indicates that the occurrence of rainy areas is more correlated in the East-West direction than in the North-South direction (and anomalously so compared to the scaling of its marginal moments). This is suggested visually in the data where the rainy areas are elongated in the East-West direction. As we go to  $p = q = 0.5$  (Figures 4.11 and 4.14), the cross moments exponents for both directions fall relative to the predicted value; in the East-West direction they lie quite nicely on top of the predicted value, while the North-South direction exponents have fallen below the predicted line. For  $p = q = 1$  (Figures 4.12 and 4.15),

this relative descent continues, although it is somewhat masked by the stretching of the y-axis, and again the North-South exponents are lower. This same result also holds for  $p = q = 2$ , which we do not show here. So we may draw the general conclusion that the GATE rainfall fields are more correlated in the East-West than the North-South direction; we came to this same conclusion via a somewhat different computation several years ago (Over and Gupta 1991).

This conclusion can be confirmed by examining the normalized cross moments at the smallest scale available in data ( $l_{min} = 4$  km). These are given by equation (4.21) for  $n = n_{max}$  and  $m = 0$  and are presented for  $p = q = 0$  and  $p = q = 1$  in Figures 4.16 through 4.19. In these plots, the choice of the function to plot along the x-axis is somewhat arbitrary, and the solid diagonal line is not to be taken as a theoretical prediction; it is merely included to help the eye compare the plots. In these plots it is shown directly that the East-West correlation is greater than the North-South correlation (at this scale) for both  $p = q = 0$  and  $p = q = 1$ .

A second reason for including these cross moment plots is to test the visual impression that real rainfall fields are “smooth”, meaning that within the rainy region, the rain rate changes more or less smoothly from low intensity regions (generally near the edges of the rainy region) to high intensity regions, generally near the center. In particular, they appear to be smoother in this sense than cascade simulations, which have a more “salt-and-peppery” appearance. One might expect that a cross moment analysis would quantitatively measure this difference, with the data being more correlated than simulations. However, the differences between data and simulations in Figures 4.16 through 4.19 are slight. Thus quantifying the visual impression of “smoothness” remains an open problem.

Returning to the discussion of the cross moment exponents in Figures 4.10 through 4.15, we can summarize and interpret the differences from the theoretical re-

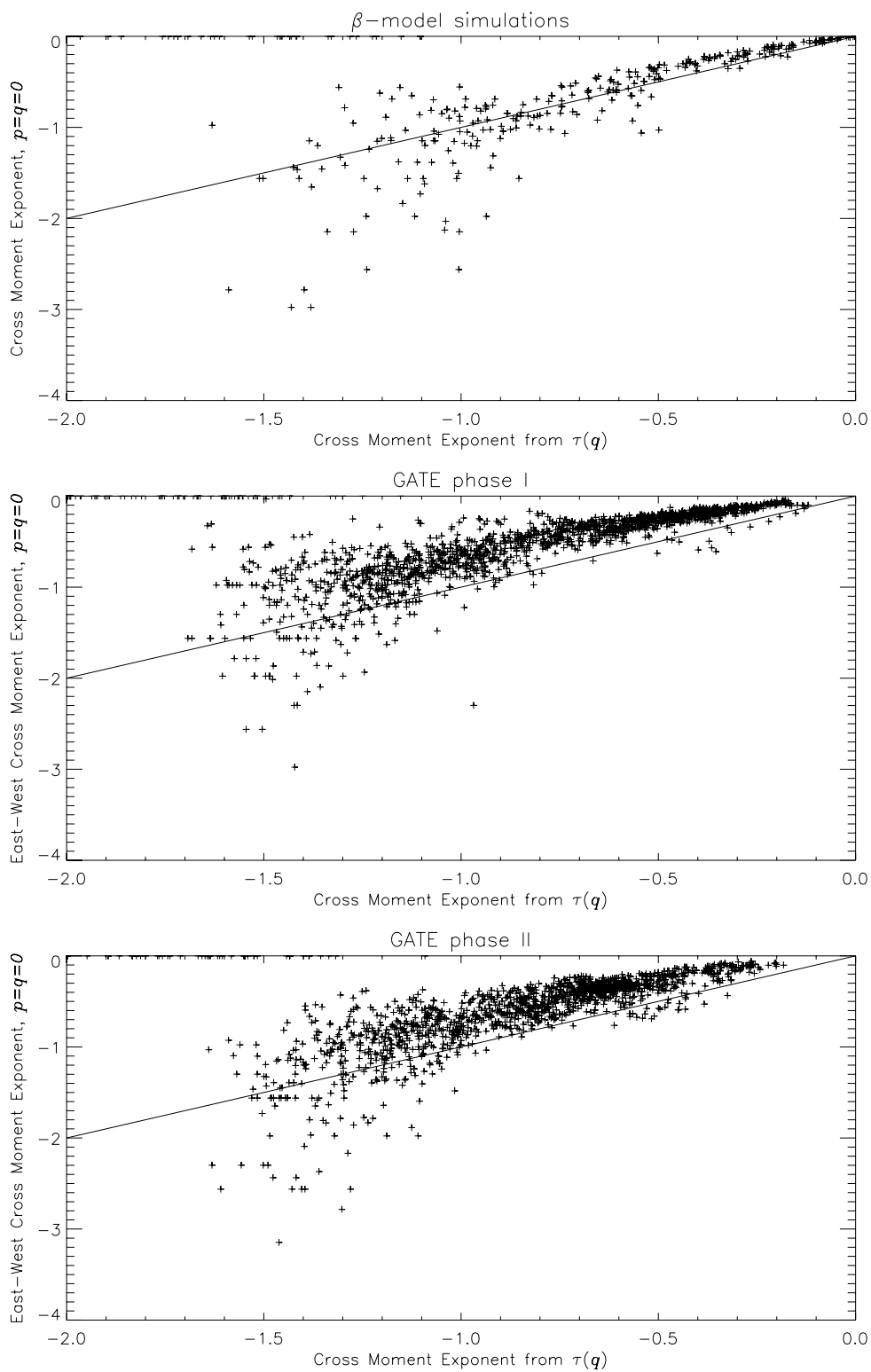


**Figure 4.10** E-W cross moment exponent vs.  $\tau(q)$  cross moment exponent  
 $p=q=0$

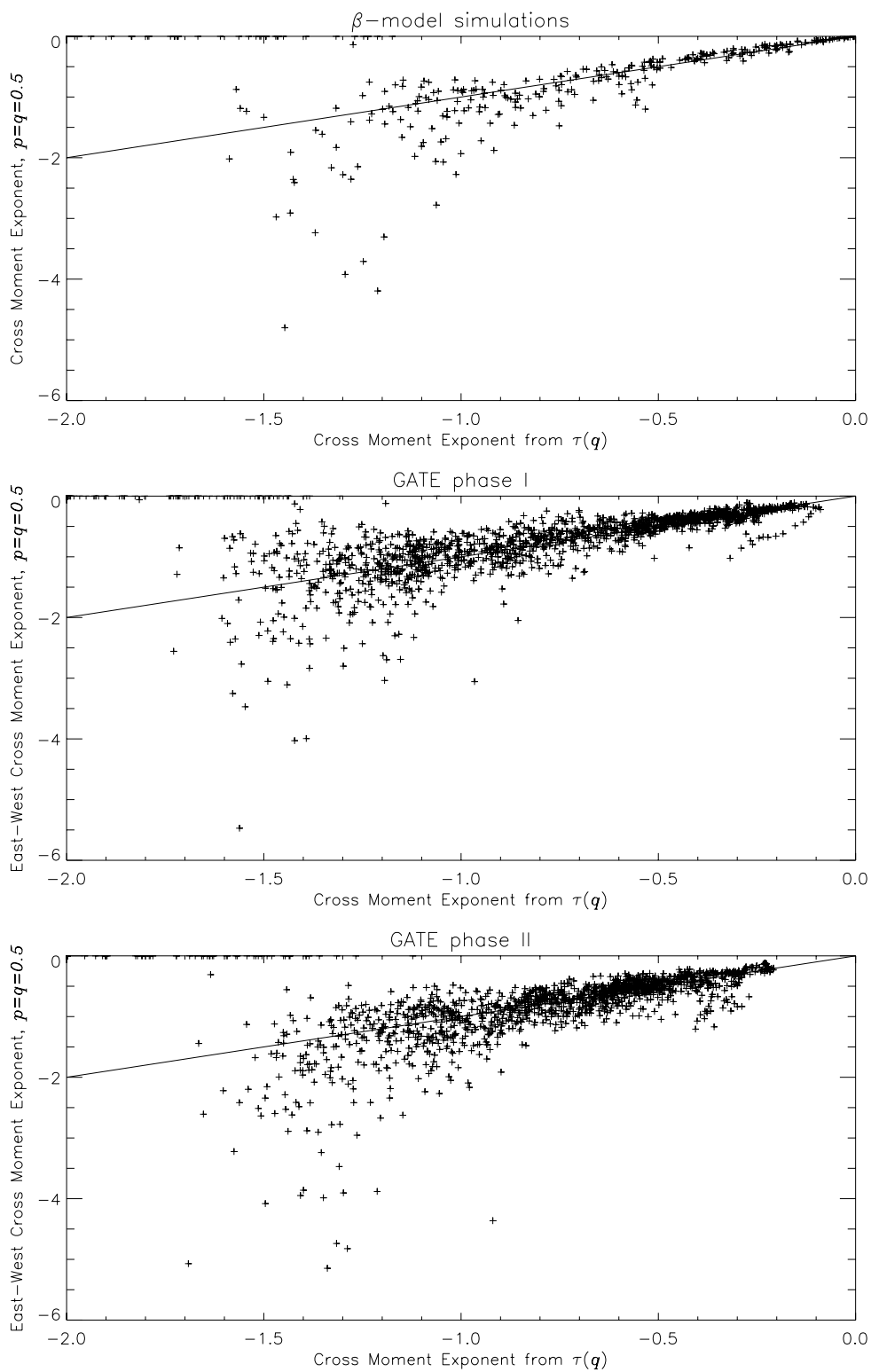


**Figure 4.11** E-W cross moment exponent vs.  $\tau(q)$  cross moment exponent  
 $p=q=0.5$

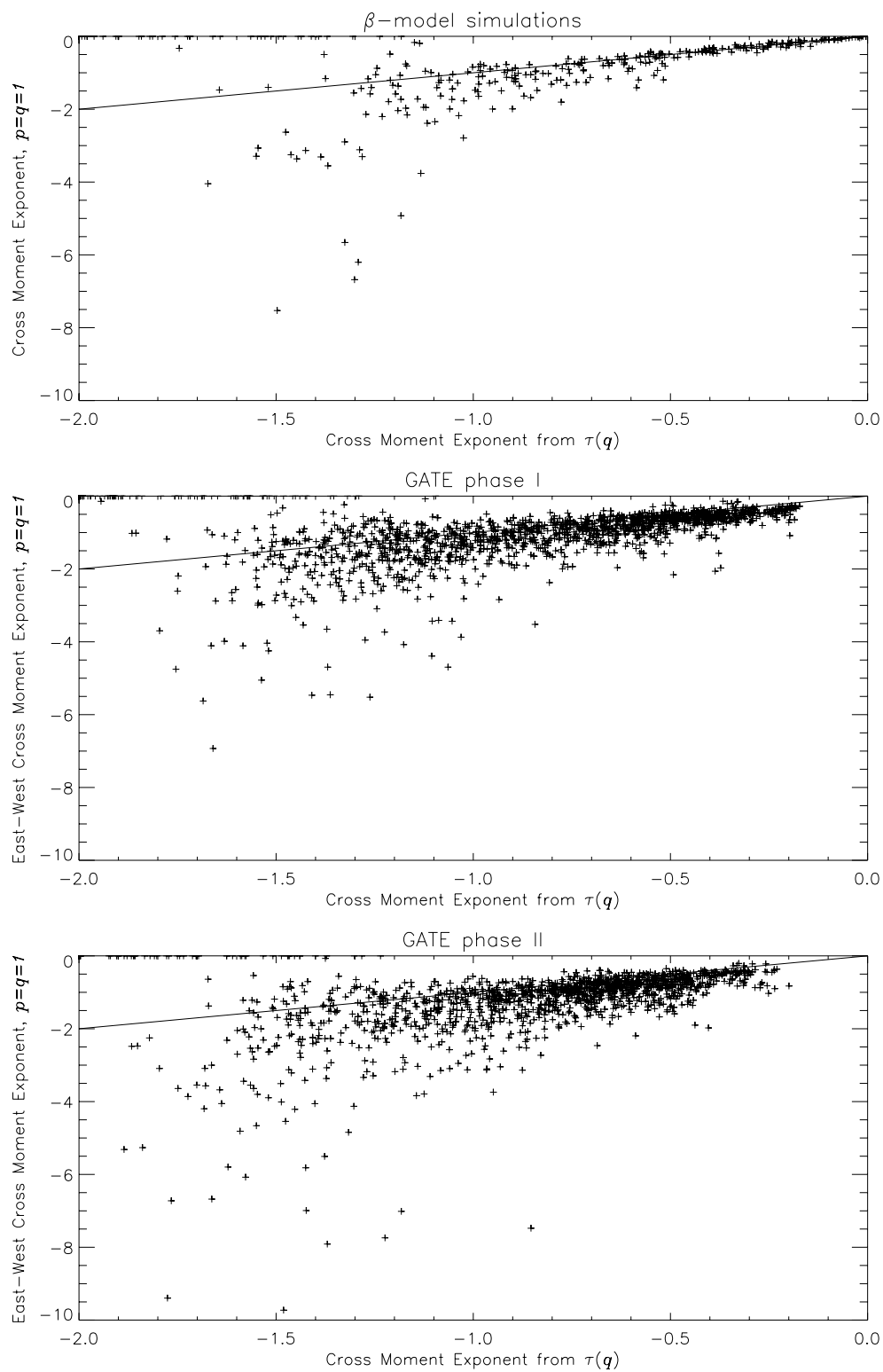


**Figure 4.12** E-W cross moment exponent vs.  $\tau(q)$  cross moment exponent  
 $p=q=1$

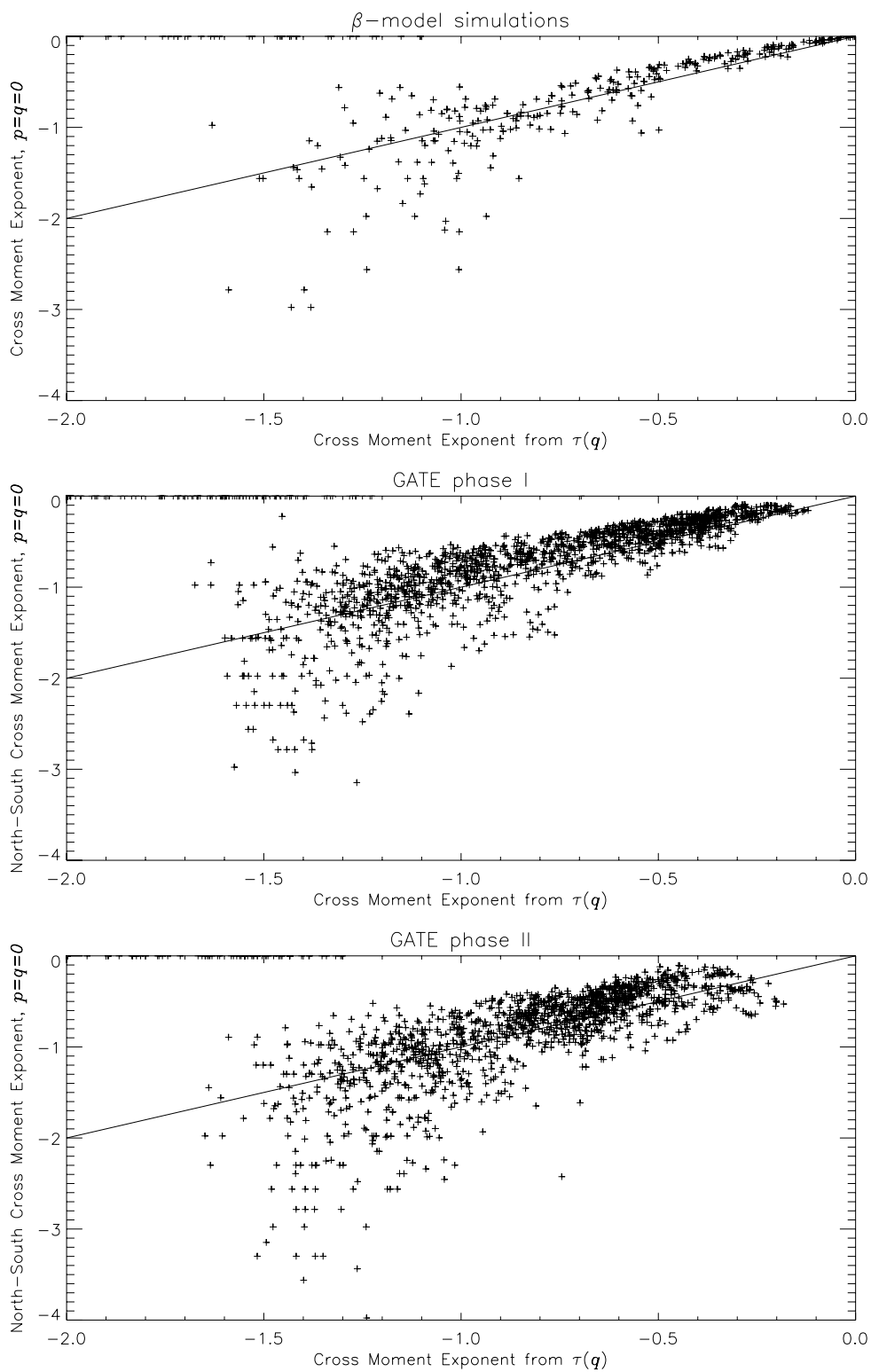


**Figure 4.13** N-S cross moment exponent vs.  $\tau(q)$  cross moment exponent  
 $p=q=0$

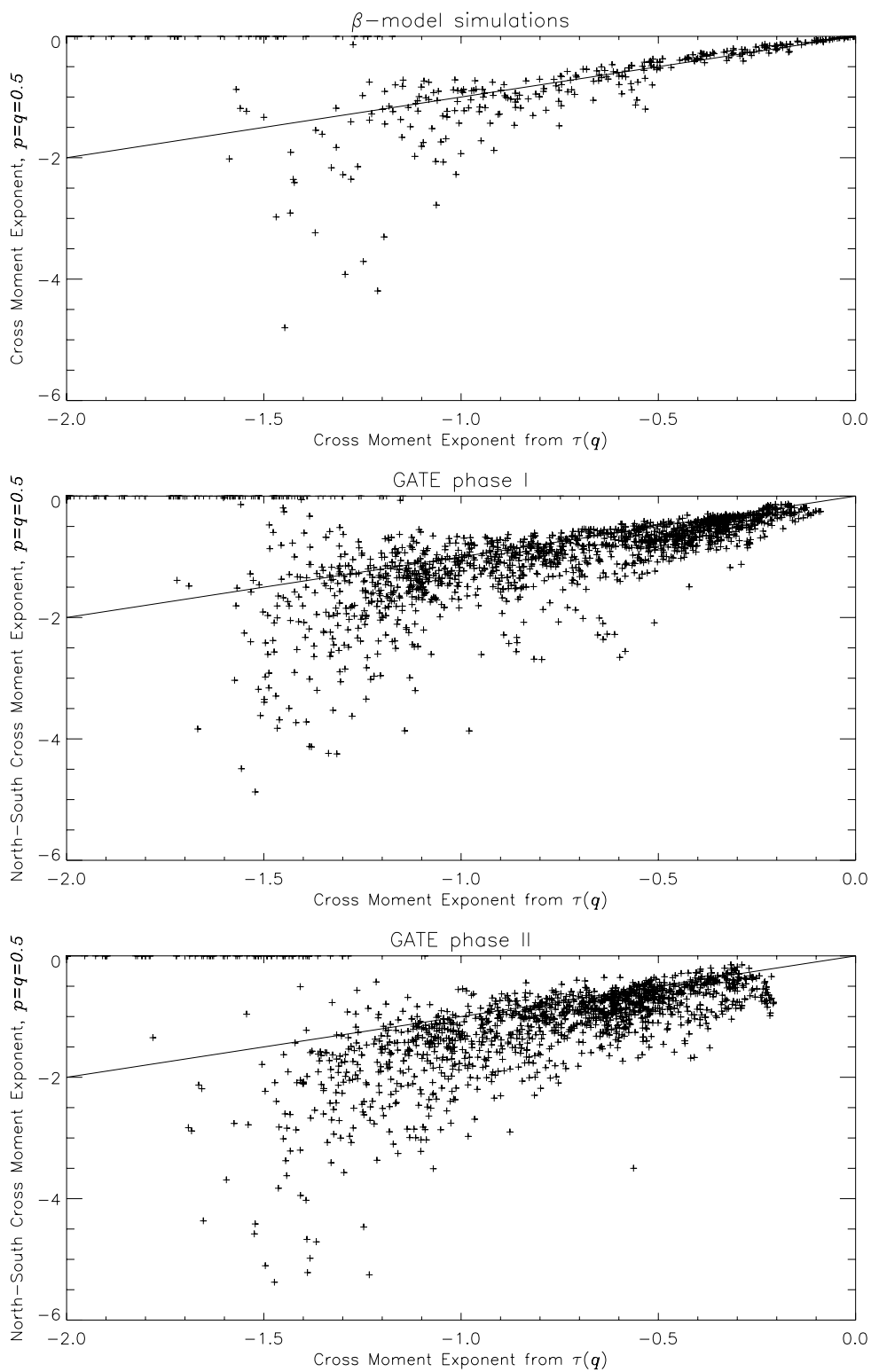


**Figure 4.14** N-S cross moment exponent vs.  $\tau(q)$  cross moment exponent  
 $p=q=0.5$

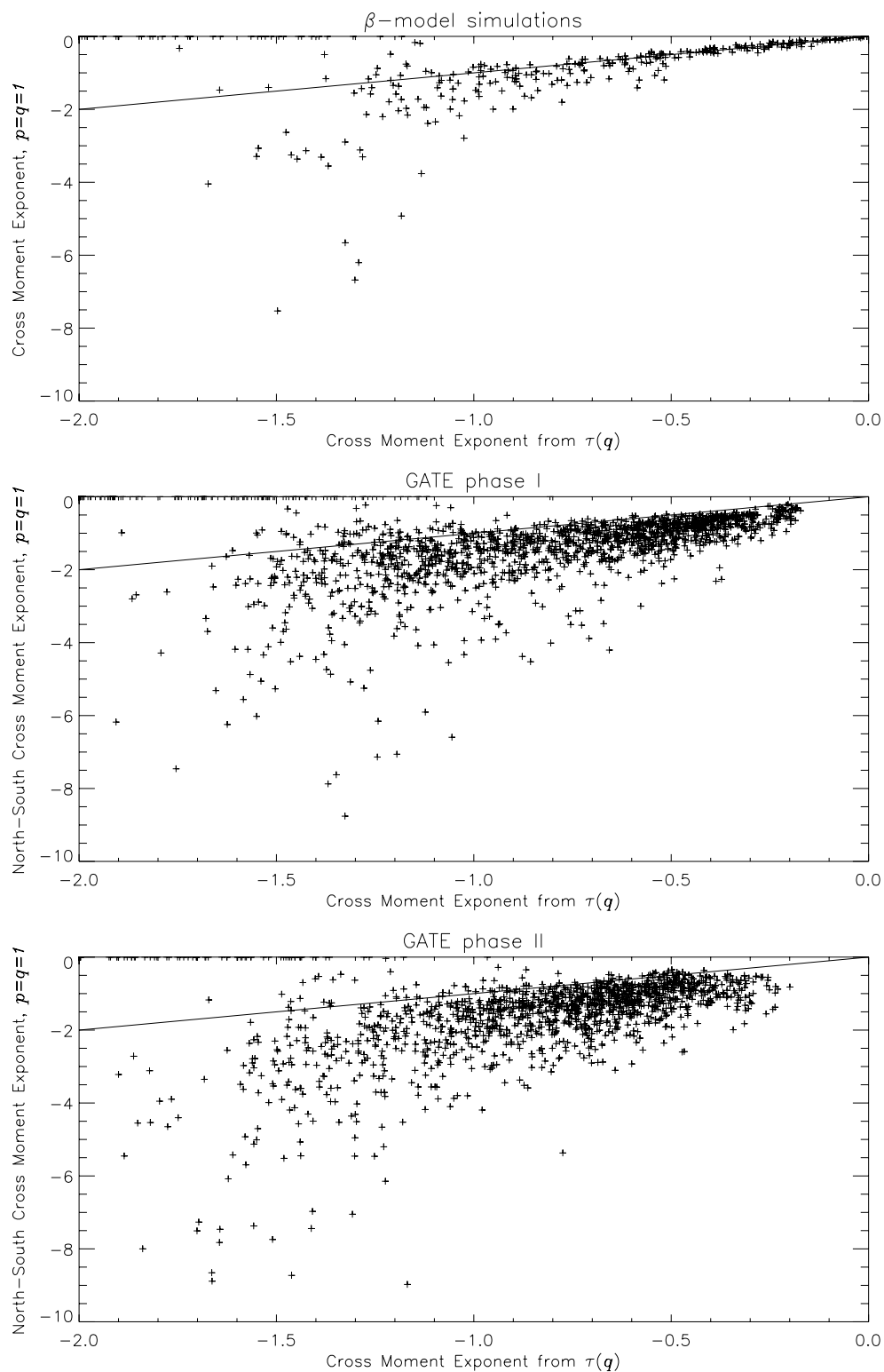


**Figure 4.15** N-S cross moment exponent vs.  $\tau(q)$  cross moment exponent  
 $p=q=1$

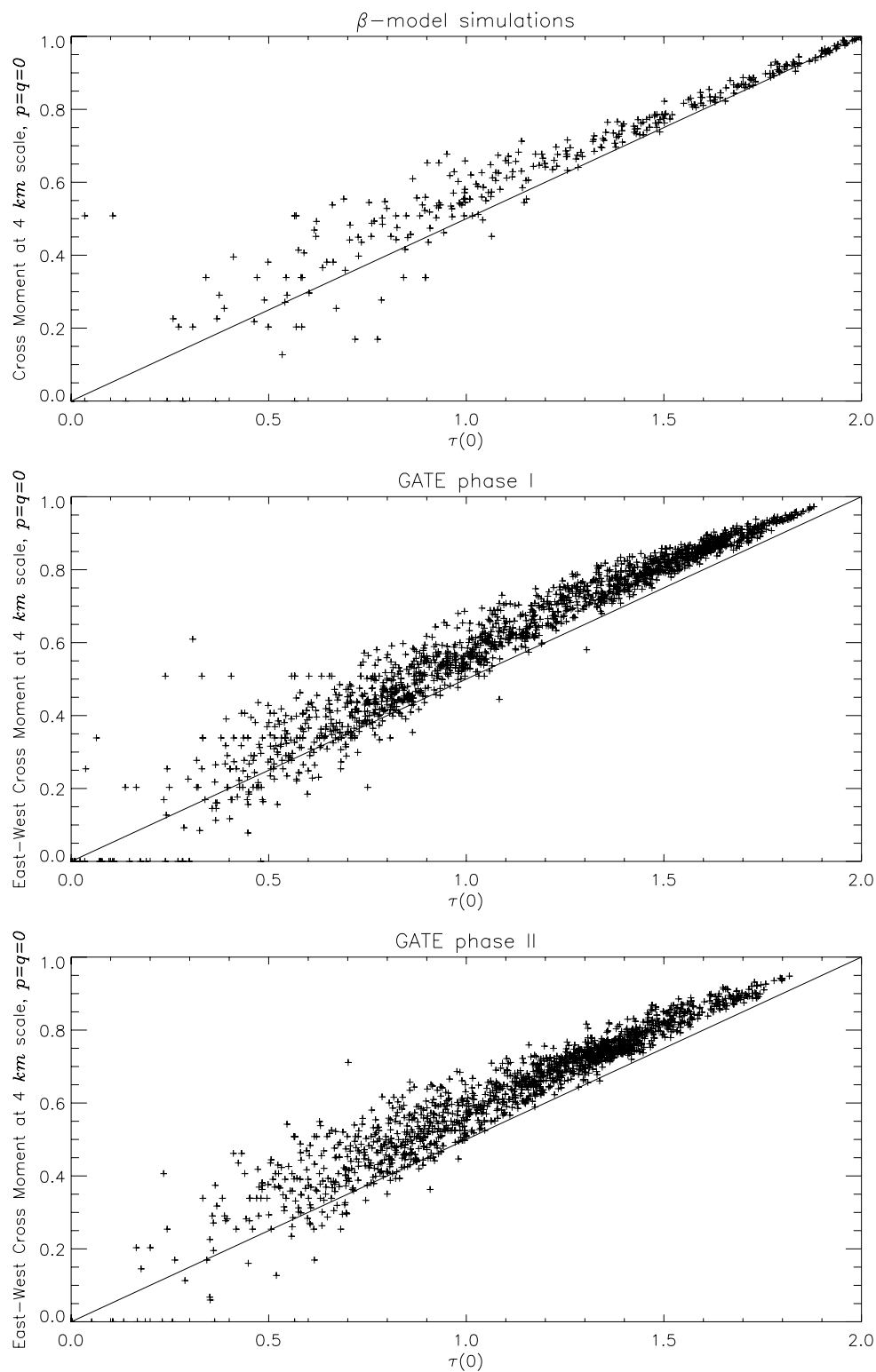


**Figure 4.16** E-W cross moment,  $p=q=0$

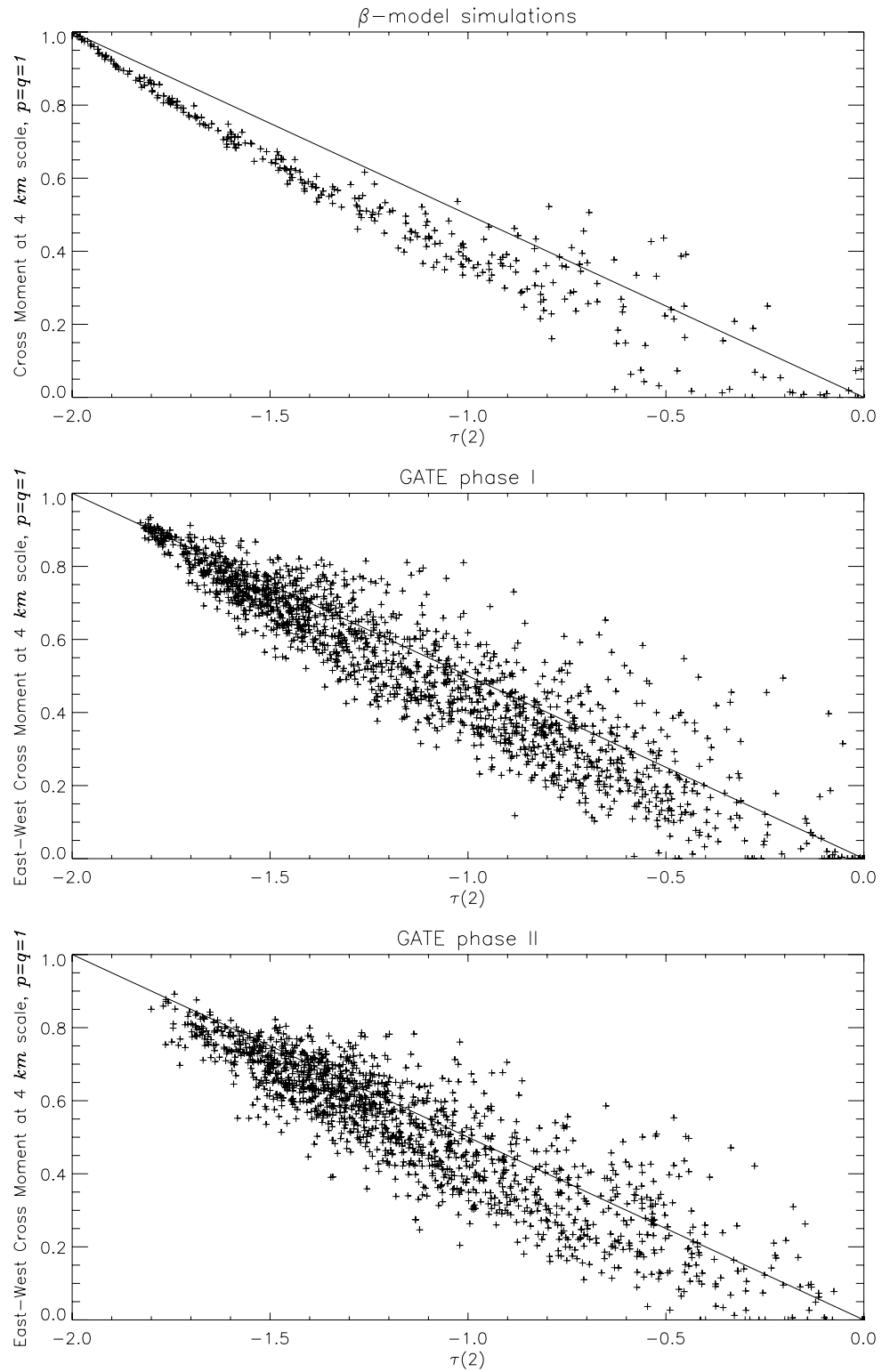


Figure 4.17 E-W cross moment,  $p=q=1$

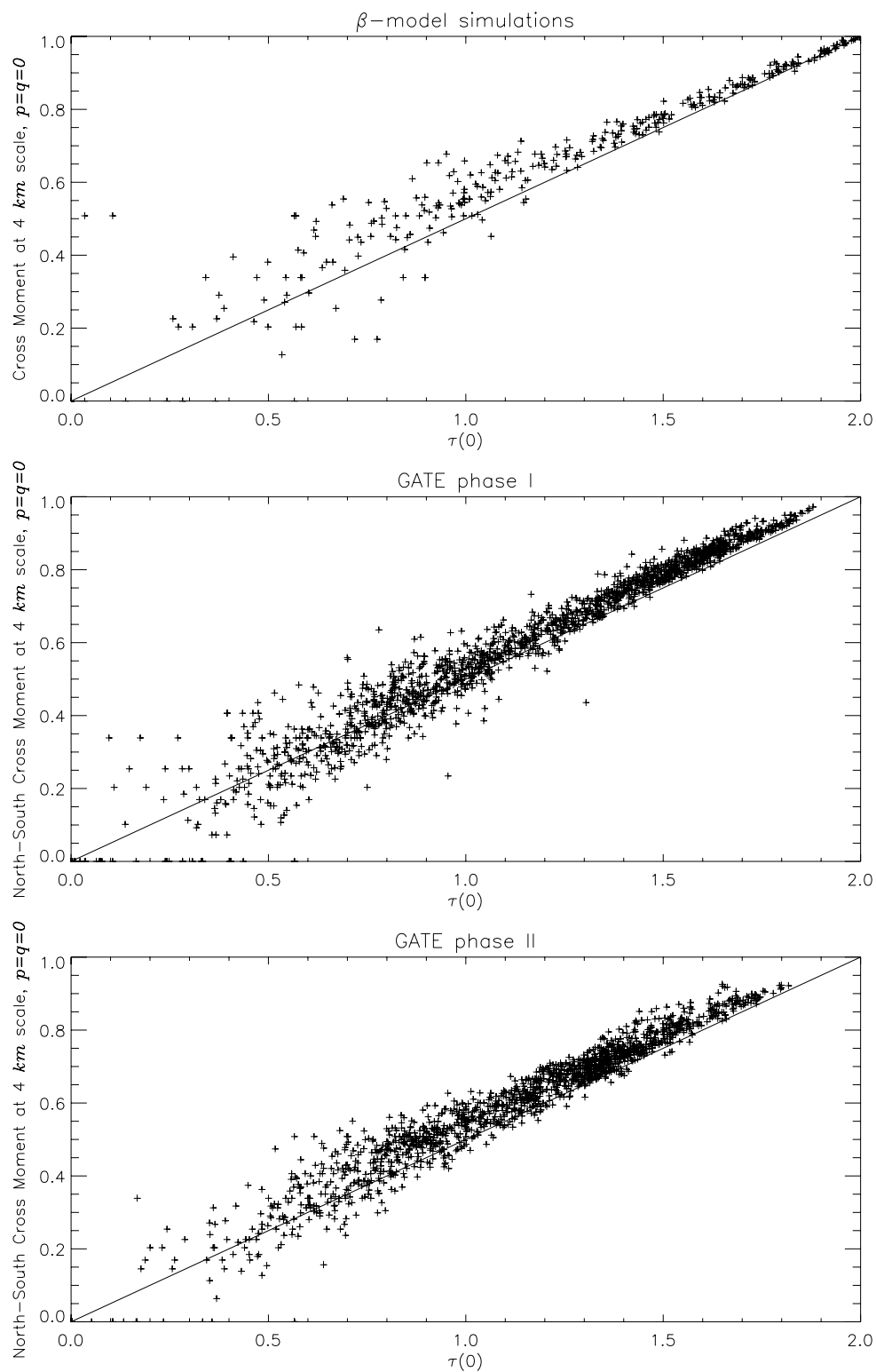


Figure 4.18 N-S cross moment,  $p=q=0$

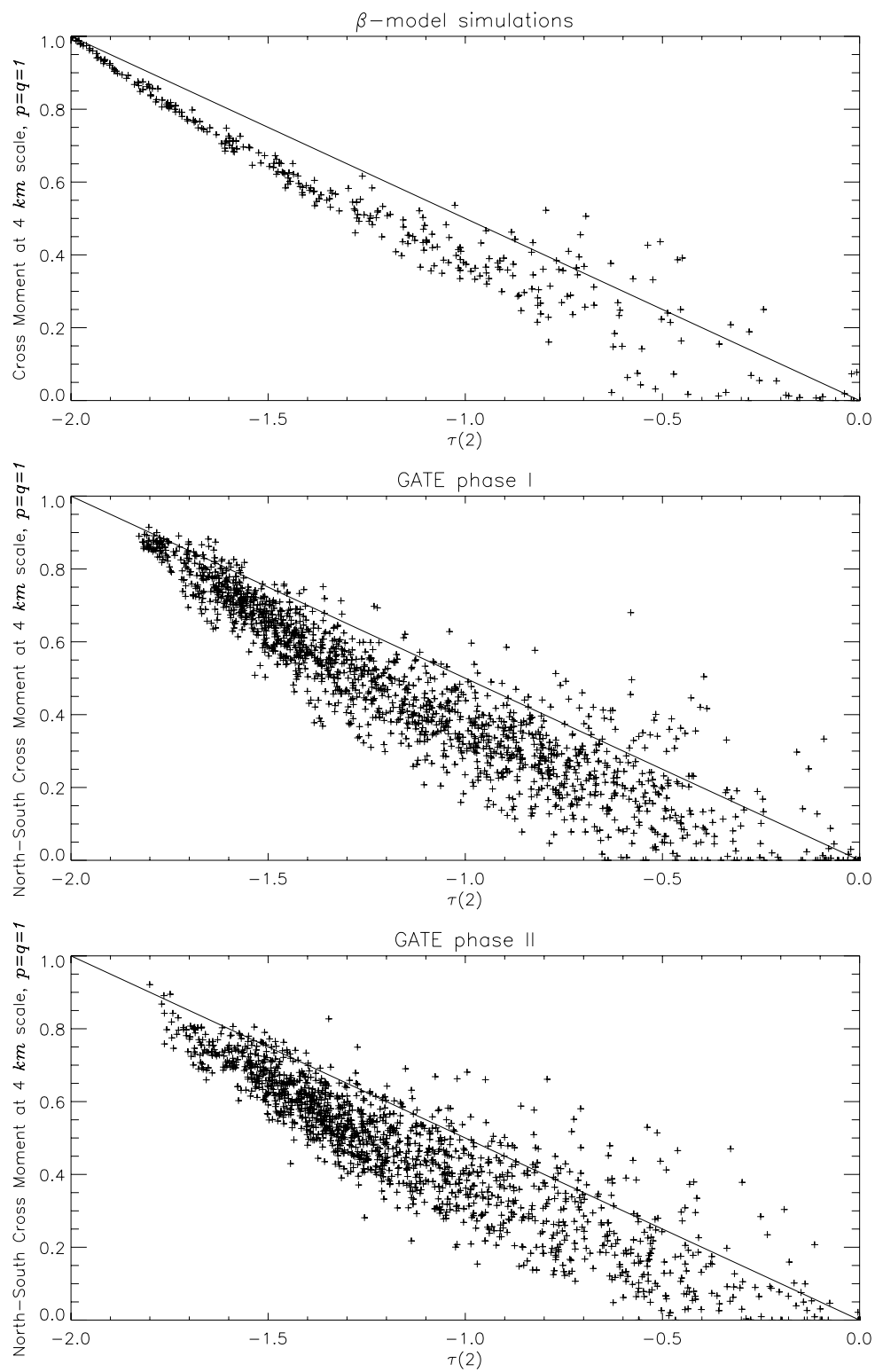


Figure 4.19 N-S cross moment,  $p=q=1$

sults as a function of moment order as follows. For  $p = q = 0$ , the cross moment exponent indicates longer correlation length than the scaling of the marginal moments would indicate, while for  $p = q = 1$ , the correlation length is shorter. Together these indicate that the GATE rainfall fields differ from the cascade theory in the direction of the traditional picture of the structure of a tropical convective rainfall field, where a few small, high intensity convective cells are imbedded in a large, low intensity region generated by the mesoscale anvil. As discussed above, both the low and high-intensity structures are elongated in the East-West direction.

While the differences from the theory indicated by the intercepts are different, they are compatible with these results. Recall that for scenes with a lot of rain, the intercepts indicated that the rainfall fields at coarse resolution are over-clustered for large scales relative to the small scales, with the opposite holding for scenes with little rain. These results can be interpreted in the convective cell / mesoscale anvil framework as saying that in scenes with a lot of rain, the rainy region consists of one or a few mesoscale anvil regions containing spatially correlated convective cells, while when there is little rain, it consists of scattered cells. The interpretation of the cross moments above matches this for scenes with a lot of rain. For scenes with little rain, the results seem opposite, but in examining the  $p = q = 1$  results further (Figures 4.12 and 4.15), one sees that the data in the left-hand tail does not fall below the theoretical line as much as the simulations do, indicating that indeed for scenes with little rain, the correlation length is anomalously large, matching the results from the intercepts.

We will see below that the further results of the scaling analysis point toward traditional ideas about the spatial structure of rainfall fields.

## 4.5 Parameter Estimation

The tests of the random cascade theory presented above show that from a standard error perspective, the scaling properties of GATE rainfall fields may be considered cascade-like. While the other tests indicate important differences from the theory in the details of the rainfall field structure, the scaling results suggest an approximate compatibility between the theory and the data. So we proceed to parameter estimation. As discussed in Section 3.3, the slope of the log-moment versus log-scale relationship as a function of moment order  $q$  gives an estimate of the  $\tau(q)$  function, which in turn provides an estimate of the MKP function of the cascade generator under certain conditions given in Theorem 3.2. Estimating the parameters of the cascade generator by this method gives a very interesting result, as we shall see. Some results from this type of analysis were published in Over and Gupta (1994). Here, however, we use somewhat different notation and perform some additional tests.

The basic result on this topic in Over and Gupta (1994) was that the estimated  $\tau(q)$  functions of the GATE and Elbow data were approximately straight lines, particularly for the low rain rate scenes, implying that the appropriate generator for modeling these scenes is the  $\beta$ -model, which is defined in Section 3.4 as

$$P(W = b^\beta) = b^{-\beta} \text{ and } P(W = 0) = 1 - b^{-\beta}. \quad (4.27)$$

(In Over and Gupta (1994) the  $\beta$ -model was parameterized as

$$P(W = (1 - p)^{-1}) = 1 - p \text{ and } P(W = 0) = p.) \quad (4.28)$$

That  $\beta$ -model generators have straight-line  $\tau(q)$  functions is demonstrated in Section 3.4, where it is shown that the  $\chi_b(q)$  function has slope  $\beta - 1$ , implying, for  $d = 2$ , that the  $\tau(q)$  function has slope  $2\beta - 2$ . The  $\beta$ -model is the simplest non-trivial cascade generator that includes an atom at zero. Notice that for a cascade with this gener-

ator, wherever there is mass, it has the same distribution

$$\mu_{\infty}(\Delta_n^i) \parallel \mu_{\infty}(\Delta_n^i) > 0 = b^{n\beta} (Z_{\infty}(\Delta_n^i) \parallel Z_{\infty}(\Delta_n^i) > 0). \quad (4.29)$$

Notice that if it were it not for the  $Z_{\infty}$  factor, each positive mass would be identical.

The “straightness” of  $\tau(q)$  is measured in Over and Gupta (1994) by comparing the value of  $p$  computed from  $\tau(0)$  with that computed from an estimate of the slope of  $\tau(q)$ . This slope estimate is such that if the  $\tau(q)$  function were a straight line, the two estimates of  $p$  would coincide. Hence their differences measure the deviation of the  $\tau(q)$  function from being a straight line. However, these estimates of  $p$  are somewhat problematical. The estimate of  $p$  from  $\tau(0)$  is problematical for the following reason. It is observed that the empirical  $\tau(q)$  functions are often concave in the neighborhood of  $q = 0.5$ . This is an anomaly because MKP functions must be convex. Because  $\tau(1)$  is always zero, this casts some doubt on the value of  $\tau(0)$ . Hence one would like to understand the origin of this anomaly before proceeding to estimate  $p$  or  $\beta$  from  $\tau(0)$ . The estimate of  $p$  from the slope of the  $\tau(q)$  function is also problematical because to estimate the slope of the  $\tau(q)$  function it uses not only  $\tau(0)$  but also the  $\tau(q)$  function where  $q$  is as large as four, and one doubts that these are very accurate, due to the use of a high moment order vis-a-vis a relatively small scene of data.

So two preliminary tasks confront us before proceeding to estimate and use the  $\beta$ -model parameter: (1) to explain the concavity of the  $\tau(q)$  function in the neighborhood of  $q = 0.5$ , particularly with regard to the accuracy of the value of  $\tau(0)$ , and (2) to determine the best method to estimate the  $\beta$ -model parameter and the parameters of random cascade generators in general.

The former task has a more limited scope, so we will begin with it. It was conjectured in Over and Gupta (1994) without the benefit of off-grid simulations that both the anomalous intercept behavior that we examined in the previous section and the

concavity of the  $\tau(q)$  function near  $q = 0.5$  had a common origin in the off-grid nature of the data. Here using off-grid simulations, we did observe in the simulation results (see, for example, Figures 4.10 and 4.13) in the previous section that the results for  $q = 0$  were particularly affected by the off-grid versus on-grid problem, but this effect was not sufficient to explain the behavior of the data. So another explanation must be found.

Let us first demonstrate the problem and consider this aspect of the  $\beta$ -model simulations specifically. We use the following approach. The local slope of the  $\tau(q)$  function at  $q = 0$  may be obtained by estimating  $\tau^{(1)}(1)$  by the method described in Section 3.3 (equation (3.50)). Using this slope a value for  $\tau(0)$  may be computed by linear extrapolation. If the estimate of  $\tau(0)$  found using  $\tau^{(1)}(1)$  lies above that derived via the scaling of moments, there is evidence of anomalous concavity in the region  $0 \leq q \leq 1$ . Applying this procedure to the  $\beta$ -model simulations will also show if the effects of being off-grid (as generated by this type of simulation) can explain some or all of the concavity. The results are given in Figure 4.20 below. For  $\beta$ -model simulations, this figure shows that for the larger values of  $\tau(0)$ , that is, the smaller values of  $\beta$ , the  $\tau^{(1)}(1)$  and direct methods of estimating  $\tau(0)$  give quite similar results and show no evidence of concavity. For the smaller values of  $\tau(0)$ , some evidence of *convexity* is apparent in the simulations. In the data, however, for the larger values of  $\tau(0)$ , the estimate of  $\tau(0)$  found using  $\tau^{(1)}(1)$  clearly lies generally above that derived from the scaling of the moments, and this difference is evident for all  $\tau(0)$  greater than about 0.6.

So just as in the previous section where we saw that the effect of generating simulations off-grid did not reproduce the moment scaling intercept behavior observed in the data, here we see that it does not explain the concavity of the  $\tau(q)$  functions estimated from data. An alternative hypothesis can be developed as follows. The value of

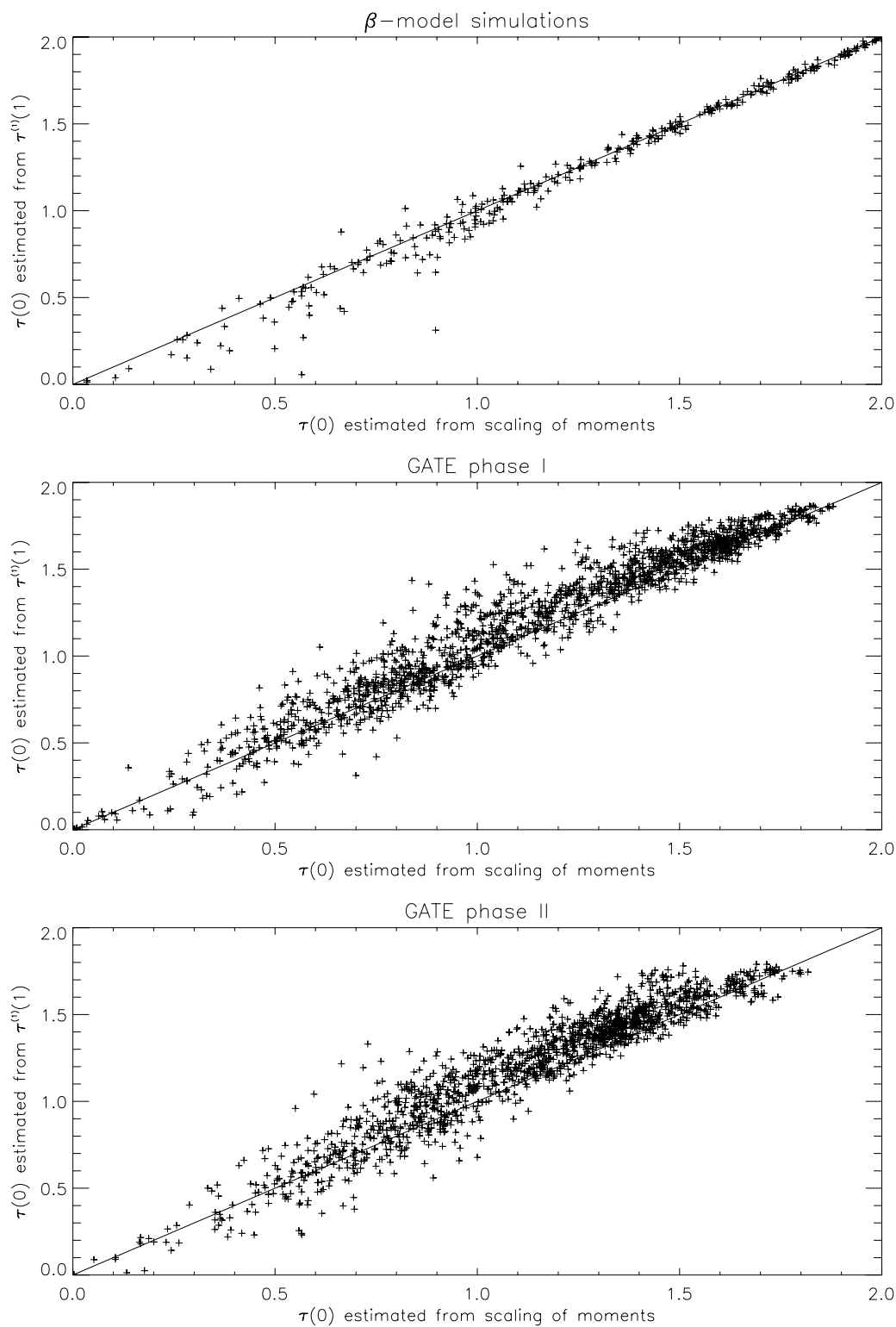


**Figure 4.20** Estimate of  $\tau(0)$  from  $\tau^{(1)}(0)$  vs. estimate from scaling of moments

$\tau(0)$  computed from the scaling of the moments, due to the weighting of the regression, is largely determined by the ratio of the two smallest-scale values, the number of boxes with rain at the smallest scale, and the number of boxes with rain at the next-to-smallest scale. Since the value of  $\tau(0)$  is anomalously low, this ratio must also be anomalously low, which implies that the number of boxes with mass does not decrease as box size increases as fast as would be expected. The beginning of the answer lies in asking why the number of boxes with mass decrease as box size increases. It decreases because we average over regions containing more than one box that has mass. So the anomaly must arise because an unusually small number of the boxes at the smallest scale lie in common boxes at the next smallest scale. One might think this effect could be reproduced by off-grid simulations, but for those produced by Voronoi tessellation subdivisions of space, we have given evidence that this effect is practically nil. The second alternative one might consider is that the rainy boxes at the smallest scale tend to be isolated, but we saw in the intercept analysis that this is true only for the smaller values of  $\tau(0)$ . The issue thus seems to be one of shape: the Voronoi tessellation scheme gives convex polygons at each subdivision, keeping the rainy areas compact. While we observed above in the intercept analysis that the rainy regions tend to be more solidly filled than the cascade theory would predict, this does not remove the possibility of quite jagged boundaries. So we add one additional element to our picture of spatial rainfall painted by deviations from the cascade theory: the mesoscale anvil regions, while tending to be almost solidly filled, have very rough boundaries.

We come now to the issue of estimating the random cascade parameters of the rainfall fields, or more generally, the question of the class of generators that is most appropriate to the data. We apply here the notion of  $k$ th order approximations developed in Section 3.4. Since from that point of view the  $\beta$ -model is the first-order model, the primary remaining question is how good a model it is, or conversely, how large are

the deviations from it. As we discussed above, Over and Gupta (1994) measured these deviations in terms of the values of the  $\tau(q)$  function. Due to the anomalous values of  $\tau(0)$  and the poor estimation accuracy that may be expected for large  $q$ , it would be nice to have a better method. Following the ideas presented in Section 3.4.3 regarding approximate generators, we use the derivatives of  $\tau(q)$  at  $q = 1$  to estimate the parameters: the first derivative to estimate  $\beta$  for the “best-fit”  $\beta$ -model and the second derivative to measure the curvature of the  $\tau(q)$  function at  $q = 1$ . The derivatives are estimated directly by the scaling of the derivatives of the moments, as described in Section 3.3

In order to illustrate the goodness-of-fit of the  $\beta$ -model and to characterize the second-order structure, we plot  $\tau^{(2)}(q)$  versus  $\hat{\beta} = 1 + \tau^{(1)}(1)/2$  for various values of  $q$  in the neighborhood of  $q = 1$  in Figures 4.21 through 4.24. For  $q = 0.5$  (Figure 4.21), the  $\tau^{(2)}(q)$  values are mostly negative, which is of course an anomaly since  $\tau(q)$  is in general convex. Hence we ignore the  $q = 0.5$  results as strongly influenced by the anomalous concavity discussed above. Most of the second derivatives for  $q = 1$  (Figure 4.22) are positive, but there are still a lot of negative values and the average is clearly smaller than in the results for  $q = 1.5$  (Figure 4.23). While it is not necessarily true that the second derivative will decrease with  $q$  for  $q > 1$  either in theory or in data, there is a strong bias toward this in data, due to asymptotic linearity of estimated  $\tau(q)$  functions (see, e.g., Schmitt et al. 1994). Hence one suspects that we see here still some effect of the anomalous concavity at  $q = 1$ , and probably the best estimate of the second derivative is given by its maximum. At  $q = 2$ , the number of negative values is smaller than at  $q = 1.5$ , but the average has decreased, so the maximum observed curvature is at  $q = 1.5$ . So we will use  $\tau^{(2)}(1.5)$  as the characteristic measure of deviation from the  $\beta$ -model.

Evidently  $\tau^{(2)}(1.5)$  is on the order of 0.15 for all three data sets, though it decreas-

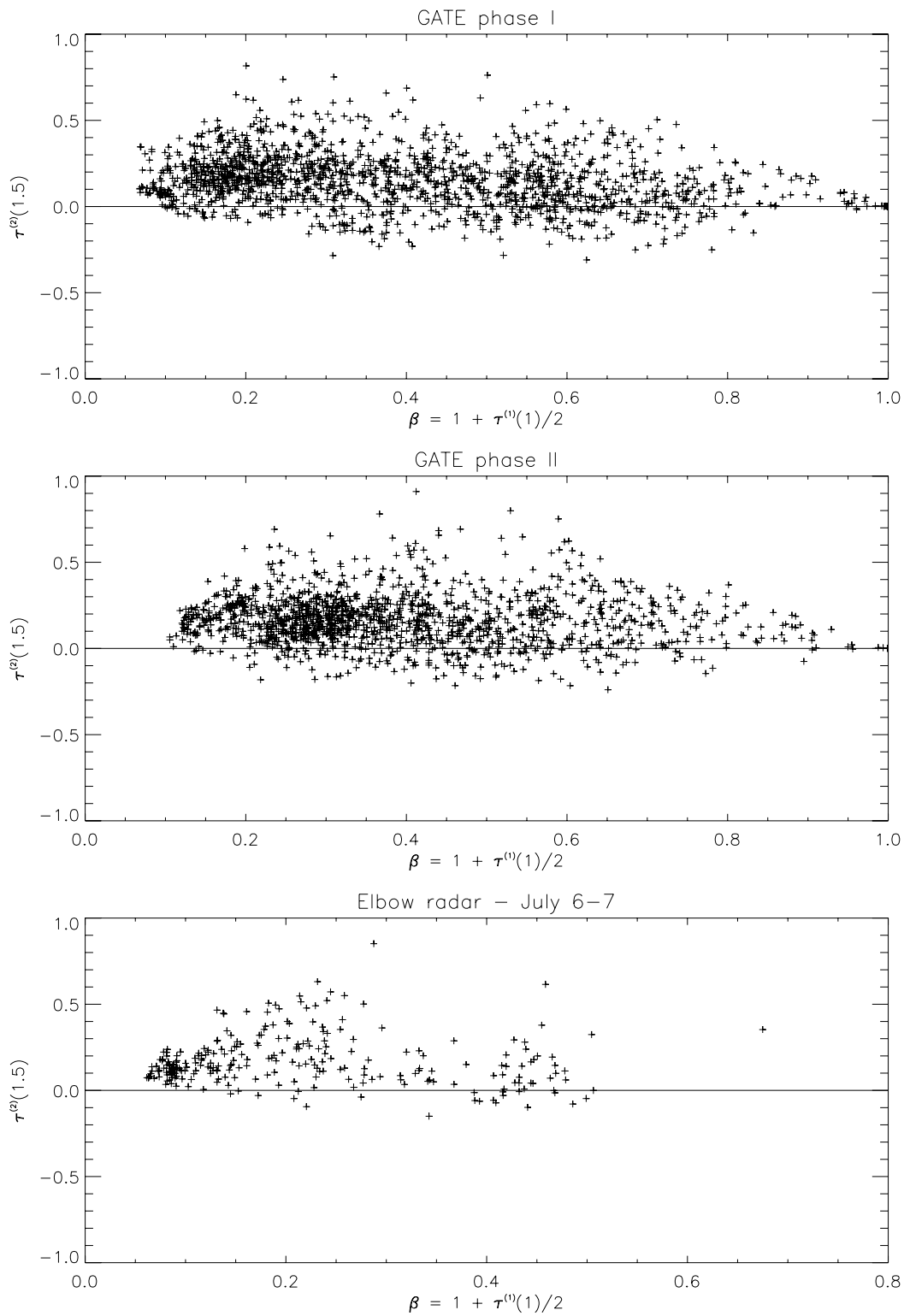


Figure 4.21  $\tau^{(2)}(0.5)$  vs. beta

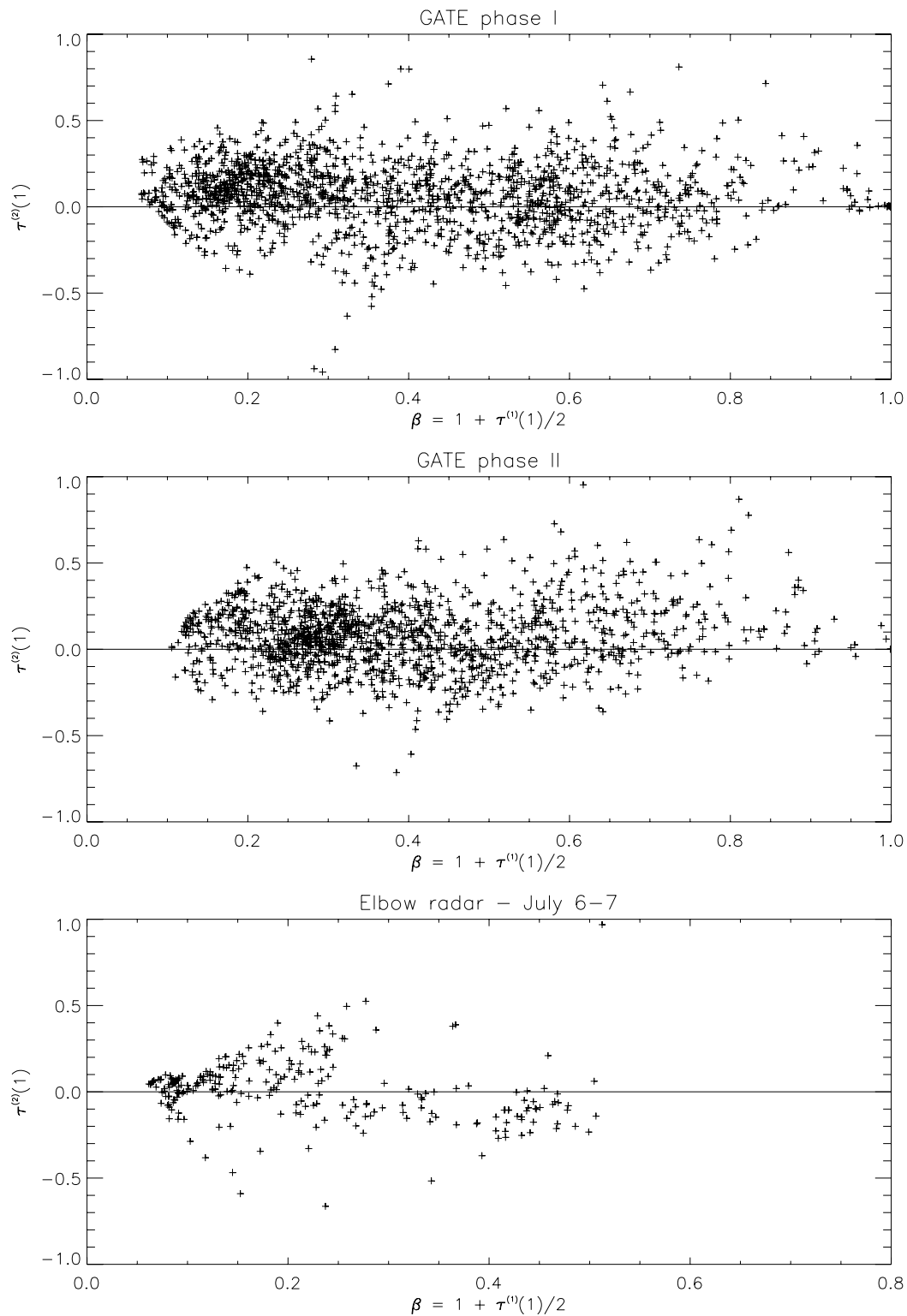
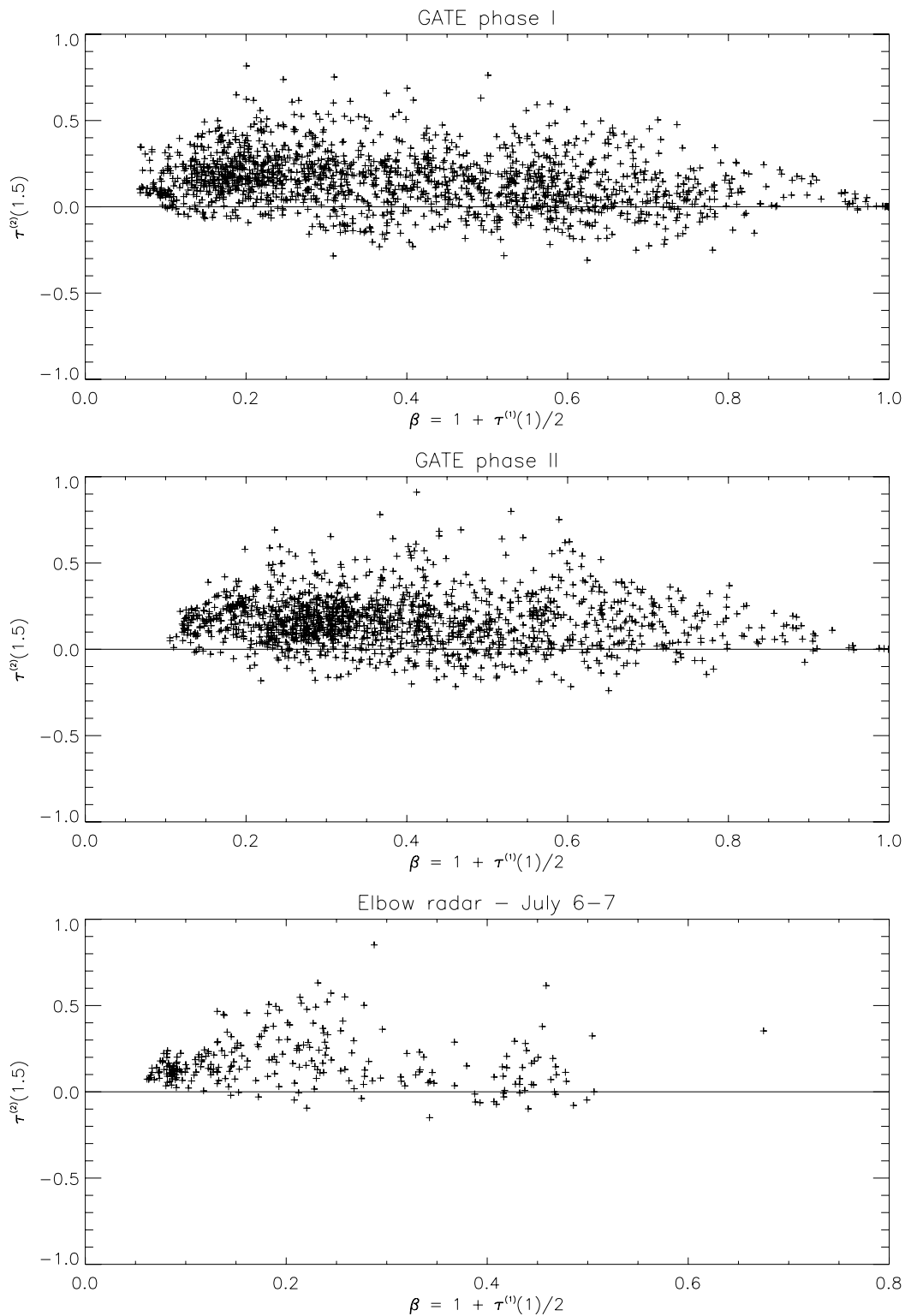
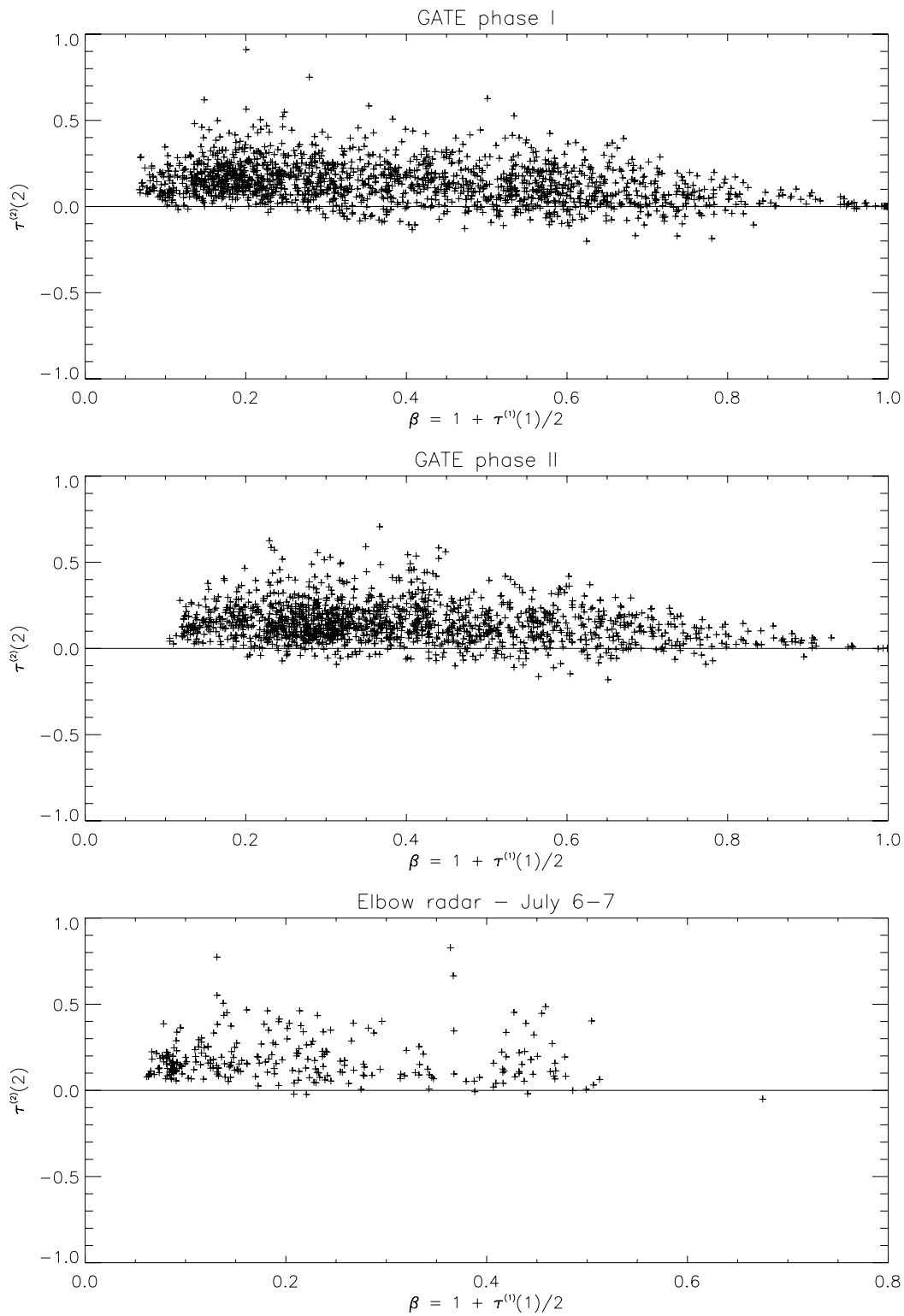


Figure 4.22  $\tau^{(2)}(1)$  vs. beta



**Figure 4.23**  $\tau^{(2)}(1.5)$  vs. beta

**Figure 4.24**  $\tau^{(2)}(2)$  vs.  $\beta$

es somewhat with  $\hat{\beta}$ . By comparison with simulation results (not shown here), this decrease could easily be an effect of sampling error. Hence there is no clear evidence that the distribution of the positive part of the cascade generator depends on the value of  $\beta$ , and thus we cannot reject the hypothesis that each data set comes from a second-order generator homogeneous sequence of scenes of data, in the sense defined in Section 3.4. Notice that this conclusion differs somewhat from the conclusions in Over and Gupta (1994), where it is reported that the  $\beta$ -model fit is good except for smaller values of  $p$  (equivalent to smaller values of  $\beta$ ). Here, using different measures of the deviation, it is more clear that  $\beta$ -model needs a roughly equal amount of correction for all  $\beta$ . It is also apparent that we cannot even reject the hypothesis that all three data sets are second-order generator homogeneous. This latter conclusion is remarkable particularly in view of the very different origin of the Elbow radar data vis-a-vis the GATE data. We will return to this issue of homogeneity between regions in the following section.

If we apply the second-order model (that is, the lognormal model) in the homogeneous form  $W^i = B^i Y$ , we have

$$Y = b^{-\sigma^2 \log b / 2 + aX}, \quad (4.30)$$

where  $X$  is a unit normal random variable. Recall that the MKP function in this case is given by

$$\chi_b(q) = (\beta - 1)(q - 1) + \frac{\sigma^2 \log b}{2}(q^2 - q) \quad (4.31)$$

(equation (3.116)) and thus has the first derivative

$$\chi_b^{(1)}(q) = \beta - 1 + \left(\frac{\sigma^2 \log b}{2}\right)(2q - 1) \quad (4.32)$$

and second derivative

$$\chi_b^{(2)}(q) = \tau^{(2)}/2 = \sigma^2 \log b. \quad (4.33)$$

We estimated from data that  $\tau^{(2)}(q) \cong 0.15$ , which corresponds to  $\chi_b^{(2)}(q) = 0.075$  and

$$\sigma = \sqrt{\frac{\chi_b^{(2)}(q)}{\log b}} = \sqrt{\frac{0.075}{\log 4}} = 0.2325\dots, \quad (4.34)$$

taking  $b = 4$  more or less arbitrarily.

So is  $\chi_b^{(2)}(q) = 0.075$  large or small? In order to be sure of our estimate of  $\chi_b(q)$ , let us first check the range of  $q$  for which the scaling of the moments estimates the MKP function according to Theorem 3.2. Since for the lognormal model

$$q_c = \frac{2(1-\beta)}{\sigma^2 \log b} = \frac{2(1-\beta)}{0.075} \quad (4.35)$$

(from equation (3.119)),  $q_c$  is quite large, even for large  $\beta$ . Thus the governing condition of Theorem 3.2 is the moment ratio condition, which is satisfied for

$$q < \sqrt{\frac{1-\beta}{\sigma^2 \log b}} \cong 3.651 \sqrt{1-\beta} \quad (4.36)$$

(from equation (3.122)). This gives a decent range of satisfaction of the conditions of Theorem 3.2; for example, when  $\beta = 0.2$ ,  $3.651 \sqrt{1-\beta} \cong 3.265$ , and when  $\beta = 0.5$ ,  $3.651 \sqrt{1-\beta} \cong 2.581$ . Thus we may be confident of our estimates of  $\chi_b(q)$  for  $q$  up to about 2.5 for most values of  $\beta$ .

One gauge of the size of  $\chi_b^{(2)}(q)$  is its statistical significance, i.e., whether it is significantly different from zero. The data analysis (Figures 4.22 through 4.24) gives good visual evidence that it is significantly greater than zero, since nearly all the points

lie above zero.

Another way to gauge whether  $\chi_b^{(2)}(q) = 0.075$  is large or small is to compare this second-order MKP function with the equivalent first-order MKP function, i.e., the MKP function of the  $\beta$ -model with the same slope at  $q = 1$ . To compute this, notice from equation (4.32) that for the second-order MKP function

$$\chi_b^{(1)}(1) = \beta - 1 + \left(\frac{a^2 \log b}{2}\right), \quad (4.37)$$

so the equivalent first-order MKP function is

$$\chi_b(q) = \left[\beta - 1 + \left(\frac{a^2 \log b}{2}\right)\right](q - 1), \quad (4.38)$$

since we need  $\chi_b(1) = 0$ . These two MKP functions are plotted against each other for  $\beta = 0.1$  and  $\beta = 0.5$  in Figure 4.25 below. There it is evident that in the neighborhood of  $q = 1$ , the differences are pretty minor, especially for small  $\beta$ , but for larger values of  $q$ , the second order effects grow increasingly important. The determination of the importance of the second order effects must come from the importance of the extremes in the application of the theory under consideration.

## 4.6 Dependence of Cascade Parameters on Large-Scale Average Rain Rate

### 4.6.1 Results

Heretofore, all of this thesis has been concerned with the description of the spatial pattern observed in rainfall field data. A fundamental problem that has not been discussed here is the issue of prediction. The basic prediction problem here is not in time, as in most modeling studies, but in scale. Another way of describing the study we have been undertaking is the following question, ‘‘Given all the available relevant information regarding the rainfall fields at some scale  $l_{max}$ , what is the ‘best’ prediction of the

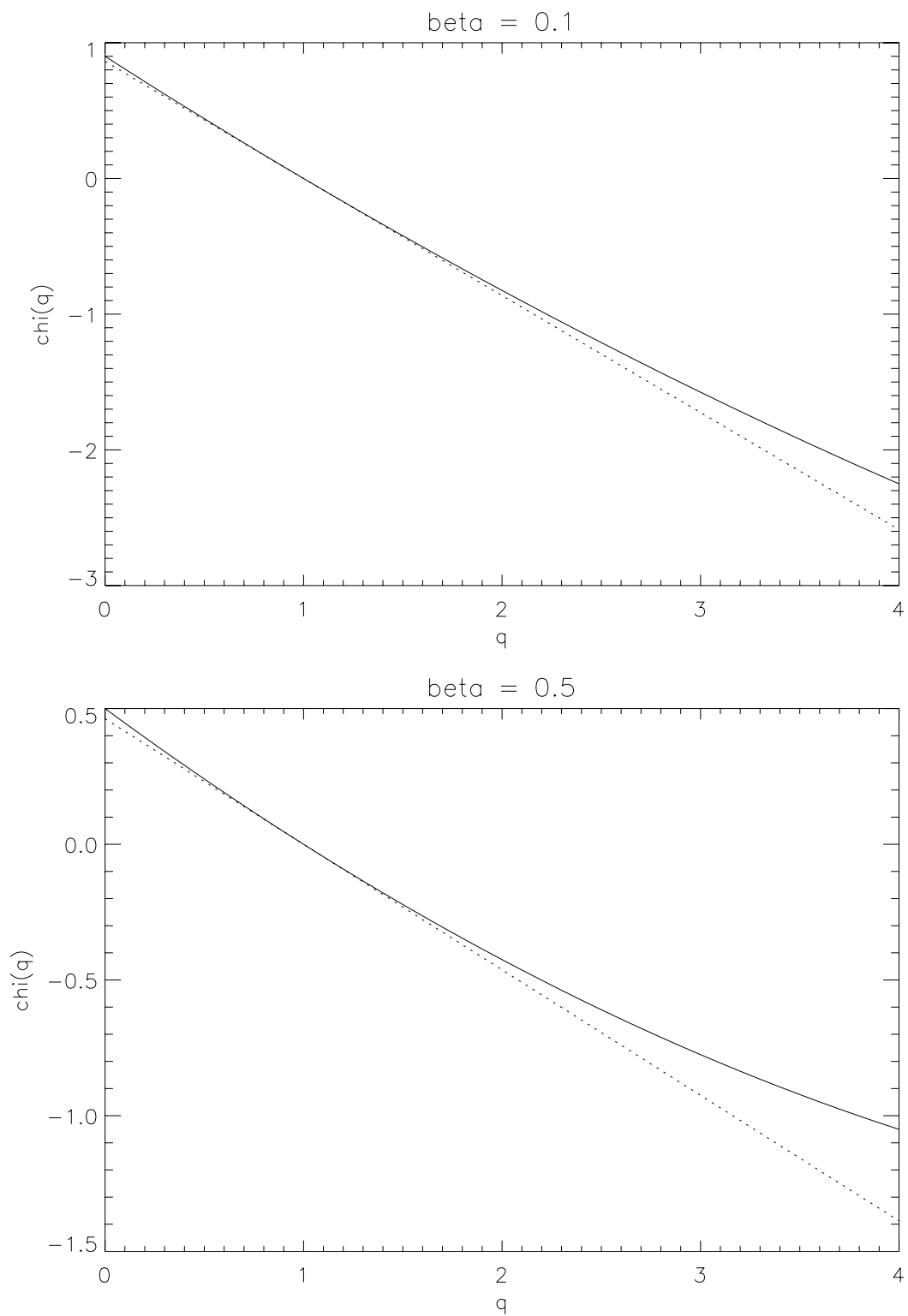


**Figure 4.25** First and second-order MKP functions with equal slopes at  $q=1$   
(a)  $\beta=0.1$ , (b)  $\beta=0.5$

structure of the field at any or all smaller scales?” An answer to this question is necessary for many applications. One important example is the problem of the parameterization of convection in large-scale atmospheric models. Because of the importance of these problems, a large literature has developed regarding the relationship between the large-scale information (or “forcing”) and the convection that arises at the small scale in response to it. Typically however the spatial structure at the small scale has not been a concern, instead, usually just the large-scale effects of the convection, such as the heating of the atmosphere due to the release of latent heat, are of concern. However, as described in the introduction, in hydrologic applications to floods, the spatial structure is critical, because the timing of runoff is sensitive to it.

We present here a very simple test of the dependence of the small-scale spatial structure on the large-scale conditions. We have seen that the scaling structure of sequences of scenes of radar rainfall data can be parameterized to the second order by a variable parameter governing the slope of the MKP function ( $\beta$ ) and a constant parameter governing its curvature. Since  $\beta$  is the only parameter that varies, it will serve as an indicator of the spatial pattern of the rainfall as modeled by a random cascade. To describe the large-scale conditions, we simply compute the average rain rate over the whole scene (the variable  $\bar{R}$  used in Chapter 3). We can then simply test how  $\beta$  depends on  $\bar{R}$ . A priori, one could imagine a number of possible relationships between  $\bar{R}$  and  $\beta$ . The simplest possibility is that  $\beta$  does not depend on  $\bar{R}$ . However, since  $\beta$  governs the fraction of rainy area, which one would expect to depend on  $\bar{R}$ , this does not seem very likely. A second, still relatively simple, possibility is that  $\beta$  and  $\bar{R}$  are related by a one-to-one function. In this case, apart from random fluctuations (which of course could be quite significant), knowing  $\bar{R}$  is equivalent to knowing  $\beta$ . The third possibility we consider is that  $\beta$  and  $\bar{R}$  are dependent, but not by a one-to-one function. There are other large-scale factors in addition to  $\bar{R}$  that have an effect on  $\beta$ .

To answer this question for these data sets, consider the following plots. They contain the value of  $\beta$  estimated by various methods plotted as a function of  $\bar{R}$ . The value of  $\beta$  plotted in Figure 4.26 was estimated from the scaling of the rainy areas ( $\tau(0)$ ). The value of  $\beta$  plotted in Figures 4.27 and 4.28 was computed from the slope of the  $\tau(q)$  function, with  $q = 1$  in Figure 4.27 and  $q = 0.5$  in Figure 4.28. All three figures clearly show that  $\beta$  and  $\bar{R}$  are related by a one-to-one function. For the moderate to large average rain rates, the form of this function is approximately exponential, and the parameters of a least-squares exponential fit, weighted so that the larger rain rates control the slope of the line, are given in the plot. The parameters of the fitted line show that at the least, the two sets of GATE rainfall data have very similar  $\beta$  versus  $\bar{R}$  relationships. The fit for the Elbow radar data differs from the GATE data primarily in its intercept, though in Figure 4.27, where the fit is not very good, the slope is also somewhat different. It is curious that the fits are not as good for  $q = 1$  as for  $q = 0$  and  $q = 0.5$ .

The exponential relationship fitted in these plots has the form

$$\beta = s \log \bar{R} + i \text{ or } e^\beta = \bar{R}^s e^i, \quad (4.39)$$

where  $s$  is the slope and  $i$  is the intercept of the regression fit. This may be written in a more illuminating form by a little algebraic manipulation. First, notice that as  $\beta$  goes to zero,  $\bar{R}$  goes to some maximum value which we will call  $R_{max}$ . When  $\beta = 0$ ,  $1 = R_{max}^s e^i$ , so  $R_{max} = e^{-i/s}$ , so equation (4.39) becomes

$$\beta = s \log \frac{\bar{R}}{R_{max}} \text{ or } e^\beta = \left( \frac{\bar{R}}{R_{max}} \right)^s \quad (4.40)$$

Because the Elbow radar data differ from the GATE data primarily in the value of the intercept, from equation (4.40) it can be seen that this means they have different maxi-

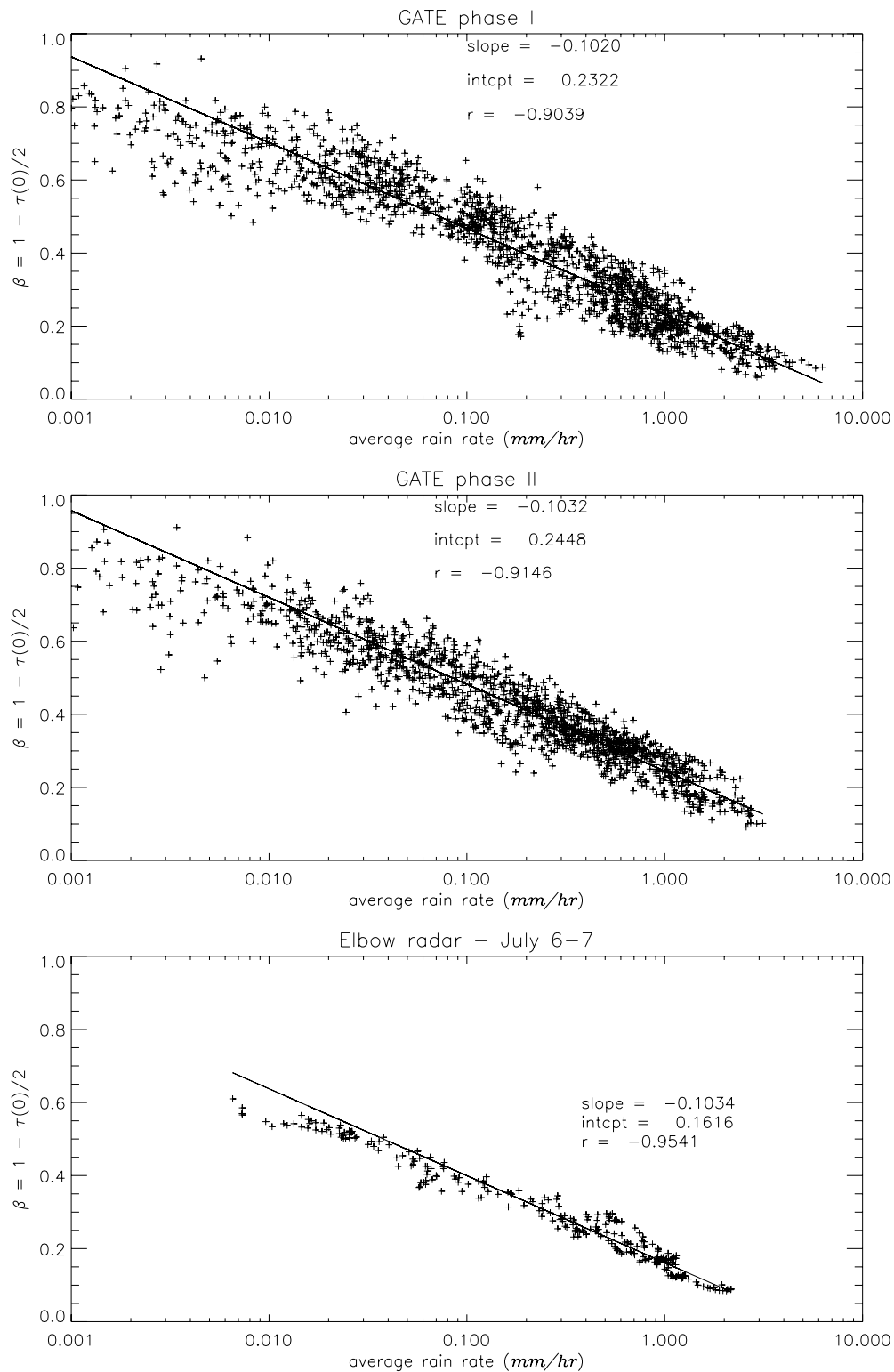


**Figure 4.26 Beta estimated from  $\tau(0)$  vs. average rain rate**

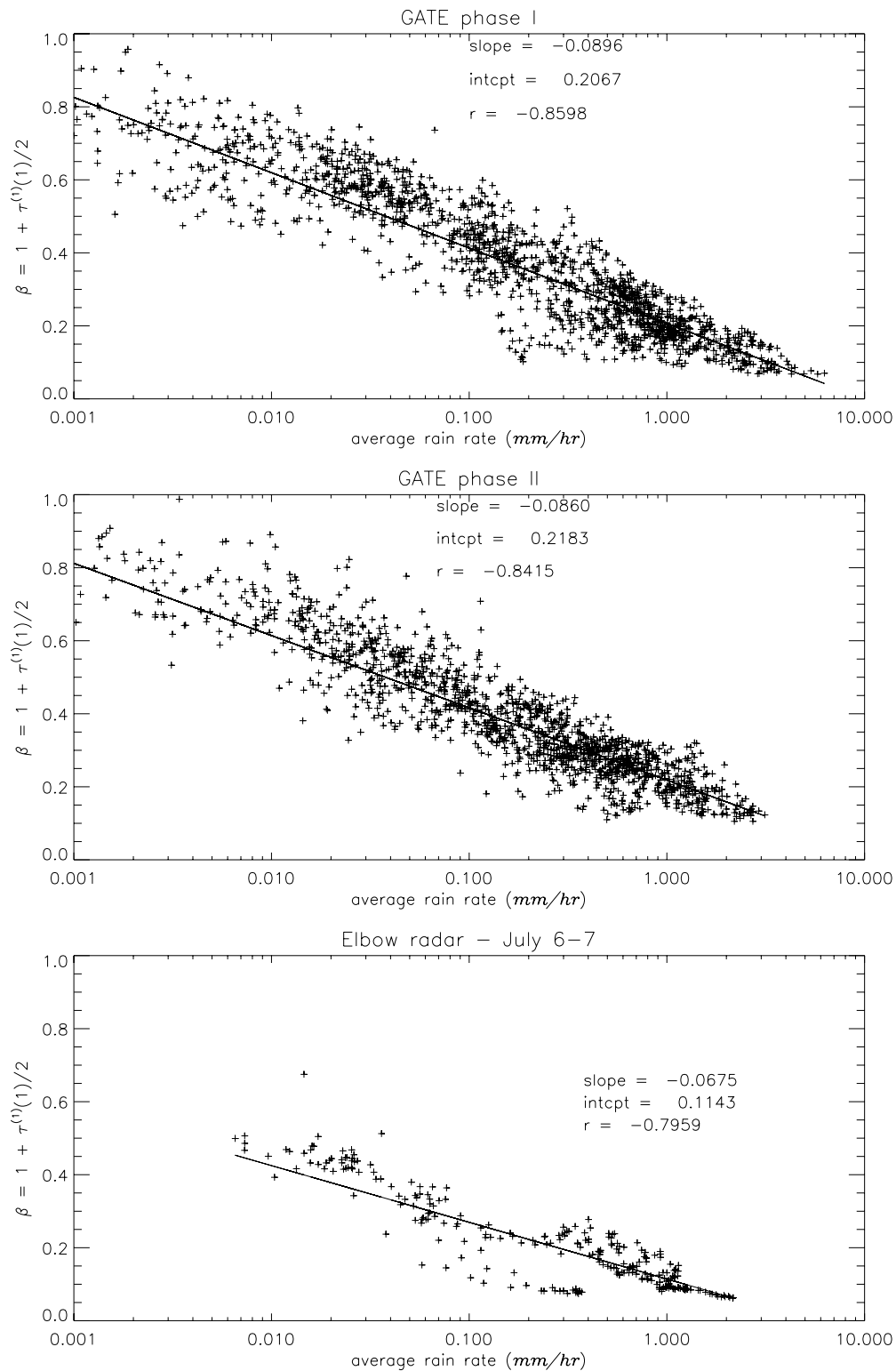


**Figure 4.27** Beta estimated from  $\tau^{(1)}(1)$  vs. average rain rate

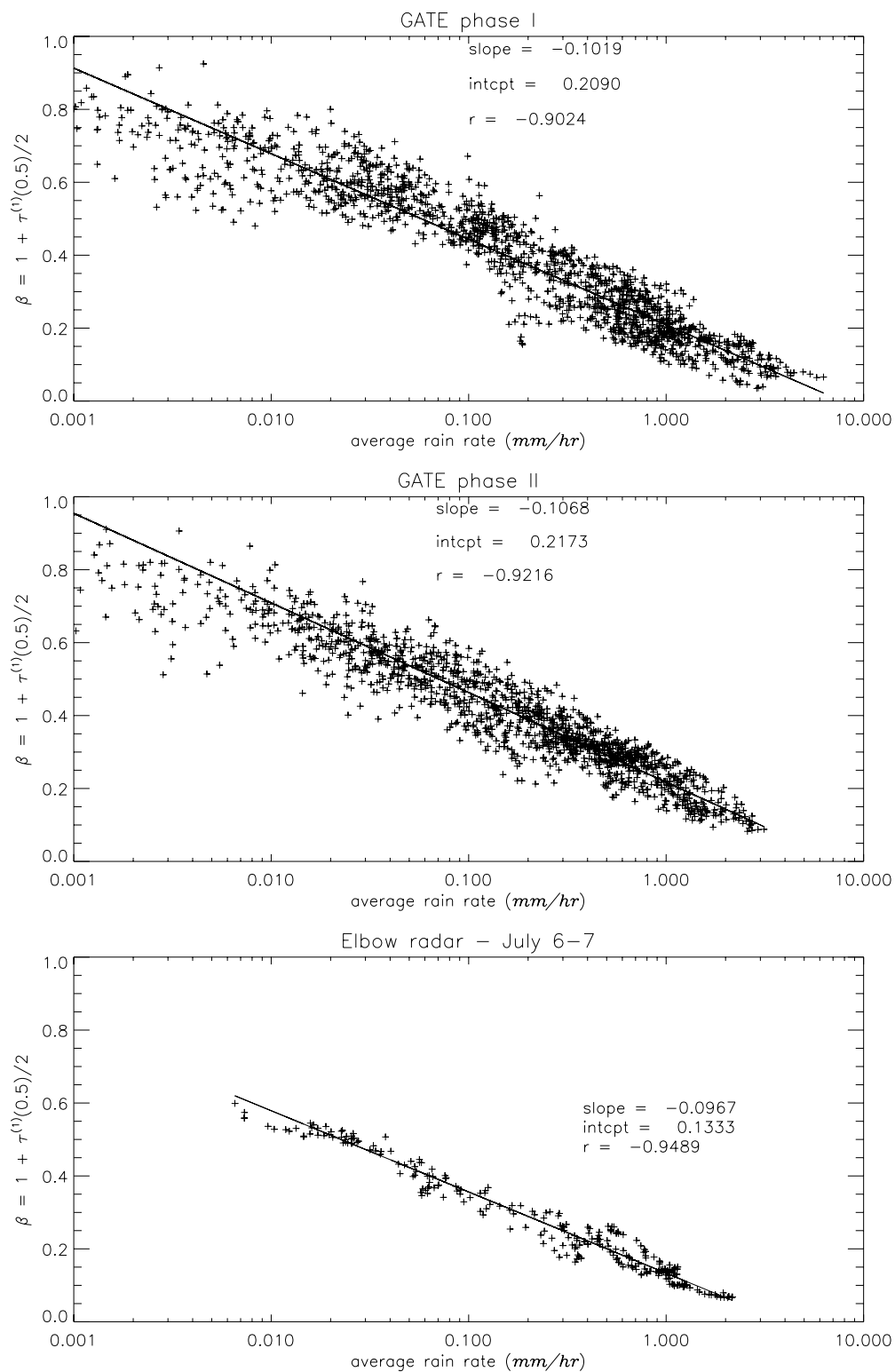


**Figure 4.28** Beta estimated from  $\tau^{(1)}(0.5)$  vs. average rain rate

imum rain rates (with the Elbow radar data being smaller), but as a function of the dimensionless average rain rate,  $\bar{R}/R_{max}$ , they are almost the same.

#### 4.6.2 Interpretation

While such a relationship as equation (4.40) is useful in itself because, given its parameters are known over some region of interest, it specifies the parameters of a subgrid-scale spatial rainfall distribution, a more basic and ultimately more useful question is why such a relationship would hold. Given the answer to this question, one might be able to compute its parameters from *a priori* considerations. We derive next an interpretation of equation (4.40) under the assumption of second-order generator homogeneity of the cascade generator by examining the distribution of rain rates conditioned on rain.

Consider the rain rate  $R_\infty^+$  in a box  $\Delta_n^i$  at level  $n$  resulting from a random cascade whose initial intensity  $R_0$  is governed by equation (4.40) conditioned on the rain rate being positive:

$$R_\infty^+(\Delta_n^i) = R_\infty(\Delta_n^i) \parallel R_\infty(\Delta_n^i) > 0 = R_{max} e^{\beta/s} \left( \prod_{j=1}^n W_j^+(\Delta_n^i) \right) Z_\infty^+(\Delta_n^i), \quad (4.41)$$

where  $Z_\infty^+(\Delta_n^i) = Z_\infty(\Delta_n^i) \parallel Z_\infty(\Delta_n^i) > 0$  and, as usual,  $W^+$  is the positive part of the generator  $W$ . Because we are considering simultaneously the behavior of the whole set of data, it is natural to assume that the generator is of the type we defined as second-order generator homogeneous, that is,  $W = BY$ , where  $B$  is a  $\beta$ -model generator and  $Y$  is generator with positive support. In this case we have

$$W \parallel W > 0 = W^+ = b^\beta Y, \quad (4.42)$$

Substituting this into equation (4.41) gives

$$R_{\infty}^+(\Delta_n^i) = R_{max} e^{\beta/s} b^{\beta n} \left( \prod_{j=1}^n Y_j(\Delta_n^i) \right) Z_{\infty}^+(\Delta_n^i). \quad (4.43)$$

Now, apart from  $Z_{\infty}^+(\Delta_n^i)$ , the only factors on the right-hand side that depend on  $\beta$  are

$$e^{\beta/s} b^{\beta n} = e^{\beta/s + n\beta \log b}. \quad (4.44)$$

Let us assume, to see where it leads, that at some level  $n$  the scaling breaks, such that the smaller scale variability is independent of that at the larger scales. A radical form of this assumption would be to posit the existence of a scale below which the spatial rainfall process is smooth, but the more general assumption we have made is sufficient. The result is that the high frequency factor  $Z_{\infty}^+(\Delta_n^i)$  no longer depends on  $\beta$ .

Therefore, when

$$\beta/s + n\beta \log b = 0, \quad (4.45)$$

the right-hand side and hence the rain rates conditioned on being positive will be independent of  $\beta$ . The only variable in equation (4.45) (apart from  $\beta$ ) is  $n$  so solving for it we obtain

$$n = \frac{-1}{s \log b}, \quad (4.46)$$

which gives a level at which the distribution of rain rates conditioned on being positive is independent of  $\beta$ . For the GATE data we have  $s \cong -0.1$  and taking  $b = 4$ , equation (4.46) gives  $n \cong 7.2$ . Since for  $b = 4$ , the data has  $n_{max} = 6$  levels, this scale is somewhat more than one level smaller in scale than the resolution of the data. More precisely, the ‘‘scale of homogeneity’’  $l_h$  is given by  $l_h = l_{max} b^{-7.21/2} \cong 1.7$  km since  $l_{max} = 256$  km.

The existence of such a scale perhaps could have been anticipated by observing

from equation (4.40) that for small  $\beta$  the initial rain rate is large while the growth of the mean positive rain rates with level is by a factor of  $b^\beta$ , only slightly greater than one. On the other hand, for large  $\beta$  the initial rain rate is small while the growth rate of mean positive rain rates  $b^\beta$  is large. Hence for any two values of  $\beta$ , there must be a scale at which their mean positive rain rates are equal. It is not however clear from this argument that this would occur at the same scale for all values of  $\beta$ , nor that it would hold for the whole distribution, since only the mean was used in the argument. Thus the  $\beta - \bar{R}$  relationship, coupled with the second-order homogeneity of the data, seems to be saying something very fundamental. The assumption of small-scale homogeneity makes the argument somewhat circular, but seen from the point of view of a consistency check, it is very nice: if, as seems at least possible intuitively, the variability at scales smaller than some level  $n$  depends only on the distribution *at* level  $n$  (like a Markov process indexed by scale), then the  $\beta - \bar{R}$  relationship, second-order homogeneity, and small-scale homogeneity fit together perfectly. Notice that this scale depends only on the slope  $s$  of the  $\beta$  versus  $\log \bar{R}$  plot, not on the intercept. The intercept is apparently fixed in some other way. Under this interpretation of the results, since the GATE and Elbow radar data have about same slope in their  $\beta$  versus  $\log \bar{R}$  plots, they have the same homogeneity scale.

In addition, consider what would occur if some break in scale did not occur at this level. Consider positive rain rates at scales smaller than the homogeneity scale. Clearly these are larger, the larger the value of  $\beta$  (i.e., the smaller the average rain rate), which could possibly be true for somewhat smaller scales, but for much smaller scales, it seems very unlikely, and the rain rates themselves would be enormous.

It is worthwhile to consider such sweeping conclusions in the light of the other literature on the subject. There is a large body of published observations from various types of storms in various locations (including GATE) of statistics describing convec-

tive updrafts and downdrafts, such as diameters and velocities (see, e.g., Lucas et al. 1994, Jorgensen and LeMone 1989, and references therein). These studies contain intercomparisons of the statistics from each type of storm with the other types, and discuss possible explanations for the differences. The main differences seem to be between oceanic convection on one hand (including hurricanes) and continental convection on the other. The continental convection is more intense, updrafts and downdrafts are larger, and it is associated with greater instability, measured by convective available potential energy (CAPE) (Lucas et al. 1994, Jorgensen and LeMone 1989). These studies do not, however, consider the dependence of the statistics within a given storm type on various environmental factors. Perhaps this is done just to obtain larger samples, but it does suggest the null hypothesis that the statistics describing convection of each type and location are homogeneous, i.e., independent of environmental factors, given that type and location.

A second relevant body of literature has developed around the issue of the estimation of tropical oceanic rainfall from satellites in anticipation of the Tropical Rainfall Measuring Mission (TRMM). A technique that seems to have a lot of promise is the so-called threshold method, originally called the area-time integral method (Doneaud et al. 1981). This method is based on the intriguing and useful empirical fact that in tropical oceanic rain (including the GATE rainfall fields), the average rain rate in a scene is linearly dependent with a very small variance on the fraction of area in the scene with rain rates greater than the threshold, for some threshold rain rate in the neighborhood of the mean of the positive rain rates.

This phenomenon can be “explained” if it is assumed, among other things, that the positive rain rates are identically distributed (see, e.g., Kedem et al. 1990). The problem with this explanation is that its assumption is easily shown to be false at the resolution at which data is available. The present results suggest however that the

assumption may actually be true (like the observationalists seem to think) at a scale that it is not typically accessible to radars, let alone passive microwave radiometers. The non-homogeneity that is evident at coarser resolution can then be understood, as Morrissey (1994) recently suggested basically on intuitive grounds, as due to clustering, which must be an increasing function of rainy area and hence of average rain rate, given the small-scale homogeneity assumption. Finding this evidence of small-scale homogeneity in a scaling context also gives hope that one of the outstanding problems of the threshold method may be solvable in this framework, that is, the effect of change of resolution of the sensor.

Finally we briefly discuss a relevant Buckingham Pi-type scaling argument put forth by Emanuel (1994, pp. 333ff.). He defines equilibrium convection as that “in which the generation of CAPE by large-scale processes nearly balances its consumption by convection” (Emanuel 1994, p. 333). Equilibrium convection is much more common than the other kind, triggered convection, in which CAPE builds up over a long time and is consumed by convection quickly, because typically the large-scale forcing varies more slowly than the time scale of convective response. In particular, equilibrium convection is observed over the oceans, while triggered convection is observed in severe continental thunderstorms. Thus Emanuel’s two types of convection appear to correspond to the two types of observations discussed above. Emanuel asks regarding equilibrium-type convection how the fractional area of convective updrafts and their velocities depend on the large-scale convective mass flux rate. While these are not the same quantities as we have been dealing with, they seem quite analogous. We have not discussed fractional rainy area in this context but it is certainly available from an argument like that resulting in equation (4.43). The updraft velocity is a measure of the intensity of the convection, as is the rain rate in a small box, conditioned on it being positive. And clearly the large-scale convective mass flux is related to the

large-scale average rain rate, though the former is more a cause and the latter more of an effect.

Emanuel argues that equilibrium convection can be characterized by three parameters,  $M_c$ , the large-scale convective mass flux (the forcing),  $N$ , the buoyancy frequency of the stable environment of the clouds, and  $D$ , the depth of the convection. By the Pi theorem, these three form one dimensionless parameter,  $F = M_c/(ND)$ . The fractional area of convective updrafts,  $\sigma$ , and their vertical velocity,  $\omega_c$ , enter through the fact that their product gives the convective mass flux, i.e.,  $M_c = \sigma\omega_c$ . Since  $\sigma$  is dimensionless, it must be given by  $\sigma \sim F^m$ , which implies  $\omega_c \sim M_c F^{-m}$ . A physical argument is used to obtain a value for  $m$ . It is based on the transience of convection, assuming that a cloud forms in response to slight environmental instability. Thus the updraft velocity is related to the amount of CAPE produced by the large-scale processes in the time it takes for surface air to ascend through the depth of the convection. For dimensional reasons, a velocity should be proportional to the square root of CAPE, giving the result that  $m = 2/3$ . Thus we have

$$\sigma \sim \left(\frac{M_c}{ND}\right)^{2/3} \quad (4.47)$$

and

$$\omega_c \sim M_c^{1/3} D^{2/3} N^{2/3}. \quad (4.48)$$

This result says that the fractional area of updrafts increases more quickly with the large-scale forcing than does the updraft velocity (the measure of convective intensity), though the updraft velocity does increase. If the conclusion was that the updraft velocity did not increase with the large-scale forcing, it would be analogous to what we have been arguing from the cascade analysis of GATE data. His conclusions indi-

cate that there may be physical reasons to believe that the updraft velocity at least, if not the positive rain rates, increase with large-scale forcing.

The tentativeness of Emanuel's argument for the exponent  $m$  and the lack of empirical study of this question leave it very much an open issue, in which the interpretation of the cascade results we have given could turn out to be largely correct.

## **Chapter 5**

# **A Theory of Space-Time Rainfall Using Random Cascades**

### **5.1 Introduction**

In this chapter the spatial theory developed in Chapter 3 and tested in Chapter 4 is extended to include temporal evolution of the spatial field. This is necessary because the sequence of scenes of data analyzed in Chapter 4 are not, as the sequential analysis might suggest, an independent sequence with varying parameters. Instead, as intuition and statistical analysis would both suggest, they are highly dependent from one scene to the next.

The variation of the parameters of the sequence of spatial scenes implies that the theory will have to be non-stationary. In correspondence with the analysis of the dependence of the spatial cascade parameters on the large-scale average rain rate in Chapter 4, the non-stationarity will be introduced by use of forcing by large-scale average rain rate, which is assumed to be prescribed.

It will become clear in the construction of the theory in Section 5.2 that it is natural to construct a Lagrangian theory (that is, following the flow). This introduces however, some difficulty in testing the theory, since data from fixed sensors has to be “tracked” to put it in the Lagrangian frame of reference. It also has implications for applications, such as modeling the rainfall over a river basin, which, of course, would be fixed in the Eulerian frame of reference. However, the Lagrangian approach is chosen because in addition to the naturalness of the construction, it also seems critical in un-

derstanding the space-time structure of rainfall to separate variability experienced over a fixed region due to advection from that due to evolution in the Lagrangian frame of reference.

A space-time random cascade theory that reflects the considerations just discussed is proposed in the next section, and various general predictions are derived. The generator process that lies at the heart of the theory consists of two components, which are specified as the second order approximation to the results of the spatial analysis of the GATE data, and are analyzed in detail in Section 5.4. Following the GATE results, the first order process is non-stationary and forced by the large-scale average rain rate, while the second order process is stationary. The primary prediction derived from the theory developed here is the scaling of two-point temporal cross-moments, which, quite analogously to the spatial case, provides a test of the theory and allows the estimation of the additional parameters introduced by the extension to space-time. This is presented in Section 5.2. The Lagrangian and Eulerian cross moments are derived in Section 5.3, with a resulting prediction regarding Taylor's hypothesis of fluid turbulence. Tests of the theory are carried out for a case study of tracked radar rainfall data and are presented interspersed with theory as predictions of the theory are derived.

## 5.2 A General Theory of Space-Time Cascades

The following natural criteria are proposed as required of a time-evolving cascade theory of space-time rainfall:

- (a) The space-time process must be *consistent* with the spatial theory, i.e., at any fixed time, the space-time process must reduce to a random cascade.
- (b) The space-time process must be *causal*, i.e., the future can depend only on the present or past. That is, at time  $t$ , the state of the system at times  $s \geq t$  must depend

only on its state at times  $r \leq t$ .

(c) The space-time process must be *contingent* on the large-scale forcing such that as  $t \rightarrow \infty$  with a constant forcing, the spatial cascade converges to the appropriate cascade model, regardless of the initial condition.

(d) The space-time process should contain fluctuations such that, as  $t \rightarrow \infty$  with constant forcing, the spatial cascades generated by the space-time process will trace out their whole sample space with the appropriate probability measure.

This last condition says essentially that the transformation of the cascade measure from one time to the next is *ergodic*. For an introduction to ergodic theory, see, for example, Breiman (1992, chapter 6). The ergodicity of the space-time process has important implications for parameter estimation for the stationary case, since then time averages would converge to ensemble averages. In fact, we assume this in Section 5.3 when estimating the ensemble average Lagrangian cross moments from temporal averages. However, a proof of the ergodicity of the space-time process will not be attempted here.

### 5.2.1 The Construction

Criterion (a) suggests the following construction: maintain the cascade structure in space, but replace the iid generators with possibly non-stationary iid stochastic processes  $W_t$  that have marginal distributions satisfying the conditions of a cascade generator, i.e.,  $P(W_t \geq 0) = 1$  and  $EW_t = 1$  for all  $t$ . A schematic of this construction is shown in Figure 5.1. At any time  $t$ , the process generated by the cascading of the  $W_t$  will then reduce to an iid cascade with generator  $W_t$ , satisfying criterion (a). This construction will also satisfy causality, as long as the processes  $W_t$  are also causal in this sense. It will be convenient to choose the processes  $W_t$  such that for them, the future depends only on the present, i.e., as Markov processes. This is convenient because

Markov processes are widely studied, so examples can be taken “off the shelf”, and because it simplifies initialization of the system: merely specifying an initial condition is sufficient to determine probabilistically the evolution of the system. Though we do not have a general proof, it appears, however, that making the generator process Markovian does not make the mass or rain rate in a pixel Markovian. We will demonstrate the fulfillment of criterion (c) using this construction for a particular choice of generator processes that model the structure of GATE rainfall as analyzed in Chapter 4.

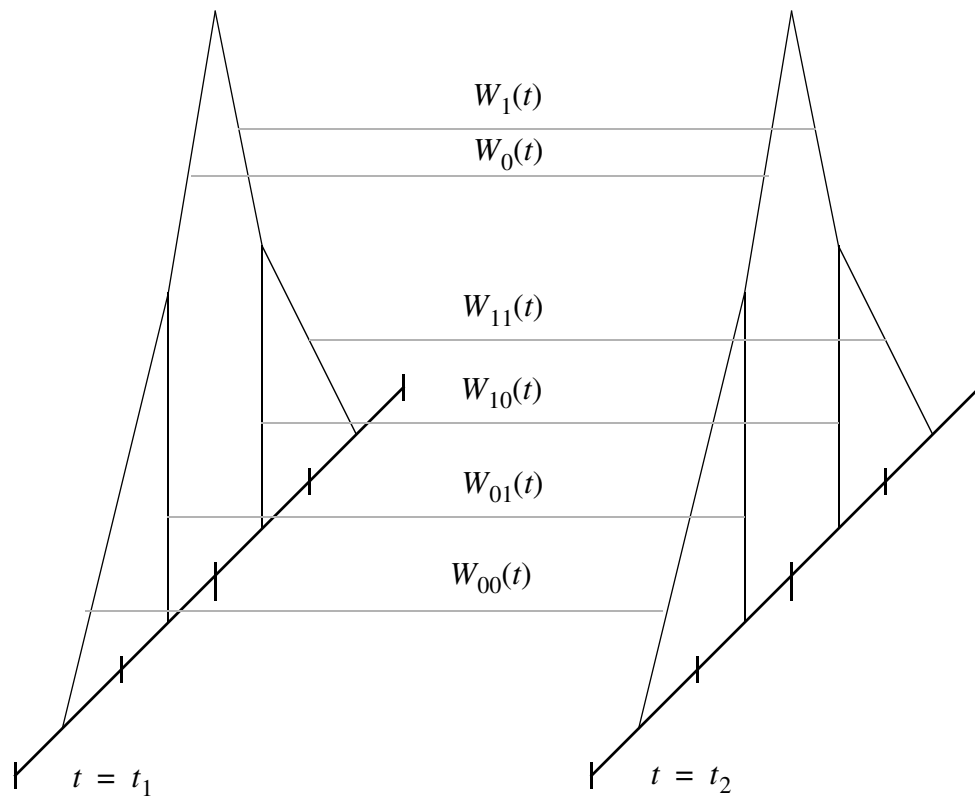


**Figure 5.1** Time-evolving cascade construction with  $d=1, b=2$

Notice that these criteria exclude the extension of the spatial model to time simply by making the cascade three-dimensional. First of all, the condition of causality would

be violated because the box  $\Delta_n^i$  over which a generator applied would have a finite extent in time, say from time  $t$  to time  $t + l_{max} v^{-1} b^{-n/3}$ , where  $l_{max}$  is the extent of the spatial cascade at the zeroth level and  $v$  is a constant (with units of velocity) that transforms  $l_{max}$  into the time domain. Thus at time  $t$  the system would “know” about the future up to time  $t + l_{max} v^{-1} b^{-n/3}$  for all  $n$ . Second, the finitude of the domain of applicability of a cascade in space, say, for all  $\tilde{x} \in [0, l_{max}]^2$  is appropriate (given, if no other scales intervene, the finitude of the size of the earth) but in time, where we would have  $t \in [0, l_{max} v^{-1}]$ , it is undesirable and in particular prevents the application of the notion of the system coming to equilibrium as  $t \rightarrow \infty$  as specified in criteria (c) and (d). Third, construction of a non-stationary version would require the spatial cascade to be non-homogeneous (i.e., having non-identically distributed generators) at any given time, since the distribution of the generators would have to change along the time axis in order to obtain the non-stationarity.

### 5.2.2 Scaling of the Moments: Testing and Parameter Estimation

Like the generators in the spatial model, the processes  $W_t$  themselves are not directly accessible in the data, so a means of testing the empirical validity of the construction and estimating its parameters is not immediately obvious. In fact, as we saw, methods that depend on ergodicity in space fail, but the generators can be recovered from the *scaling* properties of the data, which also turns out to be true for the space-time model. In fact, the scaling of a temporal cross-moment quantity will lead to a generalization of the MKP and  $\tau(q)$  functions from the spatial theory. As such, the development will be patterned after the computation of the scaling of the ensemble and spatial average moments of spatial cascades in Section 3.3. First the scaling of the expected (ensemble average) temporal cross-moments will be computed, and then it will be shown that under certain conditions on the generator process the scaling of the temporal cross-moments of a single realization of the process converge to the scaling of

the ensemble average temporal cross-moments.

To obtain the scaling of the ensemble average cross moments, define the sum of  $q$ th order cross-moments of the cascade masses at level  $n$  and at times  $t_1$  and  $t_2$  ( $t_2 \geq t_1$ ) as

$$M_n(q; t_1, t_2) = \sum_{i=1}^{b^n} \mu_\infty^q(\Delta_n^i; t_1) \mu_\infty^q(\Delta_n^i; t_2). \quad (5.1)$$

Notice that the right-hand side of equation (5.1) is the sum of the product of masses at the same location at different times. Since in data the rainfall field will have moved in this time, the tracking of this movement is critical to computing this quantity. Now consider the expectation over the ensemble of realizations:

$$EM_n(q; t_1, t_2) = \sum_{i=1}^{b^n} E[\mu_\infty^q(\Delta_n^i; t_1) \mu_\infty^q(\Delta_n^i; t_2)]. \quad (5.2)$$

Since  $\mu_\infty(\Delta_n^i; \cdot) = R_0(\cdot) l_{max}^2 b^{-n} Z_\infty(\Delta_n^i; \cdot) \prod_{j=1}^n W(\Delta_j^i; \cdot)$ , there are  $b^n$  of them, and they are identically distributed, we obtain

$$EM_n(q; t_1, t_2) = R_0^q(t_1) R_0^q(t_2) l_{max}^{4q} b^n b^{-2nq} E \left[ Z_\infty^q(t_1) \prod_{j=1}^n W_j^q(t_1) Z_\infty^q(t_2) \prod_{j=1}^n W_j^q(t_2) \right], \quad (5.3)$$

where it is understood that  $W(t_1)$  and  $W(t_2)$  refer to different times of the same process. Notice we have taken  $R_0(t_1)$  and  $R_0(t_2)$  to be non-random, since  $R_0(t)$  is prescribed. Since for each  $t$  the  $W_j(\cdot)$  are iid and independent from  $Z_\infty(\cdot)$ , equation (5.3) becomes

$$EM_n(q; t_1, t_2) = R_0^q(t_1) R_0^q(t_2) l_{max}^{4q} b^{n(1-2q)} E^n [W_{t_1}^q W_{t_2}^q] E[Z_\infty^q(t_1) Z_\infty^q(t_2)], \quad (5.4)$$

so

$$\begin{aligned} \log EM_n(q; t_1, t_2) &= n \log(b^{1-2q} E[W_{t_1}^q W_{t_2}^q]) \\ &\quad + \log E[Z_\infty^q(s) Z_\infty^q(t)] + q \log(R_0(t_1) R_0(t_2) l_{max}^4). \end{aligned} \quad (5.5)$$

Defining now a generalized MKP function

$$\chi_b(q; t_1, t_2) = \log_b E[W_{t_1}^q W_{t_2}^q] - (2q - 1), \quad (5.6)$$

we obtain

$$\begin{aligned} \log EM_n(q; t_1, t_2) &= n \log b \chi_b(q; t_1, t_2) \\ &\quad + \log E[Z_\infty^q(t_1) Z_\infty^q(t_2)] + q \log(R_0(t_1) R_0(t_2) l_{max}^4) \end{aligned} \quad (5.7)$$

(compare equation (3.34)). This result provides the form of the scaling of the expected cross moments, but does not show it can be obtained from a single realization (i.e., a single visit of the space-time cascade to its state at time  $t_1$  and its state at time  $t_2$ ). The following theorem, however, patterned after Theorem 3.2, asserts, however, that this scaling does obtain for a single realization in the small-scale limit.

**Theorem 5.1** Let  $M_n(q; t_1, t_2)$  (defined in equation (5.1)) be the temporal cross moments of a single realization of a space-time random cascade with branching number  $b$  and iid generator process  $W_t$  with generalized MKP function  $\chi_b(q; t_1, t_2)$  (defined in equation (5.6)). Assume that temporal cross moments of the generator process are such that

$$\frac{E[W_{t_1}^{2q} W_{t_2}^{2q}]}{E^2[W_{t_1}^q W_{t_2}^q]} < b \quad (5.8)$$

and

$$E[Z_\infty^{2q}(t_1)Z_\infty^{2q}(t_2)] < \infty \quad (5.9)$$

in some range  $q \in [q_{min}, q_{max}]$ .

Then with probability one,

$$\tau(q; t_1, t_2) = \lim_{n \rightarrow \infty} \frac{\log M_n(q; t_1, t_2)}{n \log b} = \chi_b(q; t_1, t_2), \quad (5.10)$$

for  $q \in [q_{min}, q_{max}]$ .

The proof, which is given in Appendix E, is quite similar to the proof of Theorem 3.2. At first glance, one might think in fact that one could take  $W_{t_1} W_{t_2}$  as a spatial cascade generator (normalized to have unit expectation), in which case Theorem 3.2 would apply directly. However, the dependence between  $W_{t_1}$  and  $W_{t_2}$  will not allow this, and a separate proof has to be made. Note also that in the proof we have neglected the  $q \log(R_0(t_1)R_0(t_2)l_{max}^4)$  term, which, it should be easy to see, has no effect, since it is non-random and does not depend on  $n$ .

Returning now to testing the theory and estimating the new parameters from data, from equation (5.7) we obtain for finite  $n$ :

$$\begin{aligned} \log_b M_n(q; t_1, t_2) \\ \approx n \chi_b(q; t_1, t_2) + \log_b E[Z_\infty^q(t_1)Z_\infty^q(t_2)] + q \log_b(R_0(t_1)R_0(t_2)l_{max}^4). \end{aligned} \quad (5.11)$$

From equation (5.11) it can be seen that according to the theory, a plot of  $\log_b M_n(q; t_1, t_2)$  versus the level  $n$  will have an approximately constant slope. Checking for this property in data thus provides a basic test of the theory.

If we define the slope of  $\log_b M_n(q; t_1, t_2)$  versus the level  $n$  as

$$\hat{\tau}(q; t_1, t_2) = \frac{d}{dn} \log_b M_n(q; t_1, t_2), \quad (5.12)$$

then according to equation (5.11), this gives an estimate of  $\chi_b(q; t_1, t_2)$ , which by solving equation (5.6) for  $E[W_{t_1}^q W_{t_2}^q]$  as function of  $\chi_b(q; t_1, t_2)$  provides a means of estimating the time-evolution parameters of the process  $W_t$ , i.e.,

$$b^{\chi_b(q; t_1, t_2) + 2q - 1} = E[W_{t_1}^q W_{t_2}^q] \cong b^{\hat{\tau}(q; t_1, t_2) + 2q - 1}. \quad (5.13)$$

Standard spatial analysis of the data at times  $t_1$  and  $t_2$  provides the spatial parameters of  $W_t$ , i.e., those governing the marginal distribution of  $W_t$  at times  $t_1$  and  $t_2$ . The interplay between the time-evolution and spatial parameters of  $W_t$  will become clear as we construct two examples of  $W_t$  below in Section 5.4.

Notice the development of this theory required no assumptions on the process  $W_t$  except those stated in Theorem 5.1, that the marginal distributions of  $W_t$  be non-negative and have mean one, and that the collection of  $W_t$  making up the space-time cascade are iid. In particular,  $W_t$  need not be Markov or even causal (but of course we assume causality), and it may have any kind of non-stationarity. Despite this, the very useful result given above regarding its scaling properties was obtained.

A further general prediction of the theory may be obtained by noticing that the generalized MKP function may be related to certain spatial MKP functions in a simple way at its temporal extremes. For zero lag we have

$$\lim_{t_2 \rightarrow t_1} E[W_{t_1}^q W_{t_2}^q] = E W_{t_1}^{2q}, \quad (5.14)$$

which implies that

$$\lim_{t_2 \rightarrow t_1} \chi_b(q; t_1, t_2) = \chi_{b, W_{t_1}}(2q). \quad (5.15)$$

For large lag, assuming short-range dependence in  $W_t$ , we have

$$\lim_{t_2 - t_1 \rightarrow \infty} E[W_{t_1}^q W_{t_2}^q] = E W_{t_1}^q E W_{t_2}^q, \quad (5.16)$$

which implies that

$$\lim_{t_2 - t_1 \rightarrow \infty} \chi_b(q; t_1, t_2) = \chi_{b, W_{t_1}}(q) + \chi_{b, W_{t_2}}(q) - 1. \quad (5.17)$$

Thus  $\chi_b(q; t_1, t_2)$  will decay as a function of  $t_2$  from  $\chi_{b, W_{t_1}}(2q)$  to  $\chi_{b, W_{t_1}}(q) + \chi_{b, W_{t_2}}(q) - 1$ , a fact which may be used without any assumption on the form of the generator  $W_t$  to test the theory and estimate the de-correlation time of  $W_t$ .

In the case of stationary  $W_t$ , the functional form of the difference between  $\chi_{b, W_t}(2q)$  and  $2\chi_{b, W_t}(q) - 1$  can be used to predict the behavior of  $\chi_b(q; t_1, t_2)$  as a function of  $t_2$  more precisely. First, consider  $q = 0$ . If  $\chi_{b, W_t}(0) < 1$ , which occurs anytime there are zeroes in the field, then

$$\chi_{b, W_t}(2q) - (2\chi_{b, W_t}(q) - 1) = 1 - \chi_{b, W_t}(q) > 0, \quad (5.18)$$

so  $\chi_b(0; t_1, t_2)$  decreases as  $t_2$  grows. Second, consider the derivative of the difference,

$$\frac{d}{dq}[\chi_{b, W_t}(2q) - (2\chi_{b, W_t}(q) - 1)] = 2\chi_{b, W_t}^{(1)}(2q) - 2\chi_{b, W_t}^{(1)}(q). \quad (5.19)$$

This result may be interpreted as follows. When  $W_t$  is a  $\beta$  model generator, the derivative is independent of  $q$ , so the right-hand side of equation (5.19) will be zero. Then  $\chi_b(q; t_1, t_2)$  will decrease at the same rate for all  $q$  as  $t_2$  grows. When  $W_t$  is not a  $\beta$  model generator,  $\chi_{b, W_t}(q)$  will be convex, which means its derivative increases with  $q$ , so the right-hand side of equation (5.19) is positive. Then the difference is increasing in  $q$ , so  $\chi_b(q; t_1, t_2)$  decreases more quickly for larger  $q$ . These results will be illustrated in the case study, for which  $W_t$  is nearly stationary.

As promised, we will test and demonstrate the predictions and parameters estimation techniques of the space-time theory using a simple case study. The data we use is from the McGill Weather Radar, located in Montreal, Canada, and it was taken on June 19, 1992. It consists of a sequence of instantaneous radar snapshots taken at five minute intervals, converted to rain rate using a  $Z$ - $R$  relation, and binned to a Cartesian grid with 2 by 2 km pixels. To obtain a Lagrangian field from this, a subset of the snapshot consisting of a 64 by 64 pixel block, was chosen at 17:00 and subsequently tracked by the method of maximum correlation (Zawadzki 1973; Austin and Bellon 1974) until the block moved out of the field of view, which occurred shortly after 20:00. The method of maximum correlation consists of finding the block at the next time that maximizes the correlation with the block at the present time. This is by no means a perfect tracking method, since it cannot account for rotation or even motion across only part of a pixel. We will refer collectively to any errors introduced into the data by tracking as “tracking error”. The case study we have chosen is particularly simple because the field does not rotate or deform appreciably, and the tracked data is approximately marginally stationary, i.e., the scaling of the spatial moments estimated from the tracked spatial scenes are approximately constant, and thus so is the sequence of spatial parameters. This may be checked by plotting the scaling of the spatial moments as a function of time, as is done in Figure 5.2.

The predictions of the theory given so far, however, do not depend on stationarity. A test of the first prediction, the scaling of the temporal cross moments, is given in Figure 5.3. It is apparent that the log-log linearity of the temporal cross moments (Figure 5.3b and c) is good, as good as that of the spatial moments (Figure 5.3a). The estimates  $\hat{\tau}(q; t_1, t_2)$  of  $\chi_b(q; t_1, t_2)$  are plotted together in Figure 5.5, along with the predicted large lag limit given by equation (5.17). Notice that the MKP function shifts down, rotates clockwise, and loses curvature as  $t_2$  increases. The first two of these

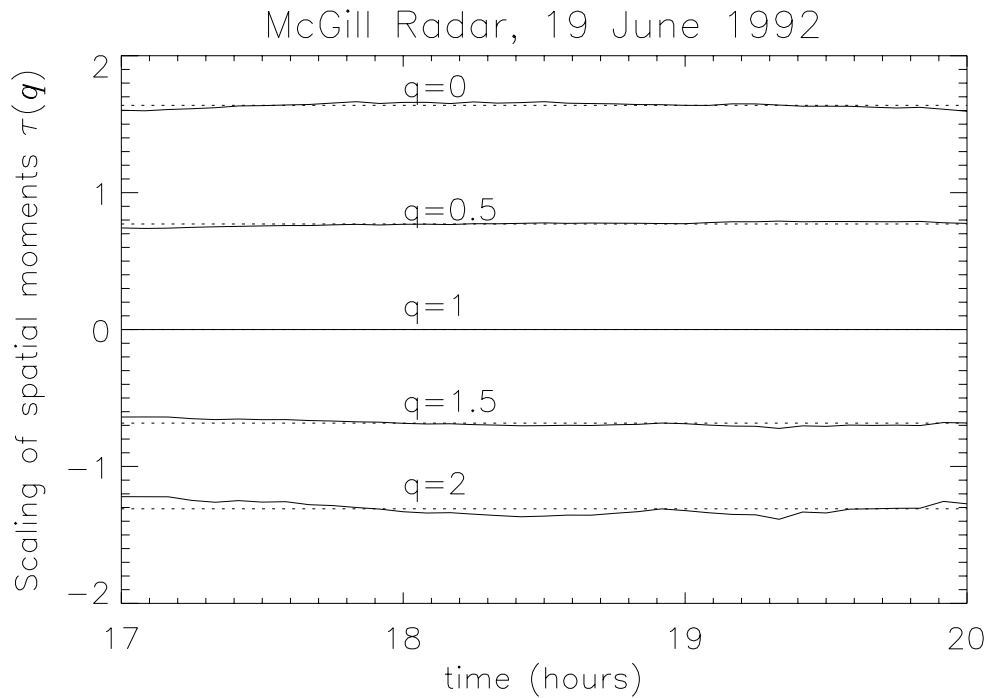


**Figure 5.2 Estimated spatial  $\tau(q)$  vs. time tracked McGill Radar rainfall field, 17:00 to 20:00 on 19 June 1992.**

properties is predicted by equations (5.15) and (5.17), as discussed above. The dependence of the second derivative on  $t_2$  is discussed below (see equations (5.30) and (5.31)).

The test of the decay of  $\chi_b(q; t_1, t_2)$  predicted in equations (5.15) and (5.17) is shown in Figure 5.5. This plot shows decay to approximately a constant for all  $q$  in about 1.5 hours, perhaps slightly less for larger  $q$ , but not exactly to the function predicted by equation (5.17). For small  $q$  ( $q < 0.5$ ),  $\hat{\tau}(q; t_1, t_2)$  for large lag never reaches the theoretical value, while for larger  $q$  ( $q > 0.5$ ), it decays beyond the theoretical value. These behaviors have the interpretation that for small  $q$  the scenes never completely de-correlate, while for large  $q$  they become anti-correlated. Whether this apparent  $q$ -

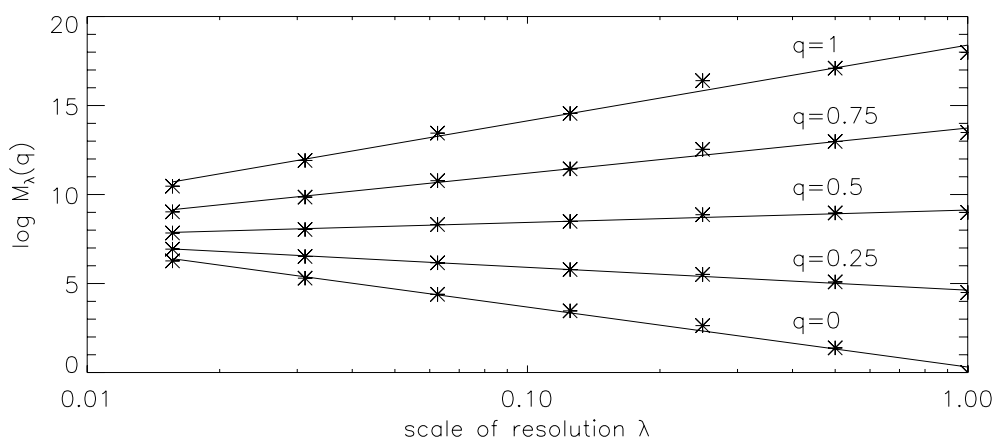
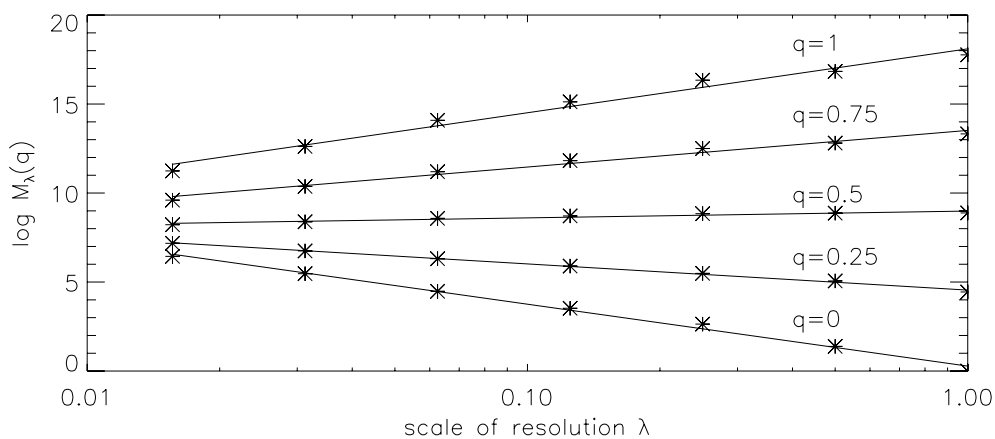
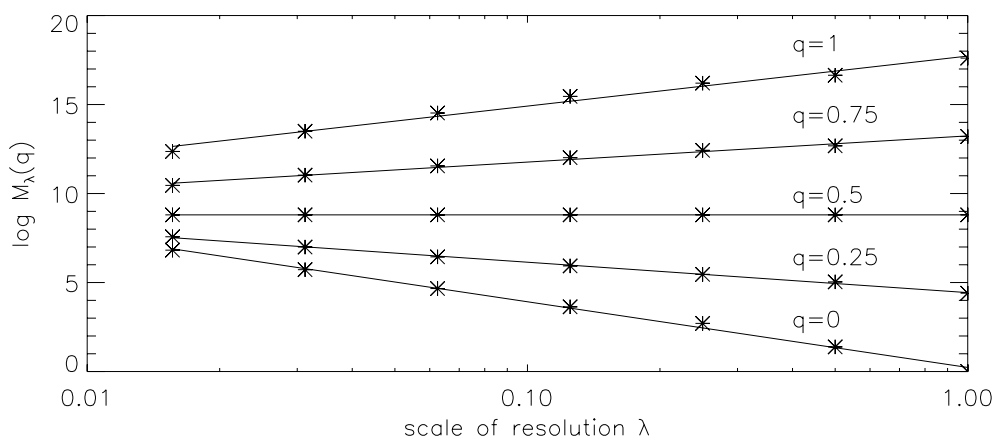


**Figure 5.3** Scaling of temporal cross moments,  $t_1 = 17:00$ .

(a)  $t_2 = 17:00$ ; (b)  $t_2 = 17:30$ ; (c)  $t_2 = 18:00$ .

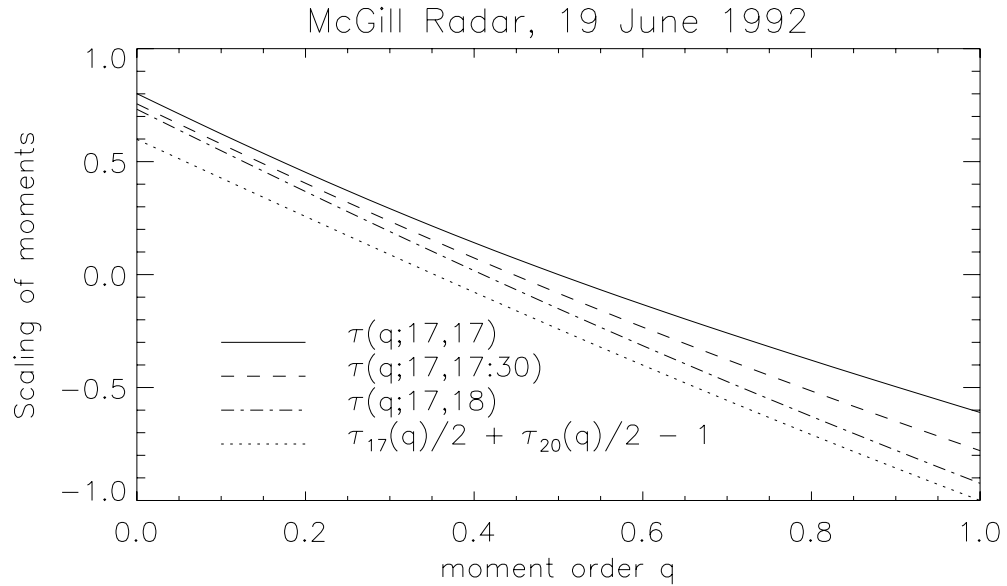


**Figure 5.4** Space-time MKP functions estimated from Figure 5.3.

dependent correlation behavior is real or the result of estimation effects such as tracking error is being investigated.

With an additional observation regarding the structure of the generator process  $W_t$ , the decay of  $\chi_b(q; t_1, t_2)$  can be used to study further aspects of its temporal behavior. The observation is, analogous to the spatial case, that  $W_t$  can be written without loss of generality as the product

$$W_t = B_t Y_t, \quad (5.20)$$

where  $B_t$  is a temporal version of the  $\beta$  model and  $Y_t$  is strictly positive, and  $B_t$  and  $Y_t$  are independent. Fully specified examples of  $B_t$  and  $Y_t$  corresponding to the first and second-order generators of the spatial theory will be given below, but equation (5.20) is sufficient for present purposes.

Consider now the MKP function with  $q = 0$ ,

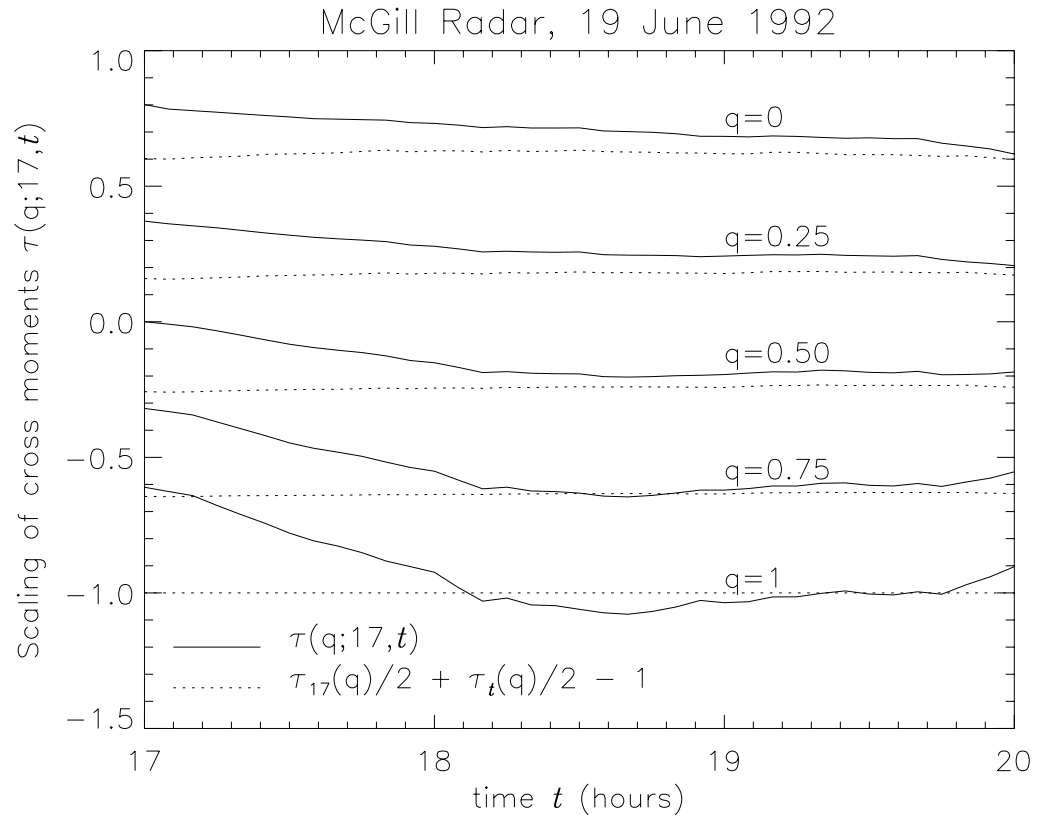


**Figure 5.5** Decay of space-time MKP function with time

The decay of  $\hat{\tau}(q;t_1, t_2)$  (solid line) from  $\hat{\tau}_{17}(2q)/2$  to  $\hat{\tau}_{17}(q)/2 + \hat{\tau}_{t_2}(q)/2 - 1$  (dashed line) as a function of  $t_2$ , as predicted by equations (5.15) and (5.17).

$$\chi_b(0;t_1, t_2) = \log_b E[B_{t_1}^0 B_{t_2}^0 Y_{t_1}^0 Y_{t_2}^0] + 1 = \log_b P(B_{t_1} B_{t_2} > 0) + 1, \quad (5.21)$$

Thus  $\chi_b(0;t_1, t_2)$  depends only on the properties of  $B_t$ . In particular we have

$$\lim_{t_2 \rightarrow t_1} \chi_b(0;t_1, t_2) = \log_b P(B_{t_1} > 0) + 1 = -\beta_{t_1} + 1 \quad (5.22)$$

and

$$\lim_{t_2 - t_1 \rightarrow \infty} \chi_b(0;t_1, t_2) = \log_b P(B_{t_1} > 0) + \log_b P(B_{t_2} > 0) = -\beta_{t_1} - \beta_{t_2} + 1. \quad (5.23)$$

Thus the decay of  $\chi_b(0;t_1, t_2)$  given in Figure 5.5 is equivalently described by equations (5.22) and (5.23).

Because  $B_t$  must take on positive values as well as zero, there is no value of  $q$  for which  $\chi_{b, W_t}(q;t_1, t_2)$  depends only on the properties of  $Y_t$ . However, since  $B_t$  is a temporal version of the spatial  $\beta$  model, its positive part has a deterministic value  $b^{\beta_t}$  for each  $t$ , which implies that

$$\chi_{b, W_t}^{(2)}(q;t_1, t_2) = \chi_{b, Y_t}^{(2)}(q;t_1, t_2). \quad (5.24)$$

To see this, notice that

$$P(B_{t_1}^q B_{t_2}^q = b^{q\beta_{t_1}} b^{q\beta_{t_2}}) = P(\{B_{t_1} > 0\} \cap \{B_{t_2} > 0\}) = p; \quad (5.25)$$

otherwise,  $B_{t_1}^q B_{t_2}^q$  is zero. Thus

$$E[W_{t_1}^q W_{t_2}^q] = E[B_{t_1}^q B_{t_2}^q Y_{t_1}^q Y_{t_2}^q] = pb^{(\beta_{t_1} + \beta_{t_2})q} E[Y_{t_1}^q Y_{t_2}^q] \quad (5.26)$$

and

$$\log_b E[W_{t_1}^q W_{t_2}^q] = \log_b p + (\beta_{t_1} + \beta_{t_2})q + \log_b E[Y_{t_1}^q Y_{t_2}^q] \quad (5.27)$$

by the independence of  $B_t$  and  $Y_t$ . Therefore

$$\frac{d}{dq} \log_b E[W_{t_1}^q W_{t_2}^q] = \beta_{t_1} + \beta_{t_2} + \frac{d}{dq} \log_b E[Y_{t_1}^q Y_{t_2}^q], \quad (5.28)$$

so

$$\frac{d^2}{dq^2} \log_b E[W_{t_1}^q W_{t_2}^q] = \chi_{b, W_t}^{(2)}(q;t_1, t_2) = \frac{d^2}{dq^2} \log_b E[Y_{t_1}^q Y_{t_2}^q] = \chi_{b, Y_t}^{(2)}(q;t_1, t_2). \quad (5.29)$$

Thus the behavior of  $\chi_{b, W_t}^{(2)}(q;t_1, t_2)$  depends only on the properties of  $Y_t$ , just as

$\chi_b^{(2)}(q)$  depends only on the second-order component in the spatial theory. Using this, by equations (5.16) and (5.17) we have

$$\lim_{t_2 \rightarrow t_1} \chi_{b, W_t}^{(2)}(q; t_1, t_2) = \frac{d^2}{dq^2} \chi_{b, Y_{t_1}}(2q) = 4\chi_{b, Y_{t_1}}^{(2)}(2q) \quad (5.30)$$

and

$$\lim_{t_2 - t_1 \rightarrow \infty} \chi_{b, W_t}^{(2)}(q; t_1, t_2) = \chi_{b, Y_{t_1}}^{(2)}(q) + \chi_{b, Y_{t_2}}^{(2)}(q). \quad (5.31)$$

Thus a decay of some kind should be evident in the behavior of  $\chi_{b, W_t}^{(2)}(q; t_1, t_2)$  as a function of lag, just as in the behavior of  $\chi_{b, W_t}(q; t_1, t_2)$ . This is confirmed in Figure 5.6 for  $q = 0.5$ , though again as in Figure 5.5 the empirical value at large lag does not match the value predicted by theory. Here this difference indicates that for large lag  $\hat{\tau}(q; t_1, t_2)$  becomes nearly a straight line, while the spatial MKP functions to which it should converge are more curved. Again, an explanation of this difference is still being sought.

### 5.3 Implications for Lagrangian and Eulerian Correlations

#### 5.3.1 Lagrangian Correlation

Temporal correlation structure in the Lagrangian frame of reference is a basic property of space-time rainfall theories of all kinds that can be used to compare the theories and test them against data. The dependence of this quantity on the scale of spatial averaging is less commonly studied but it is just as important since some averaging scale is implicit in any data set. A couple studies in which the dependence of temporal correlation on the averaging scale was explicitly studied are Laughlin (1981), who analyzed the GATE data, and Zawadzki et al. (1994), who studied the predictability of mesoscale rainfall fields at different scales. It should be noted that Laughlin's

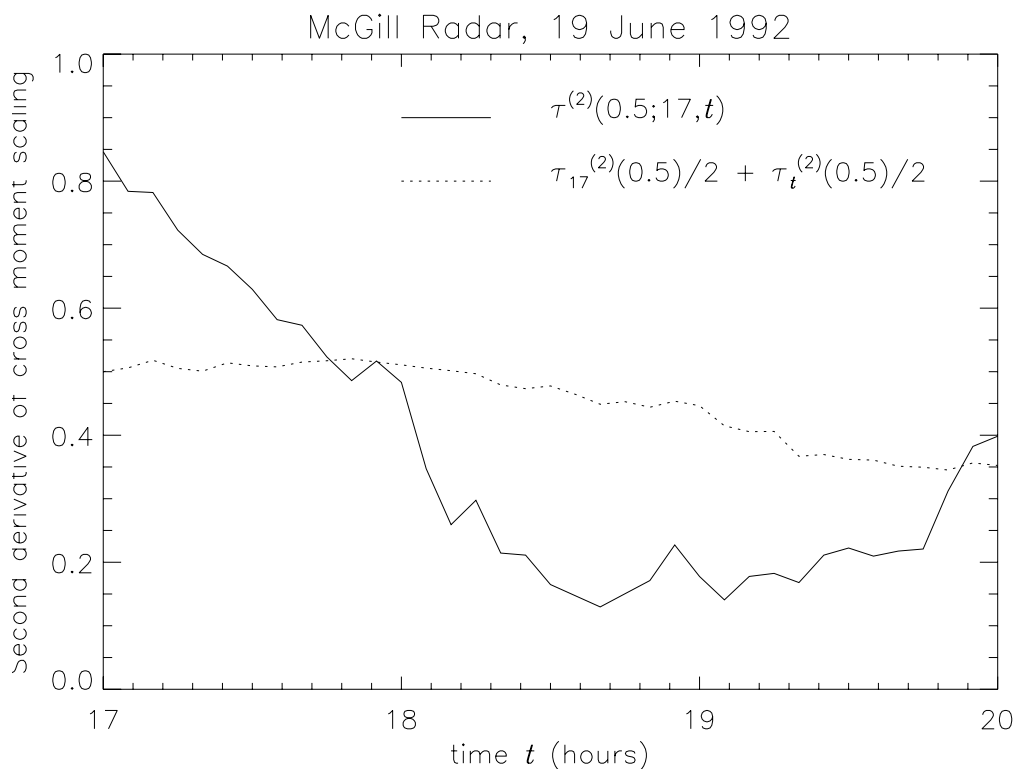


**Figure 5.6 Decay of curvature of space-time MKP function with time**

**The decay of  $\hat{\tau}^{(2)}(0.5;17, t_2)$  (solid line) from  $4\hat{\tau}_{17}^{(2)}(1)/2$  to  $\hat{\tau}_{17}^{(2)}(q)/2 + \hat{\tau}_{t_2}^{(2)}(q)/2$  (dashed line) as a function of  $t_2$ , as predicted by equations (5.30) and (5.31)**

analysis was actually Eulerian, but we list it here because his results have been used to specify the Lagrangian correlation structure, as in the space-time rainfall model of Bell (1987), and the difference is not significant for short times over larger spatial scales, because then the effect of advection is small.

The Lagrangian temporal correlation structure for the space-time cascade theory is really just a re-interpretation of the cross moments computed above. Now however we are more interested in how the cross moments evolve in time than how they vary as a function of scale of resolution. Since in estimating these moments from data we will equate a sample moment with its expectation, estimating this quantity from data requires ergodicity (in time), which we assume holds for times long compared to the de-

correlation time of the process  $W_t$ . We discussed in the previous subsection a means of estimating this de-correlation time. Unfortunately, we will find that while the change in Lagrangian cross moment as a function of scale has a simple analytical form, its dependence on time does not. For particular choices of  $W_t$  and  $q = 1$ , we can calculate and plot the result as a function of time, and compare this to data.

The sample covariance of the field in the Lagrangian reference frame at level  $n$  between two times  $t_1$  and  $t_2$  is given by

$$M_n(q; t_1, t_2) = \sum_{i=1}^{b^n} \mu_\infty^q(\Delta_n^i; t_1) \mu_\infty^q(\Delta_n^i; t_2), \quad (5.32)$$

whose expectation is given by

$$EM_n(q; s, t) = R_0^q(t_1) R_0^q(t_2) l_{max}^{4q} b^{n(1-2q)} E^n[W_{t_1}^q W_{t_2}^q] E[Z_\infty^q(t_1) Z_\infty^q(t_2)], \quad (5.33)$$

according to equation (5.4). We will consider three cases: the general case, the stationary case, and the case  $q = 1$ .

For the general case (non-stationary and any  $q \geq 0$ ), the only simplification we can make is to normalize by the moments at times  $t_1$  and  $t_2$ , computing

$$\begin{aligned} \frac{E[M_n(q; t_1, t_2)]}{EM_n(q; t_1) EM_n(q; t_2)} &= \frac{\sum_{i=1}^{b^n} \mu_\infty^q(\Delta_n^i; t_1) \mu_\infty^q(\Delta_n^i; t_2)}{\sum_{i=1}^{b^n} \mu_\infty^q(\Delta_n^i; t_1) \sum_{i=1}^{b^n} \mu_\infty^q(\Delta_n^i; t_2)} \\ &= \frac{R_0^q(t_1) R_0^q(t_2) l_{max}^{4q} b^{n(1-2q)} E^n[W_{t_1}^q W_{t_2}^q] E[Z_\infty^q(t_1) Z_\infty^q(t_2)]}{R_0^q(t_1) R_0^q(t_2) l_{max}^{4q} b^n b^{-nq} E^n W_{t_1}^q E Z_\infty^q(t_1) b^n b^{-nq} E^n W_{t_2}^q E Z_\infty^q(t_2)} \\ &= \frac{E[Z_\infty^q(t_1) Z_\infty^q(t_2)]}{E Z_\infty^q(t_1) E Z_\infty^q(t_2)} \left( \frac{E[W_{t_1}^q W_{t_2}^q]}{b E W_{t_1}^q E W_{t_2}^q} \right)^n. \end{aligned} \quad (5.34)$$

Using the normalized resolution  $\lambda = l_n / l_{max} = b^{-n/2}$ , this becomes

$$\frac{E[M_n(q;t_1, t_2)]}{EM_n(q;t_1)EM_n(q;t_2)} = \frac{E[Z_\infty^q(t_1)Z_\infty^q(t_2)]}{EZ_\infty^q(t_1)EZ_\infty^q(t_2)} \lambda^{2\left(1 - \log_b \frac{E[W_{t_1}^q W_{t_2}^q]}{EW_{t_1}^q EW_{t_2}^q}\right)}. \quad (5.35)$$

Here we see as was mentioned above that the scale-dependence of the Lagrangian cross moments has a simple analytical form, but the time-dependence does not, since it depends on  $W_t$  and  $Z_\infty(t)$ . We will see next that for stationary  $W_t$  this basic fact does not change.

For the stationary case, it is useful to normalize slightly differently and to define the lag time  $\tau = t_2 - t_1$ , and define the lag- $\tau$  stationary Lagrangian cross moments

$l_n(q;\tau)$  as

$$\begin{aligned} l_n(q;\tau) &= \frac{E[M_n(q;\tau)]}{E[M_n(2q)]} = \frac{\sum_{i=1}^{b^n} \mu_\infty^q(\Delta_n^i; t) \mu_\infty^q(\Delta_n^i; t + \tau)}{\sum_{i=1}^{b^n} \mu_\infty^{2q}(\Delta_n^i)} \\ &= \frac{R_0^q(t) R_0^q(t + \tau) l_{max}^{4q} b^{n(1-2q)} E^n[W_t^q W_{t+\tau}^q] E[Z_\infty^q(t) Z_\infty^q(t + \tau)]}{R_0^{2q} l_{max}^{4q} b^n b^{-n2q} E^n W^{2q} E Z_\infty^{2q}} \\ &= \frac{E[Z_\infty^q(t) Z_\infty^q(t + \tau)] \left( \frac{E[W_t^q W_{t+\tau}^q]}{E W^{2q}} \right)^n}{E Z_\infty^{2q}} \end{aligned} \quad (5.36)$$

$$= \frac{E[Z_\infty^q(t) Z_\infty^q(t + \tau)]}{E Z_\infty^{2q}} \lambda^{-2 \log_b \frac{E[W_t^q W_{t+\tau}^q]}{E W^{2q}}}. \quad (5.37)$$

Notice that in the stationary case,  $l_n(q;\tau)$  decays from unity at  $\tau = 0$  to a positive limit given by

$$\frac{E^2 M_n(q)}{EM_n(2q)} = b^q \left( \frac{E^2 W^q}{E W^{2q}} \right)^n \frac{E^2 Z_\infty^q}{E Z_\infty^{2q}} \quad (5.38)$$

as  $\tau \rightarrow \infty$ . Notice that this limit depends on scale; in particular, whenever  $W$  has positive variance, the limit decreases toward zero as  $n$  increases ( $\lambda_n$  decreases).

For  $q = 1$ , it is easy to compute  $E[Z_\infty(t_1)Z_\infty(t_2)]$  in terms of  $E[W_{t_1}W_{t_2}]$ , which facilitates testing of the result, since we have no other results regarding the evolution of the limit mass  $Z_\infty(t)$ . Using equation (3.29), we have

$$\begin{aligned} Z_\infty(t_1)Z_\infty(t_2) &= [b^{-1}\sum_{i=1}^b W^i(t_1)Z_\infty^i(t_1)][b^{-1}\sum_{i=1}^b W^i(t_2)Z_\infty^i(t_2)] \\ &= b^{-2}\left[\sum_{i=j} W^i(t_1)Z_\infty^i(t_1)W^j(t_2)Z_\infty^j(t_2) + \sum_{i \neq j} W^i(t_1)Z_\infty^i(t_1)W^j(t_2)Z_\infty^j(t_2)\right], \end{aligned} \quad (5.39)$$

where there are  $b$  terms in which  $i = j$  and  $b^2 - b$  terms in which  $i \neq j$ . Notice that each type of term is identically distributed and for  $i \neq j$  terms we have

$$E[W^i(t_1)Z_\infty^i(t_1)W^j(t_2)Z_\infty^j(t_2)] = EW^i(t_1)EZ_\infty^i(t_1)EW^j(t_2)EZ_\infty^j(t_2) = 1, \quad (5.40)$$

so

$$\begin{aligned} E[Z_\infty(t_1)Z_\infty(t_2)] &= b^{-2}\left\{bE[W_{t_1}W_{t_2}]E[Z_\infty(t_1)Z_\infty(t_2)] + b^2 - b\right\} \\ &= (b-1)/(b-E[W_{t_1}W_{t_2}]) \end{aligned} \quad (5.41)$$

Since  $\lim_{t_2 \rightarrow t_1} E[W_{t_1}W_{t_2}] = EW_{t_1}^2$ , we may compute a consistency check on this result as follows. For  $t_1 = t_2$  equation (5.41) reduces to  $EZ_\infty^2 = (b-1)/(b-EW^2)$ , which is indeed true for spatial cascades (see Appendix C). Using this result for

$E[Z_\infty(t_1)Z_\infty(t_2)]$  we can write

$$l_n(1;\tau) = \frac{b-EW^2}{b-E[W_{t_1}W_{t_2}]} \left(\frac{E[W_{t_1}W_{t_2}]}{EW^2}\right)^n = \frac{b-EW^2}{b-E[W_{t_1}W_{t_2}]} \lambda^{-2\log_b \frac{E[W_{t_1}W_{t_2}]}{EW^2}}. \quad (5.42)$$

Equations (5.37) and (5.42) show, as in the general non-stationary case, that while the characteristic decay time as a function of scale cannot be predicted without specifying the process  $W_t$ , the scaling properties of the Lagrangian cross moments are immediately evident. In particular, for a fixed lag  $\tau$ ,  $l_n(q;\tau)$  is log-log linear versus scale  $\lambda$  with a slope  $s(q;\tau)$  such that

$$s(q;\tau) = -2\log_b \frac{E[W_t^q W_{t+\tau}^q]}{EW^2} = 2[\chi_b(2q) - \chi_b(q;\tau)]. \quad (5.43)$$

Solving this for  $\chi_b(q;\tau)$  gives

$$\chi_b(q;\tau) = \chi_b(2q) - s(q;\tau)/2. \quad (5.44)$$

Thus if we have reason to believe that a tracked rainfall data set has a stationary generator process, the Lagrangian cross moments can be used to estimate  $\chi_b(q;\tau)$ , and its scaling can be used to test the space-time theory. Estimates of the Lagrangian cross moments with  $q = 1$  of the case study data from 17:00 to 20:00 for each scale as a function of lag are shown in Figure 5.7a (compare Figure 3a of Zawadzki et al. (1994)), while the scaling for a set of lags is given in Figure 5.7b. Scaling is approximately obeyed, and the slope increases as a function of the time lag, as it should according to equation (5.43). The estimate of  $\chi_b(q;\tau)$  computed from the slopes of the Lagrangian cross moments in Figure 5.7b is plotted in Figure 5.8. This compares reasonably well with the estimate of  $\chi_b(1;17, t)$  in Figure 5.5, though they are not estimating exactly the same quantity. The estimate of  $\chi_b(q;\tau)$  in Figure 5.8 is averaged over all instances of lag  $\tau$  in the data, whereas the estimate of  $\chi_b(1;17, t)$  is a “path-wise” quantity having only one value for each lag.

A power law in  $\lambda$  for fixed  $t - s$  is roughly consistent with the results of Laughlin (1981) and Zawadzki (1994), though again we note that Laughlin’s results are actually

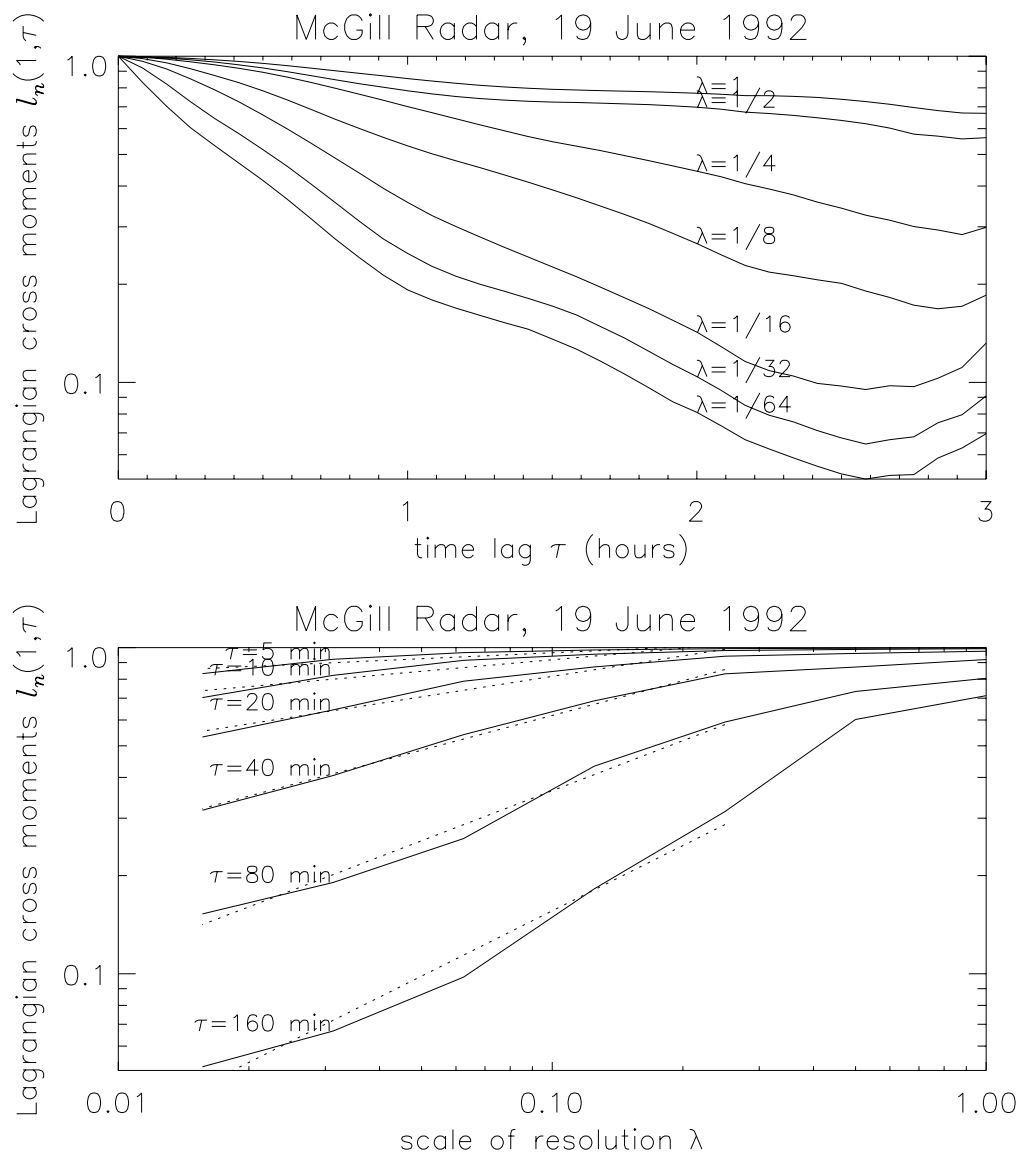


**Figure 5.7 Behavior of the Lagrangian cross moments**

(a) as a function of lag  $\tau$  for different resolutions, and (b) as a function of scale of resolution  $\lambda$  for different lags (compare equation (5.37)). In (b), the solid lines connect the values obtained from data, while the dotted line is fitted by regression to obtain a slope for use in Figure 5.8.

Eulerian. What is most significant about this is that the scaling of the Lagrangian temporal cross moment is a necessary result of the spatial cascade structure; it is not fitted by a free temporal correlation function as in, for example, the model of Bell (1987).

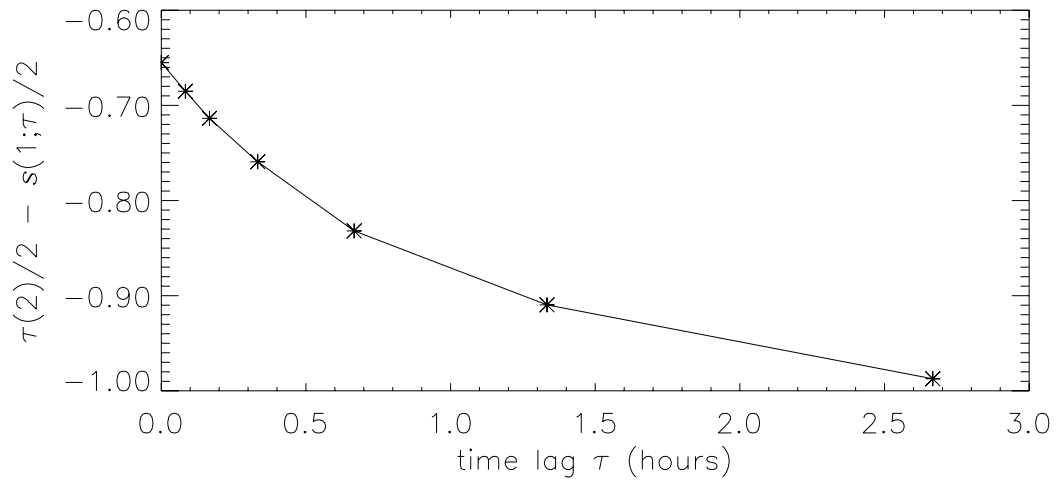


**Figure 5.8 Space-time MKP function from Lagrangian cross moments**

$\hat{\tau}(1;\tau)$  obtained from the scaling of the Lagrangian cross moments, using  $\hat{\tau}(1;\tau) = \hat{\tau}(2)/2 - s(1;\tau)/2$  (from equation (5.44)), where  $s(1;\tau)$  is the slope of the dotted lines in Figure 5.7b and  $\hat{\tau}(2)/2$  is taken from the dotted line at  $q = 2$  in Figure 5.2.

### 5.3.2 Eulerian Correlation and Taylor's Hypothesis

*Taylor's hypothesis* was proposed by G. I. Taylor as a means of solving a measurement problem in fluid turbulence research. It was (and is) desired to study the instantaneous spatial properties of the turbulent flow field by means of a time series measurement at a fixed point. Taylor (1938) proposed that for a fixed flow velocity  $u$ , the second order properties of the time series of a stationary and homogeneous random process  $\xi(t, x)$  be transformed into those of the instantaneous spatial transect by means of the following assumption:

$$\rho[\xi(s, x), \xi(t, x)] = \rho[\xi(s, x), \xi(s, x - u(t - s))], \quad (5.45)$$

where

$$\rho[X, Y] = \frac{E[XY] - E[X]E[Y]}{\sqrt{\text{Var}(X)\text{Var}(Y)}} \quad (5.46)$$

denotes the correlation of two random quantities  $X$  and  $Y$ . Since the process  $\xi(t, x)$  is by assumption homogeneous and stationary, the arguments of the correlation function are identically distributed and we can write

$$\rho[X, Y] = \frac{E[XY] - E^2 X}{\text{Var}(X)}. \quad (5.47)$$

Thus it should be clear that Taylor's hypothesis (5.45) can be written equivalently in terms of covariances or simply cross moments.

Taylor's hypothesis is sometimes generalized to require equality in joint distribution, i.e.,

$$[\xi(s, x), \xi(t, x)] = [\xi(s, x), \xi(s, x - u(t - s))]. \quad (5.48)$$

Equation (5.48) clearly implies equation (5.45). A simple way to satisfy both forms of Taylor's hypothesis is to assume a *frozen field* model, which can be written

$$\xi(t, x) = \zeta(x - u(t - s)) \quad (5.49)$$

where  $\zeta(x)$  is a homogeneous random field. In this case the random process  $\xi(t, x)$  does not vary in time in the Lagrangian reference frame; it is frozen except for being advected at velocity  $u$ .

In early works on stochastic modeling of rainfall fields, Taylor's hypothesis was often invoked as an assumption providing a means of extending a spatial model to a space-time model (see, for example, Mejia and Rodriguez-Iturbe 1974; Bras and Rodriguez-Iturbe 1976). The classic paper demonstrating that Taylor's hypothesis might hold in data is that of Zawadzki (1973), who showed that for one data set that the second order form held in his radar-derived rainfall data for times up to 40 minutes, but

not beyond. Crane (1990) also found Taylor's hypothesis to be valid in rainfall over times up to 30 minutes and spatial scales up to 20 km for one data set and up to two hours and 100 km in another data set. The so-called WGR model (Waymire et al. 1984), a clustered point process space-time rainfall model, was developed to test the circumstances under which Zawadzki's empirical findings might hold in stochastic models of this form. They found that Taylor's hypothesis holds approximately for times shorter than the correlation times of the rainfall cells in the model, with the additional requirement that the cells move at the same velocity as the cell clusters. Gupta and Waymire (1987) later generalized these results to show that any member of a quite general class of stochastic fields will satisfy Taylor's hypothesis for short times.

Since the model proposed here is not of the type considered by Gupta and Waymire (1987), it is necessary to compute the conditions under which the theory predicts that Taylor's hypothesis will hold. We will also obtain results under more a general form of the hypothesis, namely, for any positive moment order  $q$  and at any resolution. We test Taylor's hypothesis by comparing the instantaneous Eulerian cross moment with the Eulerian cross moment at a positive time lag  $\tau$ . To present the calculation requires some new notation. It is not sufficient to identify a box at level  $n$  by an arbitrary indexing,  $\Delta_n^i$ ,  $i = 1, \dots, b^n$ , because it lacks directional information, whereas the field will be assumed to be advecting in some direction. Instead we will write  $\Delta_{n,n}^{i,j}$ ,  $i = 1, \dots, b^{n/2}$ ,  $j = 1, \dots, b^{n/2}$ , where  $i$  denotes now, say, the column and  $j$  the row. To fix ideas, assume further that columns run south-to-north and rows west-to-east and that north is up. Then the box  $\Delta_{n,n}^{0,0}$  is in the southwestern (lower left) corner. We assume further that the advection occurs from west-to-east at a constant velocity  $u$ . From time  $t$  to time  $t + \tau$  it therefore shifts a distance  $u\tau$ .

Now, consider the instantaneous cross moment  $E[\mu_\infty^q(\Delta_{n,n}^{i,j})\mu_\infty^q(\Delta_{n,n}^{i+b^{m/2},j})]$ , i.e., at a separation distance  $r_n = l_{max}b^{(m-n)/2} = l_{max}b^m\lambda$ , where  $0 \leq m < n$  is a free pa-

parameter that governs (through the quantity  $b^m$ )  $r_n$  in units of the number of level  $n$  pixels, and, as usual,  $\lambda = b^{-n/2}$  is the (normalized) scale of resolution of a pixel at level  $n$ . In order to have this correspond to the right-hand side of equation (5.45), we must have

$$r_n = l_{max} b^{(m-n)/2} = l_{max} b^m \lambda = u\tau. \quad (5.50)$$

Assuming that given some  $u$ ,  $l_{max}$ , and  $n$  we choose  $m$  such that this equation holds, the Eulerian cross moment at a positive time lag  $\tau$  that corresponds to the left-hand side of equation (5.45) is therefore  $E[\mu_\infty^q(\Delta_{n,n}^{i,j};t)\mu_\infty^q(\Delta_{n,n}^{i+b^{m/2},j};t+\tau)]$ . Because the quantities  $\mu_\infty^q(\Delta_{n,n}^{i,j};t)$  and  $\mu_\infty^q(\Delta_{n,n}^{i+b^{m/2},j};t+\tau)$  appear to be at different locations, this latter quantity may not look like it corresponds to the left-hand side of equation (5.45), but in fact it does because the space-time cascade is in a Lagrangian frame of reference, which here we have assumed to be advecting at the velocity necessary such that the box  $\Delta_{n,n}^{i+b^m,j}$  is at time  $t+\tau$  where the box  $\Delta_{n,n}^{i,j}$  was at time  $t$ , according to equation (5.50).

The instantaneous spatial cross moments of a one-dimensional random cascade were discussed in Chapter 3 and their computation is given in Appendix D. For a two-dimensional cascade with branching number  $b$  and moment orders  $p = q$ , we obtain similarly

$$\frac{E[\mu_\infty^q(\Delta_{n,n}^{i,j})\mu_\infty^q(\Delta_{n,n}^{i+b^m,j})]}{E[\mu_\infty^{2q}(\Delta_{n,n}^{i,j})]} \cong \frac{E^2 Z_\infty^q}{EZ_\infty^{2q}} \frac{1}{R^n(q)} \frac{b-1}{bR(q)-1} \left(\frac{r_n}{l_{max}}\right)^{-\log_{\sqrt{b}} R(q)}, \quad (5.51)$$

where  $R(q) = EW^{2q}/E^2W^q$ . It is interesting also to write this result in terms of the pixel resolution  $\lambda = b^{-n/2}$  and the lag in units of resolution  $\lambda$  pixels  $b^{m/2}$ , which gives

$$\frac{E[\mu_{\infty}^q(\Delta_{n,n}^{i,j})\mu_{\infty}^q(\Delta_{n,n}^{i+b^m,j})]}{E[\mu_{\infty}^{2q}(\Delta_{n,n}^{i,j})]} \propto \lambda^{2\log_{\sqrt{b}}R(q) - 2\log_{\sqrt{b}}R(q)} (b^{m/2})^{-\log_{\sqrt{b}}R(q)}, \quad (5.52)$$

neglecting the terms not depending on resolution or spatial lag, which simplifies to

$$\frac{E[\mu_{\infty}^q(\Delta_{n,n}^{i,j})\mu_{\infty}^q(\Delta_{n,n}^{i+b^m,j})]}{E[\mu_{\infty}^{2q}(\Delta_{n,n}^{i,j})]} \propto (b^{m/2})^{-\log_{\sqrt{b}}R(q)}. \quad (5.53)$$

Because the resolution dependence from the  $R^{-n}(q)$  factor and that from the  $r_n/l_{max}$  factor cancel, in the final result, the resolution appears only indirectly, since it determines the size of one of the  $b^{m/2}$  pixels making up the spatial lag. Notice that  $R(q) \geq 1$  (with equality holding for  $q = 0$ ), which implies  $-\log_{\sqrt{b}}R(q) \leq 0$ , so as  $m$  grows, causing the spatial lag to grow for fixed resolution, the cross moment decreases, as would be expected.

The cross moments with positive time lag (assuming stationarity) can be computed much as the instantaneous cross moments. The only difference is that the multipliers in common between  $\mu_{\infty}(\Delta_{n,n}^{i,j};t)$  and  $\mu_{\infty}(\Delta_{n,n}^{i+b^{m/2},j};t+\tau)$  now vary in time; this makes equation (D.7) take on the form:

$$E_k[\mu_n^q(\Delta_{n,n}^{i,j};t)\mu_n^q(\Delta_{n,n}^{i+b^{m/2},j};t+\tau)] = b^{-2qn} E^{n-k} [W_t^q W_{t+\tau}^q] E^{2k} W^q. \quad (5.54)$$

Following this change through the derivation gives the final result

$$\frac{E[\mu_{\infty}^q(\Delta_{n,n}^{i,j};t)\mu_{\infty}^q(\Delta_{n,n}^{i+b^{m/2},j};t+\tau)]}{E[\mu_{\infty}^{2q}(\Delta_{n,n}^{i,j})]} \cong \frac{E^2 Z_{\infty}^q}{EZ_{\infty}^{2q}} \frac{1}{R^n(q)} \frac{b-1}{bR(q;\tau)-1} \left(\frac{r_n}{l_{max}}\right)^{-\log_{\sqrt{b}}R(q;\tau)} \quad (5.55)$$

where  $R(q;\tau) = E[W_t^q W_{t+\tau}^q]/E^2 W^q$ . Writing this result in terms of the pixel resolution  $\lambda$  and the lag in units of resolution  $\lambda$  pixels gives

$$\frac{E[\mu_{\infty}^q(\Delta_{n,n}^{i,j};t)\mu_{\infty}^q(\Delta_{n,n}^{i+b^{m/2},j};t+\tau)]}{E[\mu_{\infty}^{2q}(\Delta_{n,n}^{i,j})]} \propto \lambda^{-\log_{\sqrt{b}} \frac{E[W_t^q W_{t+\tau}^q]}{EW^{2q}}} (b^{m/2})^{-\log_{\sqrt{b}} R(q;\tau)}, \quad (5.56)$$

again neglecting terms not depending on the resolution or spatial lag. Notice here there is explicit dependence on the pixel resolution  $\lambda$ . Since

$$E[W_t^q W_{t+\tau}^q]/EW^{2q} = R(q;\tau)/R(q) \leq 1, \quad (5.57)$$

with equality holding for  $\tau = 0$ , the exponent of  $\lambda$  is non-negative but small for  $\tau$  small (relative to the de-correlation time of  $W_t$ ). Hence as  $\lambda$  decreases for fixed  $m$ , the cross moment also decreases, but only slightly for small  $\tau$ . Since  $R(q;\tau) \geq 1$ , with equality holding for  $\tau \rightarrow \infty$ , the exponent of  $b^{m/2}$  is non-positive, and thus when  $b^{m/2}$  decreases, for fixed  $\lambda$ , the cross moment increases, but only slightly for large  $\tau$ .

Comparing equation (5.55) with equation (5.51) shows that the instantaneous cross moments and the Eulerian space-time cross moments have quite similar forms, and in particular will be approximately equal, implying the validity of Taylor's hypothesis, when

$$R(q) \cong R(q;\tau), \quad (5.58)$$

which occurs, as we have noted, for  $\tau$  small.

Note the perhaps surprising scale invariance of this result. Since  $m$  can compensate, according to equation (5.50), for changes in resolution, Taylor's hypothesis can hold equally well at all scales simultaneously. The effect of changing resolution is to change the cross moment without affecting the validity of Taylor's hypothesis. Consider decreasing  $\lambda$  (increasing  $n$ ). Then we increase  $m$  in order to hold the space and time lags constant according to equation (5.50). The only effect of this is to decrease the factor  $R^{-n}(q)$  in equations (5.51) and (5.55), since  $R(q) \geq 1$ , affecting both types

of cross moment equally (i.e., without effect on the validity of Taylor's hypothesis). All this says is that two regions at some fixed separation distance in a space-time random cascade field are more correlated at coarse resolution than they are at fine resolution. Since  $r_n/l_{max}$  and  $\tau$  are fixed, no other change in the cross moments occurs through this change in resolution.

To our knowledge, no one has previously posed the problem of the validity of Taylor's hypothesis as a function of resolution or tested it in data. In fact we will not test it here, since it is a rather tricky data analysis problem, particularly with regard to the assumption of homogeneity, which often holds fairly well in the Lagrangian frame of reference, but not so well in the Eulerian. It is however an important matter to consider in the development and testing of theories of space-time rainfall, practically, because all data is averaged up to some finite resolution, and scientifically, because it will give information regarding the co-evolution of the structures at different space and time scales.

The study of Lovejoy and Schertzer (1991) has already indicated that time and space do not scale isotropically. They interpret their results as indicating that a generalization of Taylor's hypothesis for rainfall is required, which is to posit a turbulent (scale-dependent) advection velocity. In the present notation, would mean that  $u$  in equation (5.50) would depend on the level  $n$ . This implies that differential motion of the elements of the rainfall field is the key factor to be considered in going from a spatial to a space-time theory. While differential motion is certainly observed, it is not a dominant factor in the data we have examined. Our examination indicates that the most important motion that is missed by the present analysis is rotation, for which equation (5.50) in its present form remains valid. The present theory also shows that the assumption of a scale-dependent advection velocity is not required in order to have space and time scale anisotropically.

#### 5.4 A Specific Example of a Space-Time Construction

In order to give some concreteness to the arbitrary generator process  $W_t$  and to provide a pair of models that can be used in applications, we now describe the construction of space-time versions of the first and second-order approximate spatial models defined in Section 3.4 and the development of the associated parameter estimation methods. According to the approximation, the  $i$ th spatial scan has a second-order generator that can be represented as the product of independent generators

$$W^i = B^i Y^i, \quad (5.59)$$

where  $B^i$  is such that

$$P(B^i = b^{\beta_i}) = b^{-\beta_i} \text{ and } P(B^i = 0) = 1 - b^{-\beta_i}, \quad (5.60)$$

i.e., it is a  $\beta$ -model generator, and

$$Y^i = b^{-\sigma^2 \log b / 2 + \sigma X}, \quad (5.61)$$

where  $X$  is a unit normal random variable. For the first-order model, we take  $Y^i = 1$  with probability one. Thus the variation in parameters (and thus the influence of the large-scale forcing) enters only through the changes in  $B_i$ . Thus we propose a space-time model constructed with iid generator processes given by

$$W_t = B_t Y_t, \quad (5.62)$$

where  $B_t$  is a continuous-time version of the sequence  $B_1, B_2, \dots$  and as such has an associated sequence of time-varying parameters  $\beta_1, \beta_2, \dots$ , and  $Y_t$  is a continuous time version of the sequence  $Y_1, Y_2, \dots$  whose parameter sequence  $\sigma_1, \sigma_2, \dots = \sigma$  remains constant.

### 5.4.1 The Second-Order Process

Due to its relative simplicity as a stationary process, we construct first a candidate for the second-order process  $Y_t$ . As described above, at each time  $t$ , the spatial generator is the exponentiation of a Gaussian random variable with the same distribution at each time. Thus the process  $Y_t$  must be the exponentiation of a stationary Gaussian process. The temporal dependence structure however is not determined by this assumption. We have already argued that the process must be causal, and have noted the convenience of Markov processes. Physical intuition would suggest in addition that the process should be continuous if possible. A continuous Markov process suggests a diffusion, and making it Gaussian and stationary in addition specifies the stationary form of the Ornstein-Uhlenbeck process (Breiman, 1992, pp. 347ff.),

To define this process, we begin with  $V_t$ , the Ornstein-Uhlenbeck process beginning at  $t = 0$ .  $V_t$  is defined as

$$V_t = \frac{s}{m} \int_0^t e^{-\frac{\beta}{m}(t-\tau)} dX(\tau), \quad (5.63)$$

where  $X(t)$  is standard Brownian motion, i.e., it has continuous sample paths and independent Gaussian increments  $dX(\tau) = X(t + \tau) - X(t)$ . For the definition of an integral with respect to increments of Brownian motion, see Breiman (1992) or other standard works on stochastic processes.  $V_t$  has the interpretation of the velocity process of a particle with mass  $m$ , suspended in a liquid with “coefficient of friction”  $\beta$ , and subject to Brownian forcing with drift  $\mu = 0$  and diffusion  $s^2$ . It is convenient to write  $s/m = \gamma$  and  $\beta/m = \alpha$ .

A stationary version  $\tilde{V}_t$  can be constructed by beginning the process at an initial value selected at random from its invariant measure and appropriately scaling that value in time, i.e.,

$$\tilde{V}_t = V_t + e^{-\alpha t} V_1(0), \quad (5.64)$$

where  $V_1(0)$  is Gaussian with zero mean and variance  $\rho = \gamma^2/(2\alpha)$ , which we denote  $V_1(0) \sim N[0, \rho]$ , and independent of  $V_t$ . The process  $\tilde{V}_t$  is, as desired, Gaussian, stationary and Markov with continuous sample paths. It has stationary Gaussian transition probabilities, in particular, for  $\tau > 0$ ,

$$(\tilde{V}_{t+\tau} \parallel \tilde{V}_t = v_t) \sim N[v_t e^{-\alpha\tau}, \rho(1 - e^{-2\alpha\tau})], \quad (5.65)$$

and its invariant measure is the distribution of  $V_1(0)$ .

So that the invariant distribution has unit variance, we fix  $\rho = 1$  (leaving one new free parameter,  $\gamma$  or  $\alpha$ ) and use the resulting process  $\tilde{V}_t$  to construct the process  $Y_t$  as

$$Y_t = b^{-\sigma^2 \log b / 2 + \sigma \tilde{V}_t} = e^{-(\sigma \log b)^2 / 2 + \sigma (\log b) \tilde{V}_t}. \quad (5.66)$$

Hence  $Y_t$  is a lognormal diffusion with lognormal invariant distribution equal to the distribution of  $Y = b^{X'}$ , where  $X' \sim N[-(\sigma \log b)^2 / 2, (\sigma \log b)^2]$ .

Calculating the temporal cross moment  $E[Y_t^q Y_{t+\tau}^q]$ ,  $\tau > 0$  is fairly straightforward given the facts just presented but requires a lot of algebra. Thus the calculation is given in Appendix G. The result is

$$\begin{aligned} E[Y_t^q Y_{t+\tau}^q] &= e^{-(\sigma \log b)^2 q + (1 + e^{-\alpha\tau})(\sigma \log b)^2 q^2} \\ &= b^{-\sigma^2 (\log b) q + (1 + e^{-\alpha\tau}) \sigma^2 (\log b) q^2}. \end{aligned} \quad (5.67)$$

To perform a consistency check on this result, notice that because  $Y_t$  is a positive recurrent Markov process in its stationary distribution

$$\lim_{\tau \rightarrow \infty} E[Y_t^q Y_{t+\tau}^q] = E^2 Y^q. \quad (5.68)$$

From equation (5.67) we have

$$\lim_{\tau \rightarrow \infty} E[Y_t^q Y_{t+\tau}^q] = e^{-(\sigma \log b)^2 q + (\sigma \log b)^2 q^2} = E^2 Y^q. \quad (5.69)$$

The last equality holds because as we noted following equation (5.66),  $Y$  is distributed as the logarithm of  $X'$  where  $X' \sim N[-(\sigma \log b)^2/2, (\sigma \log b)^2]$ , which implies this equality by equation (G.5).

Thus  $\chi_{b, Y_t}(q; t, t + \tau)$  is given by

$$\chi_{b, Y_t}(q; t, t + \tau) = -\sigma^2 (\log b) q + (1 + e^{-\alpha \tau}) \sigma^2 (\log b) q^2 - (2q - 1), \quad (5.70)$$

and has a second-order (quadratic) form as a function of  $q$  that is quite similar to  $\chi_b(q)$  for the second order (lognormal) spatial model (equation (3.116)).

#### 5.4.2 The First-Order Process

Now consider the first-order process  $B_t$ . As described above, at each time instant  $t_i$ ,  $B_i$  is a  $\beta$  model generator with a time-varying parameter  $\beta_i$ . In continuous time, we assume there exists a continuous function  $\beta_t$  such that  $\beta_t = \beta_i$  for each instant corresponding to the  $i$ th observation. This implies that the sample paths of  $B_t$  consist of jumps between two states, 0 and  $b^{\beta_t}$ . This leaves two features of  $B_t$  unspecified. First, how  $B_t$  jumps between its states, and second, how  $\beta_t$  is determined.

We address the specification of  $\beta_t$  first. One approach is to give it some relatively simple but stochastic structure, essentially making the process  $\beta_t$  part of the space-time theory. This approach is similar to what has typically been done in previous space-time theories, where, for example, storm arrivals may follow a Poisson process. We will follow a different approach for two reasons. First, our goal, which is to con-

struct a theory that evolves according to the large-scale conditions, is somewhat different. Second, as suggested by the GATE results discussed in Section 4.6, we can assume that  $\beta_t$  is a function of the large-scale conditions. Thus we develop a specification of  $\beta_t$  that honors the relation that was observed in GATE between it and the large-scale average rain rate. It could turn out in other situations that the functional relation between  $\beta$  and  $\bar{R}$  is different or that additional or different large-scale variables are more predictive of  $\beta$  than is  $\bar{R}$ , but this would not invalidate the general approach.

Recall from the GATE results (equation (4.40)) that  $\beta_i$  can be predicted from the large-scale average rain rate  $\bar{R}_i$  according to the relation

$$P(B_i > b^{\beta_i}) = b^{-\beta_i} \approx \left( \frac{\bar{R}_i}{R_{max}} \right)^{-s}, \quad (5.71)$$

where  $s < 0$  and  $R_{max} > 0$  are constants. It is critical to distinguish between forcing and response. We assume that the large-scale variable that “explains” variations in the small-scale structure is the forcing. According to equation (5.71), this is the large-scale average rain rate  $\bar{R}$ . However, since  $\bar{R} = R_0 Z_\infty$  and  $Z_\infty$  arises from the cascade itself, it is really just the *expected* large-scale average  $R_0$  which ought to be taken as the forcing. Assume then that  $R_0(t)$  is prescribed. Note that prescribing the large-scale forcing precludes feedbacks from the small-scale to the large. The left-hand side of equation (5.71) describes the response of the small-scale structure to the large-scale forcing, so in continuous time,  $b^{\beta_t}$  is the response function. Assigning the forcing to the large-scale and the response to the small-scale in fact predicts a lag between changes in  $\bar{R}$  and  $\beta$  that is sometimes observed. The time scale of this lag should in general be given by the inverse of the fluctuation rate  $k$  which is introduced below (equation (5.81)). It is convenient to define a general forcing function  $r_t$  as

$$r_t = f(\text{large-scale conditions}) = \left( \frac{R_0(t)}{R_{max}} \right)^{-s}. \quad (5.72)$$

In general,  $b^{\beta_t}$  will respond to changes in  $r_t$ , and they will be in equality only when  $B_t$  is in equilibrium with the large-scale forcing. Then we have

$$P(B_t > 0) = b^{-\beta_t} = r_t = \left( \frac{R_0(t)}{R_{max}} \right)^{-s}, \quad (5.73)$$

from which it is seen that the forcing  $r_t$  is a probability. It is shown in Appendix F that requiring  $B_t$  to come to equilibrium with  $r_t$  in the long time limit when  $r_t$  is constant is sufficient to satisfy the contingency criterion (c) presented in Section 5.2 above.

To specify the manner by which  $B_t$  jumps between its states  $S = \{0, b^{\beta_t}\}$ , it is sufficient to assume that it is a Markov process. Notice that its state space  $S$  is time-varying. This turns out to be cumbersome. In order to simplify matters, we construct  $B_t$  via a process  $I_t$  whose sample paths consist of jumps between 0 and 1 with marginal probabilities

$$P(I_t = 1) = p_1(t) \text{ and } P(I_t = 0) = p_0(t). \quad (5.74)$$

We then define

$$B_t = p_1^{-1}(t) I_t \quad (5.75)$$

and assume that  $I_t$  is a non-homogeneous birth-death Markov process on the state space  $S = \{0, 1\}$ . It is non-homogeneous because its parameters vary in time, even though its state space does not.

The basic property  $B_t$  must have is that it reduces to a spatial cascade generator (in particular, a  $\beta$ -model generator) for fixed  $t$ . This can be demonstrated using equation (5.75), from which it is seen that

$$P(B_t = 0) = P(I_t = 0) \text{ and } P(B_t = p_1^{-1}(t)) = p_1(t), \quad (5.76)$$

i.e.,  $B_t$  is a  $\beta$ -model generator with  $b^{-\beta_t} = p_1(t)$ .

So this construction satisfies the consistency criterion (see Section 5.2) of reducing to a spatial cascade. Since we have assumed it is Markov, it also satisfies the causality criterion. Specifying the process so that it satisfies the contingency criterion will be discussed below.

As a Markov process,  $I_t$  is characterized by its transition probabilities, which are given by

$$p_{ij}(t_1, t_2) = P(\{I_{t_2} = j\} \parallel \{I_{t_1} = i\}), \quad t_2 > t_1. \quad (5.77)$$

A rigorous definition of finite-state non-homogeneous birth-death Markov processes is given in Appendix F. The transition probabilities are characterized in turn by their right-handed partial derivatives

$$q_{ij}(t_2) = \lim_{t_2 \rightarrow t_1} \frac{p_{ij}(t_1, t_2)}{t_2 - t_1} = \frac{\partial}{\partial t_2} p_{ij}(t_1, t_2). \quad (5.78)$$

The evolution of the transition probabilities are given by *Kolmogorov's forward equations*, which are given for finite state space birth-death processes by

$$\frac{\partial}{\partial t_2} p_{ik}(t_1, t_2) = q_{ik}(t_1) = \sum_j p_{ij}(t_1, t_2) q_{jk}(t_2) \quad (5.79)$$

(see, e.g., Bhattacharya and Waymire (1990, p. 335)).

Thus the  $q_{ij}$  are free parameters of the process, so it is these parameters that must be specified in a way that satisfies the contingency criterion. To do this, we first need to write the criterion in a more definite form. Using the notion of equilibrium described above (equation (5.73)), for a time-invariant forcing  $r_{t_2} = r_0$ , we require

$$\lim_{t_2 \rightarrow \infty} p_1(t_2) = \lim_{t_2 \rightarrow \infty} b^{-\beta_{t_2}} = b^{-\beta_0} = r_0, \quad (5.80)$$

i.e.,  $B_t$  must converge to equilibrium with a constant forcing in the long time limit. It can be shown in that the condition given by equation (5.80) is satisfied by taking

$$q_{ij}(t_1) = k(r_{t_2}) \begin{bmatrix} (-r_{t_2}) & (r_{t_2}) \\ (1 - r_{t_2}) & (r_{t_2} - 1) \end{bmatrix}, \quad (5.81)$$

where  $k(r_{t_2})$  is an arbitrary positive function. Although, as this shows,  $k$  may be a function of the forcing without violating the contingency criterion, we will take it to be a constant. Taking the  $q_{ij}$  as in equation (5.81) actually implies the stronger result that  $B_t$  satisfies a “dynamical” contingency criterion

$$\frac{d}{dt_2} p_1(t_2) = -k[p_1(t_2) - r_{t_2}], \quad (5.82)$$

i.e.,  $p_1(t) = P(B_t = p_1^{-1}(t))$  responds in a first-order linear manner to the forcing  $r_t$ . It is easy to see that the satisfaction of the general contingency criterion (5.80) in fact follows from (5.82) by taking  $r_t = r_0$  in (5.82) and solving for  $p_1(t)$ . The details are given in Appendix F.

With  $q_{ij}$  specified as in equation (5.81) with constant  $k$ , the time behavior of the transition probabilities  $p_{ij}$  may be computed from the forward equations. Fixing  $t_1$  so that we just have functions of  $t_2$ , we obtain

$$\frac{d}{dt_2} p_{01}(t_2) = -k(p_{01}(t_2) - r_{t_2}) \quad (5.83)$$

and

$$\frac{d}{dt_2} p_{11}(t_2) = -k(p_{11}(t_2) - r_{t_2}). \quad (5.84)$$

From these results we see that the transition probabilities respond to changes in the forcing in a first-order linear manner with rate constant  $k$ . Analytical solutions of these equations depend of course on the form of  $r_{t_2}$ . When  $r_{t_2} = r_0$ , a constant, we obtain

$$p_{01}(t_1, t_2) = r_0(1 - e^{-k(t_2 - t_1)}) \quad (5.85)$$

and

$$p_{11}(t_1, t_2) = r_0 + (1 - r_0)e^{-k(t_2 - t_1)}. \quad (5.86)$$

The time behavior of the marginal probabilities  $p_i(t) = P(I_t = i)$  may be calculated from the equations

$$p_i(t_2) = \sum_j p_{ji}(t_1, t_2) p_j(t_1), \quad (5.87)$$

which arise from the definition of conditional probability and the theorem of total probability. From these we obtain  $p_1(t_2)$  as

$$p_1(t_2) = p_{11}(t_1, t_2) p_1(t_1) + p_{01}(t_1, t_2) (1 - p_1(t_1)). \quad (5.88)$$

In the  $r_{t_2} = r_0$  case this becomes

$$p_1(t_2) = p_1(t_1) e^{-k(t_2 - t_1)} + r_0 (1 - e^{-k(t_2 - t_1)}), \quad (5.89)$$

which simply reduces to  $p_1(t_2) = r_0$  when  $p_1(t_1) = r_0$ , i.e., when  $p_1$  is in equilibrium with the forcing at time  $t_1$ .

Using these results, we compute the cross moments  $E[B_{t_1}^q B_{t_2}^q]$ . It follows from equation (5.75) that

$$E[B_{t_1}^q B_{t_2}^q] = \frac{E[I_{t_1}^q I_{t_2}^q]}{p_1^q(t_1)p_1^q(t_2)}, \quad (5.90)$$

where

$$E[I_{t_1}^q I_{t_2}^q] = E[I_{t_1} I_{t_2}] = P(\{I_{t_1} = 1\} \cap \{I_{t_2} = 1\}) = p_{11}(t_1, t_2)p_1(t_1), \quad (5.91)$$

so

$$E[B_{t_1}^q B_{t_2}^q] = \frac{p_{11}(t_1, t_2)}{p_1^{q-1}(t_1)p_1^q(t_2)}. \quad (5.92)$$

For the case of  $B_t$  in equilibrium with a constant forcing  $r_0$  all the unknowns in the cross moments have been computed and we obtain

$$E[B_{t_1}^q B_{t_2}^q] = \frac{p_{11}(t_1, t_2)}{p_1^{q-1}(t_1)p_1^q(t_2)} = \frac{r_0 + (1 - r_0)e^{-k(t_2 - t_1)}}{r_0^{2q-1}}. \quad (5.93)$$

An analogous expression can be computed in principle for any specified forcing function; for examples, see Appendix F.

### 5.4.3 Parameter Estimation

Now let us combine the results for  $B_t$  and  $Y_t$  and consider testing and estimation methods. Since

$$\chi_b(q; t_1, t_2) = \log_b E[W_{t_1}^q W_{t_2}^q] - (2q - 1), \quad (5.94)$$

we have

$$\chi_b(q; t_1, t_2) = \log_b E[B_{t_1}^q B_{t_2}^q] + \log_b E[Y_{t_1}^q Y_{t_2}^q] - (2q - 1) \quad (5.95)$$

$$= \log_b \frac{p_{11}(t_1, t_2)}{p_1^{q-1}(t_1)p_1^q(t_2)} - \sigma^2 \log_b q + (1 + e^{-\alpha(t_2-t_1)})\sigma^2 \log_b q^2 - (2q-1). \quad (5.96)$$

As noted above in Section 5.2,  $\chi_b(0; t_1, t_2)$  depends only on the properties of  $B_t$ , which, as constructed here, has one free parameter, the fluctuation rate  $k$ . From equation (5.96) we have

$$\chi_b(0; t_1, t_2) = \log_b p_{11}(t_1, t_2) + \log_b p_1(t_1) + 1. \quad (5.97)$$

To get this as a function of  $k$  explicitly, we must assume a functional form for the forcing  $r_t$ . The only really simple case is for  $r_t = r_0$ ; other cases are given in Appendix F. In this case we have

$$\chi_b(0; t_1, t_2) = \log_b [r_0 + (1 - r_0)e^{-k(t_2-t_1)}] + \log_b p_1(t_1) + 1, \quad (5.98)$$

which gives a specific functional form to the decay of  $\chi_b(0; t_1, t_2)$  which was left unspecified in Section 5.2. Note that essentially this functional form was obtained by assuming that  $B_t$  is a Markov process. Solving for  $e^{-k(t_2-t_1)}$  yields

$$e^{-k(t_2-t_1)} = \frac{b^{\chi_b(0; t_1, t_2)-1} p_1^{-1}(t_1) - r_0}{1 - r_0}, \quad (5.99)$$

which provides an easy way to test this specification of  $B_t$ , viz, if a tracked rainfall field is first-order stationary (that is,  $r_t$  is a constant  $r_0$ ), the theory predicts that the right-hand side will be exponential in the time lag  $\tau$ , providing a test of the theory, with the inverse of the time constant of the exponential giving an estimate of the rate constant  $k$ . In Figure 5.9 we replot the decay of  $\chi_b(0; t_1, t_2)$  in this form and obtain roughly an exponential. Ignoring the last half hour, we may conclude that insofar as an exponential decay is evident here, its characteristic time  $k^{-1}$  appears to be on the order of about two hours.

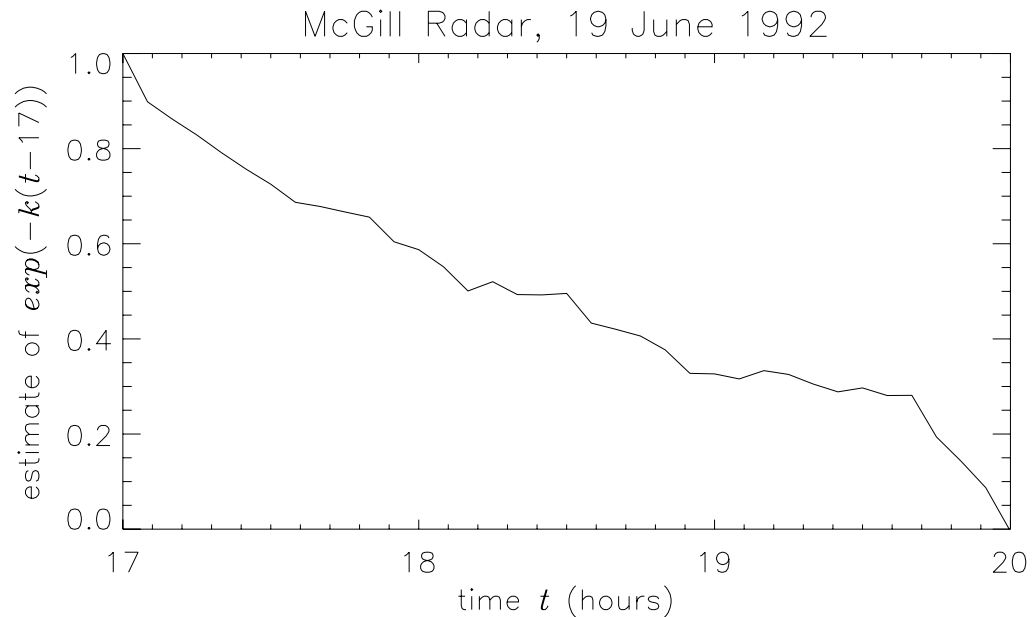


**Figure 5.9 Estimator of first-order fluctuation rate**

**Test of the exponential decay of  $(b^{\hat{\tau}(0;t_1, t_2)-1} p_1^{-1}(t_1) - r_0)/(1 - r_0)$ , which, according to equation (5.99), should estimate  $e^{-k(t_2 - t_1)}$ .**

We also showed in Section 5.2 that  $\chi_b^{(2)}(q; t_p, t_2)$  depends only on the properties of the positive process  $Y_t$  and computed its limiting values in terms of  $\chi_{b, Y_t}^{(2)}(q; t_p, t_2)$ . Now that we have specified the process  $Y_t$ , we may compute the functional form of the decay, obtaining from equation (5.96) that

$$\chi_b^{(2)}(q; t_p, t_2) = 2(1 + e^{-\alpha(t_2 - t_1)})\sigma^2 \log b. \quad (5.100)$$

This may be compared to Figure 5.6, from which we conclude that, again, insofar as an exponential decay is evident, its characteristic time  $\alpha^{-1}$  is on the order of an hour.

We conclude this section by summarizing the parameterization of the approximate models presented here. The first-order model has the generator  $B_t$ , which depends on two parameters, the forcing function  $r_t$ , which governs the value of the

spatial model  $\beta$ , and the fluctuation rate  $k$ . We have assumed that  $k$ , which governs the rate at which  $B_t$  fluctuates between the values of its state space  $S = \{0, b^{\beta_t}\}$ , is a constant. Its value can be estimated by a plot like Figure 5.9. Following the results of the spatial analysis of the GATE data, we have assumed that  $r_t$  varies according to a function of the large-scale average rain rate  $\bar{R}$ , though this should only be thought of as an example. Plots like Figure 4.6 can be used to estimate this function. The second-order model consists of the product  $W_t = B_t Y_t$ , where the second-order component  $Y_t$  is assumed to be a stationary lognormal diffusion with rate constant  $\alpha$  and spatial parameter  $\sigma$ . The rate constant can be estimated by a plot like Figure 5.6. A plot like Figure 4.22 can be used to estimate to check the stationarity of  $\sigma$  and to estimate its value.

## Chapter 6

### Conclusions

We demonstrated that the theory of multiplicative random cascades provides an accurate, easily tested model for spatially homogeneous rainfall fields and extends to space-time in a natural way. We identified a class of cascade generators that are relevant to modeling spatial rainfall, and showed that parameters could be estimated for each realization (scene) of the rainfall field. This enabled us to test the scaling invariance of statistical moments predicted by the theory. These tests were carried out on a large database of mesoscale rainfall fields, and the scaling invariance was found to be good for the “typical” field. More significant deviations were found for the high and low rain rate extremes, but it was possible to interpret these deviations in terms of the geometry of the fields and to hypothesize what kind of generalization of the theory would accommodate these features. An empirical finding of great potential significance was the variation of the parameters with the large-scale meteorological conditions, as measured by the average rain rate over the scene. In particular, only the parameter governing the division of the field into rainy and non-rainy regions depended on the average rain rate. The parameter governing the fluctuations within rainy regions was found to be invariant with respect to average rain rate. These two results suggest, at least for this data, that the large-scale forcing determines how much it rains, but how that rain is organized spatially is determined independently by the small-scale processes of convection.

A space-time theory was constructed by making the spatial theory evolve according to a non-stationary large-scale forcing. It requires that the iid random generators of

the spatial theory be regarded as iid stochastic processes indexed by time. Markov processes were used as a first approximation of this extension. In the presence of advection of the rainfall field by the ambient winds, this theory follows the flow, i.e., it is in the Lagrangian frame of reference. The path-wise properties of the spatial theory extend naturally to the space-time theory. In particular, the space-time theory predicts path-wise scale-invariance of the two-point Lagrangian temporal cross moments, which can be used to test the theory and estimate its parameters. Tests of this general prediction, as well as more specific predictions from space-time extensions of first and second-order approximations developed for the spatial theory, were carried out on a case study of tracked radar rainfall data. It was found that the characteristic de-correlation times of the generator processes are on the order of one to two hours.

Certain important predictions of the theory in the time domain were also computed. It was found that the Lagrangian correlation decreases in a power law manner as the resolution increases, as is roughly observed empirically. Under the condition of stationarity, the Eulerian correlation was computed and the prediction of the theory regarding the breakdown of Taylor's hypothesis was worked out. The theory predicts that Taylor's hypothesis will hold at any resolution up to the time scale of the generator processes, which, as noted above, is one to two hours. This also roughly matches empirical observations.

This research has identified a number of open problems in both the spatial and space-time domains. A major open problem is to test this theory on a wider variety of types of rainfall, both tropical and extratropical. Even though observations of extratropical cyclone storms motivated the notion of a scaling hierarchy of structures in space-time rainfall, the theory has not been tested on these storms. It is important to find out to what extent the small-scale rainfall is forced by large-scale dynamics and what generalizations might be needed in extratropical storms. Another open problem is an ex-

planation of the systematic curvature of the log-moments versus log-scale. One useful and defensible approach to this problem is to use equally weighted regression, rather than weighting the scales proportionally to the number of boxes at that scale, as was done here. The result of such an approach would give the “average” scaling over the range of scales in the data, which seems the appropriate approach for applications to downscaling. Preliminary results using this weighting method in the GATE data indicate a substantial reduction in the error of the fit and a disappearance of the problem of concavity in the estimated  $\tau(q)$  curve. However, as discussed in the thesis, there is physical information in these deviations that should be taken into account. This result also suggests exploration of a generalization of the theory to the case where the distribution of the generators depends on scale.

The space-time theory has been tested in depth only on the case study presented here, and in a preliminary manner on a few other cases with similar results, so further testing is an important priority in assessing its general validity. It is also important to work out sample path properties of the theory in the temporal domain. For example, disregarding the high frequency component  $Z_\infty(t)$ , the sample paths of a single pixel at some scale in the first-order space-time theory consist of jumps between zero and some positive rain rate, the rate of fluctuations being determined by the scale of the pixel. It is an open question how physically realistic such a sample path structure is, as is the question of the implications of the sample path properties for applications.

Despite these open problems regarding the generality of the theory and certain of its properties, we feel that the basic structure is secure enough that the applications of the theory to the problems in runoff generation, floods, and measurement of rainfall outlined in the introduction can begin to be explored. One such application has already been developed; see Gupta et al. (1995) and Castro (1995). In this work, the scaling exponents of floods from an idealized scale-invariant Peano river basin under instant-

neous application of spatial cascade rainfall were computed analytically. These computations required a thorough understanding of the cascade theory described here. While there are many aspects of the rainfall-runoff problem which were ignored or simplified, Gupta et al. (1995) nevertheless provides an elegant basic framework in which to develop a physical-statistical theory of floods.

This application to floods gives one hope that similar results may be possible in other areas where the space-time variability of rainfall is crucial. For one further example, consider satellite estimation of rainfall. We demonstrated in Chapter 4 a connection between the independence of the second-order parameter from average rain rate and the homogeneity, at some scale smaller than the resolution of the data, of the distribution of rain rates conditioned on positive rain. Since, as explained there, homogeneity of the distribution of rain rate conditioned on positive rain can be used to explain the so-called threshold method of rainfall estimation, it appears that it should be possible to use the present results to improve the method. In particular, one would like to predict the behavior of the method as a function of sensor resolution, which is identified as an important open problem in the estimation of rainfall from satellites by Morrissey (1994).

## References

- Austin, P. M., 1960: Microstructure of storms as described by quantitative radar data. *Physics of Precipitation: Proceedings of the Cloud Physics Conference, 3-5 June 1959, Woods Hole, Mass.*, H. Weickmann, ed. American Geophysical Union of the N.A.S.-N.R.C., Geophysical Monograph No. 5., 86-93.
- Austin, G. L. and A. Bellon, 1974: The use of digital weather records for short-term precipitation forecasting. *Q. J. R. Met. Soc.*, **100**, 658-664.
- Austin, P. M. and R. A. Houze, Jr., 1970: Analysis of mesoscale precipitation areas. *14th Radar Meteorology Conference*. Boston: American Meteorological Society, 329-334.
- Austin, P. M. and R. A. Houze, Jr., 1972: Analysis of the structure of precipitation patterns in New England. *J. Appl. Meteorol.*, **11**, 926-935.
- Bell, T. L., 1987: A space-time stochastic model of rainfall for satellite remote-sensing studies. *J. Geophys. Res.*, **92**(D8), 9631-9643.
- Bhattacharya, R. N. and E. C. Waymire, 1990: *Stochastic Processes with Applications*. New York: John Wiley & Sons, 672 pp.
- Billingsley, P., 1986: *Probability and Measure*, 2nd ed. New York: John Wiley & Sons, 622 pp.
- Bras, R. L. and I. Rodriguez-Iturbe, 1976: Rainfall generation: a nonstationary time-varying multidimensional model. *Water Resour. Res.*, **12**(3), 450-456.
- Breiman, L., 1992: *Probability*. Philadelphia: Society for Industrial and Applied Mathematics, 421 pp.
- Browning, K. A., 1974: Mesoscale structure of rain systems in the British Isles. *J. Meteorol. Soc. Japan*, **52**(3), 314-327.
- Byers, H. R. and R. R. Braham, Jr., 1949: *The Thunderstorm*. Washington: US Government Printing Office.
- Castro, S. L., 1995: Scaling Exponents of Floods from Scale-Invariant Spatial Rainfall and River Networks. M.S. Thesis, University of Colorado, Boulder, in preparation.
- Cates, M. E. and J. M. Deutsch, 1987: Spatial correlations in multifractals. *Phys. Rev. A*, **35**, 4907-4910.
- Chhabra, A. and R. V. Jensen, 1989: Direct determination of the  $f(\alpha)$  singularity spectrum. *Phys. Rev. Lett.*, **62**(12), 1327-1330.

- Chiu, L. S., G. R. North, D. A. Short and A. McConnell, 1990: Rain estimation from satellites: effect of finite field of view. *J. Geophys. Res.*, **95**(D3), 2177-2185.
- Collier, C. G., 1989: *Applications of Weather Radar Systems - A Guide to Uses of Radar Data in Meteorology and Hydrology*. Chichester, England: Ellis Horwood Limited, 294 pp.
- Cox, D. R. and V. Isham, 1988: A simple spatial-temporal model of rainfall. *Proc. R. Soc. Lond. A*, **415**, 317-328.
- Cowpertwait, P. S. P., 1995: A generalized spatial-temporal model of rainfall based on a clustered point process. *Proc. R. Soc. Lond. A*, **450**, 163-175.
- Crane, R. K., 1990: Space-time structure of rain rate fields. *J. Geophys. Res.*, **95**(D3), 2011-2020.
- Dobrushin, R. L., 1980: Automodel generalized random fields and their reform-group. *Multicomponent Random Systems*, R. L. Dobrushin and Y. G. Sinai, eds. Advances in Probability and Related Topics, vol. 6. New York: Marcel Dekker, 153-198.
- Doneaud, A., P. L. Smith, A. S. Dennis and S. Sengupta, 1981: A simple method for estimating convective rainfall over an area. *Water Resour. Res.*, **17**, 1676-1682.
- Dubrulle, B., 1994: Intermittency in fully developed turbulence: log-Poisson statistics and generalized scale covariance. *Phys. Rev. Lett.*, **73**(7), 959-962.
- Eagleson, P. S., 1984: The distribution of catchment storm coverage by stationary rainstorms. *Water Resour. Res.*, **20**(5), 581-590.
- Eagleson, P. S., N. M. Fennessy, W. Qinliang and I. Rodriguez-Iturbe, 1987: Application of spatial Poisson models to air mass thunderstorms. *J. Geophys. Res.*, **92**(D8), 9661-9778.
- Emanuel, K. A., 1994: *Atmospheric Convection*. New York: Oxford University Press, 580 pp.
- Falconer, K., 1990: *Fractal Geometry: Mathematical Foundations and Applications*. Chichester, England: John Wiley & Sons, 288 pp.
- Fritsch, J. M., R. A. Maddox and A. G. Barnston, 1981: The character of mesoscale convective complex precipitation and its contribution to warm season rainfall in the U. S. *Preprints, Fourth Conf. on Hydrometeorol.* Boston: American Meteorological Assoc., 94-99.
- Goodall, C. R. and M. J. Phelan, 1991: Edge-preserving smoothing and the assessment of point process models for GATE rainfall fields. *Statistical Inference in Stochastic Processes*, N. U. Prahhu and I. V. Basawa, eds. New York: Marcel Dekker, 35-66.

- Gupta, V. K. and D. R. Dawdy, 1995: Physical interpretations of regional variations in the scaling exponents of flood quantiles. *Hydrol. Proc.*, **9**, 347-361.
- Gupta, V. K. and E. Waymire, 1987: On Taylor's hypothesis and dissipation in rainfall. *J. Geophys. Res.*, **92**(D8), 9657-9660.
- Gupta, V. K. and E. Waymire, 1990: Multiscaling properties of spatial rainfall and river flow distributions. *J. Geophys. Res.*, **95**(D3), 1999-2009.
- Gupta, V. K. and E. Waymire, 1991: On lognormality and scaling in spatial rainfall averages? *Non-Linear Variability in Geophysics: Scaling and Fractals*, D. Schertzer and S. Lovejoy, eds. Dordrecht: Kluwer Academic, 175-183.
- Gupta, V. K. and E. C. Waymire, 1993: A statistical analysis of mesoscale rainfall as a random cascade. *J. Appl. Meteor.*, **32**(2), 251-267.
- Gupta, V. K. and E. C. Waymire, 1995: Multiplicative cascades and spatial variability in rainfall, river networks and floods. To appear in: *Reduction and Predictability of Natural Disasters*. Santa Fe, New Mexico: Santa Fe Institute.
- Gupta, V. K., S. L. Castro and T. M. Over, 1995: Scaling exponents of peak flows from spatial rainfall and channel networks. *J. Hydrol.*, under review.
- Ha, E. and G. R. North, 1995: Model studies of beam-filling error for rain-rate retrieval with microwave radiometers. *J. Atmos. Oceanic Technol.*, **12**, 268-281.
- Harrold, T. W., 1973: Mechanisms influencing the distribution of precipitation within baroclinic disturbances. *Quart. J. R. Meteorol. Soc.*, **99**, 232-251.
- Harrold, T. W. and P. M. Austin, 1974: The structure of precipitation systems - a review. *J. Rech. Atmos.*, **8**, 41-57.
- Hobbs, P. V., 1978: Organization and structure of clouds and precipitation on the mesoscale and microscale in cyclonic storms. *Rev. Geophys. Space Phys.*, **16**(4), 741-755.
- Hobbs, P. V. and J. D. Locatelli, 1978: Rainbands, precipitation cores and generating cells in a cyclonic storm. *J. Atmos. Sci.*, **35**, 230-241.
- Holley, R. and E. C. Waymire, 1992: Multifractal dimensions and scaling exponents for strongly bounded random cascades. *Ann. Appl. Prob.*, **2**(4), 819-845.
- Houze, R. A., Jr., 1981: Structures of atmospheric precipitation systems: a global survey. *Radio Sci.*, **16**(5), 671-689.
- Houze, R. A., Jr. and A. K. Betts, 1981: Convection in GATE. *Rev. Geophys. Space Phys.*, **19**, 541-576.
- Houze, R. A., Jr. and P. V. Hobbs, 1982: Organization and structure of precipitating cloud systems. *Adv. Geophys.*, **24**, 225-315.

- Houze, R. A., P. V. Hobbs, K. R. Biswas and W. M. Davis, 1976: Mesoscale rainbands in extratropical cyclones. *Mon. Wea. Rev.*, **109**, 868-878.
- Islam, S., R. L. Bras and I. Rodriguez-Iturbe, 1988: Multidimensional modeling of cumulative rainfall: parameter estimation and model adequacy through a continuum of scales. *Water Resour. Res.*, **24**(7), 985-992.
- Johnson, K. D., D. Entekhabi and P. S. Eagleson, 1993: The implementation and validation of improved land-surface hydrology in an atmospheric general circulation model. *J. Clim.*, **6**, 1009-1026.
- Jorgensen, D. P. and M. A. LeMone, 1989: Vertical velocity characteristics of oceanic convection. *J. Atmos. Sci.*, **46**(5), 621-640.
- Kahane, J.-P., 1974: Sur le modele de turbulence de Benoit Mandelbrot. *C. R. Acad. Sci. Paris, Ser. A*, **278**, 621-623.
- Kahane, J.-P., 1985: Sur le chaos multiplicatif. *Ann. Sci. Math. Quebec*, **9**(2), 105-150.
- Kahane, J.-P., 1987: Positive martingales and random measures. *Chin. Ann. Math.*, **8B**(1), 1-12.
- Kahane, J.-P., 1989: Random multiplications, random coverings, multiplicative chaos. *Analysis at Urbana*, Vol. 1, E. Berkson et al., eds., London Math. Soc. Lecture Note Series **137**. Cambridge, England: Cambridge University Press, 196-255.
- Kahane, J.-P. and J. Peyriere, 1976: Sur certaines martingales de Benoit Mandelbrot. *Adv. Math.*, **22**, 131-145.
- Kedem, B. and L. S. Chiu, 1987: Are rain rate processes self-similar? *Water Resour. Res.*, **23**(10), 1816-1818.
- Kedem, B., L. S. Chiu and Z. Karni, 1990: An analysis of the threshold method for measuring area-average rainfall. *J. Appl. Meteor.*, **29**, 3-20.
- Kolmogorov, A. N., 1941: The local structure of turbulence in incompressible liquid for very high Reynolds numbers. *C. R. Acad. Sci. USSR*, **30**, 301-305.
- Kolmogorov, A. N., 1962: A refinement of previous hypotheses concerning the local structure of turbulence in a viscous inhomogeneous fluid at high Reynolds number. *J. Fluid Mech.*, **13**, 82-85.
- Kumar, P. and E. Foufoula-Georgiou, 1993a: A multicomponent decomposition of spatial rainfall fields, 1. Segregation of large- and small-scale features using wavelet transforms. *Water Resour. Res.*, **29**(8), 2515-2532.
- Kumar, P. and E. Foufoula-Georgiou, 1993b: A multicomponent decomposition of spatial rainfall fields, 2. Self-similarity in fluctuations. *Water Resour. Res.*, **29**(8), 2533-2544.

- Lamperti, J., 1962: Semi-stable stochastic processes. *Trans. Am. Math. Soc.*, **104**, 62-78.
- Lau, K. M., T. Nakazawa and C. H. Sui, 1991: Observations of cloud cluster hierarchies over the tropical western Pacific. *J. Geophys. Res.*, **96**, Supplement, 3197-3208.
- Laughlin, C. R., 1981: On the effect of temporal sampling on the observation of mean rainfall. *Precipitation Measurements from Space, NASA Report*, D. Atlas and O. W. Thiele, eds. Greenbelt, MD: NASA Goddard Space Flight Center, D59-D66.
- Lavallee, D., D. Schertzer and S. Lovejoy, 1991: On the determination of the codimension function. *Non-Linear Variability in Geophysics, Scaling and Fractals*, D. Schertzer and S. Lovejoy, eds. Dordrecht: Kluwer Academic, 99-109.
- Lavallee, D., S. Lovejoy, D. Schertzer and F. Schmitt, 1992: On the determination of universal multifractal parameters in turbulence. *Topological Aspects of the Dynamics of Fluids and Plasmas*, H. K. Moffatt et al., eds. Dordrecht: Kluwer Academic, 463-478.
- LeCam, L., 1961: A stochastic description of precipitation. *Proc. Fourth Berkeley Symposium on Mathematical Statistics and Probability*, vol. 3, J. Neyman, ed. Berkeley: University of California, 165-186.
- Lee, S. J. and T. C. Halsey, 1990: Some results on multifractal correlations. *Physica A*, **164**, 575-592.
- Lovejoy, S., 1981: The statistical characterization of rain areas in terms of fractals. *Proc. 20th Conference on Radar Meteorology*. Boston: American Meteorological Society, 476-483.
- Lovejoy, S., 1982: Area-perimeter relation for rain and cloud areas. *Science*, **216**, 185-187.
- Lovejoy, S. and B. B. Mandelbrot, 1985: Fractal properties of rain, and a fractal model. *Tellus*, **37A**, 209-232.
- Lovejoy, S. and D. Schertzer, 1985: Generalized scale invariance in the atmosphere and fractal models of rain. *Water Resour. Res.* **21**(8), 1233-1250.
- Lovejoy, S., D. Schertzer and A. A. Tsonis, 1987: Functional box-counting and multiple elliptical dimensions in rain. *Science*, **235**, 1036-1038.
- Lovejoy, S. and D. Schertzer, 1990: Fractals, raindrops, and resolution dependence of rain measurements. *J. Appl. Meteor.*, **29**, 1167-1170.
- Lovejoy, S. and D. Schertzer, 1991: Multifractal analysis techniques and the rain and cloud fields from  $10^{-3}$  to  $10^6$  m. *Non-Linear Variability in Geophysics: Scaling and Fractals*, D. Schertzer and S. Lovejoy, eds. Dordrecht: Kluwer Academic, 99-109.

- Lucas, C., E. J. Zipser and M. A. LeMone, 1994: Vertical velocity in oceanic convection off tropical Australia. *J. Atmos. Sci.*, **51**(21), 3183-3193.
- Lukacs, E., 1970: *Characteristic Functions*, 2nd ed. London: Charles Griffin & Company, 350 pp.
- Mandelbrot, B. B., 1972: Possible refinement of the lognormal hypothesis concerning the distribution of energy dissipation in intermittent turbulence. *Statistical Models and Turbulence*, M. Rosenblatt and C. Van Atta, eds. Lecture Notes in Physics, **12**. New York: Springer-Verlag, 333-351.
- Mandelbrot, B. B., 1974: Intermittent turbulence in self-similar cascades: divergence of high moments and dimension of the carrier. *J. Fluid Mech.*, **62**(2), 331-358.
- Mandelbrot, B. B., 1983: *The Fractal Geometry of Nature*. New York: W. H. Freeman and Co., 468 pp.
- Mapes, B. E. and R. A. Houze, Jr., 1993: Cloud clusters and superclusters over the oceanic warm pool. *Mon. Wea. Rev.*, **121**, 1398-1415.
- Matsumoto, S., 1968: Smaller scale disturbances in the temperature field around a decaying typhoon with special emphasis on the severe precipitation. *J. Meteorol. Soc. Japan*, **46**(6), 483-494.
- Mejia, J. M. and I. Rodriguez-Iturbe, 1974: On the synthesis of random field sampling from the spectrum: an application to the generation of hydrologic spatial processes. *Water Resour. Res.*, **10**(4), 705-711.
- Meneveau, C. and A. B. Chhabra, 1990: Two-point statistics of multifractal measures. *Physica A*, **164**, 564-574.
- Morrissey, M. L., 1994: The effect of data resolution on the area threshold method. *J. Appl. Meteor.*, **33**(11), 1263-1270.
- Nakamoto, S., J. B. Valdes and G. R. North, 1990: Frequency-wavenumber spectrum for GATE Phase I rainfields. *J. Appl. Meteorol.*, **29**, 842-850.
- Nakazawa, T., 1988: Tropical super clusters within intraseasonal variations over the western Pacific. *J. Meteorol. Soc. Japan*, **66**(6), 823-839.
- Novikov, E. A. and R. W. Stewart, 1964: Intermittency of turbulence and the spectrum of fluctuations of energy dissipation. *Izv. Akad. Nauk USSR Geophys. Ser.*, **3**, 408-413.
- North, G. R. and S. Nakamoto, 1989: Formalism for comparing rain estimation designs. *J. Atmos. Ocean. Tech.*, **6**, 985-992.
- Nozumi, Y. and H. Arakawa, 1968: Prefrontal rainbands located in the warm sector of subtropical cyclones over the ocean. *J. Geophys. Res.* **73**, 487-492.

- Oboukhov, A. M., 1962: Some specific features of atmospheric turbulence. *J. Fluid Mech.*, **13**, 77-81.
- Ogden, F. L. and P. Y. Julien, 1994: Runoff model sensitivity to radar rainfall resolution. *J. Hydrol.*, **158**, 1-18.
- Okabe, A., B. Boots and K. Sugihara, 1992: *Spatial Tessellations: Concepts and Applications of Voronoi Diagrams*. Chichester, England: John Wiley & Sons, 532 pp.
- Over, T. M. and V. K. Gupta, 1991: Correlations in random cascades: theoretical results and a test of GATE rainfall data. Abstract, *Eos, Transactions, American Geophysical Union*, **72**(44) Supplement, 202.
- Over, T. M. and V. K. Gupta, 1993: Inference for random cascades using wavelet transforms. Abstract, *Eos, Transactions, American Geophysical Union*, **74**(16) Supplement, 55.
- Over, T. M. and V. K. Gupta, 1994: Statistical analysis of mesoscale rainfall: dependence of a random cascade generator on large-scale forcing. *J. Appl. Meteor.* **33**(12), 1526-1542.
- Over, T. M. and V. K. Gupta, 1995: A space-time theory of mesoscale rainfall using random cascades. *J. Geophys. Res.*, under review.
- Patterson, V. L., M. D. Hudlow, P. J. Pytlowany, F. P. Richards, and J. D. Hoff, 1979: *GATE Radar Rainfall Processing System*. Washington: United States Department of Commerce, NOAA Technical Memorandum EDIS 26.
- Perica, S. and E. Foufoula-Georgiou, 1995a: Linkage of scaling and thermodynamic parameters of rainfall: results from midlatitude mesoscale convective systems. *J. Geophys. Res.*, to appear.
- Perica, S. and E. Foufoula-Georgiou, 1995b: Multiscale disaggregation of spatial rainfall based on scaling and thermodynamic parameters: 1. Model development and performance evaluation. *J. Geophys. Res.*, under review.
- Peyriere, J., 1974: Turbulence et dimension de Hausdorff. *C. R. Acad. Sc. Paris, Ser. A*, **278**, 567-569.
- Phelan, M. J., 1991: Point processes and inference for rainfall fields. *Selected Proc. of the Sheffield Symp. on Appl. Prob.*, I. V. Basawa and R. L. Taylor, eds. IMS Lecture Notes-Monograph Series, vol. 18, 127-148.
- Phelan, M. J., 1992: Aging functions and their nonparametric estimation in point process models of rainfall. *Statistics in the Environmental and Earth Sciences*, A. T. Walden and P. Guttorp, eds. London: Edward Arnold, 90-116.

- Phelan, M. J. and C. R. Goodall, 1990: An assessment of a generalized Waymire-Gupta-Rodriguez-Iturbe model for GARP Atlantic Tropical Experiment rainfall. *J. Geophys. Res.*, **95**(D6), 7603-7615.
- Pitman, A. J., Z.-L. Yang and A. Henderson-Sellers, 1993: Sub-grid scale precipitation in AGCMs: re-assessing the land surface sensitivity using a single column model. *Clim. Dynam.*, **9**, 33-41.
- Polyak, I., G. R. North and J. B. Valdes, 1994: Multivariate space-time analysis of PRE-STORM precipitation. *J. Appl. Meteorol.*, **33**, 1079-1087.
- Ramirez, J. A. and R. L. Bras, 1990: Clustered or regular cumulus cloud fields: the statistical character of observed and simulated cloud fields. *J. Geophys. Res.*, **95**(D3), 2035-2045.
- Ramirez, J. A., R. L. Bras and K. A. Emanuel, 1990: Stabilization functions of unforced cumulus clouds: their nature and components. *J. Geophys. Res.*, **95**(D3), 2047-2059.
- Reed, R. J., D. C. Norquist and E. E. Recker, 1977: The structure and properties of African wave disturbances as observed during phase III of GATE. *Mon. Wea. Rev.*, **105**, 317-333.
- Richardson, L. F., 1965: *Weather Prediction by Numerical Process*. New York: Dover Publications, 236 pp.
- Rodriguez-Iturbe, I. and P. S. Eagleson, 1987: Mathematical models of rainstorm events in space and time. *Water Resour. Res.*, **23**(1), 181-190.
- Rodriguez-Iturbe, I., D. R. Cox and P. S. Eagleson, 1986: Spatial modelling of total storm rainfall. *Proc. R. Soc. Lond. A*, **403**, 27-50.
- Rodriguez-Iturbe, I., D. R. Cox and V. Isham, 1987: Some models for rainfall based on stochastic point processes. *Proc. R. Soc. Lond. A*, **410**, 269-288.
- Ross, K. A., 1980: *Elementary Analysis: The Theory of Calculus*. New York: Springer-Verlag, 264 pp.
- Schertzer, D. and S. Lovejoy, 1987: Physical modeling and analysis of rain and clouds by anisotropic scaling multiplicative processes. *J. Geophys. Res.*, **92**(D8), 9693-9714.
- Schmitt, F. D., Schertzer, S., Lovejoy and Y. Brunet, 1994: Empirical study of multifractal phase transitions in atmospheric turbulence. *Nonlin. Proc. Geophys.*, **1**, 95-98.
- She, Z.-S. and E. C. Waymire, 1995: Quantized energy cascade and log-Poisson statistics in fully developed turbulence. *Phys. Rev. Lett.*, **74**(2), 262-265.

- Siebesma, A. P. and L. Pietronero, 1988: Correlations in multifractals. *J. Phys. A*, **21**, 3259-3267.
- Simmons, G. F., 1972: *Differential Equations with Applications and Historical Notes*. New York: McGraw-Hill Book Company, 465 pp.
- Smith, J. A. and A. F. Karr, 1985: Parameter estimation for a model of space-time rainfall. *Water Resour. Res.*, **21**(8), 1251-1257.
- Sui, C.-H. and K.-M. Lau, 1992: Multiscale phenomena in the tropical atmosphere over the western Pacific. *Mon. Wea. Rev.* **120**, 407-430.
- Taylor, G. I., 1938: The spectrum of turbulence. *Proc. Roy. Soc. London, Ser. A*, **164**, 476-490.
- Tessier, Y., S. Lovejoy and D. Schertzer, 1993: Universal multifractals: theory and observations for rain and clouds. *J. Appl. Meteor.*, **32**(2), 223-250.
- Thompson, R. M., S. W. Payne, E. E. Recker and R. J. Reed, 1979: Structure and properties of synoptic-scale wave disturbances in the intertropical convergence zone of the eastern Atlantic. *J. Atmos. Sci.*, **36**, 53-72.
- Valdes, J. B., I. Rodriguez-Iturbe and V. K. Gupta, 1985: Approximations of temporal rainfall from a multidimensional model. *Water Resour. Res.*, **21**(8), 1259-1270.
- Valdes, J. B., S. Nakamoto, S. S. P. Shen and G. R. North, 1990: Estimation of multi-dimensional precipitation parameters by areal estimates of oceanic rainfall. *J. Geophys. Res.*, **95**(D3), 2101-2111.
- Valdes, J. B., E. Ha, C. Yoo and G. R. North, 1994: Stochastic characterization of space-time precipitation: implications for remote sensing. *Adv. Water Resour.*, **17**, 47-59.
- Waymire, E., 1985: Scaling limits and self-similarity in precipitation fields. *Water Resour. Res.*, **21**(8), 1271-1281.
- Waymire, E., V. K. Gupta and I. Rodriguez-Iturbe, 1984: A spectral theory of rainfall intensity at the meso- $\beta$  scale. *Water Resour. Res.*, **20**, 1453-1465.
- Waymire, E. C. and S. C. Williams, 1993: A cascade decomposition theory with applications to Markov and exchangeable cascades. Preprint.
- Waymire, E. C. and S. C. Williams, 1995: Multiplicative cascades: dimension spectra and dependence. *J. Fourier Anal. Appl.*, to appear.
- Weger, R. C., J. Lee and R. M. Welch, 1993: Clustering, randomness, and regularity in cloud fields, 3, The nature and distribution of clusters. *J. Geophys. Res.*, **98**(D10), 18,449-18,463.

- Wilson, C. B., J. B. Valdes and I. Rodriguez-Iturbe, 1979: On the influence of the spatial distribution of rainfall on storm runoff. *Water Resour. Res.*, **15**, 321-328.
- Yaglom, A. M., 1966: The influence of fluctuations in energy dissipation on the shape of turbulence characteristics in the inertial interval. *Sov. Phys.-Dokl.*, **11**, 26-29.
- Zawadzki, I. I., 1973: Statistical properties of precipitation patterns. *J. Appl. Meteor.*, **12**, 459-472.
- Zawadzki, I., 1982: The quantitative interpretation of weather radar measurements. *Atmos.-Ocean*, **20**(2), 158-180.
- Zawadzki, I., J. Morneau and R. Laprise, 1994: Predictability of precipitation patterns: an operational approach. *J. Appl. Meteor.*, **33**(12), 1562-1571.

## APPENDIX A

### A Few Concepts from Measure Theory

This material is taken primarily from Billingsley (1986, sections 2 and 3). A measure is a function that maps subsets of some space to the non-negative real numbers in a way such that the value of the measure for a given subset indicates the amount of “stuff” or “mass” associated with the subset. For a measure  $\mu$  and a set  $A$ , this amount of mass is denoted simply by  $\mu(A)$ . It should be immediately clear that a measure cannot take on negative values, and it must be *additive*, which means, for a (possibly infinite) sequence of disjoint subsets  $A_1, A_2, \dots$  and a measure  $\mu$ , we have

$$\mu\left(\bigcup_i A_i\right) = \sum_i \mu(A_i). \quad (\text{A.1})$$

Spaces with uncountably infinite numbers of subsets (such as spaces that are subsets of  $n$ -dimensional Euclidean space  $\mathfrak{R}^n$ , which we will use here) introduce some technicalities. An important concept in this connection is that of a  $\sigma$ -field. Consider first the definition of a field. A *field*  $F$  is defined as a collection of subsets of some space  $\Omega$  that satisfies the following conditions:

- (a)  $\Omega \in F$ ;
- (b)  $A \in F$  implies  $A^c \in F$ ; and
- (c)  $A, B \in F$  implies  $A \cup B \in F$ .

It can be shown that the above conditions imply that unions, complements, and intersections of a finite number of sets in  $F$  are in  $F$ . The collection  $F$  is a  $\sigma$ -field if in addi-

tion to conditions (a)-(c) it satisfies

$$(d) A_1, A_2, \dots \in F \text{ implies } A_1 \cup A_2 \cup \dots \in F.$$

In this case, complements and intersections of countably many sets are also in  $F$ . In this case, of course, the space  $\Omega$  must contain infinitely many elements. Clearly condition (d) is required of the sequence of sets used in the additivity condition (A.1).

Now consider a collection of sets  $G$  which is not a  $\sigma$ -field. There always exist  $\sigma$ -fields that contain  $G$ , and the intersection of these  $\sigma$ -fields is also a  $\sigma$ -field, which will be called the  $\sigma$ -field generated by  $G$  and will be denoted  $\sigma(G)$ . Because  $\sigma(G)$  is the intersection of the  $\sigma$ -fields containing  $G$ , it is the smallest  $\sigma$ -field containing  $G$ .

An important example of this is to take the collection  $G$  to be sets of finite disjoint sub-intervals of  $\Omega = (0, 1]$ . Then the elements  $A$  of  $\sigma(G)$  are called the *Borel sets*. Therefore, any set generated by a finite or countable number of the unions, intersections, or complements of sub-intervals of  $(0, 1]$  is a Borel set and will be measurable. In particular, if we define a measure  $\Lambda$  to be the sum of the lengths of the intervals in an element  $G \in G$ , then the unique extension of  $\Lambda$  to any Borel set is called *Lebesgue measure*.

The notion of Borel sets extends naturally to any finite region of  $d$ -dimensional Euclidean space. Here where we will be mainly considering subsets of two-dimensional Euclidean space, measures are defined on the unions, intersections, and complements of rectangles. Lebesgue measure in particular generalizes the notion of area on these sets.

## APPENDIX B

### Hausdorff Measure and Dimension

As preliminaries, we first define the *supremum* and *infimum* of a set of real numbers  $A$ , denoted  $\sup A$  and  $\inf A$ , respectively.

The supremum of  $A$  is the least upper bound of  $A$ , that is, the least number  $m$  such that  $x \leq m$  for all  $x \in A$ , or  $\infty$  if no such number  $m$  exists.

The infimum of  $A$  is the greatest lower bound of  $A$ , that is, the greatest number  $m$  such that  $m \leq x$  for all  $x \in A$ , or  $-\infty$  if no such number  $m$  exists.

It is a property of the real numbers that for any subset  $A$  bounded above that  $\sup A$  exists and is a real number, or, equivalently, for any subset  $A$  of the real numbers that is bounded below,  $\inf A$  exists and is a real number. This property distinguishes the real numbers from the rationals, and as such may be used as an axiom (the “completeness axiom”) in the definition of the real numbers (see, for example, Ross (1980), Section 4).

The supremum and infimum clearly generalize the notions of maximum and minimum, respectively. One important difference is that  $\sup A$  and  $\inf A$  need not be members of the set  $A$ .

Now to Hausdorff measure and dimension. We will closely follow the presentation in Falconer (1990), Chapter 2.

(a) For a non-empty subset  $U$  of  $\mathfrak{R}^n$  define the *diameter* of  $U$  as

$$|U| = \sup\{|x - y|; x, y \in U\}, \quad (\text{B.1})$$

i.e., the greatest separation distance of any pair of points in  $U$ .

(b) If  $\{U_i\}$  is a finite or countable collection of sets of diameter of at most  $\delta$  that cover a set  $F \subset \mathfrak{R}^n$ , i.e.,  $F \subset \bigcup_{i=1}^{\infty} U_i$  with  $0 < |U_i| \leq \delta$  for each  $i$ , we say that  $\{U_i\}$  is a  $\delta$ -cover of  $F$ .

(c) Define for some  $s \geq 0$  and  $\delta > 0$

$$H_{\delta}^s(F) = \inf \left\{ \sum_{i=1}^{\infty} |U_i|^s; \{U_i\} \text{ is a } \delta\text{-cover of } F \right\}, \quad (\text{B.2})$$

i.e., one finds the  $\delta$ -cover of  $F$  that minimizes the sum  $H_{\delta}^s(F)$  of the  $s$ th powers of the diameters.

(d) Define the  $s$ -dimensional Hausdorff measure  $H^s(F)$  as

$$H^s(F) = \lim_{\delta \rightarrow 0} H_{\delta}^s(F). \quad (\text{B.3})$$

This limit exists for any  $F \subset \mathfrak{R}^n$  and may be shown to have the properties of a measure.

(e) As we shall see,  $s$  may be interpreted as a dimension, hence one may expect that  $H^s(F)$  gives the size in some sense of  $F$  in  $s$  dimensions. One way to demonstrate this is to show the relation of Hausdorff measure to Lebesgue measure  $\lambda$ , which, one may recall, generalizes the notion of volume to  $n$ -dimensional Euclidean space. For a subset  $F \subset \mathfrak{R}^n$ , Hausdorff measure is a constant multiple of Lebesgue measure, precisely, for  $F$  a Borel subset of  $\mathfrak{R}^n$ ,

$$H^n(F) = \frac{\pi^{n/2}}{2^n (n/2)!} \lambda^n(F), \quad (\text{B.4})$$

where the prefactor is the volume of an  $n$ -dimensional ball.

(f) From equation (B.2), it is clear for  $\delta < 1$  that  $H_{\delta}^s(F)$  is non-increasing in  $s$ .

This implies by equation (B.3) that  $H^s(F)$  is non-increasing in  $s$ . In fact, if  $t > s$  and

$\{U_i\}$  is a  $\delta$ -cover of  $F$ , then

$$\sum_i |U_i|^t \leq \delta^{t-s} \sum_i |U_i|^s, \quad (\text{B.5})$$

which implies by taking infima that

$$H_\delta^t(F) \leq \delta^{t-s} H_\delta^s(F), \quad (\text{B.6})$$

which implies by taking the limit  $\delta \rightarrow 0$  that

$$\text{if } H^s(F) < \infty \text{ then } H^t(F) = 0 \text{ for } t > s. \quad (\text{B.7})$$

Equation (B.7) shows that there exists a value of  $s$  at which  $H^s(F)$  jumps from infinity to zero for increasing  $s$ . This critical value of  $s$  is the Hausdorff dimension of  $F$ , denoted  $\dim_H(F)$ . Formally,

$$\dim_H(F) = \inf\{s; H^s(F) = 0\} = \sup\{s; H^s(F) = \infty\}, \quad (\text{B.8})$$

so that

$$H^s(F) = \begin{cases} \infty & \text{if } s < \dim_H(F) \\ 0 & \text{if } s > \dim_H(F) \end{cases}. \quad (\text{B.9})$$

If  $s = \dim_H(F)$ , then  $H^s(F)$  may be zero, finite and positive, or infinity.

## APPENDIX C

### Calculation of the Moments of the Cascade Limit Mass

We first develop the tool required for the calculation. The Laplace transform  $\phi_X(r)$  of the distribution function  $F_X$  of a non-negative random variable  $X$  is defined as follows:

$$\phi_X(r) = \int_0^{\infty} e^{-rx} dF_X = E[e^{-rX}]. \quad (\text{C.1})$$

A useful fact about Laplace transforms that we will use in this appendix is that the positive integer moments of  $X$  can be recovered from the Laplace transform of its distribution by differentiation. To see this, notice

$$(-1)^n \phi^{(n)}(r) = \int_0^{\infty} e^{-rx} x^n dF_X, \quad (\text{C.2})$$

so if the limit  $\phi^{(n)}(0)$  exists then the moment  $EX^n$  exists and we have (Feller 1971, p. 435)

$$(-1)^n \phi^{(n)}(0) = EX^n. \quad (\text{C.3})$$

The idea of the calculation is to represent the basic cascade identity (Chapter 3, equation (3.29)) in terms of  $\phi_{Z_\infty}(r)$ , differentiate  $n$  times, take the limit  $r \rightarrow 0$ , and solve for  $EZ_\infty^n$ . The basic identity cascade identity is

$$Z = b^{-1} \sum_{i=1}^b W_i Z_i \text{ or } bZ = \sum_{i=1}^b W_i Z_i, \quad (\text{C.4})$$

where  $Z$  has the distribution of the cascade limit mass, written above as  $Z_\infty$ , and the

equality is in distribution. Taking the Laplace transforms of both sides of the second form of the basic identity, we obtain from the left-hand side

$$\phi_{bZ}(r) = E[e^{-rbZ}] = \phi_Z(br), \quad (\text{C.5})$$

and from the right-hand side

$$\phi_{\sum_{i=1}^b W_i Z_i}(r) = E\left[e^{-r\sum_{i=1}^b W_i Z_i}\right] = \prod_{i=1}^b E[e^{-rW_i Z_i}] = (E[e^{-rWZ}])^b, \quad (\text{C.6})$$

since the  $W_i$  are iid, the  $Z_i$  are iid, and the  $W_i$  and  $Z_i$  are independent.

The left-hand side is already in terms of  $\phi_Z$ . The right-hand side needs some work. First write

$$E[e^{-rWZ}] = \int_0^\infty e^{-rwz} dF_{W,Z}, \quad (\text{C.7})$$

where  $F_{W,Z}$  is the joint distribution function of  $W$  and  $Z$ . By the independence of  $W$  and  $Z$ , we can factor  $F_{W,Z}$  as  $F_W F_Z$ , so

$$\int_0^\infty e^{-rwz} dF_{W,Z} = \int_0^\infty \left(\int_0^\infty e^{-rwz} dF_Z\right) dF_W. \quad (\text{C.8})$$

But

$$\int_0^\infty e^{-rwz} dF_Z = E_Z[e^{-rwZ}] = \phi_Z(wr), \quad (\text{C.9})$$

so

$$E[e^{-rWZ}] = \int_0^\infty \phi_Z(wr) dF_W. \quad (\text{C.10})$$

So the basic identity can be written in terms of Laplace transforms of  $Z$  as

$$\phi_Z(br) = \left( \int_0^\infty \phi_Z(wr) dF_W \right)^b. \quad (\text{C.11})$$

To get moments of  $Z$ , we differentiate both sides of equation (C.11) with respect to  $r$ , take the limit  $r \rightarrow 0$ , and solve for  $EZ^n$ .

We begin with the first moment. Differentiating the left-hand side gives

$$\frac{d}{dr} \phi_Z(br) = b \phi_Z^{(1)}(br), \quad (\text{C.12})$$

and the right-hand side

$$\frac{d}{dr} \left[ \left( \int_0^\infty \phi_Z(wr) dF_W \right)^b \right] = b \left( \int_0^\infty \phi_Z(wr) dF_W \right)^{b-1} \int_0^\infty \phi_Z^{(1)}(wr) w dF_W. \quad (\text{C.13})$$

Setting these equal to each other and taking the limit  $r \rightarrow 0$  yields

$$b \phi_Z^{(1)}(0) = b \left( \int_0^\infty \phi_Z(0) dF_W \right)^{b-1} \int_0^\infty \phi_Z^{(1)}(0) w dF_W. \quad (\text{C.14})$$

Solving for  $\phi_Z^{(1)}(0) = -EZ$  gives

$$\phi_Z^{(1)}(0) = \phi_Z(0) \left( \int_0^\infty dF_W \right)^{b-1} \phi_Z^{(1)}(0) \int_0^\infty w dF_W, \quad (\text{C.15})$$

so

$$EZ = 1 \cdot 1^{b-1} EZEW, \quad (\text{C.16})$$

which doesn't provide any new information, but it is consistent with  $EW = 1$ .

Consider now the second derivative. Differentiating the left-hand side of equation (C.11) twice gives

$$\frac{d}{dr} b \phi_Z^{(1)}(br) = b^2 \phi_Z^{(2)}(br), \quad (\text{C.17})$$

and the right-hand side

$$b \left[ (b-1) \left( \int_0^\infty \phi_Z(wr) dF_W \right)^{b-2} \left( \int_0^\infty \phi_Z^{(1)}(wr) w dF_W \right)^2 + \left( \int_0^\infty \phi_Z(wr) dF_W \right)^{b-1} \int_0^\infty \phi_Z^{(2)}(wr) w^2 dF_W \right]. \quad (\text{C.18})$$

Setting these equal and taking the limit  $r \rightarrow 0$  yields

$$\phi_Z^{(2)}(0) = EZ^2 = b^{-1} [(b-1)(EW)^2(EZ)^2 + EW^2EZ^2] \quad (\text{C.19})$$

$$= b^{-1}(b-1) + b^{-1}EW^2EZ^2. \quad (\text{C.20})$$

Solving for  $EZ^2 = \phi_Z^{(2)}(0)$  yields

$$EZ^2 = \frac{b-1}{b-EW^2}. \quad (\text{C.21})$$

Obviously, this process can be continued ad infinitum. We make use of the third and fourth moments of  $Z$  as well, so we record the results here.

$$EZ^3 = \frac{3(b-1)EW^2EZ^2 + (b-1)(b-2)}{b^2 - EW^3} \quad (\text{C.22})$$

and

$$EZ^4 = \frac{1}{b^3 - EW^4} [4(b-1)EW^3EZ^3 + 3(b-1)(EW^2)^2(EZ^2)^2 + 6(b-1)(b-2)EW^2EZ^2 + (b-1)(b-2)(b-3)]. \quad (\text{C.23})$$

We finally note a connection to the conditions for existence of the moments of  $Z$  given in Theorem 2.2. Recall that in Theorem 2.2b we have that  $Z$  has a finite moment

of order  $q$  if and only if  $q < \inf\{q \geq 1; \chi_b(q) \geq 0\}$ . Assuming the non-degeneracy condition (see Theorem 2.2a), this condition is equivalent to the requirement that  $\chi_b(q) < 0$ . Rewriting this condition in terms of  $EW^q$ , we obtain  $EW^q < b^{q-1}$ . Notice that in equations (C.21), (C.22), and this same condition must be satisfied in order that the moments of  $Z$  are finite and positive.

## APPENDIX D

### The Ensemble Average Cross Moments for a One-Dimensional Cascade

Consider the limit measure of a one-dimensional iid discrete random cascade on the unit interval  $[0, 1]$  with generator  $W$  and branching number  $b$ . Let  $\mu(\Delta_n^i)$  denote the limit measure integrated over the  $i$ th of the  $b^n$  boxes of side length  $b^{-n}$  at level  $n$  of the cascade. Then  $\mu(\Delta_n^{i+b^m})$ ,  $1 \leq i + b^m \leq b^n$ , is the measure in the box at the distance  $r_n = b^{m-n}$ . Of course, the largest  $m$  for which the box  $\Delta_n^{i+b^m}$  can lie within the unit interval is  $m = n - 1$ , and for all such  $m$  there are some  $i$  for which the box  $\Delta_n^{i+b^m}$  is not inside the unit interval, an issue we will come back to later. Finally, define the  $p, q$  order lag- $r_n$  ensemble average cross moment as

$$E[\mu^p(\Delta_n^i)\mu^q(\Delta_n^{i+b^m})]. \quad (\text{D.1})$$

To begin the calculation, we recall that the distribution of  $\mu(\Delta_n^i)$  is given by

$$\mu(\Delta_n^i) = \mu_n(\Delta_n^i)Z(\Delta_n^i) = b^{-n} \left( \prod_{j=1}^n W_j(\Delta_n^i) \right) Z(\Delta_n^i), \quad (\text{D.2})$$

where  $Z(\Delta_n^i)$  is distributed as the total mass,  $\mu([0, 1])$  and is independent of the  $W_j(\Delta_n^i)$  and hence of the  $\mu_n(\Delta_n^i)$ . We assume a non-degenerate limit measure, which implies that  $E[Z] = 1$ , and the existence of any additional moments of  $Z$  that are required (conditions on the generator that ensure these assumptions hold are given in Theorem 2.2). Therefore, we can write

$$E[\mu_n^p(\Delta_n^i)\mu_n^q(\Delta_n^{i+b^m})] = E[Z^p(\Delta_n^i)\mu_n^p(\Delta_n^i)Z^q(\Delta_n^{i+b^m})\mu_n^q(\Delta_n^{i+b^m})] \quad (\text{D.3})$$

$$= EZ^pEZ^qE[\mu_n^p(\Delta_n^i)\mu_n^q(\Delta_n^{i+b^m})], \quad (\text{D.4})$$

for all  $i$  for which the box  $\Delta_n^{i+b^m}$  lies in the unit interval.

Now define  $k$  as the number of cascade levels above  $n$  where  $\mu_n(\Delta_n^i)$  and  $\mu_n(\Delta_n^{i+b^m})$  have their last common weight. Pick a box  $\Delta_n^i$  at random. Then  $k$  is a random variable, which we denote by  $K$  and

$$E[\mu_n^p(\Delta_n^i)\mu_n^q(\Delta_n^{i+b^m})] = \sum_{k=1}^n P_{r_n}(K=k)E_k[\mu_n^p(\Delta_n^i)\mu_n^q(\Delta_n^{i+b^m})], \quad (\text{D.5})$$

where  $P_{r_n}(K=k)$  indicates the probability that  $K=k$  given the value of  $r_n$ ,  $E_k[\cdot]$  indicates the expectation given  $k$ , and again we restrict ourselves to the  $i$  such that the box  $\Delta_n^{i+b^m}$  lies in the unit interval.

Consider the expectation part of the right-hand side of equation (D.5). Since, for a given  $k$ , the weights of  $\mu_n(\Delta_n^i)$  and  $\mu_n(\Delta_n^{i+b^m})$  are the same from level 1 to level  $n-k$  and independent from level  $n-k+1$  to level  $n$ , we have

$$E_k[\mu_n^p(\Delta_n^i)\mu_n^q(\Delta_n^{i+b^m})] = b^{-(p+q)n} E \left[ \prod_{j=1}^{n-k} W_j^{p+q} \prod_{j=n-k+1}^n W_j^p(\Delta_n^i) W_j^q(\Delta_n^{i+b^m}) \right]. \quad (\text{D.6})$$

Since the  $W_j$  are iid, it follows that

$$E_k[\mu_n^p(\Delta_n^i)\mu_n^q(\Delta_n^{i+b^m})] = b^{-(p+q)n} (EW^{p+q})^{n-k} (EW^pEW^q)^k. \quad (\text{D.7})$$

Now consider  $P_{r_n}(K=k)$ . Reviewing,  $P_{r_n}(K=k)$  is the probability, given  $r_n$ , that the  $\mu(\Delta_n^i)$  and  $\mu(\Delta_n^{i+b^m})$  designated by a randomly chosen  $\Delta_n^i$  have their last common weight  $k$  levels above  $n$  at level  $n-k$ . If we consider only those  $r_n$  of the form

$r_n = b^{m-n}$ ,  $m = 0, 1, \dots, n-1$ , then it can be shown that

$$P_{r_n}(K = k + m) = \frac{b-1}{b^k}, \quad k + m = 1, 2, \dots, n \quad (\text{D.8})$$

at those  $\Delta_n^i$  where  $\Delta_n^{i+b^m}$  lies in the unit interval. In fact,  $b^m$  of the  $\Delta_n^{i+b^m}$  do not, so, leaving them undefined, we get finally

$$P_{r_n}(K = k + m) = \frac{b-1}{b^k} / \frac{b^n - b^m}{b^n} = \frac{b-1}{b^k(1-b^{m-n})}, \quad k + m = 1, 2, \dots, n. \quad (\text{D.9})$$

Therefore, we can write equation (D.5) as

$$E[\mu_n^p(\Delta_n^i) \mu_n^q(\Delta_n^{i+b^m})] = \sum_{k=1}^{n-m} P_{r_n}(K = k + m) E_{k+m}[\mu_n^p(\Delta_n^i) \mu_n^q(\Delta_n^{i+b^m})]. \quad (\text{D.10})$$

Substituting from equations (D.7) and (D.9) gives

$$= \sum_{k=1}^{n-m} \frac{(b-1)b^{-(p+q)n}}{b^k(1-b^{m-n})} (EW^{p+q})^{n-k-m} (EW^p EW^q)^{k+m}. \quad (\text{D.11})$$

Factoring out those terms not depending on  $k$  gives

$$= \frac{(EW^{p+q})^{n-m} (EW^p EW^q)^m}{(b-1)^{-1} b^{(p+q)n} (1-b^{m-n})} \sum_{k=1}^{n-m} \left( \frac{EW^p EW^q}{bEW^{p+q}} \right)^k. \quad (\text{D.12})$$

Defining  $R(p, q) = EW^{p+q} / (EW^p EW^q)$  and summing the series gives

$$= \frac{(R(p, q))^{n-m} (EW^p EW^q)^n}{(b-1)^{-1} b^{(p+q)n} (1-b^{m-n})} \frac{1 - (bR(p, q))^{m-n}}{bR(p, q) - 1}. \quad (\text{D.13})$$

Our goal is to compute the  $r_n$ -dependence of the cross moments, so we substitute

$\log_b r_n$  for  $m-n$ , getting

$$= \frac{(EW^p EW^q)^n}{(b-1)^{-1} b^{(p+q)n} (1-r_n)} (R(p, q))^{-\log_b r_n} \frac{1 - (bR(p, q))^{m-n}}{bR(p, q) - 1} \quad (\text{D.14})$$

$$= \left( \frac{EW^p EW^q}{b^{p+q}} \right)^n \frac{b-1}{bR(p, q) - 1} \left( \frac{1 - r_n^{1 + \log_b R(p, q)}}{1 - r_n} \right) r_n^{-\log_b R(p, q)}. \quad (\text{D.15})$$

We now show that the cross moment has an approximate power law dependence on  $r_n$ . First consider the range of values of  $R(p, q)$ . Because  $EW^q$  is convex as a function of  $q$ , we have  $R(p, q) \geq 1$  for  $p, q > 0$ . In general, the maximum value of  $R(p, q)$  could be infinite, but generators that are bounded above by  $b$  figure importantly in the theorems about the limit measure of the cascade. So consider the member of this class with the largest positive moments, which occurs when  $P(W = b) = 1/b$  and  $P(W = 0) = \frac{b-1}{b}$ , i.e., a  $\beta$ -model with  $\beta = 1$ . This cascade has zero limit mass with probability one, but it makes a useful upper bound. It has  $EW^q = b^{q-1}$ , which gives  $R(p, q) = b$ . So we may assume  $0 \leq \log_b R(p, q) \leq 1$  without restricting ourselves unduly.

Given these bounds on  $\log_b R(p, q)$  and since  $0 < r_n < 1$ , we have

$$\frac{1 - r_n^{1 + \log_b R(p, q)}}{1 - r_n} \cong 1. \quad (\text{D.16})$$

Furthermore, in the limit has  $n \rightarrow \infty$  with  $m$  fixed (hence  $r_n \rightarrow 0$ ),

$$\frac{1 - r_n^{1 + \log_b R(p, q)}}{1 - r_n} \rightarrow 1. \quad (\text{D.17})$$

Therefore we can write

$$E[\mu_n^p(\Delta_n^i)\mu_n^q(\Delta_n^{i+b^m})] \cong \left(\frac{EW^p EW^q}{b^{p+q}}\right)^n \frac{b-1}{bR(p,q)-1} r_n^{-\log_b R(p,q)}, \quad (\text{D.18})$$

so

$$E[\mu^p(\Delta_n^i)\mu^q(\Delta_n^{i+b^m})] \cong EZ^p EZ^q \left(\frac{EW^p EW^q}{b^{p+q}}\right)^n \frac{b-1}{bR(p,q)-1} r_n^{-\log_b R(p,q)}, \quad (\text{D.19})$$

which shows that the ensemble average cross moment has an approximate power law dependence on  $r_n$  with exponent

$$-\log_b R(p,q) = -\log_b \frac{EW^{p+q}}{EW^p EW^q}. \quad (\text{D.20})$$

It will prove convenient to normalize this result by dividing by the marginal moment

$$E[\mu^{p+q}(\Delta_n^i)] = b^{-(p+q)n} (EW^{p+q})^n EZ^{p+q}, \quad (\text{D.21})$$

which, combining with equation (D.19) gives

$$\frac{E[\mu^p(\Delta_n^i)\mu^q(\Delta_n^{i+b^m})]}{E[\mu^{p+q}(\Delta_n^i)]} \cong \frac{EZ^p EZ^q}{EZ^{p+q}} \left(\frac{EW^p EW^q}{EW^{p+q}}\right)^n \frac{b-1}{bR(p,q)-1} r_n^{-\log_b R(p,q)} \quad (\text{D.22})$$

$$\cong \frac{EZ^p EZ^q}{EZ^{p+q}} R(p,q)^{-n} \frac{b-1}{bR(p,q)-1} r_n^{-\log_b R(p,q)}. \quad (\text{D.23})$$

## APPENDIX E

### Proof of Convergence of the Spatial Average Temporal Cross Moments

We wish to prove Theorem 5.1, i.e.,

$$\tau(q; s, t) = \lim_{n \rightarrow \infty} \frac{\log M_n(q; s, t)}{n \log b} = \chi_b(q; s, t), \quad (\text{E.1})$$

where

$$M_n(q; s, t) = \sum_{i=1}^{b^n} \mu_\infty^q(\Delta_n^i; s) \mu_\infty^q(\Delta_n^i; t) \quad (\text{E.2})$$

(equation (5.1)), and

$$\chi_b(q; s, t) = \log_b E[W^q(s)W^q(t)] - (2q - 1) \quad (\text{E.3})$$

(equation (5.6)).

We begin as in the proof of Theorem 3.2 (Holley and Waymire 1992) by showing that

$$\{X_n\} = \left\{ \frac{\sum_{i=1}^{b^n} \mu_n^q(\Delta_n^i; s) \mu_n^q(\Delta_n^i; t)}{b^{n(1-2q)} E^n[W^q(s)W^q(t)]} \right\}, \quad n = 1, 2, \dots \quad (\text{E.4})$$

is a martingale sequence with respect to the sequence of sets of events  $\{F_n(s, t)\}$ , defined as the realization of the values of the generator processes  $W_s(\Delta_j^i)$  and  $W_t(\Delta_j^i)$  for all  $j \leq n$ , but only for times  $s$  and  $t$ . The conditions defining a martingale are given in

Section 3.2. Due to the construction of the set of events  $\{F_n(s, t)\}$ , conditions (a) and (b) are automatically satisfied. Condition (c) is satisfied by virtue of  $\{X_n\}$  being the ratio of a quantity and its expected value, hence  $EX_n = 1$  for all  $n$ .

As usual, condition (d),

$$E[X_{n+1} \parallel F_n] = X_n \text{ with probability one,} \quad (\text{E.5})$$

takes a bit more work. We must show that

$$E \left[ \frac{\sum_{i=1}^{b^{n+1}} \mu_{n+1}^q(\Delta_{n+1}^i; s) \mu_{n+1}^q(\Delta_{n+1}^i; t)}{b^{(n+1)(1-2q)} E^{n+1}[W^q(s)W^q(t)]} \parallel F_n \right] = \frac{\sum_{i=1}^{b^n} \mu_n^q(\Delta_n^i; s) \mu_n^q(\Delta_n^i; t)}{b^{n(1-2q)} E^n[W^q(s)W^q(t)]}. \quad (\text{E.6})$$

i.e.,

$$E \left[ \sum_{i=1}^{b^{n+1}} \mu_{n+1}^q(\Delta_{n+1}^i; s) \mu_{n+1}^q(\Delta_{n+1}^i; t) \parallel F_n \right] = b^{\chi_b(q; s, t)} \sum_{i=1}^{b^n} \mu_n^q(\Delta_n^i; s) \mu_n^q(\Delta_n^i; t). \quad (\text{E.7})$$

To do this, expand the left-hand side as follows:

$$= \sum_{i=1}^{b^{n+1}} E[\mu_{n+1}^q(\Delta_{n+1}^i; s) \mu_{n+1}^q(\Delta_{n+1}^i; t) \parallel F_n] \quad (\text{E.8})$$

$$= \sum_{i=1}^{b^n} E \left[ \mu_n^q(\Delta_n^i; s) \mu_n^q(\Delta_n^i; t) \left( \sum_{j=1}^b \left( \frac{W_{ij}(s)}{b} \right)^q \left( \frac{W_{ij}(t)}{b} \right)^q \right) \parallel F_n \right] \quad (\text{E.9})$$

$$= \sum_{i=1}^{b^n} b^{1-2q} E[W_{ij}^q(s)W_{ij}^q(t)] E[\mu_n^q(\Delta_n^i; s) \mu_n^q(\Delta_n^i; t) \parallel F_n] \quad (\text{E.10})$$

$$= b^{\chi_b(q; s, t)} \sum_{i=1}^{b^n} \mu_n^q(\Delta_n^i; s) \mu_n^q(\Delta_n^i; t), \quad (\text{E.11})$$

completing the demonstration of condition (d).

Hence all the conditions for  $\{X_n\}$  to be a martingale sequence are fulfilled. Thus

by the submartingale convergence theorem (see, e.g., Billingsley 1986, p. 490) the sequence converges to a random variable, say  $Y$ .

To proceed, we continue to follow the proof of Theorem 3.2 in Holley and Waymire (1992). Dropping the box identifier  $\Delta_n^i$ , which should still be understood in random variables in summands, we write

$$\frac{\sum_{i=1}^{b^n} \mu_{\infty}^q(s) \mu_{\infty}^q(t)}{b^{n\chi_b(q;s,t)}} = \frac{\sum_{i=1}^{b^n} \mu_n^q(s) Z_{\infty}^q(s) \mu_n^q(t) Z_{\infty}^q(t) - \sum_{i=1}^{b^n} \mu_n^q(s) \mu_n^q(t) E[Z_{\infty}^q(s) Z_{\infty}^q(t)]}{b^{n\chi_b(q;s,t)}} + \frac{\sum_{i=1}^{b^n} \mu_n^q(s) \mu_n^q(t) E[Z_{\infty}^q(s) Z_{\infty}^q(t)]}{b^{n\chi_b(q;s,t)}} \quad (\text{E.12})$$

$$= A_n + B_n. \quad (\text{E.13})$$

Notice that

$$\lim_{n \rightarrow \infty} B_n = E[Z_{\infty}^q(s) Z_{\infty}^q(t)] \lim_{n \rightarrow \infty} \frac{\sum_{i=1}^{b^n} \mu_n^q(s) \mu_n^q(t)}{b^{n\chi_b(q;s,t)}} = E[Z_{\infty}^q(s) Z_{\infty}^q(t)] Y, \quad (\text{E.14})$$

by the martingale convergence proved above.

We will next show that  $\lim_{n \rightarrow \infty} A_n = 0$  with probability one. We show below that  $EA_n = 0$  and  $\sum_n \text{Var}(A_n) < \infty$ , which implies that  $\lim_{n \rightarrow \infty} A_n = 0$  by Chebyshev's inequality and the Borel-Cantelli lemma. To see this, notice that by Chebyshev's inequality (Battacharya and Waymire 1990, p. 630),

$$P(|A_n| \geq \varepsilon) \leq \varepsilon^{-2} EA_n^2 = \varepsilon^{-2} \text{Var}(A_n) \text{ for all } \varepsilon > 0. \quad (\text{E.15})$$

Then since  $\sum_n \text{Var}(A_n) < \infty$ , we have  $\sum_n \varepsilon^{-2} \text{Var}(A_n) < \infty$  so  $\sum_n P(|A_n| \geq \varepsilon) < \infty$  from

(E.15), which implies that  $P(|A_n| \geq \varepsilon \text{ infinitely often}) = 0$  by the Borel-Cantelli lemma, part 1 (Battacharya and Waymire 1990, p. 647). Since  $\varepsilon > 0$  is arbitrary, we have  $\lim_{n \rightarrow \infty} A_n = 0$ .

Now we show that  $EA_n = 0$ .  $A_n$  can be written

$$A_n = \frac{\sum_{i=1}^{b^n} \mu_n^q(s) \mu_n^q(t) \{Z_\infty^q(s) Z_\infty^q(t) - E[Z_\infty^q(s) Z_\infty^q(t)]\}}{b^{n\chi_b(q;s,t)}}, \quad (\text{E.16})$$

so

$$EA_n = \frac{b^n E[\mu_n^q(s) \mu_n^q(t)] \{E[Z_\infty^q(s) Z_\infty^q(t)] - E[Z_\infty^q(s) Z_\infty^q(t)]\}}{b^{n\chi_b(q;s,t)}} = 0. \quad (\text{E.17})$$

And now we show  $\sum_n \text{Var}(A_n) < \infty$ . First, since  $EA_n = 0$ ,  $\text{Var}(A_n) = EA_n^2$ , and

$$EA_n^2 = \frac{E\left[\left(\sum_{i=1}^{b^n} \mu_n^q(s) \mu_n^q(t) \{Z_\infty^q(s) Z_\infty^q(t) - E[Z_\infty^q(s) Z_\infty^q(t)]\}\right)^2\right]}{b^{2n\chi_b(q;s,t)}}. \quad (\text{E.18})$$

Consider first the expectation of the cross-terms resulting from squaring the numerator of equation (E.18), i.e., for  $i \neq j$ ,

$$\begin{aligned} & E[\mu_n^q(i, s) \mu_n^q(i, t) \{Z_\infty^q(i, s) Z_\infty^q(i, t) - E[Z_\infty^q(i, s) Z_\infty^q(i, t)]\} \times \\ & \mu_n^q(j, s) \mu_n^q(j, t) \{Z_\infty^q(j, s) Z_\infty^q(j, t) - E[Z_\infty^q(j, s) Z_\infty^q(j, t)]\}] \\ &= E[\mu_n^q(i, s) \mu_n^q(i, t) \mu_n^q(j, s) \mu_n^q(j, t)] E[Z_\infty^q(i, s) Z_\infty^q(i, t) - E[Z_\infty^q(i, s) Z_\infty^q(i, t)]] \times \\ & \quad E[Z_\infty^q(j, s) Z_\infty^q(j, t) - E[Z_\infty^q(j, s) Z_\infty^q(j, t)]] = 0, \end{aligned} \quad (\text{E.19})$$

using, for the first equality, the independence of the  $Z_\infty(\cdot, \cdot)$  from the  $\mu_n(\cdot, \cdot)$ . So only

the  $i = j$  terms contribute, so

$$\text{Var}(A_n) = EA_n^2 = \frac{\sum_{i=1}^{b^n} E[\mu_n^{2q}(i, s)\mu_n^{2q}(i, t)] \text{Var}(Z_\infty^q(s)Z_\infty^q(t))}{b^{2n\chi_b(q; s, t)}}. \quad (\text{E.20})$$

Now

$$\sum_{i=1}^{b^n} E[\mu_n^{2q}(i, s)\mu_n^{2q}(i, t)] = b^n E[\mu_n^{2q}(i, s)\mu_n^{2q}(i, t)] \quad (\text{E.21})$$

$$= b^n \left\{ b^{-2nq} E\left[\prod_{j=1}^n W_j^{2q}(s)\right] \right\} \left\{ b^{-2nq} E\left[\prod_{j=1}^n W_j^{2q}(t)\right] \right\} \quad (\text{E.22})$$

$$= b^{n-4nq} (E[(W(s)W(t))^{2q}])^n = (b^{1-4q} E[W^{2q}(s)W^{2q}(t)])^n. \quad (\text{E.23})$$

Therefore

$$\text{Var}(A_n) = \left( \frac{1}{b} \frac{E[W^{2q}(s)W^{2q}(t)]}{(E[W^q(s)W^q(t)])^2} \right)^n \text{Var}(Z_\infty^q(s)Z_\infty^q(t)) \quad (\text{E.24})$$

So we have  $\sum_n \text{Var}(A_n) < \infty$  when

$$\frac{E[W^{2q}(s)W^{2q}(t)]}{(E[W^q(s)W^q(t)])^2} < b \quad (\text{E.25})$$

(compare the condition  $EW^{2q}/E^2W^q < b$  in Theorem 3.2). So assuming the condition

(E.25), we have  $\lim_{n \rightarrow \infty} A_n = 0$  as desired.

We can now prove the theorem (equation (E.1)). Write

$$\lim_{n \rightarrow \infty} \frac{\log M_n(q; s, t)}{n \log b} = \lim_{n \rightarrow \infty} \frac{\log \sum_{i=1}^{b^n} \mu_\infty^q(\Delta_n^i; s) \mu_\infty^q(\Delta_n^i; t)}{n \log b} \quad (\text{E.26})$$

$$= \lim_{n \rightarrow \infty} \frac{\log \sum_{i=1}^{b^n} \mu_{\infty}^q(\Delta_n^i; s) \mu_{\infty}^q(\Delta_n^i; t) + \log b^{n\chi_b(q; s, t)}}{b^{n\chi_b(q; s, t)} n \log b} \quad (\text{E.27})$$

$$= \lim_{n \rightarrow \infty} \frac{\log(A_n + Y)}{n \log b} + \lim_{n \rightarrow \infty} \frac{n \log b^{n\chi_b(q; s, t)}}{n \log b} = \chi_b(q; s, t). \quad (\text{E.28})$$

QED.

## APPENDIX F

### Finite-State Non-Homogeneous Birth-Death Processes

#### F.1 Definition

A non-homogeneous birth-death process is a continuous-time Markov process with non-homogeneous transition probabilities defined as

$$p_{ij}(t_1, t_2) = P(I_{t_2} = j \mid I_{t_1} = i), t_2 > t_1$$

with the following properties (Bhattacharya and Waymire 1990, p. 335):

- (a) The  $p_{ij}(t_1, t_2)$  are continuous for  $t_1$  in the (closed) interval  $[0, t_2]$ .
- (b) The  $p_{ij}(t_1, t_2)$  have “initial” conditions given by

$$p_{ij}(t_1, t_1) = \delta_{ij}, \tag{F.1}$$

where  $\delta_{ij}$  is *Kronecker's delta*, which is given by  $\delta_{ij} = 1$  if  $i = j$ ; otherwise  $\delta_{ij} = 0$ .

- (c) The right-handed partial derivatives with respect to  $t$ , defined by

$$\lim_{t_2 \rightarrow t_1} \frac{p_{ij}(t_1, t_2)}{t_2 - t_1} = q_{ij}(t_1), \tag{F.2}$$

exist and are finite for all  $t_1$ .

The equations that describe the evolution of the transition probabilities in time are *Kolmogorov's forward equations*, which are given for finite state space  $S$  by (Bhattacharya and Waymire 1990, p. 335):

$$\frac{\partial}{\partial t_2} p_{ik}(t_1, t_2) = q_{ik}(t_1) = \sum_j p_{ij}(t_1, t_2) q_{jk}(t_2). \quad (\text{F.3})$$

As will be shown below, for a two-state process as we have proposed, the forward equations yield a pair of uncoupled first order linear ordinary differential equations for the transition probabilities, which can be integrated for essentially an arbitrary forcing  $r_t$ .

## F.2 Response to Forcing

Our next task is to specify the parameters of the process so that it responds appropriately to the forcing (criterion (c) in Section 5.2). It is clear from this formulation of a birth-death process that the free parameters of the process are the derivatives  $q_{ij}(t_1)$  of the transition probabilities. Thus it will be these that will be specified so that the process  $I_t$  responds appropriately to the forcing. In particular, we want

$$\lim_{t_2 \rightarrow \infty} P(I_{t_2} = 1) = r_0, \quad (\text{F.4})$$

where  $r_0$  is a constant forcing (or, equivalently,  $\lim_{t_2 \rightarrow \infty} P(I_{t_2} = 0) = 1 - r_0$ ). Notice that this implies that the forcing  $r_{t_2}$  is in principle a probability and hence must be bounded such that  $0 \leq r_{t_2} \leq 1$ . We will show that the requirement of equation (F.4) is satisfied by the following choice of the  $q_{ij}(t_1)$ :

$$q_{ij}(t_1) = k(r_{t_2}) \begin{bmatrix} (-r_{t_2}) & (r_{t_2}) \\ (1 - r_{t_2}) & (r_{t_2} - 1) \end{bmatrix}, \quad (\text{F.5})$$

where  $k(r)$  is an arbitrary positive function. As described in Section 5.4, this actually gives something stronger, namely what we have called a “dynamical” contingency criterion

$$\frac{d}{dt_2}p_1(t_2) = -k[p_1(t_2) - r_{t_2}] \quad (\text{F.6})$$

(equation (5.82)).

### F.3 Probabilities and Transition Probabilities

To show that equation (F.5) satisfies equations (F.4) and (F.6), it is necessary to find the equation of evolution of  $p_1(t) = P(I_t = 1)$ . To do this, first notice that from equation (5.87)

$$p_1(t_2) = p_{11}(t_1, t_2)p_1(t_1) + p_{01}(t_1, t_2)p_0(t_1). \quad (\text{F.7})$$

Using  $p_0(t_1) = 1 - p_1(t_1)$ , we obtain

$$p_1(t_2) = p_{11}(t_1, t_2)p_1(t_1) + p_{01}(t_1, t_2)(1 - p_1(t_1)) \quad (\text{F.8})$$

To obtain the transition probabilities, we use the forward equations (equations (F.3)). From those we obtain for  $p_{01}(t_1, t_2)$ :

$$\frac{\partial}{\partial t}p_{01}(t_1, t_2) = p_{00}(t_1, t_2)q_{01}(t_2) + p_{01}(t_1, t_2)q_{11}(t_2) \quad (\text{F.9})$$

$$= (1 - p_{01}(t_1, t_2))q_{01}(t_1, t_2) + p_{01}(t_1, t_2)q_{11}(t_1, t_2). \quad (\text{F.10})$$

Fixing  $t_1 = 0$  (hence  $t_2 = t_2 - t_1$ ) and substituting for the  $q_{ij}$  from equation (F.5) gives

$$\frac{d}{dt_2}p_{01}(t_1, t_2) = (1 - p_{01}(t_1, t_2))kr_{t_2} - p_{01}(t_1, t_2)k(1 - r_{t_2}) \quad (\text{F.11})$$

$$= -k(p_{01}(t_1, t_2) - r_{t_2}). \quad (\text{F.12})$$

An equation for  $p_{11}(t_1, t_2)$  can be obtained similarly, giving

$$\frac{d}{dt_2} p_{11}(t_1, t_2) = -k(p_{11}(t_1, t_2) - r_{t_2}). \quad (\text{F.13})$$

From equations (F.12) and (F.13) it can be seen that the transition probabilities decay exponentially toward the forcing with rate  $k$ .

Now, to obtain equation (F.6), differentiate equation (F.8) with respect to  $t_2$ , which gives

$$\frac{d}{dt_2} p_1(t_2) = \frac{d}{dt_2} p_{11}(t_1, t_2) p_1(t_1) + \frac{d}{dt_2} p_{01}(t_1, t_2) (1 - p_1(t_1)), \quad (\text{F.14})$$

then substitute equations (F.12) and (F.13) into (F.14) and simplify, obtaining

$$\frac{d}{dt_2} p_1(t_2) = -k[p_1(t_1)p_{11}(t_1, t_2) + p_0(t_1)p_{01}(t_1, t_2) - r_{t_2}] \quad (\text{F.15})$$

Substituting for  $p_1(t_1)p_{11}(t_1, t_2) + p_0(t_1)p_{01}(t_1, t_2)$  from equation (F.7) gives equation (F.6).

Now to compute  $\lim_{t \rightarrow \infty} P(I_t = 1)$  under the constant forcing  $r_0$ , we set  $r_t = r_0$  in equation (F.6) and solve for  $p_1(t_2)$ . These equations are first-order linear ordinary differential equations, for which the standard form is (Simmons 1972, pp. 47-48)

$$\frac{dx}{dt} + P(t)x = Q(t), \quad (\text{F.16})$$

and whose solution is given by

$$x(t) = e^{-\int P(t)dt} \left( \int Q e^{\int P(t)dt} dt + c \right). \quad (\text{F.17})$$

Applying this to the equation for  $p_1(t_2)$ , we take  $t_1 = 0$ ,  $x(t) = p_1(t_2)$ ,  $P(t) = k$ , and  $Q(t) = kr_{t_2}$ , so  $p_1(t_2)$  is given by

$$p_1(t_2) = e^{-kt_2} \left( \int k r_{t_2} e^{kt_2} dt_2 + c \right) \quad (\text{F.18})$$

for arbitrary  $r_{t_2}$ . Taking  $r_{t_2} = r_0$  and simplifying we obtain

$$p_1(t_2) = r_0 + (p_1(0) - r_0)e^{-kt_2}. \quad (\text{F.19})$$

So it is clear that in the limit  $t_2 \rightarrow \infty$  we obtain equation (F.4) regardless of the initial condition  $p_1(0)$  at  $t_2 = t_1$ .

The equations of evolution of the transition probabilities may be obtained similarly. Applying the general solution (F.17) to the equation for  $p_{11}(t_1, t_2)$  ((F.13)) with  $t_1 = 0$ , we take  $x(t) = p_{11}(t)$ ,  $P(t) = k$ , and  $Q(t) = kr_t$ , so  $p_{11}(t)$  is given by

$$p_{11}(0, t_2) = e^{-kt_2} \left( \int k r_{t_2} e^{kt_2} dt_2 + c \right) \quad (\text{F.20})$$

for arbitrary  $r_{t_2}$ . Here we take  $r_{t_2} = r_0$ ; results for two other choices of  $r_{t_2}$  are given below. The initial condition is  $p_{11}(0, 0) = 1$  (from equation (F.1)). Substituting these in, we obtain

$$p_{11}(0, t_2) = r_0 + (1 - r_0)e^{-kt_2}. \quad (\text{F.21})$$

For  $p_{01}(0, t_2)$  we have the same general solution (F.20) but a different initial condition  $p_{01}(0, 0) = 0$  and so obtain similarly

$$p_{01}(0, t_2) = r_0(1 - e^{-kt_2}). \quad (\text{F.22})$$

#### F.4 Waiting Probabilities

The parameter  $k$  describes the rate at which  $I_t$  jumps between states, thereby determining the fluctuation rate and the rate at which the process responds to changes in the forcing. To see this, consider that the probability that a continuous time Markov

process in state  $i$  at time  $t_1$  will not have jumped out at a later time  $t_2$  is given by

$$\tilde{p}_i(t_1, t_2) = e^{-\int_{t_1}^{t_2} q_{ii}(u) du}, \quad (\text{F.23})$$

which means in particular that for a homogeneous process the waiting time distribution in state  $i$  is exponential with parameter  $-q_{ii}$  (Bhattacharya and Waymire 1990, p. 275). In the present case, we have (see equation (F.5))

$$\tilde{p}_0(t_1, t_2) = e^{-\int_{t_1}^{t_2} q_{00}(u) du} = e^{-k \int_{t_1}^{t_2} r(u) du} \quad (\text{F.24})$$

and

$$\tilde{p}_1(t_1, t_2) = e^{-\int_{t_1}^{t_2} q_{11}(u) du} = e^{-k \int_{t_1}^{t_2} (1-r(u)) du}. \quad (\text{F.25})$$

Solving these in the case of a constant forcing  $r_0$  (and taking  $t_1 = 0$ ) gives

$$\tilde{p}_0(0, t_2) = e^{-kr_0 t_2} \text{ and } \tilde{p}_1(0, t_2) = e^{-k(1-r_0)t_2}. \quad (\text{F.26})$$

## F.5 Summary

For purposes of parameter estimation we require  $p_1(t_2)$  and  $p_{11}(t_1, t_2)$ , which can be calculated from the general relations given above (equations (F.20) and (F.20), respectively, the latter with initial condition  $p_{11}(t_1, t_1) = 1$ ) for whatever forcing functions are required in applying this theory to data. For completeness, we also include  $p_{01}(t_1, t_2)$ , which can also be obtained from equation (F.20) with  $p_{01}(t_1, t_1) = 0$ , and  $\tilde{p}_1(t_1, t_2)$ . If need be, equations (F.20), (F.20) and (F.25) could be integrated numerically, but analytical solutions are obviously preferable. Clearly they can be easily integrated analytically for sums of polynomial and exponential terms, and so we will

perform analytical computations for some of these as examples. For  $r_t = r_0$ , the results are already given in equations (F.21), (F.21), (F.22) and (F.26). To display these results more conveniently, they have been collected into Table F.1.

**Table F.1 Properties of a Birth-Death Process: Example 1**

	$r_{t_2} = r_0$
$p_{11}(0, t_2)$	$r_0 + (1 - r_0)e^{-kt_2}$
$p_{01}(0, t_2)$	$r_0(1 - e^{-kt})$
$p_1(t_2)$	$p_1(0)e^{-kt} + r_0(1 - e^{-kt})$
$p_1(t_2) \Big _{p_1(0) = r_0}$	$r_0$
$\tilde{p}_{11}(0, t_2)$	$exp[-k(1 - r_0)t_2]$

The results for some other choices of  $r_t$  are given in the tables below. A non-stationary forcing  $r_t$  can be fit to one of these functions (or others as appropriate), and the results in these tables can then be used to calculate the moments  $E[B_{t_1}^q B_{t_2}^q]$  in order to test the theory and estimate  $k$ , as was done for  $r_t = r_0$  in Section 5.4.

**Table F.2 Properties of a Birth-Death Process: Example 2**

	$r_{t_2} = at_2 + r_0$
$p_{11}(0, t_2)$	$r_0 + a(t_2 - k^{-1}) + (1 - r_0 + ak^{-1})e^{-kt_2}$
$p_{01}(0, t_2)$	$r_0 + a(t_2 - k^{-1}) + (-r_0 + ak^{-1})e^{-kt_2}$
$p_1(t_2)$	$(p_1(0) - r_0 + ak^{-1})e^{-kt_2} + r_0 + a(t_2 - k^{-1})$
$p_1(t_2) \Big _{p_1(0) = r_0}$	$r_0 + a(t_2 - k^{-1}) + ak^{-1}e^{-kt_2}$
$\tilde{p}_{11}(0, t_2)$	$exp\{-k[(1 - r_0)t_2 - (at_2^2)/2]\}$

**Table F.3 Properties of a Birth-Death Process: Example 3**

	$r_{t_2} = a_e e^{-mt_2} + r_c$
$p_{11}(0, t_2)$	$\frac{ka_e}{k-m}(e^{-mt_2} - e^{-kt_2}) + r_c + (1-r_c)e^{-kt_2}$
$p_{01}(0, t_2)$	$\frac{ka_e}{k-m}(e^{-mt_2} - e^{-kt_2}) + r_c - r_c e^{-kt_2}$
$p_1(t_2)$	$p_1(0)e^{-kt_2} + \frac{ka_e}{k-m}(e^{-mt_2} - e^{-kt_2}) + r_c(1 - e^{-kt_2})$
$p_1(t_2) \Big _{p_1(0) = r_0}$	$a_e e^{-kt_2} + \frac{ka_e}{k-m}(e^{-mt_2} - e^{-kt_2}) + r_c$
$\tilde{p}_{11}(0, t_2)$	$\exp\left\{-k[(1-r_0)t_2 - (1-e^{-mt_2})(a_e/m)]\right\}$

## APPENDIX G

### Cross Moments of the Stationary Log-Normal Diffusion

We want to calculate

$$\begin{aligned} E[Y_t^q Y_{t+\tau}^q] &= E[b^{q(-\sigma^2 \log b/2 + \sigma \tilde{V}_t)} b^{q(-\sigma^2 \log b/2 + \sigma \tilde{V}_{t+\tau})}] \\ &= b^{-q\sigma^2 \log b} E[e^{q\sigma \log b(\tilde{V}_t + \tilde{V}_{t+\tau})}]. \end{aligned} \quad (\text{G.1})$$

By definition we have

$$E[e^{q\sigma \log b(\tilde{V}_t + \tilde{V}_{t+\tau})}] = \int e^{q\sigma \log b(v_t + v_{t+\tau})} dF_{\tilde{V}_t, \tilde{V}_{t+\tau}}(v_t, v_{t+\tau}), \quad (\text{G.2})$$

where  $F_{\tilde{V}_t, \tilde{V}_{t+\tau}}$  denotes the joint distribution of  $\{\tilde{V}_t, \tilde{V}_{t+\tau}\}$ . In order to make use of the transition probability distribution of the process  $\tilde{V}_t$ , we write the integral in equation (G.2) as

$$\int e^{q\sigma(\log b)v_t} \left( \int e^{q\sigma(\log b)v_{t+\tau}} dF_{\tilde{V}_{t+\tau} \| (\tilde{V}_t = v_t)}(v_{t+\tau}) \right) dF_{\tilde{V}_t}(v_t). \quad (\text{G.3})$$

As given in equation (5.65) with  $\rho = 1$ ,

$$(\tilde{V}_{t+\tau} \| \tilde{V}_t = v_t) \sim N[v_t e^{-\alpha\tau}, 1 - e^{-2\alpha\tau}], \quad (\text{G.4})$$

so  $\int e^{q\sigma(\log b)v_{t+\tau}} dF_{\tilde{V}_{t+\tau} \| (\tilde{V}_t = v_t)}(v_{t+\tau})$  gives the moment of order  $q\sigma \log b$  of the logarithm of a normal random variable with the distribution (G.4). Recalling that when  $X \sim N[\mu, \sigma^2]$ ,

$$E[e^{qX}] = e^{\mu q + \sigma^2 q^2 / 2}, \quad (\text{G.5})$$

we have

$$\int e^{qa(\log b)v_{t+\tau}} dF_{\tilde{V}_{t+\tau} \| (\tilde{V}_t = v_t)}(v_{t+\tau}) = e^{q\sigma(\log b)v_t e^{-\alpha\tau} + (1 - e^{-2\alpha\tau})(q\sigma \log b)^2 / 2}. \quad (\text{G.6})$$

So we rewrite (G.3) as

$$e^{(1 - e^{-2\alpha\tau})(q\sigma \log b)^2 / 2} \int e^{q\sigma(\log b)v_t(1 + e^{-\alpha\tau})} dF_{\tilde{V}_\tau}(v_t), \quad (\text{G.7})$$

and essentially play the same trick again. We know that  $\tilde{V}_t$  is a unit normal random variable, so the integral in (G.7) is the moment of order  $q\sigma \log b(1 + e^{-\alpha\tau})$  of the logarithm of a unit normal random variable. Thus the value of the integral in (G.7) is

$$e^{(1 + e^{-\alpha\tau})^2 (q\sigma \log b)^2 / 2}, \quad (\text{G.8})$$

and after a little algebra (G.7) becomes

$$e^{(1 + e^{-\alpha\tau})(q\sigma \log b)^2}. \quad (\text{G.9})$$

So finally from (G.1) and (G.9) we have

$$\begin{aligned} E[Y_t^q Y_{t+\tau}^q] &= e^{-(\sigma \log b)^2 q + (1 + e^{-\alpha\tau})(\sigma \log b)^2 q^2} \\ &= b^{-\sigma^2(\log b)q + (1 + e^{-\alpha\tau})\sigma^2(\log b)q^2}. \end{aligned} \quad (\text{G.10})$$